N° d'ordre : 4253

THESE

Présentée à

L'UNIVERSITE BORDEAUX I

Ecole Doctorale Sciences et Environnements

Par M. Pierre POLSENAERE

Pour obtenir le grade de

DOCTEUR

Spécialité : Biogéochimie et Ecosystèmes

ECHANGES DE CO_2 ATMOSPHERIQUE DANS LA LAGUNE D'ARCACHON ET RELATIONS AVEC LE METABOLISME INTERTIDAL

Soutenue le 29 avril 2011

Après avis de :

M. Dominique Davoult, Professeur, Université Pierre et Marie Curie, Paris VI — Rapporteur
M. Alberto Vieira Borges, Chercheur qualifié, FNRS, Université de Liège — Rapporteur

Devant la commission d'examen composée de :

M. Dominique Davoult, Professeur, Université Pierre et Marie Curie, Paris VI — Rapporteur
M. Alberto Vieira Borges, Chercheur qualifié, FNRS, Université de Liège — Rapporteur
Mme Isabelle Auby, Chargée de Recherche, IFREMER Arcachon — Examinateur
M. Denis Loustau, Directeur de Recherche, INRA Villenave d'Ornon — Examinateur
M. Gwenaël Abril, Chargé de Recherche, CNRS-Bordeaux 1 / IRD-UFAM — Directeur de thèse
M. Pierre Anschutz, Professeur, Université Bordeaux 1 — Président

- 2011 -

Echanges de CO_2 atmosphérique dans la lagune d'Arcachon et relations avec le métabolisme intertidal

Résumé

Les zones côtières ne sont prises en compte dans les budgets globaux de CO_2 atmosphérique que depuis peu. Il s'avère que bien qu'elles ne représentent globalement que de faibles superficies, les flux de carbone et de nutriments y sont très significatifs à l'échelle globale. On sait peu de chose sur le comportement des écosystèmes lagunaires vis-à-vis du CO_2 et, encore moins des zones intertidales où les échanges avec l'atmosphère ont lieu alternativement avec l'eau et le sédiment.

Les objectifs de cette étude ont été d'une part, d'établir le bilan de carbone échangé entre la lagune d'Arcachon, l'atmosphère et le milieu terrestre, et d'autre part de mettre en relation ces flux avec la production nette de l'écosystème (NEP) afin de mieux caractériser le statut métabolique de celle-ci ainsi que les facteurs environnementaux clés. Pour cela, nous avons mis en place pour la première fois et à différentes saisons et stations, des mesures directes de flux de CO_2 par Eddy Covariance, une méthode fonctionnant en continu pendant l'immersion et l'émersion. En parallèle, les apports de carbone terrestre sous ses différentes formes ont été quantifiés par un suivi annuel sur 9 rivières alimentant la lagune.

L'export total de carbone par le bassin versant à travers les eaux de surface des rivières est estimé à 116 t C km^{-2} an^{-1} dont 39% est exporté à la lagune sous forme organique dissoute (DOC) du fait de la prédominance de podzols dans le bassin versant. La forte minéralisation de la matière organique terrestre dans les sols et eaux souterraines sursature largement les eaux en CO_2 et l'export sous forme de carbone inorganique dissoute (DIC) représente environ 21%. La formulation d'un modèle mathématique, le « StreamCO_2-DEGAS », basé sur les mesures de pCO_2, de concentrations et de compositions isotopiques en DIC a permis de montrer que 43% de l'export total de carbone était dégazé sous forme de CO_2 depuis les rivières vers l'atmosphère, réduisant alors le flux net entrant dans la lagune à 66 t C km^{-2} an^{-1}.

Concernant la mesure de flux verticaux, l'analyse cospectrale ainsi que les résultats obtenus en adéquation avec les contrôles physiques et biologiques aux différentes échelles tidale, diurne et saisonnière, ont permis de valider la méthode de l'Eddy Covariance en zone intertidale. Sur l'ensemble de la période de mesures, les flux de CO_2 étaient faibles, variant entre -13 et 19 µmol m^{-2} s^{-1}. Des puits de CO_2 atmosphérique à marée basse le jour ont été systématiquement observés. Au contraire, pendant l'immersion et à marée basse la nuit, des flux positifs ou négatifs ou proche de zéro ont été observés suivant la saison et la station étudiées. L'analyse concomitante des flux de CO_2 et des images satellites du platier à marée basse le jour a clairement permis de discriminer l'importance relative des deux cycles métaboliques distincts des principaux producteurs primaires avec (1) les herbiers de *Zostera noltii* à cycle annuel long, dominant la NEP en été et en automne à la station la plus centrale et (2) les communautés microphytobenthiques, dominant la production primaire brute (PPB) au printemps à la même station et en automne au fond du bassin. Un recyclage rapide de cette production durant l'immersion et l'émersion a aussi clairement été mis évidence. Au vue des différents résultats, la technique d'Eddy Covariance utilisée en zone intertidale laisse envisager d'intéressantes perspectives en termes de connaissances sur les budgets de carbone et les processus écologiques et biogéochimiques dans la zone côtière.

Mots Clés: carbone, CO_2, pCO_2, export, bassin versant, flux, dégazage, échange net de l'écosystème, production nette de l'écosystème, production primaire brute, respiration de l'écosystème, métabolisme, puits, source, zone côtière, zone intertidale, lagune, *Zostera noltii*, microphytobenthos, Eddy Covariance, image satellite.

Atmospheric CO_2 exchange in the Arcachon lagoon and relationships with the intertidal metabolism

Abstract

The coastal zone is only taken into account since recently in global carbon budgeting efforts. Although covering globally modest surface areas, carbon and nutrient fluxes in the coastal zone appear significant at the global scale. However, little is known about the CO_2 behaviour in lagoons and even less in intertidal zones where exchanges with the atmosphere occur alternatively with the water and the sediment.

The purposes of this work are, on one hand, to establish the carbon budget between the Arcachon lagoon, the atmosphere and the terrestrial watershed and on the other hand, to link these fluxes with the net ecosystem production (NEP) and better characterize its metabolic status along with the relevant environmental factors. For the first time, CO_2 flux measurements by Eddy Correlation have been carried out at different seasons and stations in the tidal flat. In parallel, the total terrestrial carbon export from river waters has been quantified throughout a complete hydrological cycle in nine watercourses flowing into the lagoon.

The total carbon export from the watershed through surface river waters is estimated at 116 t C km^{-2} yr^{-1} on which 39% is exported to the lagoon as dissolved organic carbon (DOC) owing to the predominance of podzols in the watershed. Intense organic matter mineralization in soils and groundwaters largely over-saturate river waters in CO_2 on which export accounts for 21% as dissolved inorganic carbon (DIC). The mathematical "StreamCO_2-DEGAS" model formulation based on water pCO_2, DIC concentrations and isotopic composition measurements permits to show that 43% of the total carbon export was degassed as CO_2 from the riverine surface waters to the atmosphere, lowering then this latter to 66 t C km^{-2} yr^{-1}.

With respect to the CO_2 flux measurements in the lagoon, cospectral analysis and the well accordance of results with physical and biological controls at the tidal, diurnal and seasonal time scales permit to validate the Eddy Correlation technique over tidal coastal zone. CO_2 fluxes with the atmosphere, during each period, were generally weak and ranged between -13 and 19 µmol m^{-2} s^{-1}. Low tide and daytime conditions were always characterized by an uptake of atmospheric CO_2. In contrast, during the immersion and during low tide at night, CO_2 fluxes where either positive or negative, or close to zero, depending on the season and the site. The concomitant analysis of CO_2 fluxes with satellite images of the lagoon at low tide during the day clearly discriminate the relative importance of the two distinct metabolic carbon cycling involving the main primary producers, i.e. (1) the *Zostera noltii* seagrass meadow predominance on the NEP in autumn and summer in the more central station, with an annual cycling and (2) the microphytobenthos community predominance on the gross primary production (GPP) in spring at the same station and in autumn in the inner part of the bay where a rapid carbon cycling during the immersion and the emersion was clearly highlighted. The different results obtained with the Eddy Correlation technique over tidal flats opens interesting perspectives on the knowledge of the carbon budget and the biogeochemical and ecological processes within the coastal zone.

Key words: carbon, CO_2, pCO_2, export, watershed, degassing, net ecosystem exchange, net ecosystem production, gross primary production, ecosystem respiration, metabolism, sink, source, coastal zone, intertidal zone, lagoon, *Zostera noltii*, microphytobenthos, Eddy Correlation, satellite image.

Adresse: UMR 5805 CNRS/ Université Bordeaux 1, Avenue des Facultés, 33405 Talence Cedex, France.

Ce travail de trois ans et demi n'aurait jamais pu aboutir sans l'aide des nombreuses personnes, collègues, amis et famille que je tiens à remercier sincèrement et chaleureusement maintenant.

Tout d'abord, je remercie Philippe Bertrand et Jacques Giraudeau, les directeurs de l'UMR 5805 CNRS/Bordeaux 1, dans laquelle et grâce à qui j'ai pu réaliser ma thèse dans les meilleures conditions possibles, ainsi qu'Antoine Grémare et Thierry Corrège, qui ont pris la relève, pour les mêmes raisons.

J'aimerai ensuite remercier les membres du jury qui ont jugé et examiné mon travail, en particulier Pierre Anschutz en tant que président de ce jury et chef de l'équipe « ECOBIOC Talence », Dominique Davoult, Alberto Borges en tant que rapporteurs, Isabelle Auby et Denis Loustau en tant qu'examinateurs. Merci pour vos conseils ainsi que pour la discussion tenue lors de la soutenance. Cela m'a énormément apporté.

Je n'aurais jamais pu mener à bien ce projet sans l'aide, les conseils, l'encadrement et la confiance de mon directeur de thèse Gwenaël Abril qui m'a suivi et soutenu tout au long de ce travail. Un très grand merci Gwen pour tout ce que tu as pu m'apporter tant sur le plan professionnel que personnel, ce fut un plaisir de travailler ensemble, j'espère de tout cœur que cela pourra continuer.

Je tiens également à remercier Patrice Bretel qui a co-encadré la première moitié de ma thèse et sans qui la « lady covariance » n'aurait pu être mise en place. Merci pour ta sympathie tant au laboratoire qu'à l'extérieur sur le terrain ou ailleurs autour d'une petite bière bien méritée.

J'ai également eu la chance de travailler en collaboration avec certaines personnes qui ont eu un rôle primordial dans l'aboutissement de ce travail, notamment Jean-Marc Bonnefond que je remercie pour son aide précieuse dans le traitement des données de l'eddy covariance. Je remercie aussi tout particulièrement Eric Lamaud, et ce pour de nombreuses raisons : au-delà de son aide dans le traitement des données de l'eddy covariance, je le remercie pour sa disponibilité, ses conseils et son soutien dans l'analyse des résultats et la rédaction des articles, et ce, jusque dans les derniers moments. Ce travail n'aurait pu aboutir sans cette collaboration avec l'INRA de Villenave d'Ornon. Un très grand merci aussi à Virginie Lafon de la cellule de transfert de l'UMR EPOC pour sa gentillesse, ses disponibilités et son travail sur les images satellites de la lagune d'Arcachon, qui a permis d'aboutir à des résultats si intéressants. Enfin je tiens à remercier sincèrement Bruno Delille, de l'université de Liège, pour son aide sur le terrain lors des mises en place de l'eddy covariance ou sur les cycles de 24h dans la lagune ainsi que pour son accueil chaleureux lors de mon passage à Liège.

J'ai également bénéficié de la présence de nombreuses personnes dans l'UMR qui de près ou de loin m'ont également beaucoup apporté, je pense à Henri Etcheber, ce fut un plaisir de travailler ensemble, avec sa gentillesse et sa bonne humeur, ainsi que son expérience sur le carbone organique mais aussi pour son soutien tout au long des trois ans. Nicolas Savoye pour son aide précieuse et son suivi sur mes manips' et résultats isotopiques. Karine Charlier pour sa gentillesse et son aide dans le même domaine des

isotopes. Benoit Sautour pour la valorisation de ce travail de thèse lors des conférences régions, et aussi pour ses conseils, m'ayant motivé à m'orienter vers la recherche en écologie aquatique en fin de Master 1. Yolanda Del Amo et Corine Glé lors de mon tout premier stage à la station marine à la fin du DEUG qui m'ont aussi soutenu vers cette orientation. Jean-Charles Massabuau, Gilles Durrieu et Damien Tran, mes directeurs de stage de Master 2 qui m'ont accompagné au mieux vers ce travail de thèse. Xavier de Montaudouin en tant que chef d'équipe ECOBIOC et Aldo Sottolichio pour leurs conseils juste avant ma soutenance. Merci aussi Pascal Lecroart, Cyril Langlois, Philippe Martinez, et Bruno Malaizé.

J'aimerai aussi remercier sincèrement Bruno Deflandre et Olivier Maire qui m'ont soutenu dans le projet de postdoc eddy covariance sous-marine vers lequel j'ai la chance de me diriger maintenant, en continuité de ce travail de thèse.

Les résultats obtenus pendant cette étude ont été le fruit d'un travail important mené sur le terrain en équipe. Je tiens ici à exprimer toute ma gratitude, en particulier à Dominique Poirier toujours présent à mes côtés pour les échantillonnages « rivières » et cycles de 24h. Merci à Francis Prince mais aussi à Laurent Letord, les marins de la Planula, toujours disponibles et qui ont fait que les cycles de 24h resteront de très bons moments. Merci à Guillaume Detandt qui a pris la relève de l'eddy à Arcachon, à Aurélia Mouret pour son aide précieuse sur le terrain lors des sorties rivières, à Georges Oggian pour la mise en place « physique » du mat de l'eddy lors d'un certain mois d'avril 2009. Merci à Mathieu Canton, le spécialiste du bassin versant de la lagune d'Arcachon pour la sortie terrain sur la Leyre, à Jo pour le plaisir de travailler avec toi sur le terrain par tous les temps, je m'en souviendrai longtemps, toi aussi je pense. Enfin, merci à tous les étudiants qui ont été là aussi pour m'aider, je ne les oublie pas….je n'oublie pas non plus Gwen car je pense là aussi, avoir eu de la chance d'avoir un directeur de thèse aussi présent sur le terrain.

J'en arrive maintenant à tous ceux qui m'ont soutenu et accompagné lors de ce travail lors des « très bons, bons, moyens, mauvais » moments, en particulier les thésards, ex-thésards, étudiants, non étudiants, stagiaires, amis…bref, Aurélie (L.) et Marie-Lise, pour leurs soutiens, leurs bonnes humeurs et leurs rires dans le bureau, Loic pour ne pas m'avoir fait reprendre la cigarette lors de la rédaction, Florent pour sa sympathie et sa grande gentillesse (à part sur le court !), Laurie pour ce fameux gâteau au citron dont je raffole, Aurélie (L.) pour son humour fin et relevé…allez maintenant je dois faire court pour que le manuscrit ne dépasse pas 300 pages, je remercie sincèrement Laurent, Sophie, Céline, Emilie, Marie, Bruno, Vincent, Vincent, Sylvain, Mathieu, Aurélie, Julien, Muriel, Benjamin, Camille, Ana, Ha, Audrey, Mohamedou, Ika, Romain, Elodie, Raphael, Delphine, Caroline…
Merci aussi à David, ses parents Laura et Simon, Bibi, Ju, Gui, Guigui, Nini, Tom, Tom, Baptoch, Rico, Younes, Manu, Gretou, Shaktie, Harold, Totor, Naïdie et tous ceux que j'ai oublié mais uniquement sur le papier ici !

Merci à vous trois Aurélia, Romain et Jo, lors du congrès à St John's c'était mémorable !

Merci au secrétariat pour son aide administrative, à Cathy pour son aide dans les reliures du manuscrit et à Brigitte Bordes pour sa gentillesse et son efficacité au niveau de l'école doctorale !

Merci beaucoup à Jean-Rémi Pape pour sa confiance dans mon expérience de monitorat.

Merci aussi au club de Tennis des Coqs Rouges !

Merci à Laura qui m'a accompagné lors de cette dernière année, non la plus facile soutenu tout au long de la rédaction jusqu'à la soutenance et encore maintenant.

Enfin, j'aimerai terminer ces longs remerciements par ma famille à qui je dois tout et en particulier d'être arrivé jusque là, mon père, mon grand frère Henry pour son écoute, son courage et son soutien, je n'oublie pas non plus la petite Flo qui l'accompagne.
Merci à mon deuxième grand frère Hubert pour tout ce qu'il m'apporte, soutien, amour et force sur le terrain, dans l'eau, dans la tête... ma p'tite sœur adorée Pénélope pour toutes ces mêmes raisons, son humour, sa joie de vivre.....la liste est longue mais surtout et avant tout je tiens à remercier ma maman à qui je dois énormément, pour son soutien quotidien, sa force, sa bonne humeur qu'il pleuve, qu'il neige....pour son amour....pour tout !

A ma Maman

CHAPITRE I.

INTRODUCTION GENERALE

PARTIE I.1. LE CYCLE GLOBAL DU CARBONE

PARTIE I.2. METABOLISME DU CARBONE ET FLUX DE CO_2 : DE LA ZONE COTIERE AUX LAGUNES INTERTIDALES

PARTIE I.3. PRESENTATION DU SITE D'ETUDE : LA LAGUNE D'ARCACHON

PARTIE I.4. OBJECTIF ET ORGANISATION DE L'ETUDE

I. INTRODUCTION GENERALE

I.1. LE CYCLE GLOBAL DU CARBONE

"Yes, the increases in atmospheric carbon dioxide (CO_2) and other greenhouse gases during the industrial era are caused by human activities" (Denman et al., 2007 (IPCC 2007)).

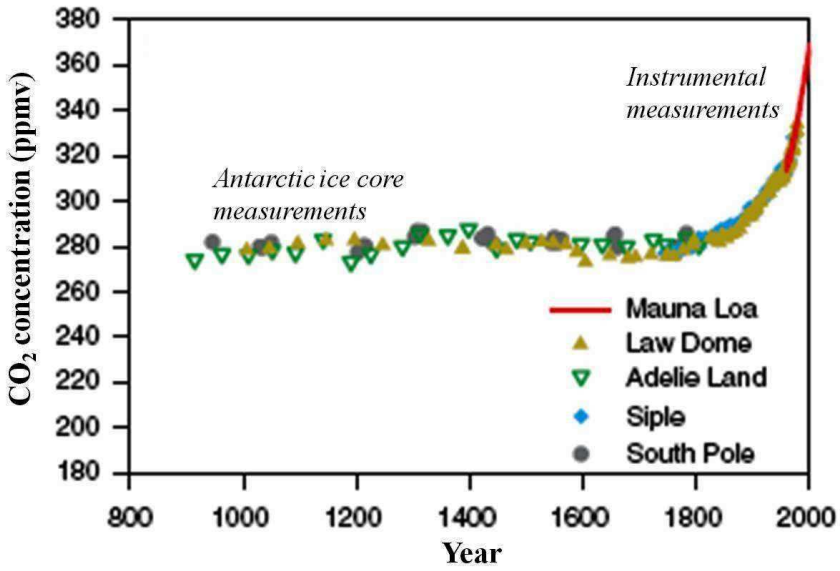

Figure 1.1. Evolutions de la concentration en CO_2 dans l'atmosphère au cours des derniers siècles (Prentice et al., 2001 (IPCC 2001)). L'enregistrement dans le passé est donné par l'étude de différentes carottes Antarctiques (Siegenthaler et al., 1988; Neftel et al., 1994; Barnola et al., 1995; Etheridge et al., 1996) ; depuis les années 1950, les concentrations en CO_2 sont mesurées par l'Observatoire de Mauna Loa à Hawaii (Keeling and Whorf, 2000).

En effet, au cours des derniers siècles, l'Homme a profondément modifié l'équilibre naturel biogéochimique de la planète en émettant de larges quantités de gaz à effet de serre (GES) vers l'atmosphère. Comme le montre la Figure 1.1, la concentration en CO_2 dans l'atmosphère est passée de 280 ppmv en 1800 à une valeur de 367 ppmv en 1999 pour atteindre aujourd'hui plus de 379 ppmv (valeur mesurée par l'Observatoire de Mauna Loa, Hawaii en 2007). L'accélération récente de ce phénomène est sans précédent ; les augmentations en CO_2 dans l'atmosphère n'avaient encore jamais dépassé 30 ppmv en 1000 ans alors qu'aujourd'hui, le CO_2 s'est élevé de 30 ppmv en seulement 17 ans. L'augmentation des concentrations en GES dans l'atmosphère s'accompagne de ce que l'on appelle le « changement global » caractérisé entre autre par le réchauffement de l'atmosphère (sensible depuis plus d'une quarantaine d'année) mais aussi de la surface des océans, par la montée (de 0.7 mm par an en moyenne) du niveau de la mer par dilatation et fonte des glaces, ou encore par la modification des milieux aquatiques et terrestres avec une intensification des événements extrêmes (Prentice et al., 2001 (IPCC 2001)).

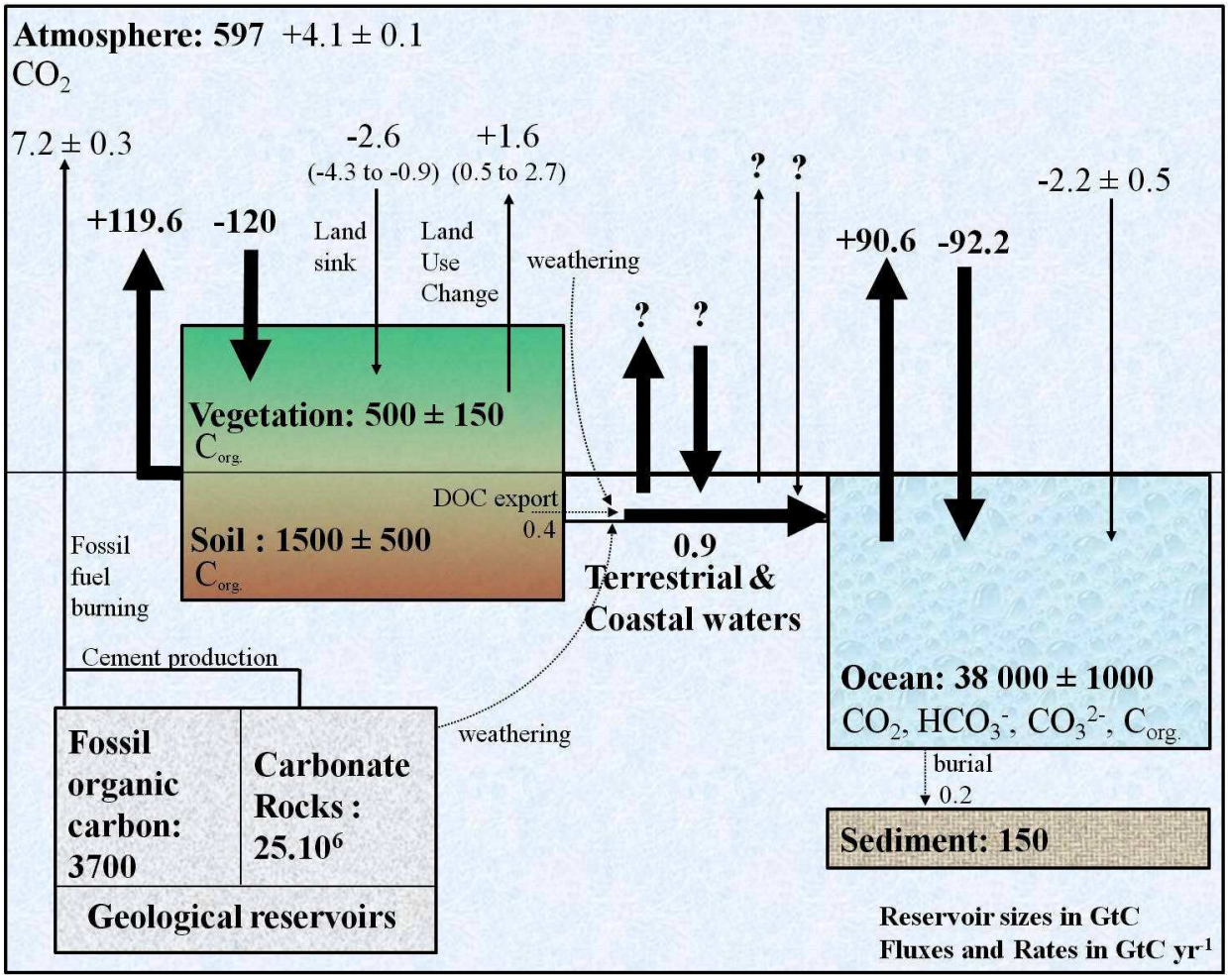

Figure 1.2. Synthèse des connaissances actuelles sur le cycle global du carbone (construit à partir des rapports IPCC 2001 et 2007). Stocks en GtC et flux en GtC an^{-1}. Les flux naturels sont représentés par les flèches épaisses et les flux anthropiques par les flèches fines. Les signes + représentent des flux depuis les réservoirs vers l'atmosphère (source de CO_2) et les signes – au contraire des puits de CO_2. $C_{org.}$: carbone organique, HCO_3^- : ions bicarbonates, CO_3^{2-} : ions carbonates. L'ensemble de ces chiffres est donné pour la période 2000-2005 par le Fourth Assessment Report AR4 (IPCC 2007).

Cette augmentation des concentrations atmosphériques en CO_2 ne révèle cependant pas la totalité des émissions anthropiques depuis 1959. En effet, seul 55% de ces émissions sont conservées dans l'atmosphère, le reste ayant été pompé par les plantes sur terre et par les océans. La Figure 1.2 montre le cycle global du carbone avec à la fois les principaux flux « naturels » avant l'ère industrielle mais aussi « anthropiques » entre les différents réservoirs. A l'Holocène, par les processus de photosynthèse, respiration, dégradation et transfert gazeux, la biosphère terrestre échangeait annuellement avec l'atmosphère environ 120 GtC (un GtC équivaut à 10^{15} grammes de carbone, i.e. un billion de tonnes) alors que l'océan en échangeait 90 GtC. Une émission de 7.2 ± 0.3 GtC an^{-1} de CO_2 vers l'atmosphère est venue s'ajouter à ces flux naturels par la combustion de

matières fossiles et la production de ciment. Cette émission anthropique est responsable de 75% de l'augmentation des concentrations en CO_2 dans l'atmosphère depuis l'ère préindustrielle. Aussi, entre 0.5 et 2.7 GtC an^{-1} de CO_2 sont rejetées vers l'atmosphère par la déforestation principalement en région tropicale et par l'utilisation agricole des écosystèmes terrestres. Ces flux montrent cependant une importante variabilité entre les différentes méthodes utilisées et sont actuellement les moins bien évalués. Sur l'ensemble de ces émissions anthropiques d'environ 9 GtC an^{-1}, 2.2 ± 0.5 sont pompées par les océans et 2.6 GtC an^{-1} (0.9 - 4.3) sont re-captées par les écosystèmes terrestres du fait de la reforestation ou encore de l'augmentation du CO_2 et de l'azote atmosphériques fertilisant la production primaire terrestre.

Les systèmes aquatiques continentaux tels que les rivières ou les fleuves transportent de larges quantités de carbone terrestre depuis le continent jusqu'à l'océan représentant le principal lien entre ces deux réservoirs. Chaque année, environ 0.9 GtC sont transportées par les rivières jusqu'aux océans, environ 40% l'étant sous forme organique et 60% sous forme inorganique (Meybeck, 1982 ; Meybeck, 1993). Sur la totalité de ce transport horizontal, près de 75% proviennent de l'atmosphère représentés par le carbone organique issu des sols et le carbone inorganique dissous issu de l'altération des roches silicatées et carbonatées. Le reste provient de la lithosphère en particulier de l'altération des roches carbonatées (Figure 2). Cependant le rôle des eaux aquatiques terrestres et côtières ne se limite pas seulement au transport passif latéral de carbone vers les océans. En effet une partie du carbone qui est transférée depuis les systèmes terrestres vers les systèmes aquatiques, est sédimentée dans les lacs et estuaires ou dégazée sous forme de CO_2 vers l'atmosphère depuis la surface des eaux continentales et côtières, et n'atteint jamais les océans (Cole et al., 2007 ; Ciais et al., 2008). De récentes compilations montrent que globalement, ce dégazage de CO_2 représenterait 40 à 48% de l'export total de carbone vers l'océan (Cole et al., 2007 ; Tranvik et al., 2009). Le transport latéral global de 0.9 GtC an^{-1} basé sur la mesure de concentrations et de débits à l'exutoire des fleuves ne correspond donc pas à l'exportation totale de carbone depuis le domaine terrestre vers le milieu aquatique. Celui-ci est certainement beaucoup plus élevé du fait de la sédimentation au niveau des eaux aquatiques continentales mais aussi et surtout du dégazage vers l'atmosphère non pris en compte ou mal évalué par les méthodes de mesure actuelles (Worrall and Landcaster, 2005 ; Worrall et al., 2007 ; Wallin et al., 2010).

Il s'avère donc nécessaire afin de préciser ce budget global, de mieux quantifier les échanges de carbone par les eaux aquatiques continentales et côtières. En particulier le transport latéral et l'exportation de carbone vers les eaux marines ainsi que les flux verticaux de CO_2 avec l'atmosphère doivent être mesurés à un pas de temps suffisamment resserré pour prendre en

compte leur dynamique et leur hétérogénéité. Le travail présenté ici s'intéresse tout particulièrement à ces échanges existant au sein de la zone côtière. Celle-ci est très sensible au changement climatique (Prentice et al., 2001 (IPCC 2001)) et actuellement l'un des objectifs majeurs dans la compréhension du fonctionnement de ces écosystèmes est d'évaluer de manière précise le budget de carbone (Yan et al., 2008).

I.2. METABOLISME DU CARBONE ET FLUX DE CO_2 : DE LA ZONE COTIERE AUX LAGUNES INTERTIDALES

I.2.1. Le « système CO_2 » et les échanges atmosphériques en milieu aquatique

Dans les eaux naturelles, le dioxyde de carbone existe sous trois formes inorganiques différentes :

- le dioxyde de carbone libre, CO_2 (aq) = dioxyde de carbone dissous,
- les ions bicarbonates, HCO_3^- et
- les ions carbonates, CO_3^{2-}.

Une quatrième forme existe, i.e. l'acide carbonique H_2CO_3 même si sa concentration est très faible par rapport à celle du CO_2 (aq) (< 0.3%). On peut alors définir par le terme CO_2 (ou $H_2CO_3^*$ ou CO_{2T}) la somme de ces deux formes (Eq. I.1) (Zeebe and Wolf-Gladrow, 2001).

$$[CO_2] = [CO_2\,(aq)] + [H_2CO_3] \qquad (I.1)$$

Les crochets représentent les concentrations totales stœchiométriques.

En raison des échanges avec l'atmosphère, le CO_2 est en équilibre thermodynamique avec le dioxyde de carbone gazeux CO_2 (g) (Eq. I.2).

$$CO_2\,(g) \overset{K_0}{\Leftrightarrow} CO_2 \qquad (I.2)$$

La concentration en CO_2 est donnée par la Loi de Henry avec K_0, le coefficient de solubilité du CO_2 dans l'eau (Eq. I.3).

$$[CO_2] = K_0(T, S).pCO_2 \qquad (I.3)$$

Où la pression partielle du CO_2 atmosphérique pCO_2 est exprimée en atm, la solubilité molaire K_0 (dépendante de la température T et la salinité S de l'eau) en mol L^{-1} atm^{-1}, et la concentration en CO_2 $[CO_2]$ en mol kg^{-1} d'eau.

Les espèces carbonatées sont reliées entre elles par l'équilibre suivant (Eq. I.4) :

$$CO_2\,(aq) + H_2O \Leftrightarrow H_2CO_3 \Leftrightarrow HCO_3^- + H^+ \Leftrightarrow CO_3^{2-} + 2H^+ \quad (I.4)$$

En utilisant le CO_2 à la place de H_2CO_3 et CO_2 (aq) dans l'Equation I.4, on obtient l'Equation I.5 simplifiée :

$$CO_2 + H_2O \overset{K_1}{\Leftrightarrow} HCO_3^- + H^+ \overset{K_2}{\Leftrightarrow} CO_3^{2-} + 2H^+ \quad (I.5)$$

Où K_1 et K_2 sont les constants d'équilibre, souvent considérées comme respectivement les première et seconde constantes de dissociation de l'acide carbonique. Pour la description du système carbonate dans les eaux naturelles, les constantes d'équilibre stœchiométrique sont utilisées (I.6 et I.7).

$$K_1^* = \frac{[HCO_3^-].[H^+]}{[CO_2]} \quad (I.6)$$

$$K_2^* = \frac{[CO_3^{2-}].[H^+]}{[HCO_3^-]} \quad (I.7)$$

Les constantes d'équilibre stœchiométrique dépendent de la température T, de la pression P et de la salinité S, et sont notées par convention avec une *.

La somme de la forme dissoute CO_2, HCO_3^- et CO_3^{2-} définit alors le carbone inorganique dissous (DIC ou $\sum CO_2$) présent dans les eaux naturelles (Eq. I.8).

$$DIC = \sum CO_2 = [CO_2] + [HCO_3^-] + [CO_3^{2-}] \quad (I.8)$$

Une dernière quantité essentielle dans la description du système carbonate est l'alcalinité de l'eau qui est intimement liée à la balance des charges dans l'eau. Elle est définie comme l'excédent de bases libres présentes dans un kilo d'eau et exprimée en équivalents protons par kilo d'eau (meq kg^{-1}) (Eq. I.9).

$$TA = [HCO_3^-] + 2[CO_3^{2-}] + [OH^-] - [H^+] + [B^-] \quad (I.9)$$

Où $[B^-]$ représente l'ensemble des bases faibles autres que les ions carbonate et bicarbonate, soit les ions borate, sulfate, fluorure…

L'équation simplifiée de l'alcalinité totale est celle de l'alcalinité carbonatée (CA) définie par l'équation suivante (Eq. I.10).

$$CA = [HCO_3^-] + 2[CO_3^{2-}] \quad (I.10)$$

Où l'ion carbonate est compté deux fois du fait de sa double charge négative.

Au cours de cette étude, la pCO_2 de l'eau a été mesurée directement par la méthode de l'équilibrateur (Frankignoulle et al., 2001), de même que l'alcalinité (TA) de l'eau, calculée par linéarisation de la fonction de Gran (1952). La concentration en DIC (la somme de chaque forme) a ensuite été calculée à partir de la pCO_2 et de la TA mesurées, en résolvant les équations du

*système des carbonates, à partir des constantes de dissociation de Mehrbach et al. (1973) (**cf. Chapitre II, Partie II**).*

L'utilisation des isotopes stables du carbone dans les eaux naturelles, permet de distinguer les différentes sources et les processus qui contrôlent le carbone inorganique dissous (Mook and Tan, 1991 ; Yang et al., 1996). Par exemple, la composition isotopique du CO_2 (g) (en ‰), déterminée par spectromètre de masse, est notée comme (Eq. I.11) :

$$\delta^{13}C\text{-}CO_2\,(g) = \left(\frac{[^{13}CO_2\,(g)] / [^{12}CO_2\,(g)]}{[^{13}Stand.] / [^{12}Stand.]} - 1 \right) \times 10^{-3} \qquad (I.11)$$

Où $[^{13}CO_2\,(g)]$ et $[^{12}CO_2\,(g)]$ correspondent respectivement aux concentrations des isotopes lourd et léger du CO_2 (g) et $[^{13}Stand.]$ et $[^{12}Stand.]$ celles du standard de référence choisi.

Le passage essentiel du $\delta^{13}C$ du DIC aux $\delta^{13}C$ des différentes espèces du système des carbonates et inversement, ne peut se faire sans connaître la chimie de celui-ci ainsi que les fractionnements isotopiques existant entre les différentes formes du système. Le bilan de masse peut alors être écrit comme (Eq. I.12) :

$$\delta^{13}C\text{-}DIC\,[DIC] = \delta^{13}C\text{-}CO_2\,[CO_2] + \delta^{13}C\text{-}HCO_3^-\,[HCO_3^-] + \delta^{13}C\text{-}CO_3^{2-}\,[CO_3^{2-}] \qquad (I.12)$$

Le $\delta^{13}C$-DIC reflète donc les contributions du DIC provenant de ses différentes sources qui présentent une composition isotopique bien distincte (Wachniew, 2006). Le $\delta^{13}C$ du CO_2 atmosphérique est d'environ -7.5‰ alors que celui des roches carbonatées est proche de 0‰ (Mook et al., 1983). Le $\delta^{13}C$ du CO_2 du sol dépend de la voix métabolique utilisée par la plante lors de la photosynthèse et des sources de matière organique alimentant les respirations microbienne et végétale (Vogel, 1993). Par exemple, dans un système où le CO_2 du sol provient de la décomposition de la matière organique d'une plante en C_3, le CO_2 produit a un $\delta^{13}C\text{-}CO_2$ proche du substrat initial (i.e. -30 à -24‰) ; La respiration de la matière organique terrestre dans les sols et les eaux va produire un DIC avec une composition isotopique similaire au substrat organique. La production primaire au contraire va fortement augmenter le $\delta^{13}C$-DIC, de même que la présence de roches carbonatées dans le système (Parker et al., 2005 ; Amiotte-Suchet et al., 1999). Enfin, les échanges gazeux génèrent une équilibration isotopique avec l'atmosphère et rendent le $\delta^{13}C$-DIC moins négatifs. *L'ensemble de ces considérations sont précisément traitées dans le **Chapitre II**, **Partie I**.*

Les flux verticaux de CO_2 entre l'atmosphère et un système aquatique peuvent être obtenus par différentes méthodes. Notamment, à partir de mesures de pCO_2 dans l'eau de surface par la technique de l'équilibrateur (Frankignoulle et al., 2003) ou calculés indirectement à partir des constantes d'équilibre du système des carbonates et de mesures de température, salinité, pH et de concentrations en DIC (Cai and wang, 1998). Les flux de CO_2 peuvent alors être calculés en utilisant l'Eq. I.13 :

$$F_c = K_0 K [pCO_2 (w) – pCO_2 (a)] \quad (I.13)$$

Où K_0 est le coefficient de solubilité du CO_2 dans l'eau, K, le coefficient d'échange ou la vitesse de transfert de gaz à l'interface air/eau et pCO_2 (w) et pCO_2 (a) les pressions partielles respectivement dans l'eau et l'air.

Les échanges de CO_2 atmosphérique peuvent également être calculés à partir de mesures réalisées lors d'incubations de courte durée, soit par chambres flottantes à l'interface air/eau (Frankignoulle, 1988) soit par chambres benthiques à l'interface air/sédiment (Migné et al., 2002). Ces méthodes, qui fournissent de précieux renseignements sur les processus qui contrôlent les échanges de CO_2 aux différentes interfaces, décrivent plus ou moins bien les grandes variabilités spatiales et temporelles de certains systèmes. Par exemple, les flux de CO_2 peuvent être sujets à d'importantes incertitudes du fait des imprécisions dans la quantification du coefficient d'échanges (Raymond and Cole, 2001). Depuis quelques années, de nouvelles techniques micro-météorologiques comme celle de l'Eddy Covariance paraissent particulièrement appropriées dans la mesure des flux de CO_2 dans des systèmes aquatiques hétérogènes et variables comme les zones côtières (Kathilankal et al., 2008 ; Zemmelink et al., 2009). En effet, cette technique permet d'obtenir à très haute fréquence des chroniques temporelles de flux de CO_2 en continu aux deux interfaces, de manière non intrusive et à l'échelle de l'écosystème (Aubinet et al., 2000 ; Baldocchi, 2003). Le flux vertical moyen de CO_2 (F_c) peut alors être calculé comme la covariance entre les fluctuations de la vitesse verticale du vent (w') et celles de la concentration en CO_2 dans l'air (ρ_c') (Eq. I.14).

$$F_c = \overline{w' \rho_c'} \quad (I.14)$$

Où la barre représente la moyenne réalisée sur la période d'intégration des flux et les ' les fluctuations turbulentes instantanées par rapport à cette moyenne.

Cette technique a notamment été utilisée au cours de cette étude et précisément décrite dans le ***Chapitre III*** *(****Parties I*** *et* ***II*** *+* ***Annexes****) en plus des considérations portant sur le coefficient d'échanges et les autres techniques (****Chapitres II*** *et* ***III****).*

I.2.2. Métabolisme et flux en zone côtière : définitions, problématiques et synthèse

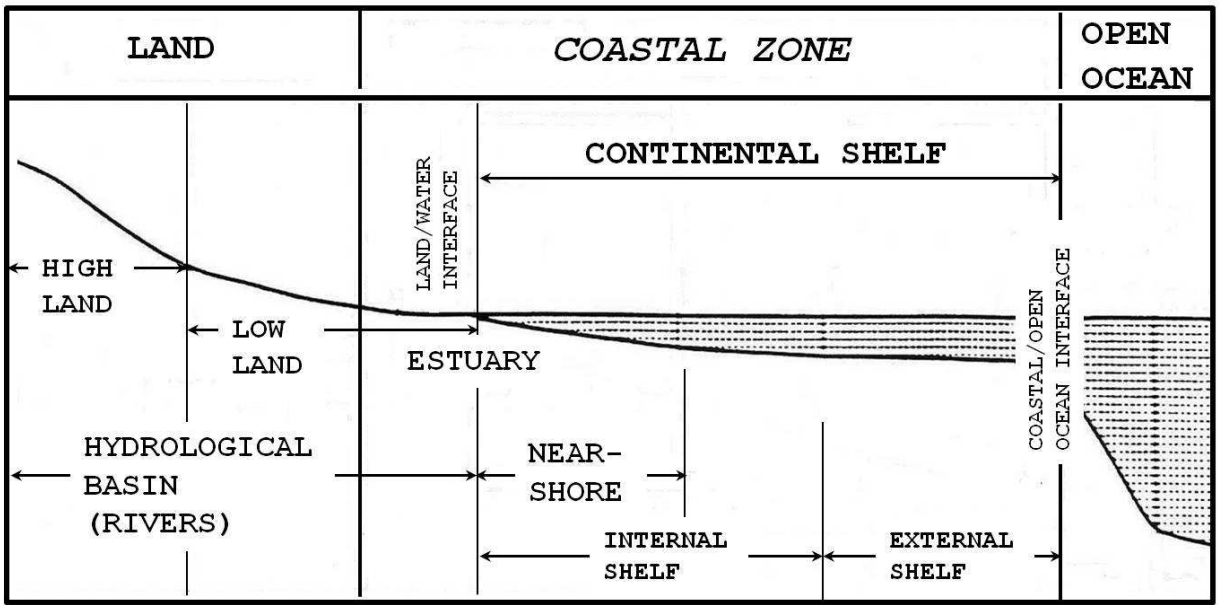

Figure 1.3. Schéma de la morphologie générale de la zone côtière.

La zone côtière est la surface de transition entre le continent et l'océan ouvert. Sa morphologie générale ainsi que les différents termes associés sont représentés en Figure 1.3. Elle est définie comme l'aire océanique située sur le plateau continental, avec une profondeur inférieure à 200 m (en moyenne), incluant toute la surface estuarienne jusqu'à la limite amont de la zone d'influence des marées. A l'intérieur de la zone côtière peut être différenciée la bande littorale comprenant par exemple les lagunes et les estuaires (« near-shore systems », Figure 1.3). Pritchard (1967) a défini un estuaire comme une baie semi-fermée ayant une ouverture sur l'océan ouvert et à l'intérieur de laquelle l'eau salée se mélange à l'eau douce provenant de son bassin versant.

Cette zone reçoit des quantités considérables de nutriments et de matière organique provenant du milieu terrestre, échange de grandes quantités de matière et d'énergie avec le milieu océanique et constitue ainsi un des environnements les plus actifs de la biosphère d'un point de vue biogéochimique (Gattuso et al., 1998; Borges et al., 2005). Néanmoins, elle n'est prise en compte dans les budgets globaux du carbone que depuis peu. En effet, même si les flux de nutriments et de carbone y sont significatifs, elle ne représente qu'une faible surface, i.e. environ 7% de l'océan global (Smith and Hollibaugh, 1993; Borges, 2005). En conséquence, d'intenses échanges de CO_2 entre l'atmosphère et les environnements côtiers sont mesurés, ceux-ci étant significatifs pour les budgets globaux du carbone (Borges et al., 2006 ; Laruelle et al., 2010).

Le métabolisme ou plus précisément la production nette d'un écosystème (net ecosystem production, NEP) est un concept central dans les recherches menées sur le cycle du carbone. Ce terme décrit la capacité d'un écosystème aquatique ou terrestre à consommer du CO_2 et à produire de la matière organique. Woodwell et Whittaker (1968) ont été les premiers à définir la NEP comme (1) la différence entre l'assimilation de CO_2 par l'activité photosynthétique de l'écosystème (production primaire brute ou gross primary production, GPP) et les pertes de CO_2 par la respiration de la communauté de l'écosystème (community respiration, CR) et (2) comme l'accumulation nette de carbone au sein de l'écosystème. La GPP représente la fixation brute de carbone par les tissus et/ou organismes autotrophes, et la CR la respiration de l'ensemble des organismes d'un écosystème, par unité de surface et de temps. La CR regroupe la respiration des autotrophes (autotrophic respiration, AR) et des hétérotrophes (heterotrophic respiration, HR). La production primaire nette (net primary production, NPP) est finalement définie comme la différence entre la GPP et la AR. En général, un écosystème accumule du carbone lorsque la GPP excède la CR (NEP positive) ou lorsque le rapport GPP/CR est plus grand que un ; on parle alors d'un système autotrophe. Au contraire, un écosystème perd du carbone lorsque GPP/CR est inférieur à 1 (NEP négative) ; on parle dans ce cas d'un système hétérotrophe (Odum, 1956).

Dans les environnements côtiers, un système autotrophe stocke nécessairement ou exporte du carbone organique vers le domaine océanique ouvert. Au contraire, dans un écosystème hétérotrophe, il se produit une perte nette de matière organique (Gattuso et al., 1998 ; Borges et al., 2006). Dans ce cas, son métabolisme est alimenté par des apports externes de matière organique, majoritairement en provenance du continent pour ce qui est de la zone littorale. La CR inclut ici la respiration totale des organismes benthiques et pélagiques, autotrophes et hétérotrophes de la colonne d'eau et du sédiment. Sur des échelles de temps relativement courtes, la GPP et la CR sont les processus qui respectivement consomment et produisent la majeure partie du carbone inorganique dans l'écosystème. Typiquement, pendant la journée, la GPP prédomine sur la CR donnant une NEP positive ; il se produit une baisse de la concentration en CO_2 dans les eaux générant un gradient qui peut conduire à un pompage de CO_2 atmosphérique. Au contraire, pendant la nuit, la CR excède la GPP et la NEP est négative ; la CR génère un enrichissement des eaux en CO_2 et conduit alors à une réduction du puits de CO_2 ou à un dégazage vers l'atmosphère. Ainsi, l'échange net de l'écosystème (net ecosystem exchange, NEE) définit comme l'échange vertical de CO_2 avec l'atmosphère, est en principe égal à la NEP dans la plupart de ces écosystèmes terrestres (Chapin III et al., 2006). Cependant, comme l'ont souligné Gattuso et al. (1998) et Borges et al. (2006), dans les environnements côtiers, la relation entre la NEP et les échanges de CO_2 avec l'atmosphère n'est pas toujours directe. En effet, les flux de CO_2 en zone

côtière peuvent être influencés par un certain nombre d'autres processus comme : la dissolution des carbonates et la calcification, l'advection de CO_2 avec les masses d'eau en provenance de zones adjacentes, ainsi que le découplage entre production et dégradation de matière organique en relation avec les propriétés physiques des masses d'eau. En effet, dans les milieux stratifiés, la GPP a lieu en surface mais la CR a lieu en partie en profondeur, dans des couches d'eau isolées de l'atmosphère, ce qui favorise le pompage de CO_2 atmosphérique (Borges et al., 2006). Enfin, dans le cas particulier de la zone intertidale, la NEP est uniquement benthique durant l'émersion et strictement égale au NEE, tandis que durant l'immersion, l'advection de carbone avec la marée peut générer de grandes différences entre la NEP totale (pélagique et benthique) et le NEE. Ainsi, Gazeau et al. (2005a) ont pu observer dans un estuaire microtidal, le Randers fjord au Danemark une NEP négative (hétérotrophie) des masses d'eaux concomitante avec un pompage de CO_2 depuis l'atmosphère. Ce résultat d'un point de vue qualitatif s'explique par le fait que les flux de CO_2 sont en partie gouvernés par les processus métaboliques dans la couche d'eau de mélange. La NEP mesurée rend compte au contraire de la stratification haline permanente des masses d'eau (Borges et al., 2006).

Aujourd'hui, les flux nets de CO_2 entre l'océan global et l'atmosphère tendent à être de mieux en mieux connus même si de larges incertitudes persistent dans les estimations. Takahashi et al. (2009) ont récemment calculé un puits de -1.6 ± 0.9 GtC an^{-1} en compilant des mesures de pressions partielles de CO_2 (pCO_2) dans les eaux de surface des océans globaux. Cependant, ces incertitudes restent mineures si l'on s'intéresse aux flux dans la zone côtière. En effet, la zone côtière couvre un large ensemble d'écosystèmes très diversifiés où le comportement du carbone est très différent, ce qui la rend fortement hétérogène. Cette hétérogénéité spatio-temporelle, le manque relatif de données en zone côtière ainsi que le manque de précision dans l'évaluation des surfaces, s'accompagne d'une grande variabilité dans les flux mesurés, i.e. en termes de puits ou de source de CO_2 (Borges, 2005 ; Borges et al., 2005 ; Chen and Borges, 2009). Les plateaux continentaux faisant partie intégrante de la zone côtière représentent une exception. En effet, Chen and Borges (2009) ont montré qu'ils absorbaient entre 0.33 et 0.36 GtC an^{-1} ce qui correspond à un puits additionnel d'environ 30% du pompage de CO_2 par l'océan global (Chen and Borges, 2009). La dernière étude réalisée par Laruelle et al. (2010) évalue à la baisse ce puits à -0.21 ± 0.36 GtC an^{-1} en utilisant une typologie des estuaires et plateaux continentaux basée sur un système d'information géographique à haute résolution (Dürr et al, 2011).

Toute une série d'écosystèmes existent au sein de la zone côtière comme les plateaux continentaux, déjà cités, mais aussi les estuaires, les marais, les lagunes, les systèmes intertidaux ou encore les fjords, les mangroves, les récifs coralliens. Une classification estuarienne simplifiée par typologies a été proposée par Dürr et al. (2011). Le Tableau 1.1 donne les principales caractéristiques influençant la dynamique du CO_2 dans chacun de ces types de systèmes côtiers.

Type	Length (km)	Depth (m)	Residence time (yr)	Total suspended solids (TSS)	Stratification	O_2	Sensivity to river flow
Delta	1 - 100	≤ 10	$10^{-3} – 10^{-2}$	medium	limited	high O_2	high
Lagoon	1 – 100	< 10	$10^{-2} – 10^{-1}$	low/medium	limited	variable O_2	medium
Macrotidal/ria	10 – 100	≤ 10	$10^{-2} – 10^{-1}$	ETM*	none	low O_2 at ETM*	medium
Fjord	10 > 100	> 100	$10^{1} – 10^{2}$	very low	high	high O_2 in surface, anoxic botom layer**	very low
Fjärd	1 – 10	≥ 10	10^{2}	low	medium	medium O_2	low

***** estuarine turbidity maximum: TSS> 100 to 10 000 mg L^{-1} depending on depth
** in fjörds with sills.

Tableau 1.1. Principales caractéristiques influençant la dynamique du CO_2 dans les environnements estuariens (Borges et Abril, 2012).

L'hétérogénéité et la complexité des écosystèmes côtiers se traduisent par une grande variabilité en termes d'écophysiologie de l'ensemble des organismes autotrophes et hétérotrophes via les facteurs environnementaux, physiques et biologiques de l'écosystème considéré. Un certain nombre de facteurs vont fortement contrôler la GPP et la CR des différents organismes, se répercutant sur le métabolisme de l'écosystème (NEP) et sur l'intensité et direction des flux de CO_2 (NEE).

- La lumière : elle agit sur les organismes autotrophes et hétérotrophes de différentes manières (1) quantitativement en contrôlant l'équilibre GPP/CR de la colonne d'eau dans le cas du compartiment planctonique des écosystèmes côtiers. En pénétrant dans la colonne d'eau, 5 à 40% de l'énergie lumineuse est perdue et on définit une profondeur de compensation, c'est-à-dire l'éclairement pour lequel le bilan GPP/CR est égal à 1 (NEP nulle). Au-dessus de cette limite, c'est la couche euphotique où la NEP est positive ; sa profondeur varie entre 150 m dans les lagons tropicaux à 5 m dans les eaux turbides (Del Amo, communication personnelle). En dessous de cette zone, c'est la zone oligophotique où la CR prédomine sur la GPP (NEP négative) et encore plus en profondeur se trouve la zone aphotique où la photosynthèse n'est

plus possible et (2) qualitativement sur les différents pigments photosynthétiques des organismes autotrophes, ceux-ci ayant des absorptions préférentielles en ce qui concerne les longueurs d'ondes du spectre lumineux. La lumière reste le moteur de la photosynthèse ; elle stimule la GPP comme c'est le cas dans les estuaires où un maximum de GPP survient dans les parties amont durant l'été suite au développement d'un bloom phytoplanctonique (Borges and Abril, 2012). Aussi, différentes courbes P/I (photosynthèse-irradiance) peuvent être mesurées dans les compartiments pélagique (Curl and McLeod, 1961) et benthique comme chez les phanérogames marines (Vermaat and Verhagen, 1996 ; Plus et al., 2005) ou les communautés microphytobenthiques. Migné et al. (2007) y ont notamment montré différentes courbes GPP/PAR (photosynthetically active radiation) en fonction des saisons et des sites choisis le long des côtes françaises (Manche). Des mécanismes de photoinhibition ou photoadaptation peuvent enfin exister chez ces organismes sous forte irradiance diminuant généralement la NEP. Certaines phanérogames marines (i.e. herbiers de *Zostera noltii*) sont en effet capables de dissiper l'excès d'énergie lumineuse sous forme de chaleur (régulation de la photosynthèse par le bas (Silva et al., 2005)) ; aussi les communautés microphytobenthiques vont se protéger en impliquant les pigments caroténoïdes dans le cycle des xanthophylles ou encore en réalisant des migrations verticales à l'intérieur du sédiment (Blanchard et al., 2004 ; Hubas et al., 2006 ; Serôdio et al., 2008).

- La température et la salinité : ces deux facteurs peuvent agir de manière conjointe ou séparée sur l'équilibre GPP/CR. La température influence non seulement l'activité photosynthétique (GPP) des organismes autotrophes pélagique (Curl and MacLeod, 1961) ou benthique (Admiraal, 1984) mais surtout la CR des communautés benthiques (Hubas, 2006) ou de la colonne d'eau comme l'ont montré Wang and Cai (2004) dans des eaux de marais (Géorgie, U.S). La température agit également sur l'activité enzymatique des organismes. Il a été montré par exemple que l'activité de la nitrate réductase chez les diatomées était plus élevée que celles des dinoflagellés pour une même gamme de température basse (Del Amo, communication personnelle). C'est pourquoi il est souvent observé une efflorescence précoce de diatomées au printemps dans les eaux côtières, celles-ci étant mieux adaptées aux intensités lumineuses et températures basses. La salinité peut également intervenir en particulier dans les estuaires ou les baies en contrôlant la répartition des organismes suivant la tolérance des espèces à résister au stress halin. Cependant, celle-ci agit plutôt avec la température formant des barrières physiques séparant différentes masses d'eau et ayant une importance en termes de NEP. En effet dans le domaine pélagique, les populations phytoplanctoniques ne vont pouvoir s'en

affranchir et se déplacer uniquement dans une couche dite de mélange. En fonction de sa position par rapport à la profondeur de compensation, la NEP pélagique va soit augmenter dans le cas où la couche de mélange est plus profonde que la couche euphotique soit diminuer dans le cas inverse.

- Les nutriments : ils vont principalement contrôler la croissance des organismes autotrophes. Si le CO_2 n'est généralement pas limitant pour les producteurs primaires, les nutriments majeurs peuvent présenter un caractère limitant et vont influencer la dynamique de ces populations. En effet, Larsen et al. (2004) ont montré que, dans les eaux côtières norvégiennes, une floraison de diatomées survenait au début du printemps après augmentation des concentrations en silice et nitrate dans la colonne d'eau, et qu'avant et après celle-ci, les cyanobactéries et pico-eucaryotes dominaient le compartiment pélagique, mieux adaptés aux faibles teneurs en sels nutritifs. La formation de Particules Exopolymériques Transparentes (TEP), à partir de l'exsudation de DOC par le phytoplancton, permet également de compenser les rapports de Redfield en cas de limitation par les nutriments inorganiques (DIC) en période oligotrophe (Beauvais, 2003). En milieu marin, certains groupes (i.e. coccolithophoridés) peuvent enfin utiliser de l'azote ou du phosphore sous forme organique et se développer lorsque ces deux éléments sous forme inorganique sont limitants pour d'autres groupes (Borges, communication personnelle). D'autre part, il a été montré que certaines microalgues benthiques (diatomées) ont la capacité de découpler l'absorption de sels nutritifs et leur utilisation lors de la production ; en zone intertidale, le microphytobenthos pourrait absorber les éléments nutritifs pendant l'immersion profitant du flux à l'interface et produire ensuite durant l'émersion de jour en utilisant ces réserves lorsque les conditions deviennent limitantes (Guarini, 1998).

- Les interactions entre les populations : les relations trophiques vont influencer la NEP et les flux de matières au sein d'un écosystème. Brussaard et al. (1995) ont notamment mis en évidence les effets du broutage, de la sédimentation et de la mort cellulaire dans la structure d'un système côtier pélagique de la Mer du Nord. Un autre exemple concerne le compartiment benthique avec les herbiers de phanérogames marines qui vont favoriser l'activité des organismes hétérotrophes (épiphytes et bactéries autour des racines) et vont supporter une CR importante (Middelburg et al., 2005)[1]. Enfin d'autres communautés microphytobenthiques peuvent être contrôlées par les consommateurs primaires suspensivores de la colonne d'eau ou

[1] Les herbiers semblent faire exception à l'idée de Smith and Hollibaugh (1993) quant au métabolisme de la zone côtière, i.e. « plus un système est oligotrophe et plus il sera hétérotrophe » (cf. Duarte et al., 2010).

bien déposivores des sédiments de surface et être ainsi transférées aux échelons supérieurs du réseau trophique (Guarini, 1998).

- L'hydrodynamique : c'est un paramètre englobant une large gamme de processus allant de l'action de la houle (i.e. distribution des macroalgues en fonction du mode d'exposition abrité, semi-abrité ou battu) à la turbulence en général, avec les formations de gradients de densité dans la colonne d'eau ou encore avec la stratification/mélange des masses d'eau. Prenons l'exemple du rythme tidal en zone côtière présenté en Figure 1.4. En fonction de l'amplitude de la marée le rythme tidal va plus ou moins influencer l'activité biologique des organismes ainsi que les flux de CO_2.

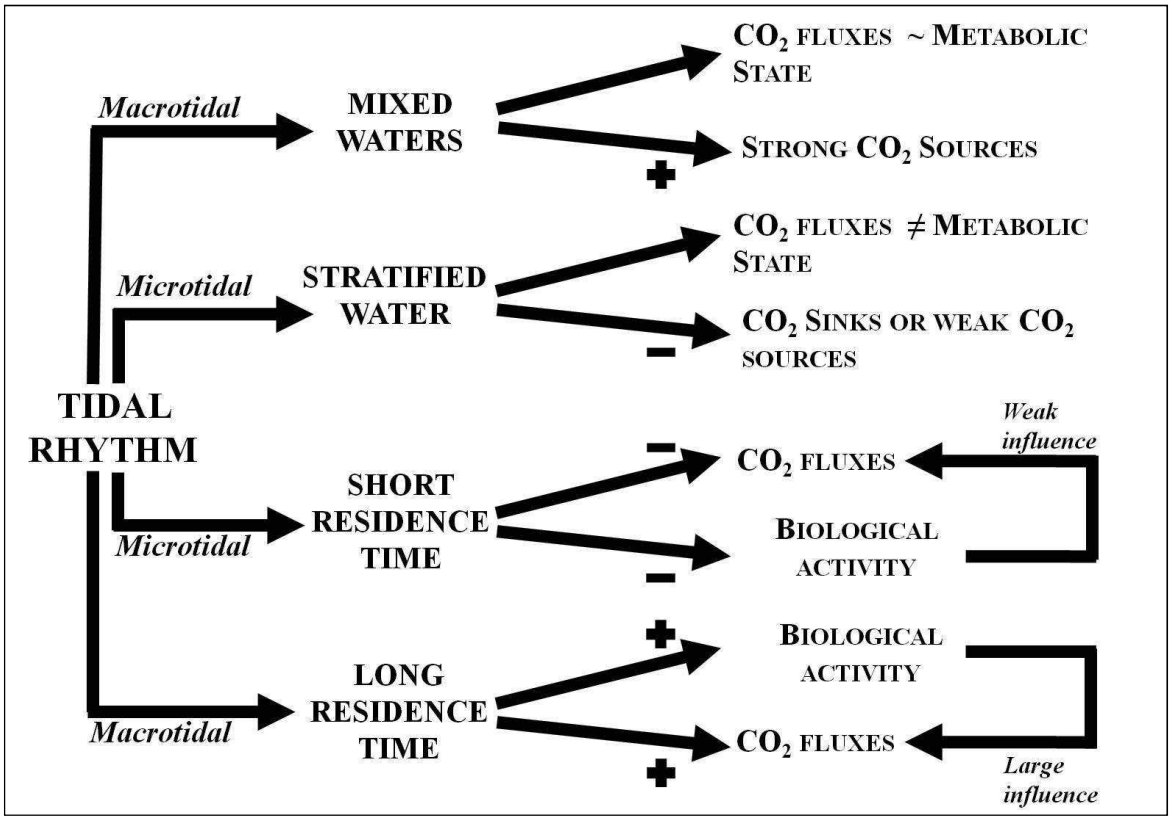

Figure 1.4. Influence du rythme tidal sur les propriétés physiques de la colonne d'eau et sur les flux de CO_2 à l'interface air/eau en relation avec le statut métabolique dans le cadre des systèmes côtiers. Des systèmes macrotidal et microtidal sont caractérisés par des amplitudes de marée supérieure à 4 m et inférieure à 2 m respectivement (Davies, 1964).

Dans un système macrotidal de type estuaire par exemple, les eaux sont en général bien mélangées et souvent turbides et dans ce cas la NEP est négative. Ceci est dû à l'intense dégradation de la matière organique labile en provenance des rivières qui favorise la CR alors que la GPP est limitée par la disponibilité en lumière due aux forts taux de matières en suspension

(Smith and Hollibaugh, 1993 ; Gattuso et al., 1998). Dans ce cas, les flux verticaux de CO_2 sont relativement proches de la NEP. Au contraire dans un système stratifié de type microtidal, l'activité biologique est favorisée. Koné et al. (2009) ont par exemple montré une forte production phytoplanctonique en relation avec une stratification haline permanente dans deux lagunes de Côte d'Ivoire. Ce type de système stratifié est généralement puits ou faible source de CO_2, ces flux ne rendant pas toujours compte de la NEP puisque ces derniers intègrent toute la couche d'eau de mélange et non la stratification des masses d'eau (Borges et al., 2006). Aussi, le rythme de la marée favorise ou au contraire diminue l'activité biologique d'un système en contrôlant le temps de résidence de ses masses d'eau ceci se répercutant sur l'intensité des flux de CO_2 (Figure 1.4). Gazeau et al. (2005b) ont par exemple montré que dans la baie de Palma (Méditerranée), du fait du mouvement très rapide des masses d'eau, l'activité biologique des herbiers de Posidonie avait un impact limité sur les pCO_2 et les flux de CO_2 à l'interface air/eau.

La NEP (GPP et CR) ainsi que les flux de CO_2 (NEE) en zone côtière vont donc montrer une très grande variabilité de manière qualitative et quantitative. La Figure 1.5 représente les flux de CO_2 entre les environnements estuariens et l'atmosphère ainsi que le nombre d'études réalisées sur chacun de ces types estuariens et la surface relative qu'ils représentent selon la classification de Dürr et al. (2011).

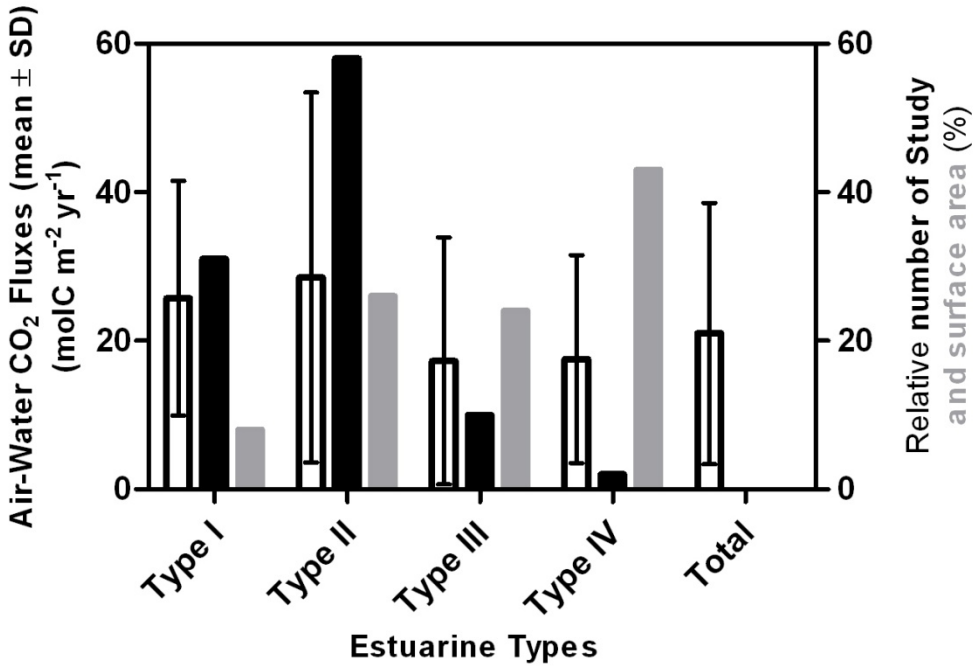

Figure 1.5. Flux de CO_2 entre les différents types d'environnements estuariens et l'atmosphère (barres blanches) repris de Laruelle et al. (2010) en rapport avec le nombre d'études correspondant à chacun des types (barres noires) et la surface relative qu'ils représentent (barres grises). Type I : deltas et estuaires ; Type II : systèmes tidaux ; Type III : lagons et Type IV : fjords et fjärds.

Au total, l'émission globale de CO_2 vers l'atmosphère par les environnements estuariens est estimée à +0.27 ± 0.23 GtC an^{-1} (Figure 1.5). Il apparaît que la majorité d'entre eux se comporte comme des sources de CO_2 vers l'atmosphère couplées à une NEP négative (hétérotrophie nette)[2]. C'est le cas en particulier des Type I et II avec respectivement 27.5 ± 15.8 et 28.5 ± 24.9 molC m^{-2} an^{-1}. Les systèmes III et IV représentent aussi une source de CO_2 équivalente proche de 17.5 ± 16 molC m^{-2} an^{-1} ainsi qu'une surface relative significative de 24 et 43% respectivement (Figure 1.5). Cependant certaines parties de ces systèmes estuariens, peu profondes avec une forte proportion de producteurs primaires (i.e., la composante macrophyte d'un estuaire), peuvent agir au contraire comme un puits net de CO_2 et être caractérisées par une NEP positive (autotrophie nette). Duarte et al. (2010) dans une synthèse sur le métabolisme des communautés d'herbiers ont reporté des rapports GPP/CR en moyenne supérieurs à 1 avec une GPP et NEP estimées à 224.9 ± 11.1 et 27.2 ± 5.8 mmolC m^{-2} jr^{-1} respectivement.

Les échanges de CO_2 en zone côtière malgré leur forte variabilité spatio-temporelle sont donc de mieux en mieux connus (Laruelle et al., 2010 ; Borges and Abril, 2012). Cependant à une échelle encore plus petite, si les systèmes tidaux en particulier les estuaires (Type II) ainsi que les petits deltas (Type I) sont relativement bien caractérisés, les autres systèmes tels que les fjords et fjärds (Type IV) et les lagunes (Type III) le sont beaucoup moins, représentant pourtant une forte surface relative au sein des systèmes estuariens (Figure 1.5). En effet, très peu d'études se sont focalisées sur la dynamique des flux de CO_2 entre les milieux lagunaires et l'atmosphère comme l'étude menée par Koné et al. (2009) dans cinq lagunes contigües de Côte d'Ivoire, en Afrique (Figure 1.5). De ce fait, l'étude des flux de CO_2 et de carbone dans ce type d'écosystème, système ubiquiste que l'on retrouve à toutes les latitudes, et qui plus est, soumis à un rythme des marées, paraît tout à fait justifiée. Avant de présenter le site de ce travail de thèse, le bassin d'Arcachon, voyons d'abord les spécificités d'une lagune intertidale d'un point de vue échanges de CO_2 et métabolisme du carbone.

[2] Il est à noter que les flux verticaux de CO_2 vers l'atmosphère et le statut hétérotrophe de ces différents systèmes estuariens étudiés correspondent dans ce cas (Borges and Abril, 2012).

I.2.3. Spécificités des lagunes (intertidales) d'un point de vue du carbone

Les lagunes font partie intégrante de la zone côtière, en tant que système littoral, occupant 13% du trait de côte mondial (Kjerfve, 1985). Kjerfve (1994) définit les lagunes comme étant des masses d'eau peu profondes séparées de l'océan par une barre, connectées au moins de façon intermittente à l'océan par un ou plusieurs chenaux et généralement orientées parallèlement à la côte. Cependant, il n'en reste pas moins difficile d'en donner une définition précise puisqu'aucun critère ne permet de les distinguer des autres systèmes comme les baies, les estuaires ou encore les marais, d'autant plus lorsque celles-ci sont soumises à l'influence des marées. Les principales caractéristiques physico-chimiques des lagunes sont rappelées dans le Tableau 1.1. Ces milieux saumâtres présentent en général une longueur de 1 à 100 km pour une profondeur faible (inférieure à 10 m). Les concentrations en oxygène sont variables et les concentrations en matières en suspension sont modérées. Lorsque la marée est importante, le temps de résidence des masses d'eau y est court et les phénomènes de stratification sont limités. Les lagunes sont particulièrement sensibles aux phénomènes d'eutrophisation liés aux pressions anthropiques. Ceux-ci se traduisent par des apports de nutriments à la colonne d'eau et aux sédiments liés aux activités dans le bassin versant et amenés par les rivières jusqu'à la lagune[3]. Ils peuvent alors favoriser le développement de micro- et macroalgues opportunistes au détriment des macroalgues et phanérogames autochtones (Duarte, 1995).

Le rythme de la marée va fortement influencer les spécificités de la lagune tant en termes de NEE, ou que de NEP, que d'échanges latéraux de carbone avec les systèmes adjacents. Le forçage tidal va contrôler ces différents termes qui caractérisent le métabolisme de la lagune de façon concomitante avec d'autres échelles de temps caractéristiques comme les rythmes nycthéméral, saisonnier et annuel. Une caractéristique importante des lagunes en lien avec les marées est l'alternance de périodes d'émersion à marée basse et d'immersion à marée haute ayant pour conséquence (1) une GPP pélagique qui peut être forte à marée haute du fait de la pénétration significative de la lumière dans la colonne d'eau à faible profondeur (Gazeau et al., 2004) (2) la possibilité d'une GPP benthique forte à marée basse liée par exemple à l'activité photosynthétique du microphytobenthos qui n'est effective que pendant les périodes d'exondation le jour (Guarini, 1998 ; Hubas et al., 2006 ; Migné et al., 2007) et (3) l'existence d'un fort couplage entre les compartiments benthiques et pélagiques. Par exemple, Guarini (1998) a montré, dans le bassin de Marennes-Oléron, que la GPP microphytobenthique produite à marée basse tenait une place

[3] Deborde et al. (2008) ont également mis en évidence la notion de pompage tidal, c'est-à-dire l'approvisionnement en nutriments des chenaux de marée à marée basse à partir de l'infiltration d'eaux poreuses riches en nutriments au travers des sédiments.

prépondérante dans les flux de biomasse micro-algale de cet écosystème. En effet, une grande partie du microphytobenthos peut être remis en suspension lors de la marée haute et contribuer fortement à la GPP pélagique phytoplanctonique afin de soutenir les taux élevés de production secondaire observés dans ce bassin. A l'inverse, Spilmont et al. (2005) ont observé sur une plage sableuse exposée (de la Manche) que le taux de production primaire benthique en général faible sur ce site pouvait montrer de fortes valeurs en relation après le dépôt sur le sédiment de certaines espèces phytoplanctoniques.

Une autre caractéristique des lagunes intertidales concerne le transfert de la production primaire synthétisée à marée basse vers les maillons supérieurs du réseau trophique. Par exemple dans les lagunes côtières dominées par les phanérogames marines, il a été montré que la matière organique synthétisée par ces herbiers en majorité en période d'émersion était très peu ou lentement dégradée et était surtout stockée dans les sédiments de la lagune sur plusieurs milliers d'années. Ainsi, une fraction significative de la GPP de ces herbiers n'est alors pas utilisée par les hétérotrophes, ce qui tend à rendre ce type d'écosystème autotrophe et puits de CO_2 (Duarte et al., 2010). Au contraire, Middleburg et al. (2000) ont observé que dans deux stations intertidales de l'estuaire de l'Escaut (Belgique), la production microphytobenthique réalisée au cours de la marée basse était rapidement et significativement transférée vers l'ensemble des organismes benthiques hétérotrophes, i.e. bactéries, méiofaune et macrofaune en fonction de la distribution de leur biomasse respective.

Enfin, nous pouvons mettre en relation l'ensemble de ces caractéristiques concernant la NEP benthique et pélagique des lagunes intertidales avec celles des flux verticaux de CO_2 et des mouvements horizontaux des masses d'eau avec les systèmes adjacents. La Figure 1.6. synthétise les relations entre ces différentes caractéristiques. En particulier, en fonction du rythme tidal, les interfaces d'échanges, en termes de NEE avec l'atmosphère, vont changer ainsi que la contribution des différents producteurs primaires benthiques et pélagiques en termes de NEP. A marée basse, la NEE va se produire à l'interface air-sédiment mettant en jeu uniquement la NEP benthique qui va assurer une forte production durant le jour. A ce moment, l'influence des rivières est restreinte aux chenaux et les échanges horizontaux en particulier avec l'océan restent faibles (Figure 1.6.A). A marées montante et haute, la matière organique synthétisée durant l'émersion va être transférée aux compartiments benthiques et pélagiques soit en contribuant à la production primaire planctonique soit à la production secondaire benthique ou pélagique via les différents couplages (Figure 1.6.B). Par conséquence, à cette période, la NEE va être le résultat de la NEP planctonique et de la NEP benthique mais aussi des transports horizontaux de carbone entre la lagune et les eaux douces continentales d'une part et les eaux océaniques d'autre part.

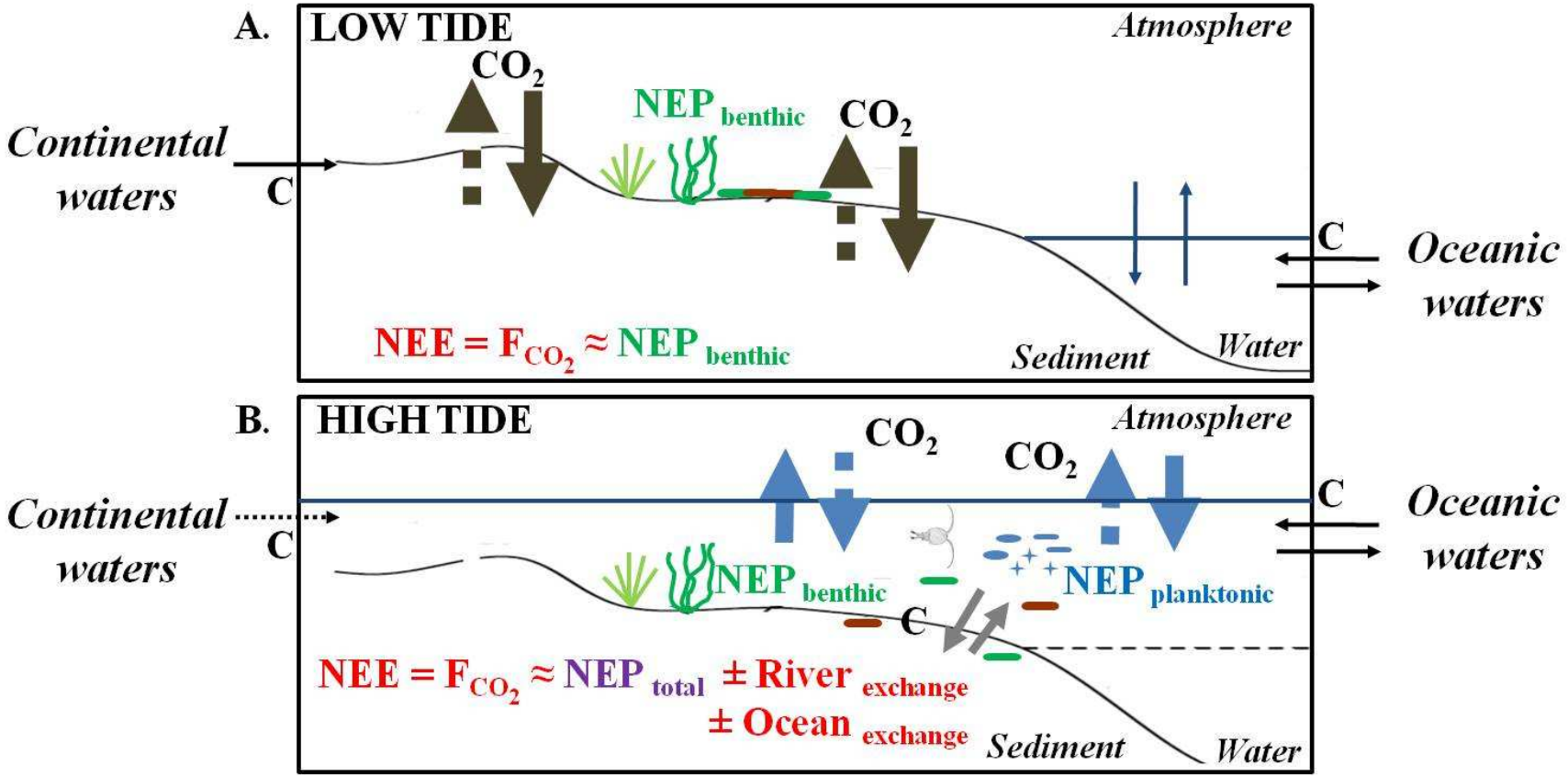

Figure 1.6. Relation NEE, NEP et échanges horizontaux dans une lagune intertidale. A : marée basse : NEE ou flux verticaux de CO_2 à l'interface air/sédiment (NEP benthique), influence des rivières prédominantes et échanges latéraux faibles ; B : marée haute : flux à l'interface air/eau (NEP totale, planctonique et benthique), influence océanique prédominante et échanges latéraux faibles. L'intensité des flux varie en fonction de l'épaisseur des flèches ; couplage entre les compartiments benthiques et pélagiques (voir texte).

Voyons maintenant les principales caractéristiques du site adopté pour ce travail, le bassin d'Arcachon.

I.3. PRESENTATION DU SITE D'ETUDE : LA LAGUNE D'ARCACHON

Le bassin d'Arcachon est une lagune intertidale située sur la côte Atlantique (France) à l'ouest de l'Europe par 44°40' de latitude Nord et 01°10' de longitude Ouest (Figure 1.7.A). Elle est soumise à la fois aux influences marines de l'Océan Atlantique et continentales par un ensemble de cours d'eau de son bassin versant (Figure 1.7.B).

I.3.1. Caractéristiques du bassin versant

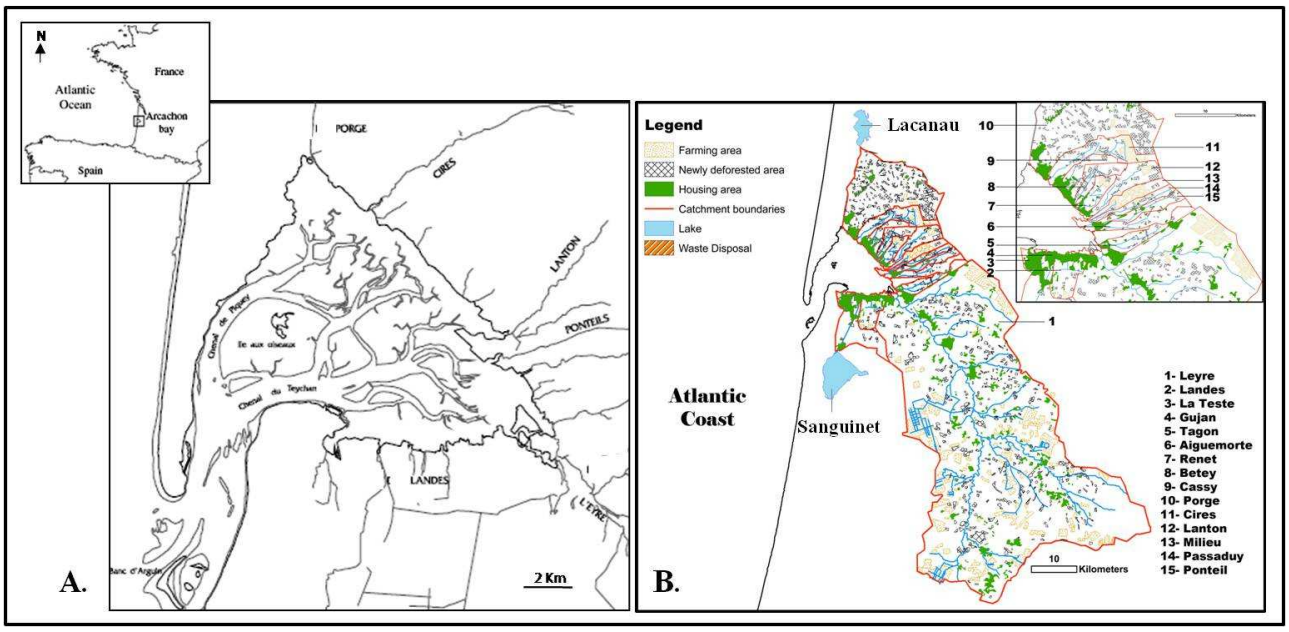

Figure 1.7. Le bassin versant de la lagune d'Arcachon; A : principaux cours d'eau alimentant la lagune ; B : délimitation de chaque sous-bassin.

Le basin versant total affluent à la lagune d'Arcachon couvre une surface de basse altitude de 4138 km^2 où les pentes ne dépassent généralement pas 25%. Ce bassin est relativement homogène d'un point de vue topographique, climatique (de type océanique, isohyètes entre 900 et 1000 mm) et géologique (Auby et al., 1994). Le bassin versant est constitué de 1136 km^2 de bassins de type indirect via les lacs (le système Hourtin-Carcans et Lacanau au Nord et le système Cazaux-Sanguinet au Sud) et 3000 km^2 de bassins de type direct via les cours d'eau (Figure 1.7.B). 84% du bassin est occupé par une forêt de pin maritime (*Pinus pinaster)* couvrant un sol sableux d'origine Pléistocène appelé « le Sables des Landes » (Trichet et al., 1997). Ces sols appelés

podzols se sont formés à partir d'un matériau mère grossier pauvre et siliceux (i.e. dépôts sableux périglaciaires) sous des climats tempérés humides (Lundström et al., 2000). Ces sols sont acides (pH 4-5), pauvres en minéraux mais aussi riches en carbone dont la teneur peut atteindre 50 g par kg de sol (Jolivet et al., 2007). Principalement silicaté, quelques affleurements carbonatés peuvent s'observer localement dans le bassin versant en particulier le long de la Leyre (Folliot et al., 1993). De même, au niveau du sous-bassin du Ponteils, le centre d'enfouissement de déchets de la ville d'Audenge a utilisé pendant de nombreuses années de la chaux qui a enrichi les sols en carbonates (Canton et al., 2010).

Au niveau du Sables des Landes se trouve une nappe d'eau libre et continue, couvrant plus de 4000 km^2 à proximité de la lagune d'Arcachon[4]. Celle-ci, avec une épaisseur qui varie entre 10 et 130 m, est localisée très près de la surface. Le régime de cette nappe détermine trois types de Landes (Righi and Wilbert, 1984). La lande hydrophile qui occupe la majeure partie du bassin avec une nappe d'eau inférieure à 1 m de profondeur ; la lande mésophile présente dans les parties basses et au milieu du bassin dont l'amplitude de la nappe supérieure à 2 m créé des périodes humides et sèches ; et enfin la lande xérophile, en bordure de ruisseaux, avec une nappe profonde à plus de 3 m. Le bassin versant a été massivement drainé par la plantation de la forêt de pins suite à un décret impérial de 1857. Même si la forêt est encore très largement majoritaire, une agriculture intensive de maïs est maintenant bien présente couvrant une surface totale de 130 à 280 km^2 au détriment de l'agriculture traditionnelle et de la forêt (Auby et al., 1994 ; Canton et al., 2010).

Concernant le réseau hydrographique, le bassin d'Arcachon reçoit les eaux douces de plusieurs cours d'eau (Figures 1.7, 1.8 ; Tableau 1.2). La plus importante en termes de débit et de surface (70% de la surface totale) est la Leyre, localisée dans la partie sud-est du bassin (Figure 1.8.A). En plus, 17 ruisseaux caractérisés par de très faibles débits (Tableau 1.2) sont répartis tout autour du bassin comme par exemple le Tagon (Figure 1.8.B). Enfin, deux canaux, celui du Porge au nord et celui des Landes au sud, transportent les eaux des lacs respectivement de Lacanau et de Cazaux-Sanguinet (Manaud et al., 1997 ; De Wit et al., 2005). Annuellement, la lagune reçoit en moyenne 1.25 10^9 m^3 d'eau douce dont 8% par les eaux-souterraines, 13% par les précipitations et 79% par les cours d'eau (Rimmelin, 1998).

[4] En comptant à la fois les bassins versants direct (environ 3000 km^2) et indirect via les lacs (environ 1100 km^2)

	Watershed Surface (km^2)	Runoff ($m^3 s^{-1}$)	Drainage ($L s^{-1} km^{-2}$)	Population density (inhab km^{-2})	Inhabitants/ runoff (inhab $m^{-3} s$)
Porge (Arès)	221.6	3.63	18	310	17263
Cirès (Andernos)	48.7	0.63	13	445	34402
Renet (Lanton)	17.9	0.61	34	43	1283
Lanton (Lanton)	36.1	0.28	8	43	5562
Milieu (Audenge)	21.3	0.63	19	63	3313
Ponteils (Audenge)	23.3	0.23	10	63	6414
Tagon (Biganos)	29.6	0.67	23	113	4939
Leyre (Biganos)	2141.4	18.16	8	113	13360
Landes (Gujan-Mestras)	116.6	0.52	4	315	70703
Total	2656.5	25.34	137	1510	157239

Tableau 1.2. Caractéristiques générales des principaux cours d'eau du bassin versant de la lagune d'Arcachon. La Leyre et le canal du Porge représentent respectivement 73% et 24% du total des apports d'eaux douces par les cours d'eau. Les débits ont été moyennés sur les années 1989-1993.

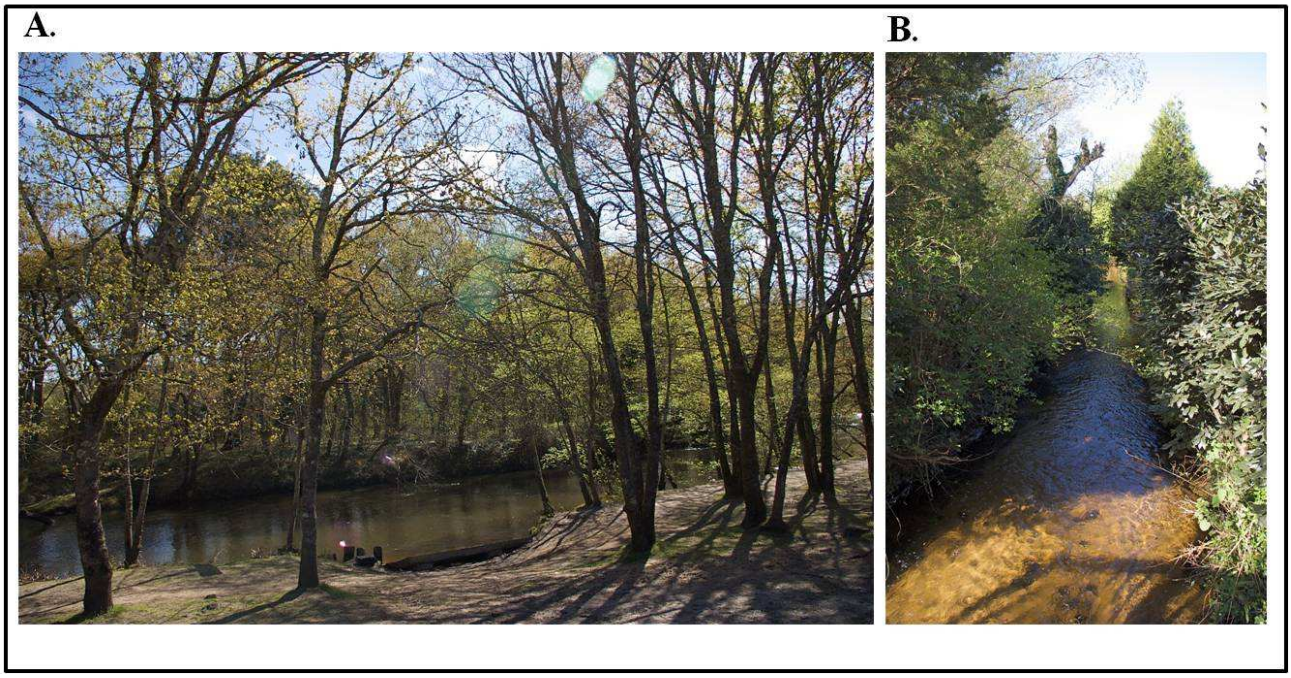

Figure 1.8. Photographies de cours d'eau du bassin versant de la lagune d'Arcachon ; A : la rivière Leyre, B : le ruisseau Tagon.

I.3.2. Caractéristiques de la lagune d'Arcachon

I.3.2.a. Morphologie et physico-chimie de la lagune

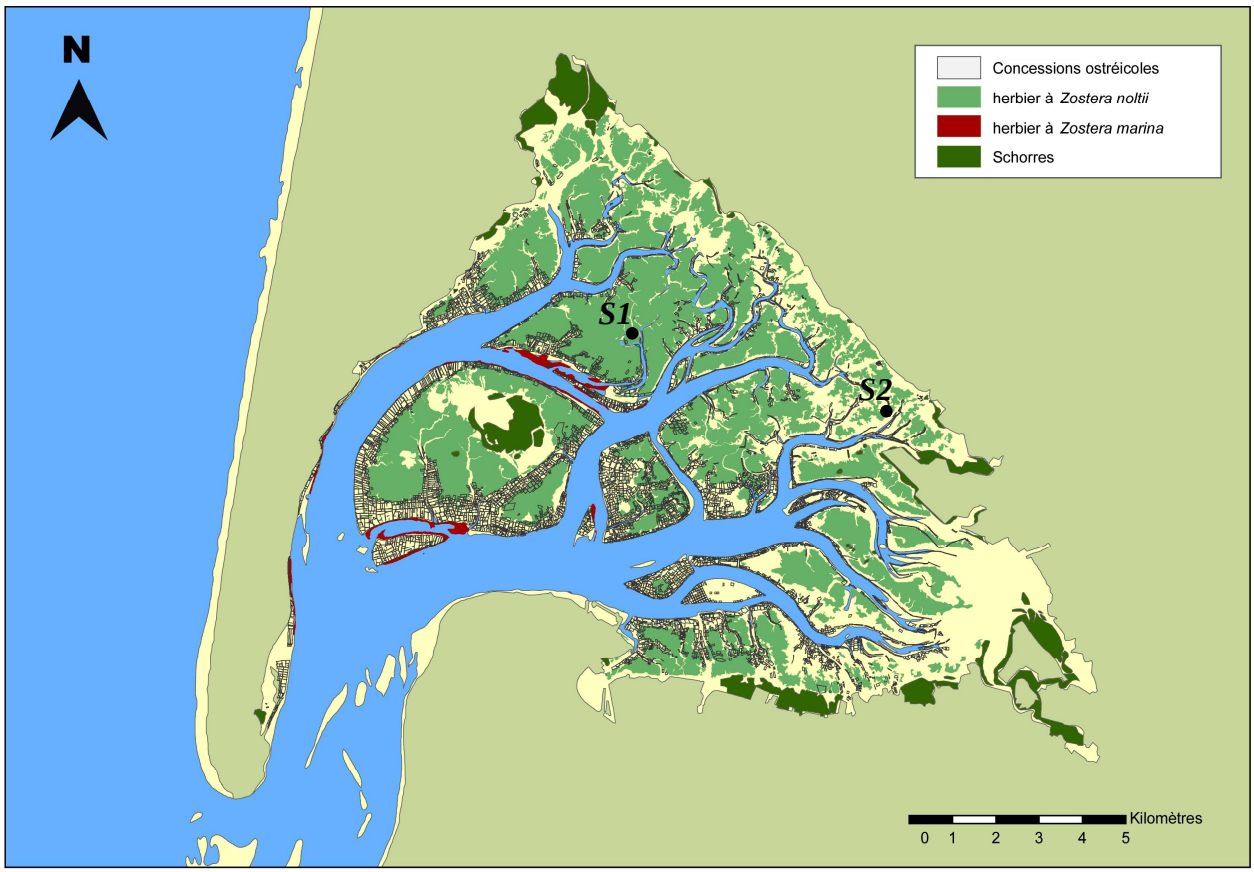

Figure 1.9. La lagune d'Arcachon : cartographie obtenue à partir de photographies aériennes et de mesures *in situ*, d'après Gilles Trut, Ifremer ; concessions ostréicoles (données de 2009), herbiers (données de 2008) et schorres (données de 1989). La zone subtidale (chenaux) est représentée en bleu. L'herbier de *Zostera noltii* colonise 60% du platier intertidal.

Cette lagune intertidale de 174 km^2 en forme de triangle équilatéral s'insère dans la plaine côtière des Landes de Gascogne et communique avec l'Océan Atlantique via un réseau de chenaux et de barres sableuses appelées « passes », de largeur : 2-3 km et de longueur : 12 km (Figure 1.9). Avec une profondeur moyenne de 4.6 m, cette lagune présente des marées de type semi-diurne dont l'amplitude varie de 0.8 à 4.6 m (Plus et al., 2008) ; en fonction du coefficient de marée, le bassin est donc considéré comme une lagune mésotidale à macrotidale. Le volume d'eau contenue dans la lagune évolue de près de 264 10^6 m^3 (coefficient de 45) à près de 492 10^6 m^3 (coefficient de 95) (Plus et al., 2008). Pendant un cycle de marée, la lagune échange avec l'océan entre 130 et 200 10^6 m^3 et entre 370 et 400 10^6 m^3 d'eau pendant des marées moyennes de morte-eau et de vive-eau, respectivement. Le bassin reçoit aussi pendant la durée de chaque cycle de marée, de 1.2 à 1.8 10^6 m^3 d'eau douce provenant de son bassin versant (Manaud et al., 1997). Le nombre de Canter

Cremer est donc de 110-170 ce qui classe le bassin d'Arcachon dans une catégorie d'estuaire relativement bien mélangé à forte influence marine (Pritchard, 1967). En comparaison, ce nombre dans l'estuaire de la Gironde est de 30-40 (Abril et al., 2002). Du fait de la faible profondeur des passes (5 m à marée basse et 9 m à marée haute), seule la partie superficielle de la tranche d'eau du large peut pénétrer dans le bassin créant ainsi une stratification horizontale des masses d'eau (Figure 1.9.). Des passes vers l'intérieur du bassin, elles sont classées selon trois catégories distinctes par leurs variations annuelles de température et salinité (Boucher, 1968) :

- Les eaux néritiques externes (T = 9.5-21°C ; Salinité 34-35)
- Les eaux néritiques moyennes (T = 6-22°C ; Salinité 27-33)
- Les eaux néritiques internes (T = 1-25°C ; Salinité 22-32)

En plus de la marée, le vent est le second moteur hydrodynamique de la lagune. Les vents dominants soufflent de l'ouest avec une dominante nord à la belle saison et un partage nord-sud à la mauvaise saison (Manaud et al., 1997). Le temps de renouvellement des eaux du bassin est relativement court variant entre 13 jours en hiver à 16 jours en été. Les vents de nord et d'ouest favorisent nettement plus ce renouvellement que ceux d'est ou de sud. Néanmoins, les eaux expulsées lors du jusant sont en grande partie reprises durant le flot suivant, ceci ne favorisant pas le renouvellement. Enfin, une arrivée d'eau extérieure localisée dans le fond de la baie par les rivières diminue le confinement et favorise aussi le renouvellement de façon importante (Plus et al., 2008).

La surface du bassin d'Arcachon se divise en deux zones principales (Figures 1.9 et 1.10) :

- la zone subtidale, immergée en permanence avec une surface de 57 km^2 représentée par trois types de chenaux ; les chenaux principaux à fort hydrodynamisme (profondeur maximale : 25 m et courants supérieurs à 1 m s^{-1}) ; les chenaux transversaux, perpendiculaires à la circulation principale des courants de marée et caractérisés par une forte sédimentation vaseuse ; et les chenaux secondaires, en prolongement des chenaux principaux de faible profondeur composés de sédiments sableux en majorité.
- La zone intertidale, immergée à marée haute et découverte à marée basse deux fois par jour alternativement et qui représente 117 km^2 (en période de vive-eaux pour un coefficient de 120) soit les 2/3 de la lagune. La température des sédiments de surface à marée basse fluctue entre -3 et 43°C sur l'année largement influencée par les conditions atmosphériques (Blanchet, 2004). Enfin, une large gamme de sédiments se retrouve sur l'estran avec des sédiments perméables sableux fins dans la partie amont recouverts par une couche de sédiments silto-vaseux vers l'aval (Bouchet, 1968).

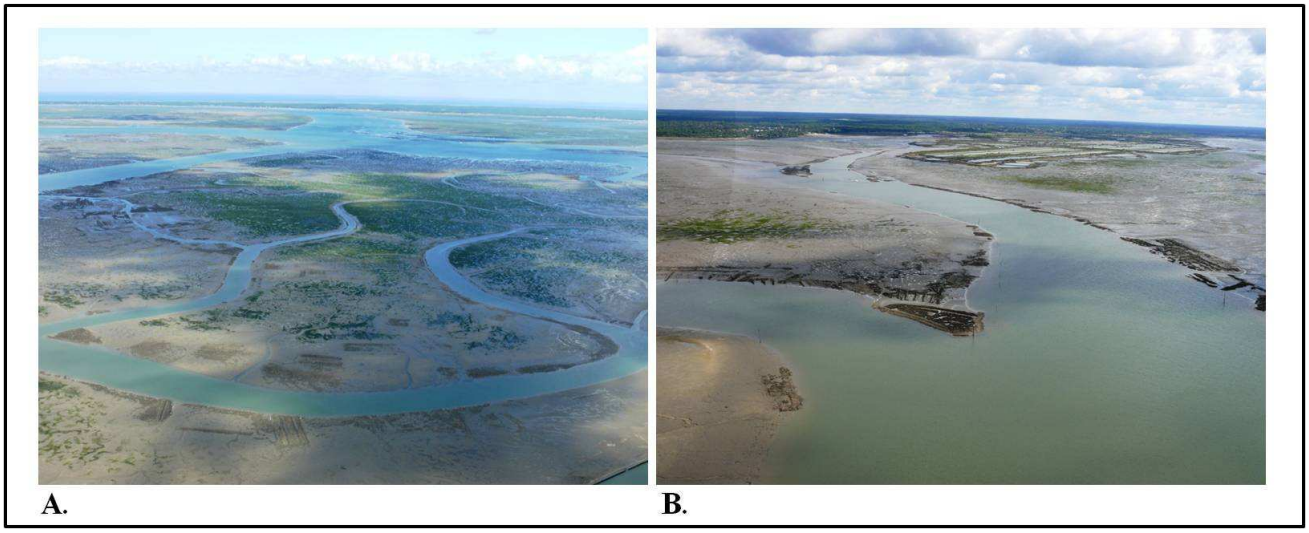

Figure 1.10. Photographies aériennes du bassin d'Arcachon à marée basse (J.M. Froidefond) montrant la zone subtidale avec le réseau de chenaux transversaux et secondaires (A, B) et la zone intertidale avec notamment les herbiers de *Zostera noltii*, les sédiments vaseux et les récifs d'huitres sauvages.

I.3.2.b. Ecologie de la lagune

	Annual Primary Production Estimation			
	t C yr^{-1}	**g C m^{-2} yr^{-1}**	**Contribution (%)**	**References**
***Zostera noltii* Seagrass meadows**	8880-12709	127-181	20	Auby, 1991
***Zostera marina* meadows**	2336	584	5	Auby, 1991
Benthic macroalgae (*Monostroma obscurum)*	2508	17	5	Auby et al., 1994
Benthic macroalgae (épiphytes des herbiers de *Zostera marina)*	390-584	97-146	1	Auby, 1991
Schorre halophyte plants (above-ground production)	3045-3639	397-474	7	Sorianno-Sierra, 1992
Microphytobenthos	16133-17621	104-114	32	Auby (personal communication)
Phytoplankton	16068	103	30	Glé et al., 2008
Total	**49360-55465**	**1429-1619**		

Tableau 1.3. Synthèse des estimations concernant la production primaire de la lagune d'Arcachon. Les estimations en g C m^{-2} an^{-1} ont été obtenues en normalisant les productions annuelles par les surfaces respectives de chacun des compartiments. Les productions des herbiers de *Zostera noltii*, des macroalgues et des plantes halophytes correspondent à des productions nettes estimées à partir de mesures de biomasses sur une couverture annuelle. Les productions des herbiers de *Zostera marina* et de ses épiphytes ont été estimées à partir de valeurs calculées à Roscoff (France). La production du microphytobenthos correspond à une production brute estimée à partir de mesure de concentrations en Chl *a* sur une couverture temporelle limitée. Enfin, la production du phytoplancton se situe entre une production brute et nette obtenue par incubations au ^{14}C pendant une certaine année (2003) (cf. références citées).

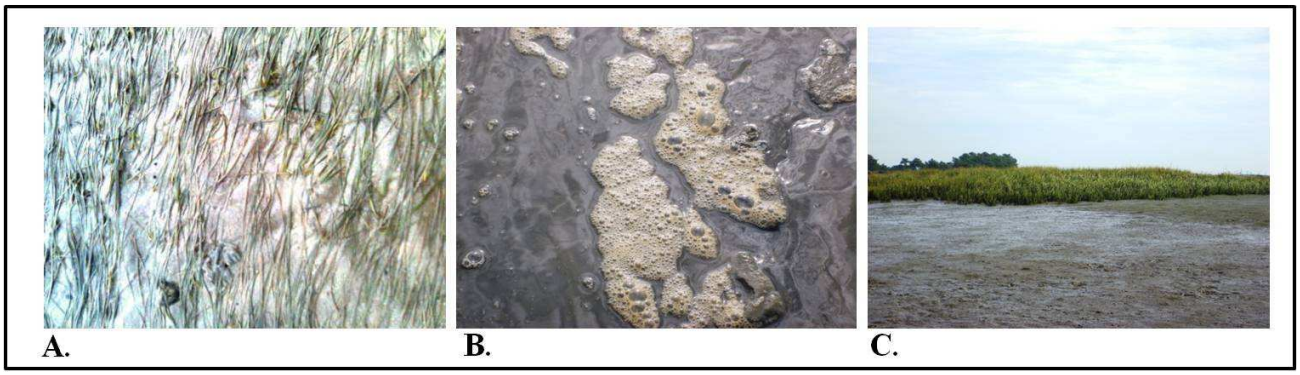

Figure 1.11. Photographies des principaux producteurs primaires benthiques du bassin d'Arcachon ; A : l'angiosperme marine *Zostera noltii*, B : le microphytobenthos (ici en exsudation au début de l'immersion), C : le schorre.

L'ensemble de ces spécificités, qui caractérisent une zone côtière en général, font de la lagune d'Arcachon une zone très active des points de vue biologique et de son métabolisme. Celui-ci est initié par un ensemble diversifié de producteurs primaires benthiques et pélagiques dont l'importance varie spatialement et selon les cycles diurne, tidal et saisonnier. Dans la lagune, cette production primaire totale est dominée au 2/3 par la production primaire benthique par :

- Les herbiers de *Zostera noltii* qui assurent une production annuelle variant entre 127-181 g C m^{-2}, soit 8880-12709 t C (Auby, 1991 ; Tableau 1.3). En effet, 60% (i.e. 70 km^2 en 1989) de la zone intertidale est colonisée par cette angiosperme marine ce qui fait du bassin le plus grand herbier d'Europe (Figures 1.9, 1.10.A et 1.11.A). Cette phanérogame de petite taille (maximum 30 cm de long pour quelques mm de large) est particulièrement bien développée sur le platier entre -1.9 et +0.8 m en particulier dans les substrats silto-argileux des zones intertidales basses. Dans les sédiments sableux, la pauvreté en nutriments entraine le développement d'un important système racinaire afin d'assurer le bon approvisionnement en nutriments et de résister aux agents dynamiques (Auby and Labourg, 1996). La croissance de l'herbier montre d'importantes variations saisonnières en densité et biomasse et suit un schéma unimodal avec des maxima en été (juin-septembre) et des minima en hiver, seul le système racinaire (rhizome) persistant tout au long de l'année (Duarte, 1989 ; Auby and Labourg, 1996 ; Vermaat and Verhagen, 1996). Cependant, l'herbier de *Zostera noltii* régresse de manière importante depuis les vingt dernières années, notamment établi par l'utilisation de photographies aériennes (Plus et al., 2010). Un déclin non homogène de 33% entre 1988 et 2008 a été observé dans la lagune, avec une accélération surtout depuis 2005, en particulier dans le secteur Est de la lagune alors que la couverture de l'herbier dans la partie Ouest et le Nord du bassin se maintient (Auby et al., 2009 ; Plus et al., 2010). L'herbier couvre aujourd'hui une surface de 45.7 km^2 (en 2007) soit 39% de la zone intertidale. Cette regression se traduit notamment par une augmentation des concentrations en ammonium aux embouchures des principaux cours d'eau (Leyre et Porge) (Plus et al., 2010).

- Les communautés microphytobentiques (Figure 1.11.B) avec une production comprise entre 104 et 114 g C m^{-2} an^{-1}, soit 16133-17621 t C an^{-1} (Auby, communication personnelle, Tableau 1.3). Avec les herbiers de *Zostera* noltii, elles assurent ensemble plus de la moitié de la production primaire totale de la lagune. Présentes tout au long de l'année dans le bassin, ces cellules forment de denses tapis bruns à la surface du sédiment durant la saison printanière où les maximums de biomasse sont généralement atteints (Auby, communication personnelle).

- Les herbiers de *Zostera marina* présents en bordure de chenaux, en permanence immergés, ne contribuent que faiblement à la production primaire totale (2336 t C an^{-1} soit 5%, Tableau 1.3) couvrant un espace réduit de 4 km^2 dans la lagune, en forte régression aussi (i.e. déclin de 74% observé entre 1988 et 2008, Plus et al., 2010)[5].

- Les macroalgues benthiques, de type *Monostroma obscurum* ou épiphytes des herbiers de *Zostera marina*, représentent respectivement 2508[6] et 390-584 t C an^{-1} soit 5 et 1% de la production primaire totale de la lagune (Tableau 1.3).

- Enfin en bordure interne du bassin, une végétation halophyte représentée notamment par les espèces du genre *Spartina* constituant les pré-salés ou schorre de la lagune (Figure 1.11.C), contribue à la production totale à hauteur de 7% environ avec 3045-3639 t C an^{-1} (Soriano-Sierra, 1992 ; Tableau 1.3).

La production primaire pélagique de la lagune n'en reste pas moins significative, dominée par les communautés phytoplanctoniques à raison de 103 g C m^{-2} an^{-1} (30% environ de la production totale, Tableau 1.3), plaçant la lagune parmi les systèmes de faiblement à moyennement productifs (Glé et al., 2008). Des efflorescences phytoplanctoniques précoces provenant de l'océan et dominés par de grandes diatomées (*Asterionellopsis glacialis*) entraînent de très fortes productions en période hivernale et au début du printemps. Ceux-ci font alors place à des efflorescences printanière et estivale de petites diatomées mais aussi de cellules non siliceuses de petite taille (flagellés) adaptées aux faibles concentrations en nutriments (Glé et al., 2007).

[5] Ces herbiers représentent un habitat très sensible et très riche en termes de diversité et d'abondance. Ils forment un habitat permanent et un site de nourricerie et de reproduction pour un grand nombre d'espèces (hippocampes, épiphytes, seiches…) (Blanchet et al., 2004).

[6] Cette estimation ne prend en compte que la production de *Monostroma obscurum* et pas celle des autres macroalgues, nombreuses dans la lagune.

I.3.2.c. Les pressions anthropiques

Le bassin d'Arcachon comme grand nombre de zones côtières est sujet à d'importantes pressions humaines notamment agricole, touristique, et aquacole. La population autour du bassin a augmenté de 60% sur les quarante dernières années atteignant plus de 100 000 habitants aujourd'hui. En période estivale, ce chiffre est multiplié par trois (de Montaudouin, communication personnelle). 12 000 embarcations à flot, dont 76% motorisées, sont basées sur le bassin avec la moitié dans les ports et l'autre moitié au mouillage (Rapport GEOMER 2010). D'autre part, le bassin d'Arcachon supporte une importante activité conchylicole produisant chaque année environ 18 000 tonnes d'huitres. Divisé par deux depuis 1960, elle occupe actuellement une surface de 900 ha (10 km^2) dont seulement 60% est exploité. D'importants récifs d'huîtres sauvages laissés à l'abandon se sont développés transformant de manière profonde le milieu (Figure 1.10). L'agriculture dans le bassin versant de la lagune est responsable de près de 66% des apports annuels d'azote inorganique, qui ont été multipliés par deux entre 1980 et 1993 provoquant des phénomènes d'eutrophisation (Auby et al., 1994 ; Blanchet, 2004). En particulier, le bassin a vu au début des années 1990, un développement massif d'algues vertes (*Monostroma obscurum, Enteromorpha clathrata*). Cependant, ces phénomènes ont régressé depuis et restent aujourd'hui limités, ceci étant en partie expliqué par l'hydrodynamisme et le temps de renouvellement des eaux de la lagune. Les eaux usées domestiques et industrielles sont rejetées après traitement directement à l'océan au sud du bassin, ce qui limite les apports en azote et phosphore (De Wit et al., 2005). Enfin, un certain nombre d'espèces ont été introduites volontairement dans la lagune (*Ruditapes philipinarum*, *Crassostrea gigas*) ou involontairement (*Crepidula fornicata*, *Spartina anglica*…) (Blanchet, 2004). Cependant, leur impact sur la richesse biologique et la diversité spécifique du bassin reste faible, à l'exception des spartines qui créent un envasement en zone amont et entrent en compétition spatiale avec les herbiers de zostères naines (Cottet et al., 2007).

La lagune bénéficie d'un grand nombre de mesures de protection et de classement : Natura 2000, ZNIEFF I et II (zone naturelle d'intérêt écologique, faunistique ou floristique), ZICO (zone d'importance pour la conservation des oiseaux), ZPS (zone de protection spéciale), sites classés, inscrits, propriétés du Conservatoire du Littoral ou autres réserves naturelles). Malheureusement, cette protection reste encore trop fragmentaire comme le montre par exemple l'absence de législation stricte au sein de la mesure ZNIEFF.

I.4. OBJECTIF ET ORGANISATION DE L'ETUDE

I.4.1. Les objectifs de cette étude et les opérations mises en œuvre

Ce travail de thèse porte sur les échanges de CO_2 atmosphérique dans la lagune d'Arcachon et les relations existant avec le métabolisme intertidal.

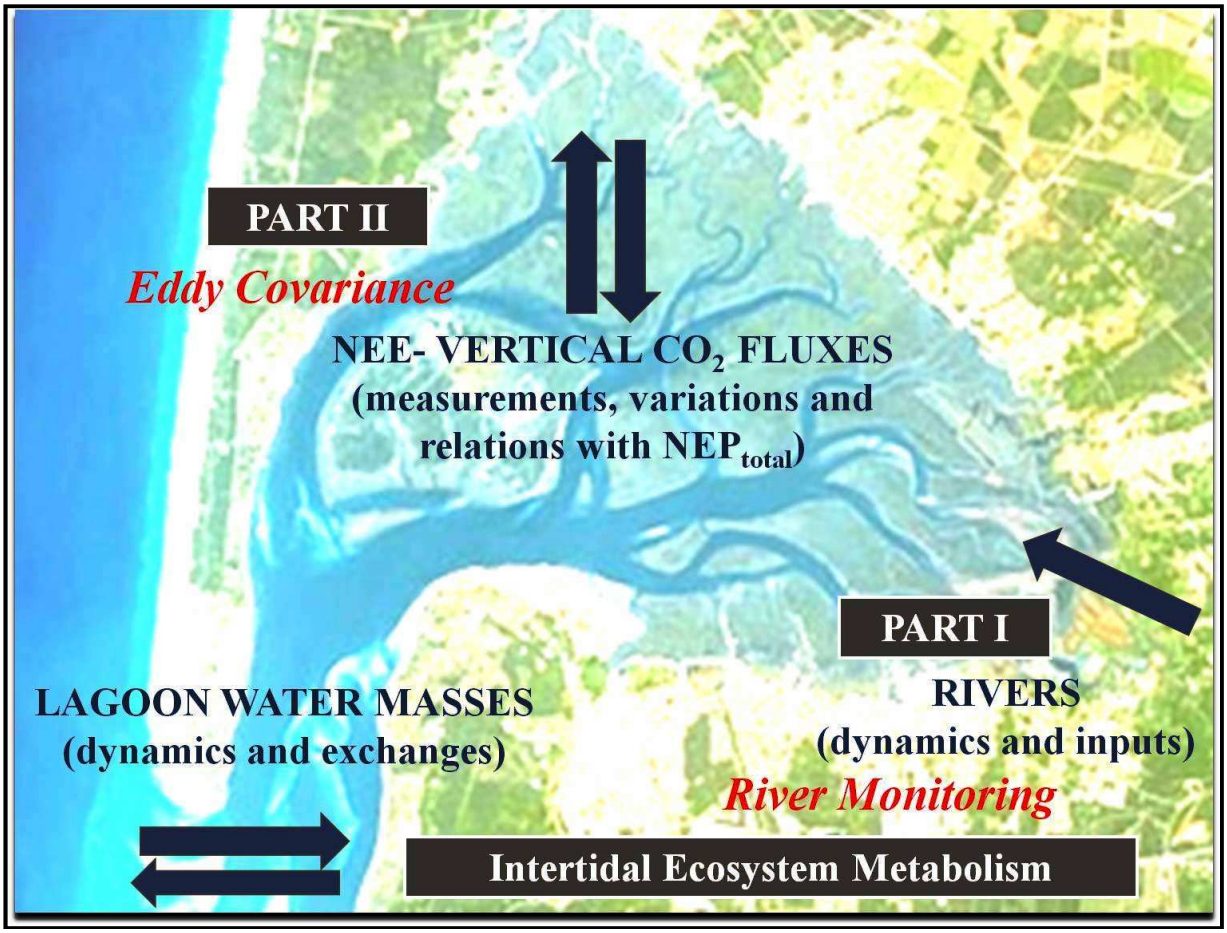

Figure 1.12. Les principaux axes de l'étude des échanges de CO_2 atmosphérique dans la lagune d'Arcachon.

Les objectifs de la présente étude se sont articulés autour de deux parties principales en relation avec le métabolisme intertidal de la lagune comme le montre la Figure 1.12 (revoir la partie I.2. avec la Figure 1.6 pour les explications).

- Une première grande partie a concerné l'étude de la dynamique du carbone dans les eaux de rivières entrant dans la lagune. En particulier, les variations saisonnières de l'ensemble des formes du carbone dans ces eaux douces ont été caractérisées. Egalement, les exports de ces différentes formes de carbone vers la lagune ont été quantifiés en estimant la part de CO_2 qui a dégazé vers l'atmosphère depuis ces eaux de rivières, n'atteignant jamais la lagune (parties I.1 et I .2).

- Une deuxième grande partie de ce travail a concerné la mise en place dans la lagune d'un système de mesure de flux turbulents par Eddy Covariance (EC). Cette technique permet de mesurer les flux de CO_2 aux deux interfaces air/eau et air/sédiment de manière continue. L'objectif principal était de réussir à appliquer cette méthode largement utilisée dans les écosystèmes terrestres à la zone côtière en particulier à la zone intertidale et d'obtenir des flux qualitatifs et quantitatifs. Ceci permit de caractériser les variations de ces flux aux échelles diurne, tidale, saisonnière, en relation avec les facteurs environnementaux, le métabolisme de l'écosystème et la distribution des producteurs primaires de la lagune. Il était également intéressant de savoir comment le bassin se comportait à l'échelle annuelle vis-à-vis du carbone en termes de puits ou de sources de CO_2 pour l'atmosphère.

Afin de mener à bien ces différents objectifs, un important travail sur le terrain (Figure 1.13) a été réalisé faisant suite à un grand nombre d'analyses en laboratoire. Concernant la dynamique et les apports de carbone en provenance du bassin versant, un suivi annuel de Février 2008 à Février 2009 a été effectué à raison d'une sortie toutes les deux semaines sur quatre rivières et d'une sortie tous les mois sur cinq autres cours d'eau (voir Figure 1.7 et Tableau 1.2). Par rapport à la mesure de flux de CO_2 entre la lagune et l'atmosphère, six déploiements ont été réalisés. Tout d'abord, en septembre-octobre 2007 à la Station 2 (Figure 1.9) durant le chantier PNEC 2007 (Programme National Environnement Côtier) où quatre jours de données ont été obtenus avec un système EC prêté par le Laboratoire d'Aérologie de Toulouse (D. Serça). Suite au financement par la Région Aquitaine de notre propre système EC en avril 2008, trois autres déploiements ont été menés dans la lagune, à la Station 1 (Figure 1.9) à proximité d'un herbier très dense de *Zostera noltii*. Ces trois déploiements se sont déroulés en juillet 2008 (7 jours), septembre-octobre 2008 (20 jours) et avril 2009 (13 jours)[7].

[7] Six déploiements ont été réalisés dans le bassin d'Arcachon au total. Cependant, ceux de décembre 2008 et juillet 2009 n'ont pas permis d'obtenir de données satisfaisantes de flux de CO_2, suite à des problèmes techniques rencontrés sur le terrain.

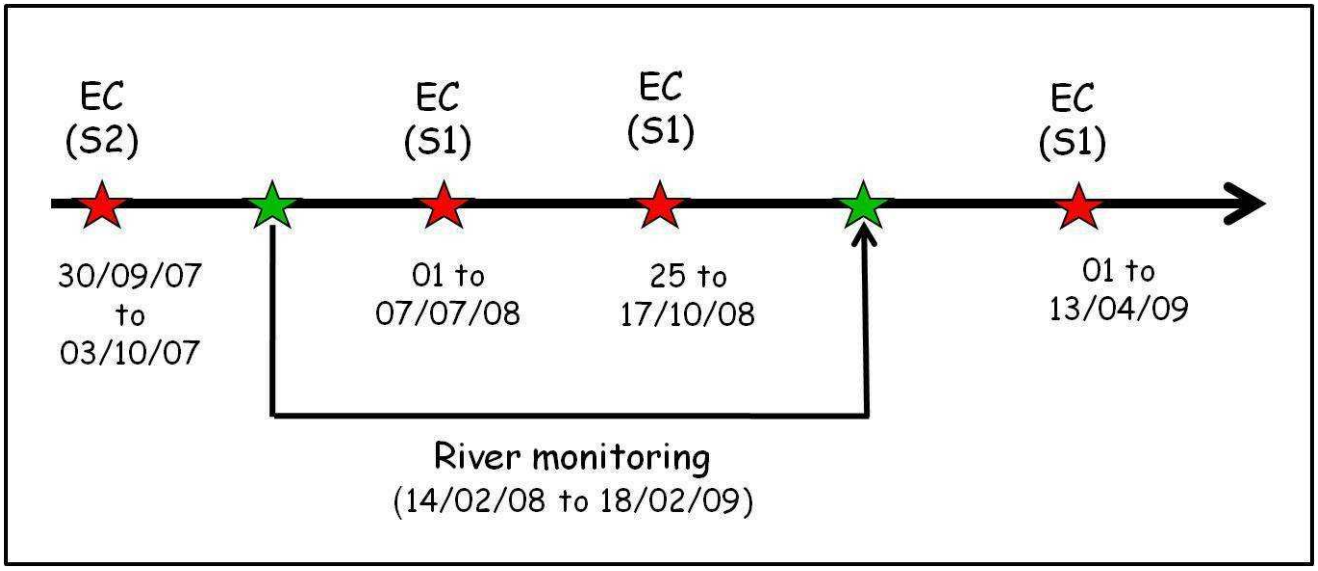

Figure 1.13. Chronologie des différentes expérimentations menées sur le terrain ; voir **Figure 1.9** pour la localisation des deux stations étudiées.

I.4.2. Organisation et présentation du mémoire

Ce mémoire s'organise ensuite en deux grandes parties (chapitres 2 et 3). Dans le chapitre 2 seront abordés la dynamique du carbone dans les ruisseaux et rivières du bassin versant de la lagune d'Arcachon ainsi que les apports à la lagune en prenant aussi en compte le dégazage de CO_2 de la surface de ces cours d'eau vers l'atmosphère. La première sous-partie du chapitre 2 présente la formulation d'un modèle totalement original, appelé « StreamCO_2 DEGAS », permettant d'estimer la part de CO_2 issu du sol et qui dégaze vers l'atmosphère avant l'entrée dans la lagune à partir de mesures isotopiques. Cette sous-partie fait l'objet d'une soumission au journal *Geochimica et Cosmochimica Acta* depuis décembre 2010. Dans une deuxième sous-partie seront abordés les variations spatio-temporelles de carbone dans neuf rivières du bassin versant ainsi que l'export de carbone à la lagune en intégrant aussi le dégazage de CO_2 obtenu à l'aide du modèle. Cette sous-partie fait l'objet d'une soumission à la revue *Limnology and Oceanography* depuis décembre 2010.

Dans un troisième chapitre, nous verrons la mesure des flux de CO_2 par EC entre la lagune et l'atmosphère ainsi que leurs variations en fonction des différents forçages environnementaux et les relations avec le métabolisme de l'écosystème intertidal. Ce chapitre se présente en deux sous-parties, la première présentant la méthode EC et sa validation en zone intertidale en se basant sur les variations de flux turbulents de CO_2, de chaleur et d'énergie obtenus durant l'expérimentation de Juillet 2008. La deuxième, en intégrant l'ensemble des quatre expérimentations, discutera les variations spatio-temporelles des flux de CO_2 en relation tout particulièrement avec la production

primaire de la lagune. En effet, une analyse détaillée d'images satellites montrant la dynamique saisonnière des herbiers de Zostères a été entreprise afin de mettre en relation cette dynamique avec celle observée dans les échanges de CO_2 mesurés dans la lagune. Ces deux sous-parties viennent tout juste d'être soumises respectivement aux revues *Journal of Geophysical research* et *Biogeosciences.*

Enfin dans une synthèse générale, nous replacerons les résultats de ce travail dans le contexte des connaissances antérieures sur les flux de carbone dans le bassin d'Arcachon. Un schéma de synthèse du budget de carbone de la lagune sera présenté et discuté en détail dans ses différents compartiments, afin de proposer des perspectives de travail pour l'améliorer. Dans celles-ci, nous discuterons notamment l'intérêt d'un outil comme l'EC pour étudier des problématiques telles que la récession de l'herbier de zostère.

CHAPITRE II.

DYNAMIQUE, EXPORT ET DEGAZAGE DE CARBONE TERRESTRE VERS LA LAGUNE D'ARCACHON DEPUIS LES EAUX DE SURFACE DE SON BASSIN VERSANT

PARTIE II.1. MODELLING CO_2 DEGASSING FROM SMALL ACIDIC RIVERS USING pCO_2, DIC AND $\delta^{13}C$-DIC DATA [8]

PARTIE II.2. EXPORT AND DEGASSING OF TERRESTRIAL CARBON FROM SMALL RIVERS AND STREAMS DRAINING A TEMPERATE SANDY PODSOLISED CATCHMENT [9]

[8] Cette partie fait l'objet d'une soumission : Modelling CO_2 degassing from small acidic rivers using pCO_2, DIC and $\delta^{13}C$-DIC data, Polsenaere P. and G. Abril, Submitted to ***Geochimica Et Cosmochimica Acta*** (anglais corrigé par American Journal Experts).

[9] Cette partie fait l'objet d'une soumission : Export and degassing of terrestrial carbon from small rivers and streams draining a temperate sandy podsolised catchment, Polsenaere P., Savoye N., Etcheber H., Canton M., Poirier D., Bouillon S. and G. Abril, Submitted to ***Limnology and Oceanography*** (anglais corrigé par American Journal Experts).

II. DYNAMIQUE, EXPORT ET DEGAZAGE DE CARBONE TERRESTRE VERS LA LAGUNE D'ARCACHON DEPUIS LES EAUX DE SURFACE DE SON BASSIN VERSANT

II.1. MODELLING CO_2 DEGASSING FROM SMALL ACIDIC RIVERS USING pCO_2, DIC AND δ^{13}C-DIC DATA

Résumé

Le dégazage de dioxyde de carbone, issu de la respiration terrestre, depuis les ruisseaux et les petites rivières vers l'atmosphère, apparaît comme une composante majeure des budgets de carbone des bassins versants. Ici, nous proposons une approche originale afin de quantifier ce flux à partir de données de pressions partielles de CO_2 (pCO_2), de concentrations en carbone inorganique dissous (DIC) (ou d'alcalinité totale, TA) et de compositions isotopiques du carbone inorganique dissous (δ^{13}C-DIC) dans les cours d'eaux. Le modèle s'applique aux eaux acides, non tamponnées (de type humique) et repose sur les hypothèses qui incluent essentiellement la composition isotopique du DIC (δ^{13}C-DIC) dans les eaux souterraines s'écoulant vers les eaux de surface (CO_2 issu du carbone organique respiré et les ions HCO_3^- issu du lessivage) et sur le fait que l'isotope 12 léger du dioxyde de carbone ($^{12}CO_2$) dégaze vers l'atmosphère plus rapidement que l'isotope lourd ($^{13}CO_2$). Nous évaluons d'abord la composition isotopique de la matière organique du sol et le fractionnement isotopique du CO_2 dans un sol afin d'obtenir le δ^{13}C-CO_2 dans ce sol et ces eaux souterraines. A partir des concentrations en HCO_3^- (TA), nous estimons la contribution relative de l'érosion des roches silicatées et carbonatées (ces dernières étant mineures dans ces eaux) à la concentration en ions HCO_3^- et à sa composition isotopique associée. Les calculs relatifs au modèle commencent à partir de la valeur de δ^{13}C-DIC déduite de la méthode citée précédemment et consistent en deux itérations emboitées. La première itération mime la diminution de pCO_2 et l'augmentation de δ^{13}C-DIC qui surviennent le long du cours d'eau pendant le dégazage, en commençant avec une pCO_2 initiale du sol qui est supposée, et en terminant avec les valeurs de pCO_2 et de δ^{13}C-DIC mesurées *in situ* dans le cours d'eau. La deuxième itération consiste à ajuster la pCO_2 du sol initiale jusqu'à ce que la pCO_2 et le δ^{13}C-DIC atteignent en même temps les valeurs mesurées *in situ*. Suite à l'obtention de cette convergence, le modèle calcule une concentration théorique en DIC, le $[DIC]_{ex}$, qui a été perdue sous forme de CO_2 vers l'atmosphère depuis la source jusqu' au point de mesure dans la rivière. Le $[DIC]_{ex}$ peut ensuite être multiplié par le débit de la rivière afin d'en déduire la quantité de carbone dégazée depuis les eaux de surface de la rivière. Le modèle a été testé sur un jeu de données, obtenu à la

suite d'un échantillonnage saisonnier sur le terrain de trois petites rivières drainant des sols sableux (podzols) dans le sud ouest de la France ; il a permis d'obtenir des dégazages annuels comparables à ceux reportés dans les autres études, bien qu'un peu supérieurs (borne supérieure des rangs pour deux cours d'eau et dix fois la moyenne pour un cours d'eau). Une partie de cette différence peut avoir été causée par un dégazage intense à proximité des eaux souterraines arrivant en surface, qui a été pris en compte par notre méthode intégrative mais pas par les méthodes classiques basées sur la pCO_2 des eaux de rivière et la vitesse de transfert du gaz. La sensibilité du modèle résulte de l'hypothèse faite sur l'importance de l'érosion de roches carbonatées, ce qui peut également expliquer ce fort dégazage. Le modèle reproduit de manière cohérente les valeurs et les tendances saisonnières des pCO_2 dans les sols (maximales en été) et des vitesses de transfert de gaz (maximales durant les forts débits). Nous discutons la sensibilité du modèle à différents paramètres et hypothèses et nous proposons quelques améliorations afin de mieux contraindre le $[DIC]_{ex}$ calculé pour une validation définitive du modèle. Nous concluons que notre approche intégrative présente un potentiel intéressant comme outil utilisé dans la quantification du dégazage de CO_2 depuis les petits cours d'eaux en amont, dépassant la difficulté de mesurer ou de choisir une vitesse adéquate de transfert de gaz.

Abstract

Degassing of terrestrially-respired CO_2 from streams and small rivers appears to be a significant component in watershed carbon budgets. Here we propose an original approach to quantifying this flux using data of pCO_2, DIC (or Total Alkalinity, TA) and δ^{13}C-DIC in stream waters. The model applies to acidic, non-buffered (humic-type) waters and basically relies on some assumptions, including the stable isotopic composition of DIC in groundwater seeping to surface water (CO_2 from respired soil organic carbon and HCO_3^- from weathering) and on the fact that $^{12}CO_2$ degases to the atmosphere more rapidly than $^{13}CO_2$. We first consider both the soil organic matter isotopic composition and the isotopic fractionation of CO_2 in a soil to derive the δ^{13}C-CO_2 in that soil and groundwater. From the HCO_3^- (TA) concentrations in streams, we estimate the relative contribution of silicate and carbonate weathering (the latter being minor in these waters) to the HCO_3^- and its associated isotopic composition. Model calculations start from the δ^{13}C-DIC value computed by the aforementioned method and consist of two interlocked iterative procedures. The first procedure mimics the decrease in pCO_2 and the increase in δ^{13}C-DIC that occur along the stream watercourse during degassing, starting from an assumed initial soil pCO_2 and ending at the *in situ* pCO_2 or δ^{13}C-DIC. The second iteration procedure consists of adjusting the initial soil

pCO_2 until pCO_2 and δ^{13}C-DIC simultaneously reach the *in situ* measured values. After convergence is obtained, the model computes a theoretical concentration of DIC, $[DIC]_{ex}$, that has been lost as CO_2 to the atmosphere from the headwater to the sampling point in the river. $[DIC]_{ex}$ can be multiplied by the river discharge to derive the quantity of carbon degassed from the river surface. The model was tested on seasonal field datasets from three small rivers draining sandy podsols in southern France and gave annual areal degassing rates comparable to those reported in other studies, though somewhat larger (upper half range in two rivers, ~10 times the average in one stream). Part of this discrepancy might have been caused by an intense degassing in the vicinity of groundwater seeps, which was accounted for our integrative method but not by classical methods based on stream water pCO_2 and gas transfer velocity. The sensitivity of the model results on the assumption of the importance of carbonate weathering might also explain this high degassing rate. The model reproduced consistent values and seasonal trends of soil pCO_2 (maximal in summer) and gas transfer velocity (maximal at high water flow). We discuss the sensitivity of the model to the different parameters and assumptions and propose some improvements for better constraining the computed $[DIC]_{ex}$ for definitive validation. We conclude that our integrative approach has great potential as an efficient tool for quantifying CO_2 degassing in small headwater bodies, overcoming the difficulty of measuring or choosing a gas transfer velocity.

1. Introduction

Laterally transporting a total flux of about 0.9 Gt C yr^{-1}, rivers represent the main linkage between the land and the ocean (Meybeck, 1982; Kempe et al., 1991). This flux is composed of ~20% particulate organic carbon (POC), ~25% dissolved organic carbon (DOC), ~45% dissolved inorganic carbon (DIC) and ~10% particulate inorganic carbon (PIC) (Meybeck, 1987; Ludwig et al., 1996; Meybeck and Vorosmarty, 1999). Except in eutrophic rivers, where phytoplankton production can produce autochthonous POC, the majority of POC is allochthonous and originates from soil erosion in most rivers (Meybeck, 1993). DOC in non-polluted rivers primarily originates from leachable organic carbon in soils and from terrestrial vegetation (Kempe et al., 1991; Sobek et al., 2007). DIC in freshwater can be differentiated into two fractions with distinct origins and behaviours: carbonate alkalinity, primarily in the HCO_3^- form, which comes from soil and bedrock weathering, and dissolved CO_2, which results from respiration in soils, groundwaters, river sediments and waters (Meybeck, 1987; Amiotte-Suchet and Probst, 1995; Abril et al., 2000). Riverine DIC is thus an open dynamic system that is closely related to the lithology of the drainage basin as well as soil and river respiration and is also affected by atmospheric CO_2 exchange. Rivers not only transport carbon laterally to the ocean, but also process carbon through biological activity and transfer it vertically as organic carbon burial in sediments and as CO_2 exchanges with the atmosphere (Cole et al., 2007; Ciais et al., 2008). Freshwaters are generally net heterotrophic, where a significant part of POC and DOC is mineralised to CO_2 and degassed to the atmosphere (Duarte and Prairie, 2005; Battin et al., 2008). Recent works have revealed that despite their small contribution to earth's cover area, freshwaters emit a significant amount of CO_2 to the atmosphere (Cole and Caraco, 2001; Cole et al., 2007). To achieve a precise carbon budget of the continental biosphere, it is necessary to quantify not only the carbon export to the ocean, but also the carbon burial in lake sediment and the CO_2 outgassing to the atmosphere all along the watershed. This CO_2 degassing is the result of instream processes but is also regulated by riparian and hyporheic/groundwater CO_2 inputs to waters (Jones and Mulholland, 1998; Abril et al., 2000; Cole and Caraco, 2001; Billet et al., 2004). Particularly supersaturated CO_2 headwaters show very high areal degassing rates (Hope et al., 2001; Johnson et al., 2008; Billett and Moore, 2008; Davidson et al., 2010). The gas transfer velocity K_{600} that, together with the water-air pCO_2 gradient drives the degassing intensity is controlled by several physical factors and subjected to large uncertainties in rivers (Raymond and Cole, 2001). Furthermore, CO_2 degassing might be underestimated because of a rapid decrease of pCO_2 from headwaters to downstream rivers (Worrall and Lancaster, 2005; Johnson et al., 2008; Davidson et al., 2010).

The stable isotopic composition of DIC (δ^{13}C-DIC) varies over a large range in freshwaters. Carbon reservoirs that act as a source of riverine DIC (soil, groundwater, bedrocks and atmosphere) have distinct isotopic signatures (Yang et al., 1996; Clark and Fritz, 1997). The δ^{13}C of atmospheric CO_2 is about -7.5‰, whereas carbonates rocks have a δ^{13}C of about 0‰ (Mook et al., 1983). The δ^{13}C of soil CO_2 depends on the plant pathways used for photosynthesis and the organic matter sources fuelling plant and microbial respiration (Vogel, 1993). In a system where soil CO_2 is primarily derived from decomposition of C_3 plant organic matter, the CO_2 produced has a δ^{13}C-CO_2 value close to the initial substrate (i.e. -30 to -24‰). Respiration of terrestrial organic matter in soils and waters will produce DIC with an isotopic composition similar to the organic substrate. Primary production, in contrast, tends to increase δ^{13}C-DIC and generate strong diel variations (Parker et al., 2005). Finally, gas exchange along river courses generates an isotopic equilibration with the atmosphere and makes the δ^{13}C-DIC less negative. In this paper, we use the latter property of isotopic air-water equilibration to estimate CO_2 degassing rates.

We present here a model called "streamCO_2-DEGAS" that uses water-air isotopic equilibration processes to compute CO_2 degassing in streams and small rivers. The model uses *in situ* data of pCO_2, Total Alkalinity (TA) (or DIC concentration) and δ^{13}C-DIC and applies to small acidic and unproductive rivers and streams. The model first assumes several hypotheses concerning the isotopic composition of the DIC initially released to surface waters. It then computes a theoretical DIC concentration that has evaded to the atmosphere upstream of the sampling point in order to reach the observed pCO_2 and δ^{13}C-DIC values due to gas isotopic equilibration. After describing the principles in detail, we test the sensitivity of the model to the *in situ* pCO_2, TA and δ^{13}C-DIC. We then apply the model to a dataset obtained in three rivers of the Arcachon lagoon catchment with known lithology and morphologies. Finally, we discuss the potential of our model and improvement measures for application in other freshwater systems.

2. Material and Methods

2.1 Study site

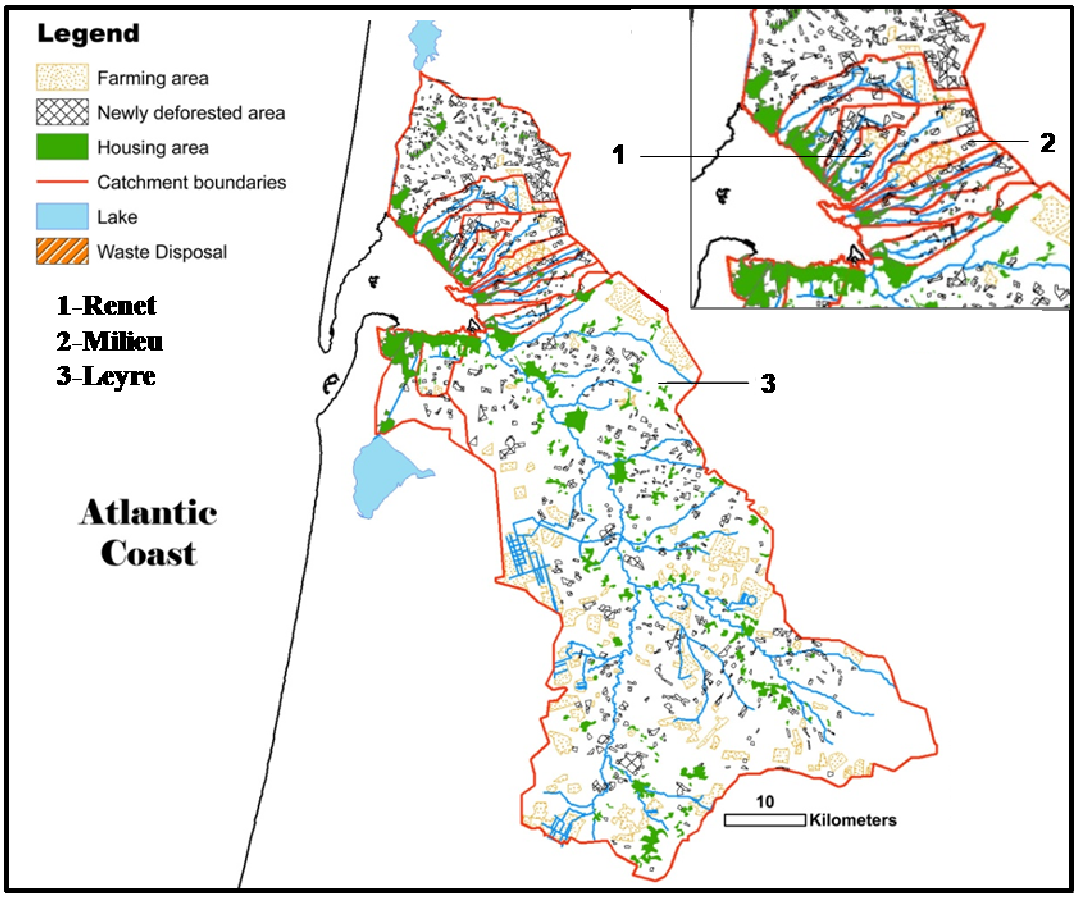

Figure 1. Map of the Arcachon lagoon and its direct catchment basin showing the three sampled rivers (the Renet and Milieu streams and the Leyre River) and the catchment boundaries with soil occupation.

The study site for this model development and validation was located in the Arcachon lagoon catchment and concerns three of its direct-flowing rivers, the Renet and the Milieu streams and the Leyre River (Figure 1). Located in Southwest France, the catchment, with a surface of 3001 km^2, is lowland (slopes below 0.25%) and relatively homogeneous topographically, climatically (isohyets between 900 and 1000 mm) and geologically (Laplana et al., 1993). The soils are composed of sandy podsols of Pleistocene origin, primarily covered by maritime pine forest (Trichet et al., 1997). The soils are crossed by a shallow, multi-layered, permeable aquifer, which is not deeper than 3 m, has a maximum thickness less than 25 m and is highly connected to surface waters (Rimmelin et al., 1998). Soils are characterised by high acidity (pH 4-5), low inorganic nutriment availability, organic matter reaching 15% (Jolivet et al., 2007) and a near absence of carbonate rocks, except a few Miocene carbonated outcrops in the Leyre catchment (Folliot et al., 1993).

	Renet		Milieu		Leyre	
Catchment Surface (Km^2)	17.9		21.3		2141.4	
Runoff (m^3s^{-1})	0.6		0.6		18.2	
Drainage ($L\ s^{-1}km^{-2}$)	33		28		8	
Water temperature (°C)	12.9 ± 2.4	6.6~16.6	12.70 ± 3.5	4.2~17.5	12.74 ± 4.2	3.8~18.6
Conductivity (μScm^{-1})	202 ± 27.9	178~277	270 ± 34	215~321	170 ± 15	151~195
pH	6.29 ± 0.07	6.23~6.40	6.24 ± 0.08	6.17~6.33	6.96 ± 0.03	6.92~7.03
Chl a (μgL^{-1})	0.6 ± 0.5	0.1~2.2	0.4 ± 0.3	0.1~1.2	1.0 ± 0.8	0.1~3.8
POC (mgL^{-1})	1.7 ± 2.8	0.1~13.4	1.5 ± 1.2	0.1~4.6	1.3 ± 0.9	0.1~4.2
DOC (mgL^{-1})	5.5 ± 1.1	4.1~9.8	4.2 ± 1.1	2.4~5.8	5.5 ± 1.8	2.7~10.1
δ^{13}C-POC (‰)	-28.6 ± 0.4	-29.4~-28	-28.1 ± 0.9	-28.9~-26.5	-28.7 ± 0.5	-29.5~-27.7
pCO_2 (ppmv)	5479 ± 1279	1437~7653	2554 ± 949	1529~5460	1604 ± 338	1046~2453
TA ($mmolL^{-1}$)	0.247 ± 0.052	0.154~0.370	0.104 ± 0.022	0.078~0.153	0.325 ± 0.114	0.12~0.52
DIC ($mmolL^{-1}$)	0.513 ± 0.081	0.317~0.674	0.229 ± 0.055	0.17~0.39	0.403 ± 0.104	0.255~0.612
δ^{13}C-DIC (‰)	-20.3 ± 0.4	-21.2~-19.6	-19.7 ± 1.7	-24.6~-17.9	-15.6 ± 2.6	-21.6~-12.5

Table 1. General characteristics and carbon concentrations (average ± standard deviation; min~max) of the three studied rivers. Data from a one-year monitoring between February 2008 and February 2009 (Polsenaere et al., submitted).

The three studied rivers have contrasting sizes, the Leyre River being much larger than the Milieu and Renet streams (Table 1). They are well channelized, with little or no floodplains; on the Leyre and Renet rivers, numerous trees trunks on the edges and across the river create substantial turbulence during high discharge. Carbon concentrations and associated parameters were monitored over a one-year sampling period (Polsenaere et al., submitted) and are summarised in Table 1. POC concentrations are moderate, between 0.1 and 4.6 mg L^{-1} throughout the year, reflecting weak erosion in the lowland sandy catchment. Throughout the year, there is an almost constant δ^{13}C-POC value of -28‰ in the three rivers, which reveals an origin from terrestrial C_3 plant and soil detritus consistent with soil occupation by pine forest. Autochthonous POC is minor, as attested by Chl *a* concentrations below 4 µg L^{-1} (Table 1). In contrast, the dominance of podsols leads to high concentrations of DOC (between 2.4 to 10.1 mg L^{-1}). Waters of the three rivers are supersaturated in CO_2 (pCO_2 between 1000 and 8000 ppmv) as a result of large inputs from soils and groundwater. The short residence time relative to that of the aquifer and the fact that maximum pCO_2 occurs in summer, when groundwater inflows are maximum (Polsenaere et al., submitted), suggest that respiration in the rivers themselves is modest in comparison to groundwater and soil CO_2 inputs as is also the case in other headwaters (Billet et al., 2004; Johnson et al., 2008; Davidson et al., 2010). TA values are low, typical for sandy catchments where silicate weathering dominates, but increase in the Leyre River where some carbonate rocks are present. In these acidic waters, TA is almost entirely composed of HCO_3^- and represents only half of the DIC in the Milieu and Renet rivers and 2/3 in the Leyre; the remaining TA is composed of carbonic acid and dissolved CO_2. δ^{13}C-DIC values are more negative in the Renet and Milieu streams throughout the year (-20.3±0.4 and -19.7±1.7‰, respectively) than in the Leyre River (-15.6±2.6‰). In the Leyre, δ^{13}C-DIC is positively correlated with the TA and DIC concentrations (Figure 2), reflecting ^{13}C-enriched DIC inputs from carbonate rocks that increase in summer, when groundwater runoff dominates (Polsenaere et al., submitted). In contrast, δ^{13}C-DIC is negatively correlated with pCO_2 in the three rivers (Figure 2b) due to the predominance of two antagonistic processes: (1) the input of CO_2 from groundwater of terrestrial C_3 material, which increases pCO_2 and decreases δ^{13}C-DIC, and (2) CO_2 degassing to the atmosphere, which has the opposite effect on both parameters (Polsenaere et al., submitted).

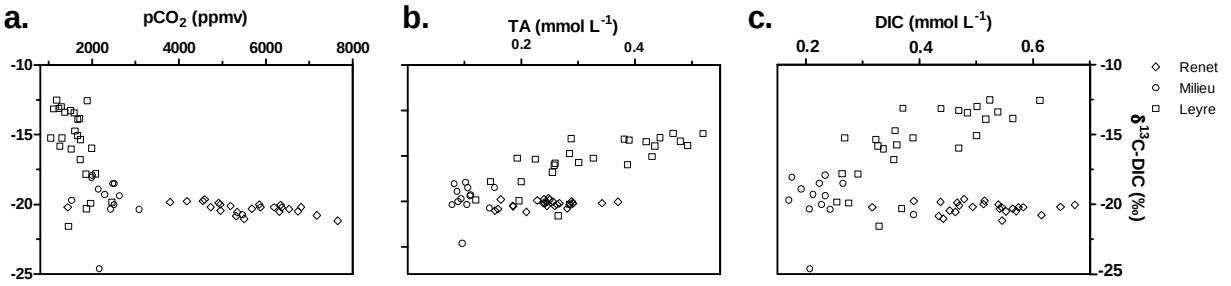

Figure 2. Isotope DIC composition (‰) variations versus a. pCO_2 values (ppmv), b. TA concentrations (mmol L^{-1}) and c. DIC concentrations (mmol L^{-1}) in the three studied rivers of the Arcachon lagoon catchment.

2.2 The stream CO_2-DEGAS model formulation

2.2.1. Initial hypothesis, general principle and validity domain

Our model that computes integrated CO_2 degassing from rivers is based on two initial hypotheses: first, the river waters must be acidic, and second, they must be unproductive. Figure 3 shows the Bjerrun diagram of typical river water, with the CO_2^* form (the sum of carbonic acid H_2CO_3 and dissolved CO_2) dominating at low pH and the HCO_3^- form dominating at higher pH. Panels b and c show the relative changes in CO_2^* and HCO_3^- concentrations that occurred when each species was introduced in the water, respectively. The buffer factors $dCO_2^*/dDIC$ and $dHCO_3^-/dDIC$ were computed, as in Abril (2009), using the carbonic acid constant sets proposed by Mehrbach et al. (1973) and the CO_2 solubility coefficient of Weiss (1974). When CO_2 from respiration was introduced in the water, and when the waters were acidic, most of the DIC change occurred in the CO_2^* pool, and the HCO_3^- was not affected: $dCO_2^*/dDIC$ was close to 1 and $dHCO_3^-/dDIC$ was zero (Figure 3b). In contrast, at high pH, as the case of seawater, CO_2 inputs generate significant changes in the HCO_3^- concentration (Abril, 2009). Conversely, when HCO_3^- inputs occurred after silicate or carbonate rock weathering, the CO_2^* concentration was affected (decreased due to increasing buffering capacity) only when the pH was lower than 4.7 (Figure 3c). At a pH higher than 4.7, DIC inputs in the HCO_3^- form conservatively generated an increase in the HCO_3^- concentration ($dHCO_3^-/dDIC$ is close to 1 in figure 3c). As a consequence, CO_2 inputs from respiration conservatively affected the CO_2^* pool when water had a pH between 4.7 and 7.2, as in the case of our study sites and many rivers and lakes worldwide. Additionally, HCO_3^- inputs from rock weathering conservatively affected the HCO_3^- (the Total Alkalinity) pool. Thus, the two dominant forms of DIC can be formulated independently in our model and still remain in dynamic chemical and isotopic equilibrium.

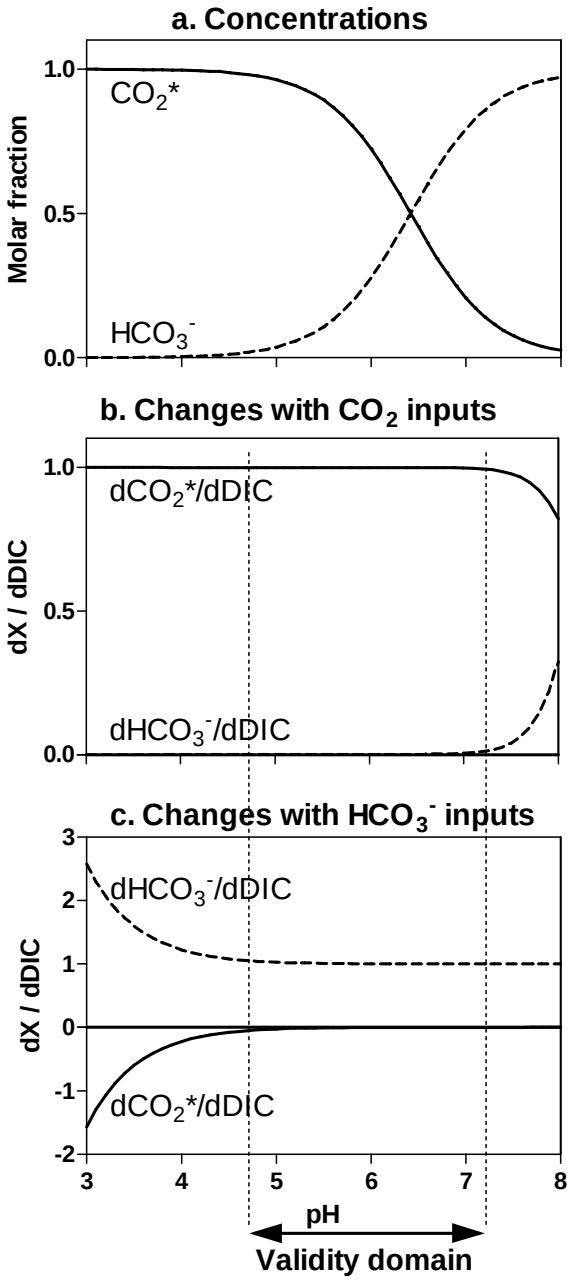

Figure 3. The carbonate system in freshwaters: a. the Bjerrun diagram (modified) of a typical river water showing molar fraction of aqueous CO_2 (CO_2^*, black lines) and bicarbonates (HCO_3^-, dotted lines) as a function of pH; b. ratio between the change in CO_2^* or HCO_3^- concentrations (dCO_2^* and $dHCO_3^-$, respectively) and the change in DIC concentration (dDIC) induced by an input of CO_2^*; and c. by an input of HCO_3^-. For pH between 4.6 to 7.2 units, there are no changes in CO_2^* and HCO_3^- concentrations with inputs of both species.

The second assumption is the application of the model only in unproductive waters, where photosynthesis by phytoplankton, microphytobenthos and submerged vegetation is limited. Primary production in rivers can generate important changes in pCO_2 and $\delta^{13}C$-DIC, particularly at the diurnal time scale (Parker et al., 2005). In fact, aquatic photoautotrophs use $^{12}CO_2$ as a carbon source at a faster rate than $^{13}CO_2$. Consequently, the remaining DIC becomes isotopically heavier (Clark and Fritz, 1997). In our model, we assumed insignificant primary production in the three studied rivers, where Chl *a* concentrations were below 4 µg L^{-1} (Table 1). This low Chl *a* concentration is also the case in many acidic headwaters worldwide (e.g., Johnson et al., 2008; Billet and Moore, 2008)

The streamCO_2-DEGAS model is based on the fact that the isotopic signature of DIC in river water is controlled by the signature of its sources and the intensity of CO_2 degassing, which tends to equilibrate dissolved CO_2 with atmospheric CO_2 (Degens, 1969; Mook et al., 1974). Knowing some basic information about the nature of the watershed, a theoretical isotopic composition and relative proportion of DIC released from terrestrial carbon respiration and rock weathering can be computed. Then, as CO_2 continuously evades from the river waters to the atmosphere, the rate of isotopic equilibration with the atmosphere can be calculated. This allows at the end to compute a theoretical quantity of CO_2 that has escaped to the atmosphere in order to reach the pCO_2 and DIC isotopic composition observed *in situ* in the rivers. The model takes into account the following parameters: the isotopic composition of the CO_2 respired in the soils, groundwater and, eventually, the rivers; the quantity and isotopic composition of HCO_3^- released from rock weathering (with the relative proportion of silicate and carbonate rocks); and the isotopic equilibration occurring between water CO_2^* and atmospheric CO_2 at the water-air interface. The streamCO_2-DEGAS model calculates a theoretical DIC concentration, the "DIC exchanged" ($[DIC]_{ex.}$), which corresponds to a quantity of CO_2 that has been degassed from the water to the atmosphere throughout the river course upstream of the sampling point. When multiplied by the water discharge, the $[DIC]_{ex}$ gives a quantity of CO_2 that has degassed between the river headwaters and the sampling point. The model formulation is depicted in Figure 4, and the variables are listed in Table 2. The scheme presents five boxes inter-connected by carbon isotope and concentration mass-balances. Each box is assimilated to a specific compartment, where sinks and sources of DIC occur, that is characterised by an isotope (‰) and a concentration (mmol L^{-1}) value.

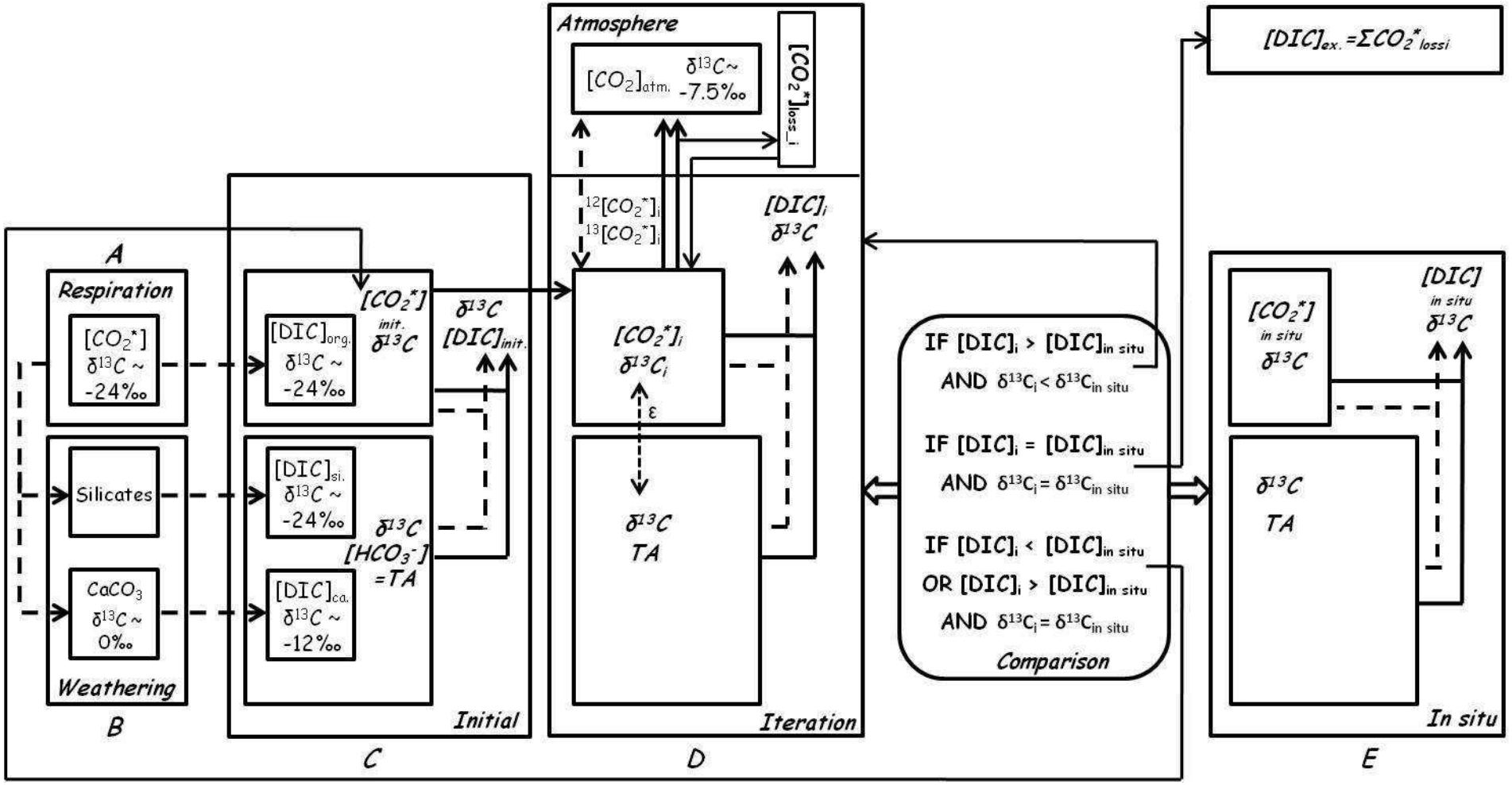
A
Respiration
[CO2*] δ13C ~ -24‰
Silicates
CaCO3 δ13C ~ 0‰
Weathering
B
[CO2*] init. δ13C
[DIC]org. δ13C ~ -24‰
[DIC]si. δ13C ~ -24‰
δ13C [HCO3-] =TA
[DIC]ca. δ13C ~ -12‰
δ13C [DIC]init.
Initial
C
Atmosphere
[CO2]atm. δ13C~ -7.5‰
[CO2*]loss_i
12[CO2*]i
13[CO2*]i
[CO2*]i δ13Ci
ε
δ13C TA
[DIC]i δ13C
Iteration
D
IF [DIC]i > [DIC]in situ AND δ13Ci < δ13Cin situ
IF [DIC]i = [DIC]in situ AND δ13Ci = δ13Cin situ
IF [DIC]i < [DIC]in situ OR [DIC]i > [DIC]in situ AND δ13Ci = δ13Cin situ
Comparison
[DIC]ex. =ΣCO2*lossi
[CO2*] in situ δ13C
[DIC] in situ δ13C
δ13C TA
In situ
E

Figure 4. Schematic representation of the streamCO_2-DEGAS model in acidic and unproductive rivers. Full and dashed lines refer to carbon concentrations and isotopic composition, respectively. The dotted line refer to the isotopic fractionation factors ε between CO_2^* and HCO_3^-. The size of each box as well as the length/direction of arrows has been drawn for understanding of the scheme. [DIC] is calculated as the sum of [CO_2^*] and [HCO_3^-], δ^{13}C-DIC is computed with the mass-balance equation and [HCO_3^-] is assumed as constant and equals TA. Box A: DIC source in the form of dissolved CO_2 (CO_2^*) from the respiration of terrestrial organic matter in soils and groundwater. Box B: DIC source in the form of HCO_3^- resulting from carbonate and silicate rock weathering. Box C: initial state; the initial [CO_2^*] value is assumed, and the initial [HCO_3^-] is fixed at the *in situ* TA value. Initial [DIC] is the sum of initial [CO_2^*] and [HCO_3^-]; the initial δ^{13}C-DIC values is computed with the [CO_2^*] and [HCO_3^-] concentration and their respective isotopic composition from Boxes A and B. Notice that in the model, A/B and C boxes are only isotopically linked (dashed lines). Box D: iterations; $^{12}CO_2^*$ and $^{13}CO_2^*$ fluxes across the interface are calculated by iterations resulting in a [CO_2^*] losses to the atmosphere; only the CO_2^* form is affected by air/water fluxes. At each iteration, new [DIC] and δ^{13}C-DIC values are calculated. Box E: *in situ* data of [DIC] and δ^{13}C-DIC are compared to the iterative values; if the iterative [DIC] > *in situ* [DIC] and iterative δ^{13}C < *in situ* δ^{13}C, iterations are continued within box D; if iterative [DIC] > *in situ* [DIC] or iterative [DIC] < *in situ* [DIC] and iterative δ^{13}C = *in situ* δ^{13}C, the initial state in box A is modified with a new initial CO_2^* (that is, a new soil pCO_2) and iterations begin again; when *in situ* and iterative [DIC] and δ^{13}C are equal at ± 10^{-5}, the model computes the CO_2 degassing ($[DIC]_{ex.}$) as the sum of the CO_2^* losses at each iteration. Throughout the modelling process, HCO_3^- stays at a constant concentration, but is affected by isotopic changes. Knowing the *in situ* water temperature, TA, pCO_2 and δ^{13}C-DIC in the river, assuming a percentage of contribution of carbonate to chemical weathering and assuming a δ^{13}C value in soils (δ^{13}C-SOM), the model allows the estimation of DIC due to respiration of soil organic carbon $[DIC]_{org}$ before the air/water exchange, the DIC due to weathering $[DIC]_{Si}$ and $[DIC]_{Ca}$, and the fraction of DIC that has degassed to the atmosphere $[DIC]_{ex}$.

Variables	Definitions	Equations and ref.
$\delta^{13}C\text{-}CO_{2soil}$	Isotope composition of soil carbon dioxide CO_2 (‰)	(1)
$\delta^{13}C\text{-}SOM$	Isotope composition of soil organic matter (‰)	(1)
$\delta^{13}C\text{-}CO_{2atm.}$	Isotope composition of atmospheric CO_2 (‰)	(1) -7.5 (Mook et al., 1983)
$pCO_{2atm.}$	Partial pressure of atmospheric CO_2 (sum of each isotope $^{13}pCO_{2atm.}$ and $^{12}pCO_{2atm.}$) (ppmv)	(1) 387 (IPCC, 2001)
pCO_{2soil}	Partial pressure of soil CO_2 (ppmv)	(1) 400-130 000 (Amundson and Davidson, 1990)
$[DIC]_{org.}$ $[CO_2^*]_{init.}$	Theoretical Dissolved Inorganic Carbon DIC (or initial dissolved CO_2) due to in- and out-stream respiration before gas exchanges (sum of concentrations of each isotope in the dissolved CO_2 form) ($mmolL^{-1}$)	(4)
K_0	Apparent solubility constant ($mmolKg^{-1}atm^{-1}$)	(4) (Weiss, 1974)
$pCO_{2init.}$	Partial pressure of initial CO_2 before gas exchanges (sum of each isotope $^{13}pCO_{2init.}$ and $^{12}pCO_{2init.}$) (ppmv)	(4)
ε_{dg}	Fractionation between dissolved and gaseous CO_2 (‰)	(5) (Zhang et al., 1995)
T	River water temperature (°C)	(5)
$\delta^{13}C\text{-}DIC_{org.}$	Isotope composition of DIC due to respiration	(6)
$[HCO_3^-]/TA$	River water alkalinity or bicarbonate ions ($mmolL^{-1}$)	(7)
$[DIC]_{si.}$	DIC due to silicate rock weathering ($mmolL^{-1}$)	(7)
$[DIC]_{ca.}$	DIC due to carbonate rock weathering ($mmolL^{-1}$)	(7)
$\delta^{13}C\text{-}DIC_{si.}$	Isotope composition of DIC due to silicate weathering (‰)	(8)
$\delta^{13}C\text{-}DIC_{ca.}$	Isotope composition of DIC due to carbonate weathering (‰)	(9)
$\delta^{13}C\text{-}CaCO_3$	Isotope composition of carbonate rocks (‰)	(9) 0 (Zeebe and Wolf-Gladrow, 2001)
$[DIC]_{init.}$	DIC at the initial state of river water before gas exchanges ($mmoL^{-1}$)	(10)
$\delta^{13}C\text{-}DIC_{init.}$	Isotope composition of initial DIC (‰)	(11)
ε_{bg}	Fractionation between bicarbonates and gaseous CO_2 (‰)	(12) (Zhang et al., 1995)
ε_{db}	Fractionation between dissolved CO_2 and bicarbonates (‰)	(13) (Zhang et al., 1995)
$\delta^{13}C\text{-}CO_2^*{}_{init.}$	Isotope composition of initial dissolved CO_2	(14)
$p^{13}CO_{2init.}$	Partial pressure of initial $^{13}CO_2$ (ppmv)	(15)
$p^{12}CO_{2init.}$	Partial pressure of initial $^{12}CO_2$ (ppmv)	(16)
$[^{13}CO_2^*]_{init.}$	Concentration of isotope 13 in the dissolved CO_2 form ($mmolL^{-1}$)	(17)
$[^{12}CO_2^*]_{init.}$	Concentration of isotope 12 in the dissolved CO_2 form ($mmolL^{-1}$)	

$p^{13}CO_{2atm.}$	Partial pressure of atmospheric $^{13}CO_2$ (ppmv)	(18)
$p^{12}CO_{2atm.}$	Partial pressure of atmospheric $^{12}CO_2$ (ppmv)	(19)
$F^{13}CO_2$	Fluxes of $^{13}CO_2$ at the air/water interface ($mmolm^{-2}h^{-1}$)	(20)
$F^{12}CO_2$	Total fluxes of $^{12}CO_2$ at the air/water interface ($mmolm^{-2}h^{-1}$)	
FCO_2	Fluxes (sum of each isotope) of CO_2 at the air/water interface ($mmolm^{-2}h^{-1}$)	
$[^{13}CO_2^*]_{loss}$	Losses of dissolved $^{13}CO_2$ at the interface ($mmolL^{-1}$)	(21)
$[^{12}CO_2^*]_{loss}$	Losses of dissolved $^{12}CO_2$ at the interface ($mmolL^{-1}$)	
$[CO2^*]_{loss}$	Total losses of dissolved CO_2 at the interface ($mmolL^{-1}$)	
K_{600}	Normalised gas transfer velocity (mh^{-1})	(20) (21)
H	River height (m)	(21)
t	Time constant (h)	(21)
$\Delta p^{13}CO_2$	Difference between water and air $^{13}pCO_2$ (ppmv)	(21)
$\Delta p^{12}CO_2$	Difference between water and air $^{12}pCO_2$ (ppmv)	
ΔpCO_2	Difference between water and air pCO_2 (ppmv)	
$[CO_2^*]_n$	Dissolved CO_2 after n iterations (gas exchanges occur) or *in situ* dissolved CO_2 ($mmolL^{-1}$)	(22)
$[DIC]_n$	*In situ* DIC ($mmolL^{-1}$)	(23)
$\delta^{13}C\text{-}CO_2^*(n)$	*In situ* isotope composition of dissolved CO_2 (‰)	
$\delta^{13}C\text{-}HCO_3^-(n)$	*In situ* isotope composition of HCO_3^- (‰)	
$\delta^{13}C\text{-}DIC(n)$	*In situ* isotope composition of DIC (‰)	
$[DIC]_{ex.}$	concentration of DIC that has been degassed from the river water to the atmosphere upstream of the sampling point ($mmolL^{-1}$)	(24)

Table 2. List of the variables used in the formulation of the streamCO_2-DEGAS model; see Figure 4 as well as equations in the text.

2.2.2. Isotopic signatures of DIC from terrestrial organic matter respiration and rock weathering

Respiration of terrestrial organic matter in soils, groundwaters and rivers liberates CO_2 that reaches the waters in the form of CO_2^* (box A in Figure 4). The isotopic composition of this carbon that contributes to the riverine DIC depends on the signature of its main source, the soil organic matter (δ^{13}C-SOM), which is directly related to the type of vegetation cover. In the case of C_3 plant organic matter, as in our study sites, the soil-respired CO_2 produced has the same isotope composition value as the initial substrate, i.e., -30 to -24‰ (Vogel, 1993). Little or no fractionation occurs during respiratory conversion of soil organic matter to respired-CO_2 (Mariotti, 1991; Amiotte-Suchet et al., 1999). However, due to selective molecular diffusion of the gas through the soil pores, the isotopic composition of soil CO_2 can become enriched in ^{13}C relative to the soil organic matter by up to 4-5‰ (Craig, 1953; Cerling et al., 1991). This fractionation value is variable and greatly depends on where the respiration occurs. If respiration primarily occurs in unsaturated soils, the fractionation is maximal (Davidson, 1995; Amundson et al., 1998). When respiration occurs in waterlogged soils, groundwaters, and river waters and sediments, the molecular diffusion, and thus the isotopic fractionation of CO_2 in soil become much less important (near 1‰, O'Leary, 1984). Due to the sandy nature of the soils in the three rivers studied here, we assumed that the majority of the CO_2 that escaped from the rivers came from respiration in unsaturated soils. Later, the sensitivity of the model results to this hypothesis will be tested. The isotopic composition of soil CO_2 is thus computed from the isotopic composition of soil organic matter (assumed to be the same as measured in the river POC) based on Cerling et al. (1991) and Davidson (1995):

$$\delta^{13}\text{C-CO}_{2\text{soil}} = 0.0044\delta^{13}\text{C-SOM} + \frac{\text{pCO}_{2\text{atm.}}}{\text{pCO}_{2\text{soil}}}\left(\delta^{13}\text{C-CO}_{2\text{atm.}} - 1.0044\delta^{13}\text{C-SOM} - 4.4\right) + 4.4 + \delta^{13}\text{C-SOM} \quad (1)$$

where δ^{13}C-CO_{2soil}, δ^{13}C-SOM and δ^{13}C-CO_{2atm} are carbon isotope ratios of soil CO_2, soil organic matter and atmospheric CO_2, respectively; in accordance with the literature, average values of 400 and 30 000 ppmv were chosen for pCO_{2atm} and pCO_{2soil}, the partial pressures of CO_2 in atmosphere and soil, respectively (IPCC, 2001; Amundson and Davidson, 1990). With a δ^{13}C-SOM of approximately -28‰, which corresponds to the δ^{13}C-POC measured in the rivers year-round, we obtained a δ^{13}C-CO_{2soil} near -24‰.

In soils and groundwaters, weathering of carbonate and silicate rocks by soil CO_2 produces bicarbonates (HCO_3^-), which contribute to the river DIC (Figure 4, Box B). For silicate

weathering, such as albite hydrolysis (Eqn. 2), HCO_3^- originates solely from soil CO_2 (Amiotte-Suchet et al., 1999).

$$2NaAlSi_3O_8 + 2CO_2 + 3H_2O \rightarrow Al_2Si_2O_5(OH)_4 + 2Na + +2HCO_3^- + 4SiO_2 \quad (2)$$

In this case, the HCO_3^- produced and released to the water has the same isotopic composition as the soil CO_2, i.e., -24‰ at our study sites.

For carbonate dissolution by soil CO_2 (Eqn. 3), one-half of the HCO_3^- originates from the mineral itself and the other half from soil CO_2.

$$CaCO_3 + CO_2 + H_2O \rightarrow Ca^{2+} + 2HCO_3^- \quad (3)$$

In the case of carbonate dissolution alone, the isotopic composition of the HCO_3^- released to the water is the average of the isotopic compositions of the soil CO_2 (-24‰) and the carbonate rock (about 0‰) (i.e., -12‰ in the case of our study sites).

2.2.3. Theoretical initial state of river DIC

In our model, we define a theoretical initial state of river DIC before any CO_2 degassing has occurred (Figure 4, Box C). At a pH between 4.7 and 7.2, this DIC is simply the sum of CO_2^* from respiration of terrestrial organic matter and HCO_3^- from rock weathering. First, an initial soil pCO_2 value is assumed, which allows for the calculation of the CO_2^* concentration from the terrestrial soil organic matter respiration (named $[DIC]_{org}$) using the apparent CO_2 solubility constant K_0 (mmol L^{-1} atm^{-1}) of Weiss (1974) for freshwater and Henry's law (Eqn. 4).

$$[DIC]_{org.} = [CO_2^*]_{init.} = K_0 pCO_{2init.} \quad (4)$$

where $[DIC]_{org}$ is the DIC originating from the respiration of soil organic matter and is equal to $[CO_2^*]_{init}$ (mmol L^{-1}); pCO_{2init} (ppmv) is the corresponding assumed partial pressure of CO_2 at the initial river water state before any degassing occurs. CO_2-supersaturated groundwater discharges first at a single point at the stream's spring and then as diffusive discharge throughout the watercourse, where it joins stream water that has already been substantially degassed (Johnson et al., 2008; Davidson et al., 2010). Consequently, the $[DIC]_{org}$ term defined in our model is a theoretical concentration that integrates all of the respiration sources occurring at distinct places (soil, groundwater, sediments and waters), but it does not represent any measurable quantity in groundwater or river water. Because we assumed that all the respiration occurred in soils for the model application for our study site, $[DIC]_{org.}$ was the average CO_2^* concentration in groundwaters.

The isotope composition CO_2^* from soil organic matter respiration (DIC_{org}) was then computed from the one of the soil gaseous CO_2 using the fractionation between both forms, defined by Zhang et al. (1995) (Eqn. 5 and 6).

$$\varepsilon_{dg} = 0.0049T - 1.31 \quad (5)$$

where ε_{dg} represents the fractionation (‰) between dissolved and gaseous CO_2 and T is the water temperature (°C).

$$\delta^{13}C\text{-}DIC_{org.} = \delta^{13}C\text{-}CO_{2soil} + \varepsilon_{dg} \quad (6)$$

where $\delta^{13}C\text{-}DIC_{org.}$ and $\delta^{13}C\text{-}CO_{2soil}$ are the respective isotope compositions of DIC originating from organic matter respiration and from soil gaseous CO_2.

Conversely, the HCO_3^- concentration results entirely from rock weathering and, at the selected pH range, is not affected by degassing to the atmosphere and equal to the alkalinity. Consequently, the HCO_3^- concentration at the initial state in groundwater is the same as measured *in situ* in rivers. In the model, we took into account the contribution of silicate and carbonate rock weathering to alkalinity according to Eqn. 7:

$$[HCO_3^-] = TA = [DIC]_{si.} + [DIC]_{ca.} \quad (7)$$

The relative contribution of both weathering pathways can be estimated by comparing the measured alkalinity (or HCO_3^-) values with those reported by Meybeck (1987) in monolithic watersheds; in rivers draining only carbonate rocks, typical alkalinity is 3.195 mmol L^{-1}, whereas in rivers draining only silicate rocks, alkalinity is 0.125 mmol L^{-1}. Based on this principle, the measured TA values at our study sites (Table 1) gave a one-year average contribution of carbonate rock weathering to alkalinity of 4 and 7% in the Renet and Leyre rivers, respectively, with alkalinity in the Milieu stream coming from silicate rock weathering alone.

In the case of silicate rock weathering alone, the isotopic signature of the DIC equals the isotopic signature of the initial dissolved CO_2 (Amiotte-Suchet et al., 1999) (Eqn. 8).

$$\delta^{13}C\text{-}DIC_{si.} = \delta^{13}C\text{-}DIC_{org.} \quad (8)$$

In contrast, the DIC originating from carbonate rock weathering has an isotopic signature of an equal mixture of soil dissolved CO_2 and $CaCO_3$ (Reaction (3) (Eqn. 9).

$$\delta^{13}C\text{-}DIC_{ca.} = (\delta^{13}C\text{-}DIC_{org.} + \delta^{13}C\text{-}CaCO_3)/2 \quad (9)$$

Although in acidic rivers, such as those studied here, carbonate weathering is generally minor; it might significantly affect the isotopic signature of the DIC inputs in the form of HCO_3^-. This was illustrated by the positive relationship between DIC and $\delta^{13}C$-DIC in the Leyre River (Figure 2a), a trend induced by deeper groundwater flow at low water stage; this groundwater is more influenced by carbonate rock weathering than surface runoff (Polsenaere et al. submitted).

From the initial CO_2^* and HCO_3^- pools, the theoretical initial river DIC isotopic composition can be computed as (Eqn. 10 and 11):

$$[DIC]_{init.} = TA + [DIC]_{org.} \quad (10)$$

$$\delta^{13}C\text{-}DIC_{init.} = \left(\delta^{13}C\text{-}DIC_{org.} \times [DIC]_{org.} + \delta^{13}C\text{-}DIC_{si.} \times [DIC]_{si.} + \delta^{13}C\text{-}DIC_{ca.} \times [DIC]_{ca.}\right) / [DIC]_{init.} \quad (11)$$

In river water, dissolved CO_2 and HCO_3^- are in isotopic equilibrium as defined by Zhang et al. (1995). Thus, the isotopic composition of dissolved CO_2 at the initial state can be obtained from the isotopic composition of DIC (Eqn. 12, 13 and 14).

$$\varepsilon_{bg} = -0.1141T + 10.78 \quad (12)$$

where ε_{bg} represents the fractionation between CO_2 and HCO_3^-.

$$\varepsilon_{db} = \varepsilon_{dg} - \varepsilon_{bg} \quad (13)$$

where ε_{db} represents the fractionation between CO_2^* and HCO_3^-, and ε_{dg} represents the fractionation between CO_2 and CO_2^* (Eqn. 5).

$$\delta^{13}C\text{-}CO_2^*{}_{init.} = \delta^{13}C\text{-}DIC_{init.} + (\varepsilon_{db} \times TA)/[DIC]_{init.} \quad (14)$$

where $\delta^{13}C\text{-}CO_2^*{}_{init.}$ and $\delta^{13}C\text{-}DIC_{init.}$ are the isotope compositions of dissolved initial CO_2 and initial DIC, respectively. In summary, the initial state of DIC (concentrations and isotopic composition) in the model is calculated from the TA measured in the river for the HCO_3^- concentration, from an assumed pCO_2 for the CO_2^* concentration, from the isotopic composition of soil organic matter that determines the $\delta^{13}C$ of soil CO_2 and from a relative proportion of carbonate and silicate weathering deduced from the measured TA. Finally, HCO_3^- and CO_2^* are assumed at the isotopic equilibrium, and CO_2^* can escape to the atmosphere, although HCO_3^- is assumed to be conservative.

2.2.4. Iterative computation of CO_2 degassing

From the initial state defined above, the evolution of river DIC with degassing consists of a decrease of the CO_2^* concentration (and the pCO_2) and an increase in $\delta^{13}C$-DIC due to the more rapid evasion of $^{12}CO_2$ relative to $^{13}CO_2$ (figure 4, Box D). The initial partial pressures of each stable isotope can be calculated from their respective initial partial pressures of CO_2 (Eqn. 15).

$$p^{13}CO_{2init.} = \delta^{13}C\text{-}PDB \times pCO_{2init.} \times \left(\left(\frac{\delta^{13}C\text{-}CO_2^*{}_{init.}}{1000}\right) + 1\right) \Big/ 1 + \delta^{13}C\text{-}PDB \times \left(\left(\frac{\delta^{13}C\text{-}CO_2^*{}_{init.}}{1000}\right) + 1\right) \quad (15)$$

where $p^{13}CO_{2init}$ is the initial partial pressure of $^{13}CO_2$ in water (ppmv), and $\delta^{13}C$-PDB refers to the Pee-Dee Belemnite standard stable isotope, equal to 0.011237.

Then, the partial pressure of $^{12}CO_2$ in river water and the concentration of ^{13}C isotope in the CO_2 form are deduced (Eqn. 16 and 17).

$$pCO_{2init.} = p^{13}CO_{2init.} + p^{12}CO_{2init.} \quad (16)$$

where $p^{13}CO_{2init.}$ and $p^{12}CO_{2init.}$ are the partial pressures of each isotope.

$$[^{13}CO_2^*]_{init.} = K_0 p^{13}CO_{2init.} \quad (17)$$

where $[^{13}CO_2^*]_{init.}$ is the concentration of isotope 13 in the CO_2 form (mmol L^{-1}).

The same calculation is done for $[^{12}CO_2^*]_{init.}$

The partial pressures of each CO_2 isotope in the atmosphere are given by (Eqn. 18 and 19).

$$p^{13}CO_{2atm.} = \delta^{13}C\text{-}PDB \times pCO_{2atm.} \times \left(\left(\frac{\delta^{13}C\text{-}CO_2^*{}_{atm.}}{1000}\right) + 1\right) \Big/ 1 + \delta^{13}C\text{-}PDB \times \left(\left(\frac{\delta^{13}C\text{-}CO_2^*{}_{atm.}}{1000}\right) + 1\right) \quad (18)$$

where $p^{13}CO_{2atm.}$ is the partial pressure of $^{13}CO_2$ in the atmosphere (ppmv); the isotope composition of atmospheric CO_2 equates to -7.5‰ (Mook et al., 1983).

$$pCO_{2atm.} = p^{13}CO_{2atm.} + p^{12}CO_{2atm.} \quad (19)$$

where $p^{13}CO_{2atm.}$ and $p^{12}CO_{2atm.}$ are the partial pressures of $^{13}CO_2$ and $^{12}CO_2$ in the atmosphere, respectively.

The streamCO_2-DEGAS model then computes CO_2 fluxes of each isotope from the following equations (Eqn. 20 and 21).

$$F^{13}CO_2 = K_{600} K_0 \Delta p^{13}CO_2 \quad (20)$$

where $F^{13}CO_2$ represents the $^{13}CO_2$ fluxes at the interface in mmol m^{-2} h^{-1}; K_0 is the apparent CO_2 solubility constant of Weiss (1974) in mol Kg^{-1} atm^{-1}; K_{600} is an arbitrary normalised gas transfer speed (for a Schmidt number of 600 in cm h^{-1}), and $\Delta p^{13}CO_2$ is the difference between the initial water and the atmospheric $p^{13}CO_2$ in ppmv.

$$[^{13}CO_2^*]_{loss} = (K_{600} t / 10^{-3} H)\, K_0 \Delta p^{13}CO_2 = \beta K_0 \Delta p^{13}CO_2 \quad (21)$$

where $[^{13}CO_2^*]_{loss}$ expresses the losses of $^{13}CO_2^*$ to the atmosphere in mmol L^{-1}, t is a time constant (h) and H is the depth of the river (m); both t and H are arbitrarily fixed. The same calculations are made for $^{12}CO_2$ fluxes and dissolved $^{12}CO_2$ losses. In equation 21, the term β is dimensionless and proportional to the ratio between the gas transfer velocity and water height. This parameter can be arbitrary fixed and defines the size of the iterations. The same value of β is applied to both isotopes. In the model, CO_2 fluxes and resulting CO_2 degassing are independent of the gas transfer velocity and river depth, two parameters subject to large variations and uncertainties.

At each iteration, an amount of CO_2 degasses to the atmosphere, which results in a decrease in water pCO_2 (and thus DIC, but HCO_3^- remains conservative) and an increase in δ^{13}C-DIC. Due to pCO_2 gradients at the river water-air interface, $^{12}CO_2$ diffuses faster than $^{13}CO_2$ and the isotope composition of water CO_2 approaches the equilibrium value of the atmospheric CO_2 isotope composition of -7.5‰ (Mook, 1970; Yang et al., 1996). Thus, at each iteration a new DIC concentration and δ^{13}C-DIC can be calculated. Figure 5 shows the variations of water pCO_2 and δ^{13}C-DIC according to the iteration steps, starting at three initial conditions that correspond to three different assumed initial pCO_2 values (see 2.2.3). pCO_2 and δ^{13}C-DIC evolve toward equilibrium values, with atmospheric pCO_2 approaching 400 ppmv and δ^{13}C-DIC approaching +1‰, corresponding to the isotopic equilibrium with atmospheric CO_2 of +9‰ (Mook et al., 1974).

To calculate the CO_2 degassing to the atmosphere from rivers, the model compares the new computed water pCO_2 and δ^{13}C-DIC values at each iteration to those measured in the field (Table 1; Figure 4, Box E). After a certain number of iterations, three different cases can occur as shown in Figure 5. In case 1, when the initial river pCO_2 is fixed at a high value (20 000 ppmv), the iterative δ^{13}C-DIC reaches the *in situ* value (-15‰ in this example) before the pCO_2 reaches the *in situ* value (1000 ppmv in this example). In this case, these rates indicate that the isotopic equilibration with the air occurs before the necessary quantity of CO_2 has degassed. In contrast, when the initial water pCO_2 is fixed at a lower value (2000 ppmv), as in case 2, the pCO_2 reaches the *in situ* value before the δ^{13}C-DIC. Finally, in case 3, the initial pCO_2 was fixed to the adequate value (3563 ppmv) so that the pCO_2 and δ^{13}C-DIC reached *in situ* values at the same time iteration. In this last case, CO_2 degassing can be computed. To summarise, because HCO_3^- is conservative, the convergence criteria of the streamCO_2-DEGAS model are expressed as follows (figure 4):

- If the iterative DIC is higher than the *in situ* DIC concentration, and the δ^{13}C-DIC is lower than the *in situ* δ^{13}C-DIC, then iterations are continued.
- If the iterative DIC is different (higher or lower) from the *in situ* DIC, and the iterative δ^{13}C-DIC is equal to the *in situ* δ^{13}C-DIC, then the initial pCO_2 is modified: either diminished when the iterative DIC is higher than *in situ*, or increased when the iterative DIC is lower than *in situ*. Then iterations begin again from this new initial pCO_2. Calculated from the measured soil organic matter isotope composition and the contribution of silicate and carbonate rock to alkalinity, the isotope composition of initial DIC is unchanged.

- If the iterative DIC concentration and the δ^{13}C-DIC values converge with the *in situ* measured values (at ±1 µmol.L^{-1} for DIC and ±0.01‰ for δ^{13}C-DIC), a "DIC exchanged" concentration $[DIC]_{ex}$ can be computed by the model as described below.

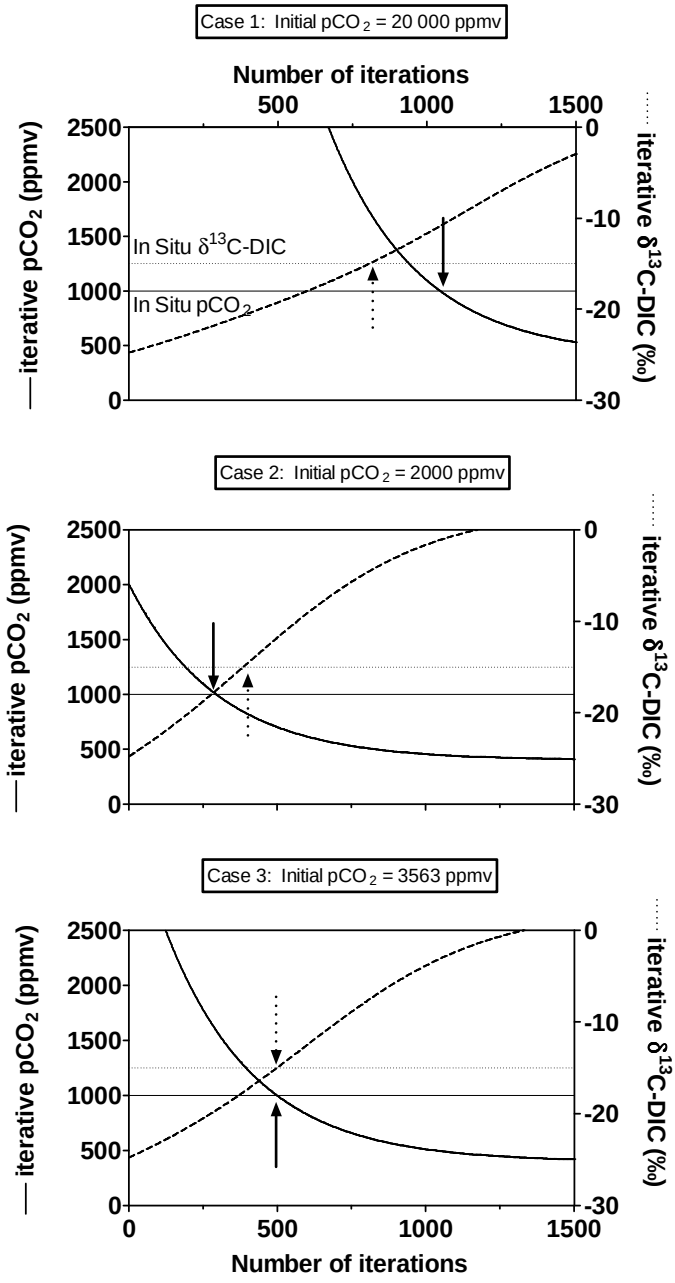

Figure 5. The convergence criteria of the streamCO_2-DEGAS model. Each graph represents iterations within box D in Figure 4. Bold and dashed curves represent iterative pCO_2 and δ^{13}C-DIC, respectively. Full and dotted lines represent *in situ* pCO_2 and δ^{13}C-DIC, respectively. pCO_2 is in ppmv and δ^{13}C-DIC is in ‰. In case 1, the initial pCO_2 was fixed at a too high value, so δ^{13}C-DIC reached the *in situ* value before pCO_2. In case 2, the initial pCO_2 was fixed at a too low value, so δ^{13}C-DIC reached the *in situ* value after pCO_2. In case 3, the initial pCO_2 was fixed at the correct value, so δ^{13}C-DIC and pCO_2 reached the *in situ* value at the same iteration. In this latter case, $[DIC]_{ex}$ can be computed.

2.2.5. The CO_2 degassing calculation

The CO_2 degassing from rivers is calculated from the DIC parameters obtained after n iterations leading to the exact data measured *in situ*. Knowing the amount of dissolved CO_2 lost to the atmosphere, the final water concentrations of CO_2^* is calculated by the following (Eqn. 22).

$$[CO_2^*]_n = [CO_2^*]_{init.} - \sum_{i=1}^{n}[CO_2^*]_{loss(i)} \quad (22)$$

where $[CO_2^*]_n$ and $[CO_2^*]_{loss}$ are the total concentration and losses of dissolved CO_2 for n iterations, respectively.

Alkalinity being conservative, the DIC concentration for n iterations, $[DIC]_n$ is given by (Eqn. 23).

$$[DIC]_n = [CO_2^*]_n + TA \quad (23)$$

where TA represents river alkalinity in mmol L^{-1}.

Finally, the DIC exchanged, or the CO_2 degassing from the rivers of the Arcachon lagoon catchment is obtained as follows (Eqn. 24).

$$[DIC]_{ex.} = [DIC]_{init.} - [DIC]_n = \sum_{i=1}^{n}[CO_2^*]_{loss(i)} \quad (24)$$

where $[DIC]_{ex.}$ represents the integrated CO_2 degassing from river waters to the atmosphere in mmol L^{-1}.

Knowing the *in situ* water temperature, alkalinity, pCO_2 and δ^{13}C-DIC measured in the river, and assuming a percentage of contribution of carbonate to the weathering and the value of δ^{13}C in soils, the model thus permits the estimation of the following chemical conditions as found in our three studied rivers: the DIC due to respiration before the air-water exchange ($[DIC]_{org.}$), the DIC due to silicate and carbonate weathering ($[DIC]_{Si.}$ and $[DIC]_{Ca.}$, respectively) and the percentage of river DIC that has degassed into the atmosphere ($[DIC]_{ex.}$).

$$[DIC]_{insitu} = [DIC]_{org.} + TA - [DIC]_{ex.} \quad (25)$$

3. Results

3.1. CO_2 degassing assuming silicate weathering alone

We started in a first step assuming only silicate weathering, as was the case in the Milieu River, where TA is lower than 0.125 mmol L^{-1}. Consequently, the isotopic composition of the initial DIC (Box B in Figure 4) was equal to the isotopic composition of the initial soil CO_2 that is close to -24‰ assuming an average isotopic composition of soil organic matter equal to the isotopic composition of POC (-28‰) observed in the study rivers (Eqn. 1).

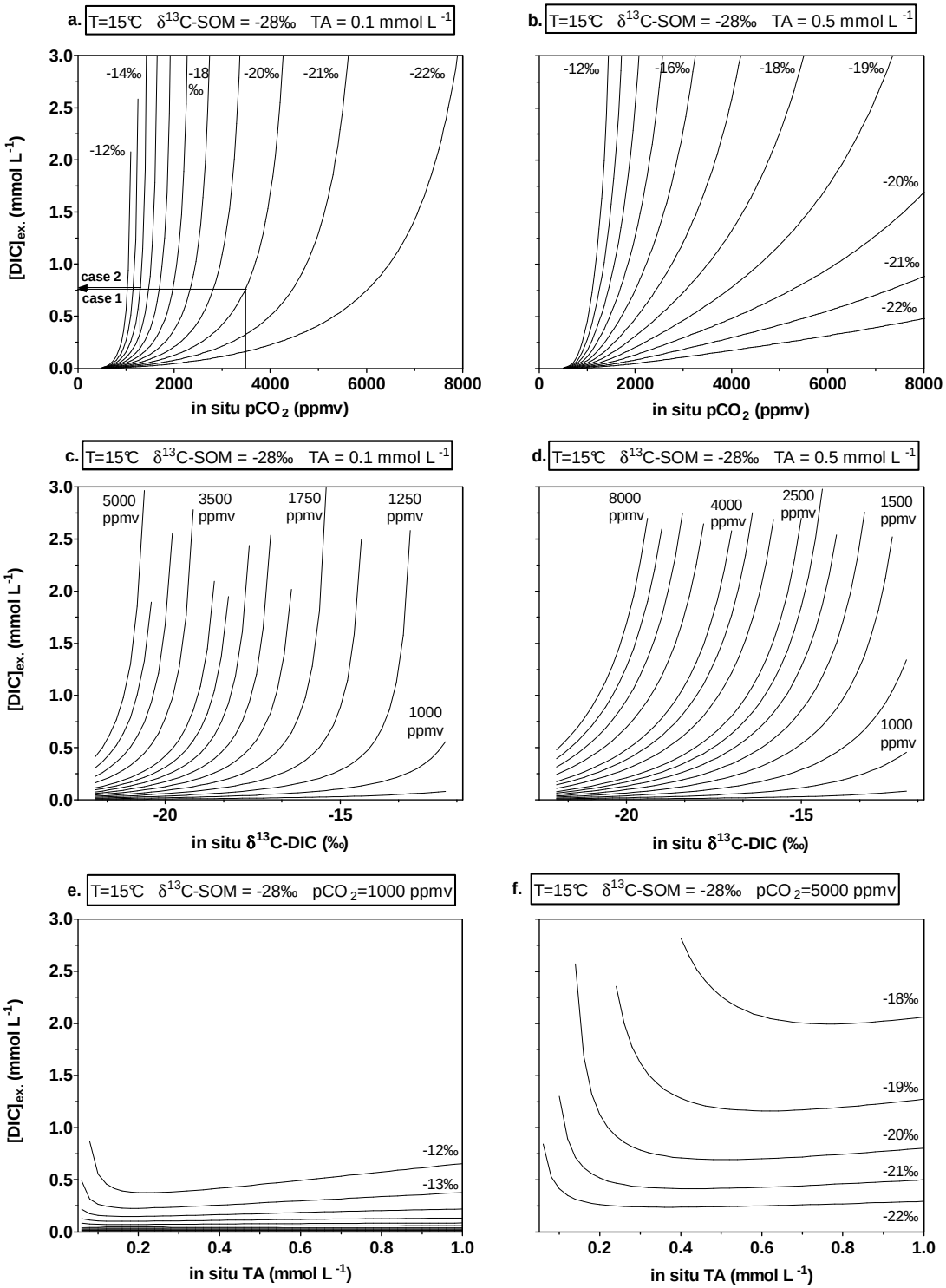

Figure 6. Influence of *in situ* pCO_2 (a. and b.), δ^{13}C-DIC (c. and d.) and TA (e. and f.) on modelled $[DIC]_{ex}$. Input parameters: T=15°C; δ^{13}C-SOM=-28‰; a. and c. TA=0.1 mmol L^{-1}; b. and d. TA=0.5 mmol L^{-1}; e. pCO_2=1000 ppmv and f. pCO_2=5000 ppmv. Cases 1 and 2 are used as examples in the Discussion.

3.1.1. Influence of the in situ river pCO_2, δ^{13}C-DIC and TA

$[DIC]_{ex.}$ was computed using three DIC parameters, i.e., *in situ* water pCO_2, δ^{13}C-DIC and TA. The influence of the three DIC parameters on the CO_2 degassing is shown in Figure 6 using ranges of variations observed at our study sites (Table 1). Although it was assumed here that only silicate weathering occurred, the sensitivity of $[DIC]_{ex}$ to *in situ* pCO_2 and δ^{13}C-DIC was tested for both non buffered water (TA=0.1 mmol L^{-1}, Figures 6a, c) and moderately buffered waters (TA=0.5 mmol L^{-1}, Fig. 6.b., d.). The sensitivity to TA was tested for low and high *in situ* water pCO_2 (1000 and 5000 ppmv in Figures 6e and 6f respectively).

Modelled $[DIC]_{ex.}$ concentrations increased with *in situ* pCO_2 at given TA and δ^{13}C-DIC values (Figures 6a, b). This means that when high pCO_2 is observed in rivers, strong degassing must have occurred upstream in order to explain the observed δ^{13}C-DIC values. Note also that $[DIC]_{ex.}$ increased extremely quickly with pCO_2 at less negative δ^{13}C-DIC values. To reach such heavy δ^{13}C-DIC in rivers, assuming a majority of silicate rock weathering, a very large quantity of CO_2 must have degassed. For the same reasons, computed $[DIC]_{ex}$ concentrations increased with the observed *in situ* δ^{13}C-DIC at given alkalinity and pCO_2 values (Figures 6c, d). The model was consistent with *in situ* observations in the studied rivers, where very negative δ^{13}C-DIC values were associated with high CO_2 and inversely (Figure 2). Situations with high pCO_2 (4000-6000 ppmv) and less negative δ^{13}C-DIC (around -12‰) are generally not encountered in acidic and unproductive rivers, as they would require an extremely high CO_2 degassing rate and $[DIC]_{ex}$ concentrations.

In non-buffered to moderately buffered waters, modelled $[DIC]_{ex}$ concentrations decrease at given *in situ* water pCO_2 and δ^{13}C-DIC values (Figures 6.a, b, c, d). When TA increases, computed $[DIC]_{ex}$ concentrations first rapidly decrease and then slowly increase (Figures 6e, f), due to two antagonist effects in the model formulation. This initial decrease is due to the fact that, at the initial state in Eq. 14, the difference in isotopic composition of CO_2^* and DIC becomes larger when TA increases. An increase in TA makes the initial $\delta^{13}C\text{-}CO_2^*$ more negative and, thus, the difference in isotopic composition between CO_2^* and atmospheric CO_2 becomes larger. As a result, the rate of isotopic equilibration becomes faster for the same quantity of CO_2 degassed, and δ^{13}C-DIC tends to reach the *in situ* value before pCO_2 (case 1 in Figure 5). As a result, the model reduces the initial pCO_2 for the two parameters so that they simultaneously converge at the *in situ* state, and $[DIC]_{ex}$ is lowered. This kinetic isotopic equilibration effect is particularly important at low TA. The second and antagonist effect is due to a buffering effect on the δ^{13}C-DIC of the

HCO_3^- pool, which is not affected by degassing during iterations. Thus, to make the δ^{13}C-DIC increase for a given value, it is necessary to release more CO_2 to the atmosphere when TA is higher. This makes pCO_2 reach the *in situ* value before δ^{13}C-DIC (case 2 in figure 5). Then, the model increases the initial pCO_2 for the two parameters so that they simultaneously converge at the *in situ* state, and $[DIC]_{ex}$ is thus increased.

3.1.2. Sensitivity of the stream CO_2-DEGAS model to temperature and isotopic composition of soil carbon

Temperature affects the isotopic fractionation equations between DIC species (Zhang et al. 1995) and the apparent CO_2 solubility constant; thus, it also affects the degassing rate (Weiss 1974). However, water temperature has a minor influence on modelled $[DIC]_{ex}$ concentrations. In the case of the three rivers, the modelled $[DIC]_{ex}$ decreased and then increased by less than 10% for temperatures varying from 5 to 25°C (not shown). In contrast, the influence of the assumed δ^{13}C-SOM on $[DIC]_{ex.}$ concentrations is much more important, particularly at high *in situ* pCO_2 (Figure 7). At high *in situ* pCO_2, the δ^{13}C-DIC value is much closer to the assumed δ^{13}C-SOM, and its convergence to the *in situ* value during iterations is faster and largely determines the final calculated $[DIC]_{ex.}$ In fact, the more negative the δ^{13}C-SOM, the larger the difference between the initial and the *in situ* δ^{13}C-DIC (Figure 5) and thus, the larger the amount of CO_2 degassed to the atmosphere to reach the observed δ^{13}C-DIC values. Here, we postulated that the majority of the CO_2 degassing from rivers comes from respiration in well drained soils (sandy soils), where the isotopic fractionation of CO_2 due to selective vertical diffusion is maximal at 4‰. If in reality, a significant fraction of respiration occurs in waterlogged soils and/or in waters and sediments, then the respired CO_2 would have an isotopic composition closer to the δ^{13}C-SOM. Consequently, computed $[DIC]_{ex}$ values would be sensitive to this in the same way because they depend on the assumed δ^{13}C-SOM, as shown in Figure 7.

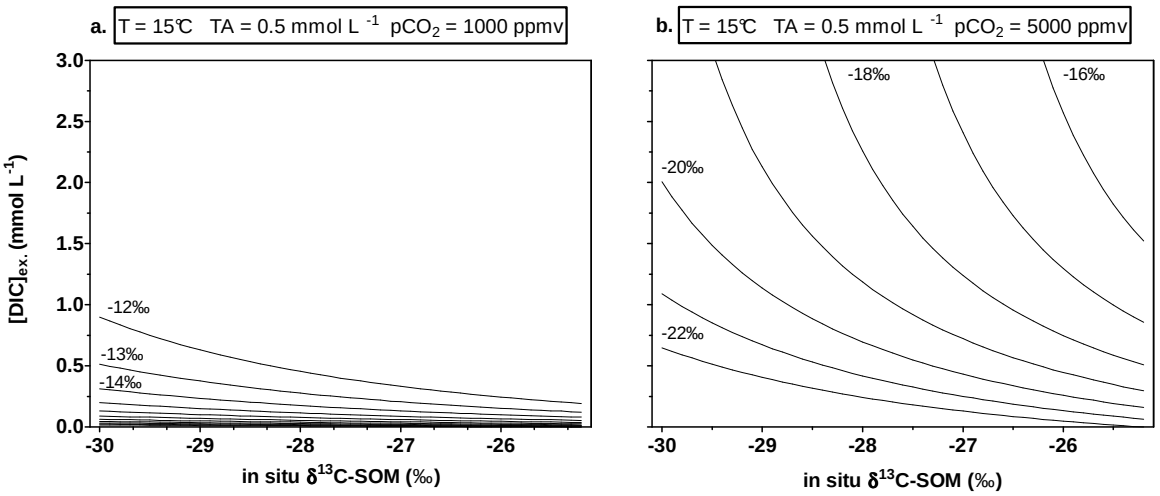

Figure 7. Influence of the isotopic composition of soil organic matter δ^{13}C-SOM on modelled $[DIC]_{ex}$. Input parameters: TA=0.5 mmol L^{-1}; pCO_2=1000 ppmv in a. and pCO_2=5000 ppmv in b.

3.2. CO_2 degassing taking into account both silicate and carbonate weathering

Even with acidic river waters, both silicate and carbonate rocks occur in many catchments. Assuming the characteristic TA values proposed by Meybeck (1987), carbonate rock weathering at our study site contributes between 0 to 7% of the HCO_3^-. Despite this small percentage, the potential effect of carbonate weathering on the isotope signature of the DIC source must be tested.

3.2.1. Sensitivity to changes in the isotopic signature of the DIC source alone

With $[DIC]_{Ca}$ ranging from 0 to 30% of the TA, we tested the influence of carbonate contribution to alkalinity for a fixed TA of 0.5 mmol L^{-1}, at a given *in situ* pCO_2 value (Figure 8a) and at a given *in situ* δ^{13}C-DIC (Figure 8b). Modelled $[DIC]_{ex.}$ concentrations decreased with carbonate contribution, particularly for the most extreme *in situ* values at high pCO_2, as previously seen when testing the sensitivity to TA (Figures 6e, f). For a carbonate weathering contribution to TA varying from 0 to 30% and a δ^{13}C-SOM of -28‰, the initial δ^{13}C-DIC changed from -24.7 to -21.2‰. Thus, the difference between initial and *in situ* δ^{13}C-DIC was diminished, and the modelled $[DIC]_{ex}$ was lowered. The dependency of modelled $[DIC]_{ex}$ on the proportion of HCO_3^- from carbonate weathering was much more pronounced at high *in situ* pCO_2. As shown in Figure 8b, an increase in carbonate contribution of 10% generated a decrease in $[DIC]_{ex}$ of 0.45 mmol L^{-1} at a pCO_2 of 7000 ppmv, but of only 0.020 mmol L^{-1} at a pCO_2 of 2000 ppmv. However, the relative sensitivity was similar at both pCO_2 values, about 20% of the modelled $[DIC]_{ex}$ value. Out

of the three study sites, very high pCO_2 only occurred in the Renet stream, where TA was close to the reference concentration proposed by Meybeck (1987) for 100% silicate weathering, and thus, carbonate contribution was extremely low.

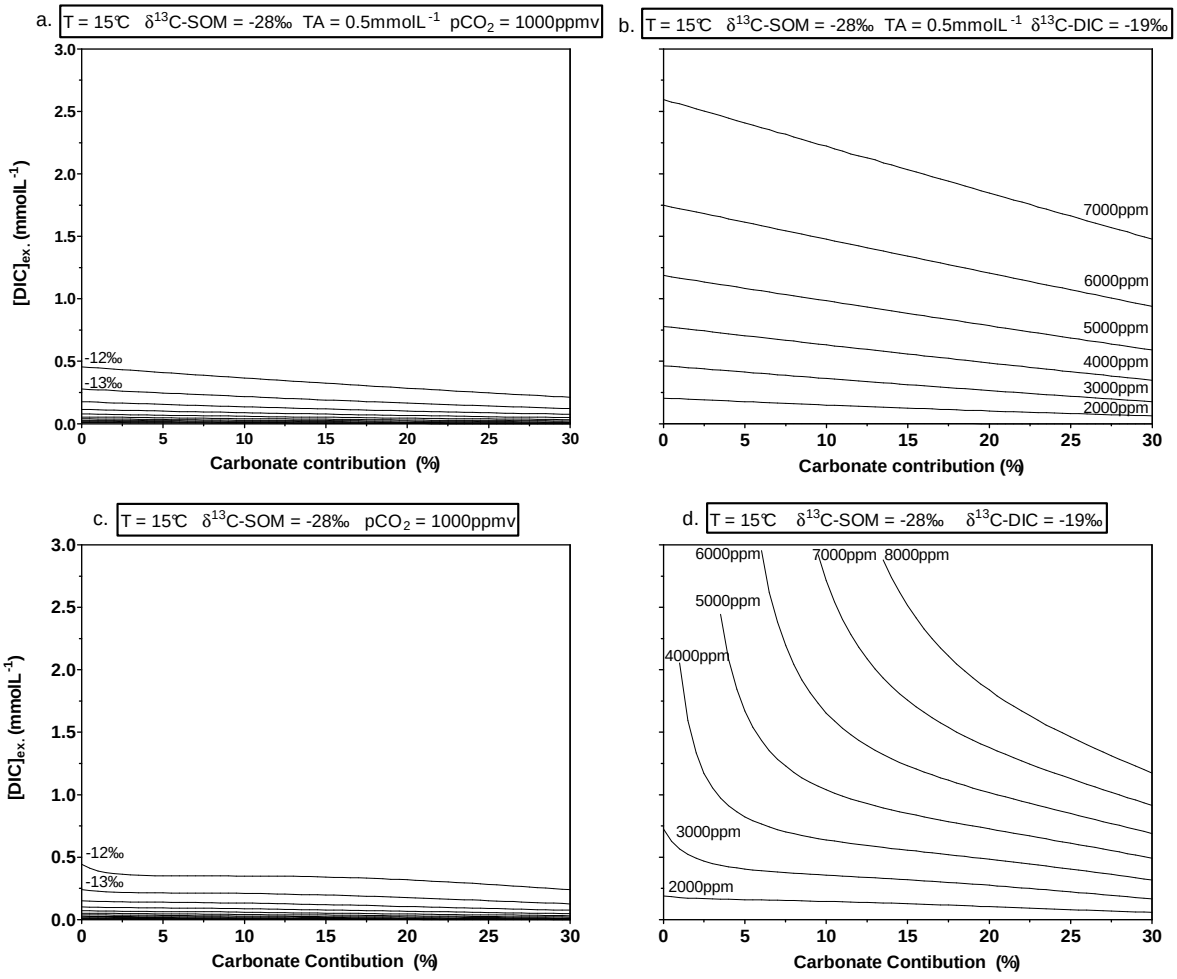

Figure 8. Influence of carbonate rock weathering contribution to TA on modelled $[DIC]_{ex}$ concentrations. a. and b.: influence of the isotopic signature of the source alone; c. and d. concomitant influence of the isotopic signature of the source and also of the TA concentration. Input parameters: T=15°C, δ^{13}C-SOM=-28‰.

3.2.2. Sensitivity to combined changes in the isotopic signature of the DIC source and in the TA

Carbonate weathering influences our model results through two simultaneous processes: first, by changing the TA, and second, by changing the isotopic signature of the DIC. Carbonate weathering releases HCO_3^- with an $\delta^{13}C$ of one-half that released by silicate weathering. Using the representative concentrations given by Meybeck (1987), from a 0 to 30% contribution of carbonates to weathering, river TA increases from 0.125 to 1.040 mmol L^{-1}. The influence of both the isotope source signature and the TA on the CO_2 degassing was tested for either a given pCO_2 value or a given isotope DIC composition (Figures 8c, d, respectively). Logically, we obtained a combined influence of the isotope signature (Figures 8a, b) and the *in situ* TA (Figures 6e, f) on modelled $[DIC]_{ex}$. Consequently, modelled $[DIC]_{ex}$ decreased with increasing carbonate. $[DIC]_{ex}$ results were very sensitive to the proportion of carbonate weathering, particularly at low carbonate contribution and at high pCO_2 (Figure 8d). In our three studied rivers, high pCO_2 values occurred during summer months, when groundwater discharge was maximal and was associated with higher TA than during the winter period. Thus, summer modelled $[DIC]_{ex}$ values must be taken with caution as they would be very sensitive to the assumed carbonate weathering contribution.

3.3. Application of the model to the three rivers of the Arcachon lagoon catchment

Applying our streamCO_2-DEGAS model to the pCO_2, TA and $\delta^{13}C$-DIC measured in rivers allows an estimation of the CO_2 degassing from waters to the atmosphere. This estimation can be added to the fluxes of other carbon species transported by rivers to provide the total carbon loss from terrestrial systems through the hydrological network. Field data show that HCO_3^- from rock weathering and CO_2^* from respiration are of the same order or magnitude (Table 1). Model results indicate that, at the three studied rivers, carbonate weathering is a minor contributor to the TA and DIC fluxes (Table 3). Modelled $[DIC]_{ex}$ were of the same order of magnitude as the *in situ* DIC concentrations. The yearly averaged contribution of TA to DIC was minor in the three rivers, with a maximum of 27% in the Leyre River, among which 20% was silicate weathering and 7% was carbonate weathering (Table 3). On a yearly average, the relative proportions of HCO_3^- export, CO_2^* export and CO_2 degassing were 10:10:80%, 13:14:73% and 27:7:66% at the outlet of the Renet, Milieu and Leyre Rivers, respectively. These proportions reveal that a large fraction of the DIC entering the river water rapidly escapes as CO_2 upstream of the sampling point, as already noted in several other studies in headwaters (*e.g.*, Billett et al., 2004; Johnson et al., 2008; Davidson et al., 2010). The highest modelled $[DIC]_{ex}$ of more than 3 mmol L^{-1} occurred in the

Renet stream in summer, when the measured *in situ* pCO_2 values were more than 7000 ppmv (Table 1 and 3). Seasonality of all DIC concentrations was much more pronounced in the Renet and Milieu small streams than in the larger Leyre River, in which there was higher observed pCO_2 and modelled $[DIC]_{ex}$ during low flow. A similar negative concentration-discharge relationship was observed in a peatland stream, as deep soil and groundwater were the major source of aquatic CO_2 (Dinsmore and Billett, 2008). Modelled soil pCO_2 varied from 2400 ppmv in the Milieu River at high discharge to more than 77 000 ppmv in the Renet stream at low discharge. When multiplied by the river discharge, modelled $[DIC]_{ex}$ provided a quantity of CO_2 that had degassed from the river water surface to the atmosphere (Table 3). After dividing this quantity by the river surface area, we obtained CO_2 water-air fluxes ranging from 20 mmol m^{-2} d^{-1} in the Milieu stream in winter to more than 6000 mmol m^{-2} d^{-1} in the Renet stream in summer (Table 3). To calculate the corresponding gas transfer velocities (K_{600}), we attempt to account for the downstream decrease in pCO_2 along small streams (Dawson et al., 1995; Johnson et al., 2008) by assuming the water pCO_2 as the average of the modelled soil pCO_2 and the observed water pCO_2 at the downstream sampling point. Gas transfer velocities, normalised to a Schmidt number of 600 according to Wanninkhof (1992), varied between 1 cm h^{-1} in the Milieu River in summer and 30 cm h^{-1} in the Renet River in winter.

	Renet		Milieu		Leyre	
DIC concentrations (mmol L^{-1})						
HCO_3^- from carbonate weathering	0.010 ± 0.002	0.007~0.015	0.000		0.022 ± 0.008	0.008~0.035
HCO_3^- from silicate weathering	0.251 ± 0.041	0.178~0.355	0.104 ± 0.019	0.082~0.153	0.296 ± 0.103	0.112~0.458
CO_2^* dissolved in water	0.263 ± 0.056	0.075~0.334	0.110 ± 0.018	0.076~0.139	0.079 ± 0.019	0.057~0.135
$[DIC]_{ex}$	2.112 ± 0.822	0.063~3.401	0.592 ± 0.425	0.015~1.402	0.800 ± 0.693	0.0290~2.540
Total DIC exported from land	2.637 ± 0.873	0.38~3.94	0.806 ± 0.436	0.222~1.626	1.197 ± 0.766	0.358~3.025
Modelled soil pCO_2 ($pCO_{2init.}$) (ppmv)	49 280 ± 18 700	2 630~77 860	14 100 ± 8 400	2 460~32 330	18 630 ± 16 400	2 120~63 670
DIC fluxes (t C day^{-1})						
HCO_3^- from carbonate weathering	0.005 ± 0.002	0.002~0.010	0.000		0.328 ± 0.094	0.19~0.548
HCO_3^- from silicate weathering	0.113 ± 0.049	0.052~0.25	0.050 ± 0.024	0.017~0.095	4.364 ± 1.251	2.518~7.278
CO_2^* dissolved in water	0.120 ± 0.059	0.034~0.273	0.056 ± 0.036	0.019~0.148	1.661 ± 1.784	0.333~8.241
CO_2 degassed to the atmosphere	0.952 ± 0.542	0.028~2.243	0.258 ± 0.199	0.009~0.631	10.671 ± 7.421	0.680~29.075
Total DIC exported from land	1.189 ± 0.627	0.169~2.704	0.364 ± 0.233	0.107~0.808	17.024 ± 9.063	7.012~41.19
River Surface Area (km^2)	0.028		0.036		1.77	
Water – air CO_2 fluxes (mmol m^{-2} d^{-1})	2 800 ± 1 600	83~6 600	596 ± 459	20~1 460	502 ± 349	32~1 368
K_{600} (cm h^{-1}) *	12 ± 7	5~30	8 ± 6	1~21	7 ± 5	2~22

Table 3. DIC parameters in the three rivers computed with the streamCO_2-DEGAS model (average ± standard deviation; min ~ max). * K_{600} was computed from the river surface area, the CO_2 modelled flux, and assumed a pCO_2 as the average of the modelled soil pCO_2 and the pCO_2 observed at the downstream sampling point.

4. Discussion

The originality of our modelling approach is involved in the estimation of CO_2 degassing from streams and rivers without the necessity of assuming a value for gas transfer velocity and water surface area, two parameters that are often difficult to estimate and that are always a matter of debate and uncertainty (e.g., Raymond and Cole, 2001). Instead of using these two parameters, our CO_2 degassing rates are computed as a theoretical $[DIC]_{ex}$, which mainly depends on initial assumptions on the carbon sources in soils and on the property of $^{12}CO_2$ to degas faster to the atmosphere than $^{13}CO_2$. This modelled $[DIC]_{ex}$ can then be multiplied by the river discharge, a parameter that is relatively easy to access. Current efforts in quantifying global CO_2 degassing from inland waters (e.g., Cole et al., 2007) are hampered by the fractal nature of these fluxes; throughout the river continuum, the smallest headwater surface areas are those that show not only the highest areal degassing rates, but also the highest heterogeneity in pCO_2 and gas transfer velocity. This is one of the main interests for developing an integrative method as proposed here with the streamCO_2-DEGAS model. After first providing some evidence of the validity of our approach based on its application at the three study sites, we then critically analysed its principle and sensitivity to some hypothesis and parameters and proposed some guidelines for future improvements and application elsewhere.

4.1. Validation of the model at the study sites

At our three study sites, modelled soil pCO_2 values (Table 3) and seasonal trend were consistent with those observed in organic-rich, acidic soils. In a compilation of data from the upper meters of soils around the world, Amundson and Davidson (1990) reported pCO_2 between 400 and 130 000 ppmv. In undisturbed forested watersheds of the Amazon basin, Johnson et al. (2008) reported a very constant and consistent pCO_2 of ~52 000 ppmv in deep (8 m) soils and in groundwater springs. In Scottish peat soils, Dinsmore and Billett (2008) measured pCO_2 between 20 000 and 30 000 ppmv. In a temperate, hardwood-forested catchment, Jones and Mulholland (1998) modelled soil pCO_2 that varied from 907 in winter to 35 313 ppmv in summer. As the result of enhanced summer soil respiration concomitant with a larger contribution of CO_2-enriched deep groundwater to the stream waters, our highest modelled soil pCO_2 occurred during low flow, as reported in other studies (Jones and Mulholland 1998; Dinsmore and Billett, 2008). Thus, our model was able to reproduce a logical seasonal pattern of soil pCO_2 from only concentrations and isotopic data in the stream waters. The highest soil pCO_2 was found in the Renet stream, which showed the highest *in situ* water pCO_2, especially during summer months (Table 1). According to

the model, the CO_2 degassing from the Renet stream was the highest, followed by the Leyre and the Milieu watercourses. Even if less negative δ^{13}C-DIC values were observed throughout the year in the Leyre River, the air/water initial pCO_2 gradient was weaker, and thus, CO_2 degassed in lower quantity to reach *in situ* values. Leading to the weakest CO_2 degassing of the three watercourses, the same phenomenon was observed in the Milieu stream, where depleted δ^{13}C-DIC values were measured. The model also showed that a maximum pCO_2 observed at a sampling point was always associated with a maximum soil pCO_2 and, thus, a maximum degassing upstream, as modelled $[DIC]_{ex}$ increased with *in situ* pCO_2 (Figure 6a,b). Due to enhanced gas exchange, lower pCO_2 levels in the river were never caused by stronger degassing upstream of the sampling point, as would be thought intuitively, but rather to lower CO_2 inputs from soils and groundwaters throughout the watercourse. In the Milieu River, water pCO_2 of less than 2000 ppmv occurred in winter and was associated with negative δ^{13}C-DIC values (about -18‰, Figure 2b) and was thus moderately impacted by isotopic equilibration with the atmosphere. In the Leyre River, pCO_2 levels of less than 1000 ppmv occurred in winter and summer and were associated with δ^{13}C-DIC values much less negative (about -12‰), which could suggest a stronger isotopic equilibration with the atmosphere and, thus, a larger CO_2 degassing. However, these lower pCO_2 values were also associated with higher DIC and TA, which were due to a significant contribution of carbonate weathering, which also raises the δ^{13}C-DIC (Figure 2a). Our model suggests that during these lower pCO_2 periods in the Leyre River, carbonate weathering has a much larger effect on the δ^{13}C-DIC than enhanced degassing upstream of the sampling point.

Our modelled areal CO_2 degassing fluxes between 20 and 6600 mmol m^{-2} d^{-1} (for instance, a yearly average of 2800 mmol m^{-2} d^{-1} in the Renet stream (Table 3)) appear larger than those reported in other streams with similar organic-rich surrounding landscapes (Table 4). Though in the upper range, yearly averages of 500 mmol m^{-2} d^{-1} in the Leyre River and 600 mmol m^{-2} d^{-1} in the Milieu stream are consistent with those previously reported. All previous studies were based on water pCO_2 data and a gas transfer velocity deduced from gas tracer injections or literature values. Such approaches do not account for the potentially high degassing rates in the vicinity of groundwater seeps in first-order headwaters and in very small, temporary streams along the stream banks, particularly at low-water stage. In four Amazonian streams, Johnson et al. (2008) reported a 90% degassing of the CO_2 transported by groundwater less than 50 m downstream of the spring emergence points. The fact that our integrative modelling approach accounts for these potential CO_2 degassing hotspots may explain why we obtain higher degassing rates. When compared to total carbon export, our modelled degassing rates are still consistent with those reported in some

other acid- and organic-rich streams. Indeed, the annual CO_2 degassing/total (organic and inorganic) carbon export ratio was 1.4 for the Renet stream, 0.5 for the Milieu stream and 0.6 for the Leyre River (Polsenaere et al. submitted). These ratios were consistent with those reported in boreal streams by Hope et al. (2001) (0.9), by Jonsson et al. (2007) (0.8) and by Rantakari et al. (2010) (between 0.5 and 2.9).

Using a water pCO_2 value as the average between the modelled soil pCO_2 (the initial pCO_2 in the model) and the observed pCO_2 at the downstream sampling point, our calculated K_{600} values were between 1 and 22 cm h^{-1} (Table 3); these values were, in contrast to the CO_2 fluxes, consistent with those reported by Wanninkhof et al. (1990) in small rivers and streams using gas tracers techniques or those given by the O'Connor and Dobbins (1958) equation. Spatial and temporal variations were consistent with the potential drivers of turbulence in the rivers. The lowest value of 1 cm h^{-1} in the Milieu stream corresponded to an unusually negative δ^{13}C-DIC of -24 ‰. At the three sites, the lowest values occurred at low water discharge. All sites had a sandy bottom with a moderate roughness, so lowering water current had a greater potential influence than lowering water height (O'Connor and Dobbins, 1958; Wanninkhof et al., 1990). The Milieu stream had a straight channel shape, where water flowed without hindrance, water height was reduced to about 10 cm in summer, and the K_{600} was consistently the lowest; the Renet stream was also shallow, but tree trunks across the river created small waterfalls consistent with higher K_{600}. In a similar shallow and turbulent stream, Wanninkhof et al. (1990) measured a K_{600} of nearly 60 cm h^{-1} using SF_6 injection. Finally, the Leyre River was always more than one meter depth, but trunks and branches near the edges generated turbulence and eddies, particularly at high flow.

Site	CO_2 degassing mmol m^{-2} d^{-1}	Method	Reference
Temperate humid hardwood forest	146-353	pCO_2 and K_{600} from propane injection (1)	Jones and Mulholland 1998
Lowland temperate peatland	42-290	pCO_2 and K_{600} from propane injection (1)	Billet et al. 2004
Boreal deciduous forest	260	pCO_2 and K_{CO2} constant at 16 cm h^{-1} (2)	Teodoru et al. 2009
Coniferous boreal forests	640	pCO_2 and K_{600} 23 cm h^{-1} (small streams) and 6.6 cm h^{-1} (main stream)	Jonsson et al. 2007
Ombrotrophic peat bog	60-980	Chamber and wind speed model	Billett and Moore 2008
Amazonian rainforest	260-780	pCO_2 and K_{600} 10-25 cm h^{-1}	Davidson et al. 2010
Temperate coniferous forest on sandy podzolised soils	502-596-2800	StreamCO_2-DEGAS model (yearly averages in 3 streams)	This study

Table 4. Comparison of CO_2 degassing areal rates in various streams

(1) Value not specified
(2) Water temperature not specified in the study, so K could not be normalised to a Schmidt number of 600.

4.2. Critical analysis and further improvements

Although our modelling approach appears to be a promising tool to compute CO_2 degassing rates in acidic rivers and streams, a careful analysis of model sensitivity to various factors must be performed to provide guidelines for further improvement and application elsewhere. The first problem that must be addressed is the extreme, non-linear dependence of modelled $[DIC]_{ex}$ on *in situ* pCO_2 and δ^{13}C-DIC, particularly at low TA. $[DIC]_{ex}$ versus pCO_2 and versus δ^{13}C-DIC are both strongly convex curves (Figure 6a, b, c, d). As a consequence, the sensitivity (and, thus, the relative error) of $[DIC]_{ex}$ due to absolute accuracy in pCO_2 and δ^{13}C-DIC measurements increases with the $[DIC]_{ex}$ value itself. In Figure 6a, $[DIC]_{ex}$ versus pCO_2 curves are close to vertical when pCO_2 is low, and δ^{13}C-DIC is less negative. Curves are wider at higher pCO_2 and at more negative δ^{13}C-DIC. This tendency is more pronounced at low TA than at moderate TA (figures 6a, b), as the HCO_3^- pool acts as a buffer for the δ^{13}C-DIC increase during degassing, while in acidic waters it does not affect the pCO_2 decrease (Figure 3). Modelled $[DIC]_{ex}$ is 0.779 mmol L^{-1} in case 1 of figure 6 (absence of carbonate rock weathering, TA = 0.1 mmol L^{-1}, δ^{13}C-DIC = -20‰ and pCO_2 = 3500 ppmv), typical conditions observed in the Milieu stream (Table 1). If pCO_2 increases by 10% (from 3500 to 3850 ppmv) and all other parameters are unchanged, $[DIC]_{ex}$ increases by 66% (from 0.779 to 1.293 mmol L^{-1}). In case 2 (absence of carbonate rock weathering, TA = 0.1 mmol.L^{-1}, δ^{13}C-DIC = -14‰ and pCO_2 = 1300 ppmv), modelled $[DIC]_{ex}$ is 0.786 mmol L^{-1}. If pCO_2 increases by only 10% (from 1300 to 1430 ppmv) and all other parameters are unchanged, $[DIC]_{ex}$ is multiplied by a factor of 5.5 (from 0.786 to 4.341 mmol L^{-1}). This effect can be explained mathematically; at the high (less negative) δ^{13}C-DIC value of case 2, the contrast in δ^{13}C between the soil and the river water downstream becomes maximal, so an extremely high initial soil pCO_2 is necessary to reach the convergence of both δ^{13}C-DIC and pCO_2 at the same iteration (boxes C and D in figure 4). As a consequence, small changes in the water pCO_2 lead to large changes in the initial pCO_2 and, thus, in the calculated $[DIC]_{ex}$ (Figure 6c). In fact, case 2 conditions probably never occur in nature: first, we obtained such high $[DIC]_{ex}$ values only when water pCO_2 was also high (the maximum $[DIC]_{ex}$ of 3.4 mmol L^{-1} in the Renet stream corresponded to an *in situ* pCO_2 of 7600 ppmv); second, such a high δ^{13}C-DIC value of -14‰ occurs in natural waters only when some carbonate weathering occurs and the TA is much higher than 0.1 mmol.L^{-1} (e.g., Jin et al., 2009). As shown in Figure 2, δ^{13}C-DIC values in the Leyre River that were higher than -15‰ were associated with higher DIC but lower pCO_2; thus, δ^{13}C-DIC values corresponded to higher TA due to some carbonate weathering (Polsenaere et al., submitted).

A second, and in some cases, more difficult problem of our modelling approach came from the sensitivity to TA and carbonate weathering, particularly at TA values below 0.3 mmol L^{-1} and at high pCO_2 (Figures 6f and 8d). $[DIC]_{ex}$ was much lower at low pCO_2 (1000 ppmv in Figure 6e) and was weakly affected by the TA value (Figure 6e) at classical δ^{13}C-DIC values of less than -15‰. In the case of the Milieu stream, which had the lowest TA, the sensitivity of modelled $[DIC]_{ex}$ on TA was modest, as also pCO_2 is moderated. In the Leyre River, where TA was higher and obviously affected by carbonate weathering, pCO_2 was low, so modelled $[DIC]_{ex}$ was not as sensitive to the assumptions regarding the quantity of carbonate weathering (Figures 8b, d). In the Renet Stream, however, where pCO_2 was often higher than 5000 ppmv, TA was exactly in the range where modelled $[DIC]_{ex}$ varied considerably with both the TA value (Figure 6f) and the assumed carbonate weathering contribution to TA (Figure 8d). If the carbonate weathering contribution in the Renet Stream was higher than the one predicted using Meybeck's (1987) end-members, it could lead to overestimated $[DIC]_{ex}$ and partly explain why, compared to the literature, the streamCO_2-DEGAS model gave high CO_2 degassing rates in this stream.

A third problem is the sensitivity to assumptions on the isotopic composition of the initial soil pCO_2. Here we assumed a year-round δ^{13}C-SOM value of -28 ‰, which corresponded to a fairly constant δ^{13}C-POC value in the three rivers. According to Eqn. 1, we assumed an isotopic fractionation of ^{13}C-CO_2 due to molecular diffusion of +4.9‰, which was consistent with those found in the laboratory and in other catchments (Cerling et al., 1991; Davidson, 1995; Jin et al., 2009). The basis of this assumption was that the majority of soil respiration occurs in well-drained conditions. If a significant part of the respiration occurs in waterlogged soils or in the aquatic system itself, the respired CO_2 will not undergo such isotopic fractionation, as molecular diffusion of CO_2 in water is weaker than in air (O'Leary, 1984; Amiotte-Suchet et al., 1999). In fact, we do not have direct field evidence that all of the respiration primarily occurs in well drained-soil. We could only expect that in these sandy soils, the upper, well drained organic-rich soil horizon was the major site of respiration. As shown in Figure 7, modelled $[DIC]_{ex}$ concentrations were very sensitive to the isotopic composition of the soil organic carbon, so they were also sensitive to the assumed isotopic fractionation of CO_2 in the soil. If respiration in groundwater and in river waters and sediments was significant, then the initial ^{13}C-CO_2 would have been more negative, and the modelled $[DIC]_{ex}$ would have been even higher than those we obtained here.

It is evident that this work is only a first attempt and needs improvement and stronger validation. The uncertainties of our approach could be significantly reduced by adapting the sampling strategy to the model needs. First, sampling groundwater would allow better constraint of the initial conditions (for both pCO_2 and δ^{13}C-DIC). Then, to validate our approach, we would conduct a well-designed study in a headwater section with a simple morphology that included the following: systematic seasonal groundwater, springs and stream water sampling, water and sediment respiration measurements and, eventually, some coupled gas tracer injection experiments. We could verify some model assumptions, concerning, for instance, isotopic fractionation of CO_2 in soils, the contribution of carbonate weathering, and the impact of TA. Comparing sites with well known and contrasting lithologies would also provide helpful information to better constrain the effect of carbonate weathering on model results

5. Conclusion

Using only pCO_2, DIC and δ^{13}C-DIC, we tested the possibility of estimating CO_2 degassing from acidic streams and small rivers draining organic rich soils. To support the field data, we developed a conceptual and numerical model that calculates a theoretical concentration of DIC that must have degassed to the atmosphere given some reasonable assumptions about carbon sources and isotopic composition in soils. The sensitivity of the model results to measured or assumed parameters suggests that, in the ranges commonly found in nature, the uncertainty in our approach should not be larger than that of classical methods. Although the model was poorly constrained (with soil or groundwater data, for instance), it computed CO_2 degassing values consistent with the literature at two study sites, but also one value relatively larger that the literature values at another site. It was not possible to fully explain why our model gave higher fluxes in the latter stream; on one hand, our method may better account for intense degassing at the vicinity or groundwater seeps; on the other hand, assumptions on the significance of carbonate weathering may be critical under the conditions encountered in this stream. Because acidic, humic-rich waters are probably a significant fraction of global freshwater CO_2 degassing, and because a large database of pCO_2, DIC and δ^{13}C-DIC is already available in some streams worldwide, our integrative method has great potential for application. Even if more efforts are necessary to definitively validate the approach, preliminary results presented here should encourage future research in this direction.

Acknowledgements

This model would not exist without setting up the δ^{13}C-DIC method at the EPOC laboratory thanks to the help of our colleague Nicolas Savoye, and the numerous advices of Steven Bouillon from the Katholieke Universiteit Leuven. We are also grateful to our colleague Vincent Marieu for his help in Matlab programming. This paper is a contribution to the ANR PROTIDAL project coordinated by Pierre Anschutz.

II.2. EXPORT AND DEGASSING OF TERRESTRIAL CARBON FROM SMALL RIVERS AND STREAMS DRAINING A TEMPERATE SANDY PODSOLISED CATCHMENT

Résumé

Les variations spatiales et temporelles des concentrations et compositions isotopiques du carbone ont été suivies durant un cycle hydrologique complet dans neuf rivières et ruisseaux du sud-ouest de la France, drainant un bassin versant sableux de type podzol et alimentant la lagune d'Arcachon. Le bassin correspond à une plaine uniforme où les formations sableuses, la forêt de pins et les sols enrichis en matière organique (podzols) dominent. Dans ces eaux de rivières acides (pH de 5.6-7), le carbone organique particulaire (POC) représente la plus faible contribution au carbone total (concentration : 0.138 ± 0.05 mmol L^{-1}) du fait d'une érosion mécanique des sols limitée. Les teneurs importantes de POC dans les matières en suspension (20 ± 3% des matières particulaires en suspension (SPM)), les faibles concentrations en Chlorophylle *a* et les compositions isotopiques du POC (δ^{13}C-POC) relativement constantes, proche de -28‰ tout le long de l'année, montrent que ce POC est issu de plantes terrestres en C_3 et des détritus du sol, avec de faibles niveaux de production autochtone. En opposition, la présence de podzols sur le bassin versant confère des niveaux d'exportation de carbone organique dissous (DOC ; concentration : 0.55 ± 0.2 mmol L^{-1}) très forts. Avec une concentration de 0.488 ± 0.19 mmol l^{-1}, le carbone inorganique dissous (DIC) représente la deuxième contribution à l'export de carbone vers la lagune ; 35% de ce DIC est sous la forme de CO_2 en excès alors que le reste est sous forme d'ions bicarbonates. La composition isotopique du DIC (δ^{13}C-DIC) reste négative (environ -20‰) tout au long de l'année dans une majorité de cours d'eau, révélant la prédominance de la minéralisation de carbone terrestre et de la dissolution des roches silicatées dans les sols, comme source majeure de DIC dans les rivières. Dans les autres rivières, l'érosion locale de roches carbonatées augmente de façon concomitante les valeurs d'alcalinité à 1 mmol L^{-1} et de δ^{13}C-DIC à -7‰. De plus, une valeur de δ^{13}C-DIC moins négative, associée à des niveaux faibles de pCO_2 mesurés dans les eaux de la rivière la plus grande du bassin, révèlent les quantités significatives de CO_2 dégazées en amont du point de mesure. Avec des valeurs de pCO_2 situées entre 1000 et 10 000 ppmv, toutes les rivières se comportent comme une source de CO_2 vers l'atmosphère, particulièrement en période de basses eaux, lorsque le débit des eaux souterraines domine celui des eaux de surface. Le dégazage de CO_2 depuis les eaux de rivières de surface vers l'atmosphère représente un flux additionnel de carbone qui est similaire ou même plus grand que l'export latéral de DOC. Le dégazage et l'export total de carbone depuis ces neuf rivières est estimé à 116 t C km^{-}

^{2} yr^{-1}, réparti entre le dégazage de CO_2 vers l'atmosphère (43%), l'export de DIC (21%), l'export de DOC (29%) et l'export de POC (7%).

Abstract

Spatial and temporal carbon concentrations and isotopic compositions were monitored during a complete hydrological cycle in nine acidic watercourses draining a lowland forested sandy podsolised catchment, flowing into the Arcachon lagoon. In river waters, particulate organic carbon (POC) was the lowest contributor to the total carbon (0.138 ± 0.05 mmol L^{-1}) because of the limited mechanical soil erosion. The general high POC content in the suspended matter (20%), low Chl *a* concentrations and the relatively constant δ^{13}C-POC value (near -28‰) throughout the year reveal that this POC originates from terrestrial C_3 plant and soil detritus. In contrast, the presence of podsols leads to large levels of dissolved organic carbon (DOC; 0.55 ± 0.2 mmol L^{-1}). Dissolved inorganic carbon (DIC) was the second largest contributor to the export of carbon to the lagoon (0.488±0.19 mmol L^{-1}). The δ^{13}C-DIC value approximately -20‰ throughout the year in many small rivers revealed the predominance of terrestrial carbon mineralisation and silicate rock dissolution in soils as the major DIC source in the rivers. In the other rivers, some local weathering of carbonate rocks concomitantly increased the total alkalinity (TA) to 1 mmol L^{-1} and the δ^{13}C-DIC to -7‰. With pCO_2 between 1000 and 10000 ppmv, all of the rivers were a source of CO_2 to the atmosphere particularly during the low river stage. CO_2 degassing represents an additional carbon flux similar to or even greater than the lateral DOC export. Finally, the total carbon degassing and export from these nine rivers was estimated to 116 t C km^{-2} yr^{-1}.

1. Introduction

Rivers deliver significant amounts of terrestrially-derived carbon from the land to the sea, representing the main linkage between these two reservoirs. Approximately 0.9 Gt C yr^{-1} is discharged by rivers to oceans (Meybeck 1982). Of this total carbon flux value, about 40% is organic and 60% is inorganic (Meybeck 1993). Nevertheless, the role of rivers in the global carbon cycle is not limited to the passive transport of carbon to the oceans. In fact, a large part of the carbon that is lost from terrestrial systems degasses as CO_2 to the atmosphere from the surfaces of inland waters and does not reach the ocean (Cole et al. 2007; Ciais et al. 2008). Recent data compilations suggest that, globally, the degassing of CO_2 from inland waters could be occurring at levels that are similar to or larger than the export to the ocean (Cole et al. 2007; Tranvik et al. 2009).

The concentration and composition of carbon in river waters is partly a product of instream processes, but is in its majority regulated by upland, riparian and hyporheic/groundwater processes that determine solute and gaseous inputs into aquatic systems (Hynes 1975; Jones and Mulholland 1998). In most rivers, the particulate organic carbon (POC) is allochthonous and originates from soil erosion; additionally, in some eutrophied rivers, phytoplankton can produce highly autochthonous POC (Etcheber 1983; Abril et al. 2002; Neal et al. 2006). Dissolved organic carbon (DOC) in unpolluted rivers mostly originates from leachable organic carbon in soils and from terrestrial vegetation (Meybeck 1993; Sobek et al. 2007). This DOC is often considered to be mainly recalcitrant to microbial degradation and is almost entirely transported to the ocean (Mantoura and Woodward 1983). However, part of this DOC serves as a substrate for heterotrophic bacteria and fuels the aquatic trophic chain through the microbial loop in freshwaters (Hollibaugh and Azam 1983; Tranvik 1988; Pace et al. 2004). Additionally, autochthonous labile DOC can be produced within rivers by phytoplankton (Bianchi et al. 2004). Most rivers and lakes are net heterotrophic and emit carbon dioxide (CO_2) to the atmosphere (Jones et al. 2003; Sobek et al. 2005; Billett and Moore 2008). CO_2 is typically supersaturated in streams and rivers that are connected to CO_2-rich groundwater and soils and because of instream organic matter decomposition, which exceeds primary production in the river itself (Kling et al. 1991; Jones and Mulholland 1998; Cole and Caraco 2001). Thus, inland aquatic systems are almost always supersaturated in CO_2 and represent net sources of CO_2 (Cole et al. 1994; Hope et al. 1994; Jones et al. 2003). The CO_2 that is found in freshwater is produced by roots and bacterial respiration in the soil, groundwaters, wetlands, waters and sediments. It is also influenced by silicate and carbonate rock weathering, producing carbonate alkalinity rather than dissolved CO_2

(Yang et al. 1996; Amiotte-Suchet et al. 1999). In the presence of carbonate rocks on the watershed, one half of the total alkalinity (TA) originates from the rock, with the rest being atmospheric carbon that has been fixed on land and recycled in the soils; these rivers generally have a high pH, high dissolved inorganic carbon (DIC) and TA, and a relatively heavy isotopic composition of DIC (Barth et al. 2003; Wachniew 2006). When, in contrast, silicate rock weathering is dominant, all of the DIC originates from soil organic matter mineralisation; these rivers are acidic, have low TA and a large fraction of the DIC is present as excess CO_2 with respect to the atmospheric equilibrium (Amiotte-Suchet et al. 1999).

Thus far, several studies on inland water carbon dynamics and their exportation to oceans have been carried out; for example, in estuaries (Frankignoulle et al. 1998; Abril et al. 2002), lakes (Kling et al. 1991; Cole et al. 1994), large rivers (Meybeck 1993; Hope et al. 1994; Gaillardet et al. 1999) and stream waters (Hynes 1983; Neal and Hill 1994; Jones and Mulholland 1998). A few studies have dealt with rivers and streams in a lowland acidic catchment with organic matter-enriched soils and have attempted to estimate not only carbon lateral export as particles and solutes but also CO_2 degassing to the atmosphere along the entire river course (Billett et al. 2004; Hope et al. 2001). Here, we present a one-year survey of carbon dynamics in rivers and streams that drain a temperate, lowland, sandy, podsolised catchment and flow into the Arcachon lagoon (southwest of France). In this paper, we describe the dynamics of all of the carbon forms (particulate, dissolved, organic, inorganic and gaseous) and we quantify simultaneously the carbon export to the lagoon and the CO_2 degassing to the atmosphere. Finally, we establish a regional carbon budget that can be compared to the net ecosystem production upstream inland and downstream in the lagoon.

2. Materials and Methods

2.1 Study site

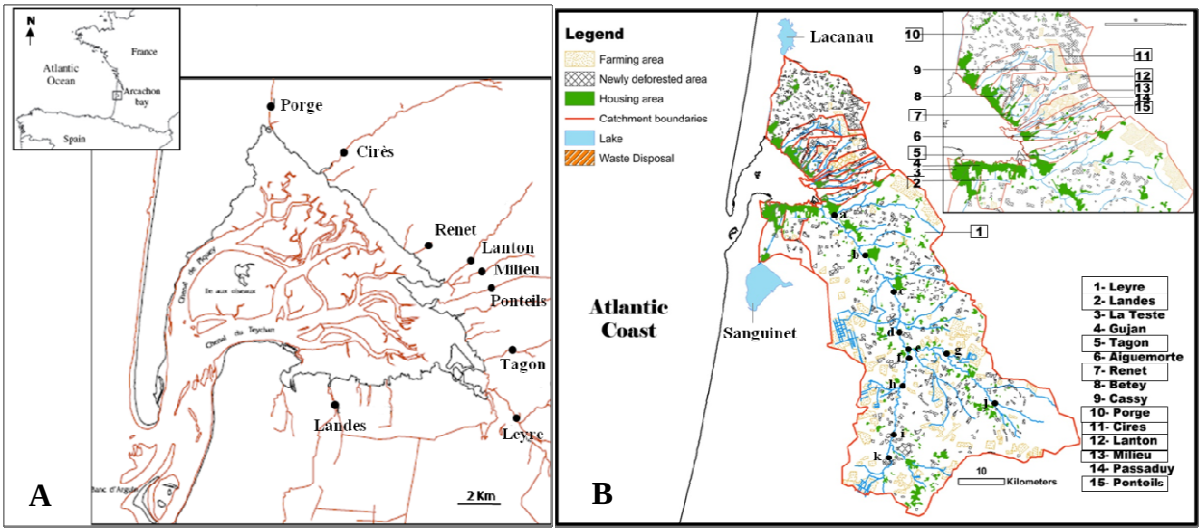

Figure 1. Map of the Arcachon lagoon and its direct catchment basin, showing A: the sampling stations for the nine watercourses, i.e., Porge, Cirès, Renet, Lanton, Milieu, Ponteils, Tagon, Leyre and Landes and B: the watercourse catchment boundaries, with soil occupation and the eleven stations that were sampled on the Leyre catchment, i.e., a, b, c, d, and e (La Leyre); f, h, i, and k (La Grande Leyre) and g, j (La Petite Leyre).

The study area is located in the Arcachon lagoon catchment in south-western France. In this area, urban wastewaters are collected and are directly delivered, after treatment, to the ocean from the lagoon; thus, they have a moderate impact on river water composition (De Wit et al. 2005). The Arcachon lagoon receives freshwater from several rivers (Fig. 1A; Table 1). The largest, in terms of watershed and discharge, is the Leyre River, located at the south-eastern corner. In addition, 17 streams with very low runoffs are distributed all around the lagoon, and two canals, Canal du Porge in the north and Canal des Landes in the south, also bring water from regulated dune lakes: the Lacanau Lake in the north, and the Cazaux-Sanguinet Lake in the south (Manaud et al. 1997; De Wit et al. 2005). The annual freshwater inputs into the lagoon average at 1.25 billion m^3, of which 8% is groundwater, 13% is rainfall and 79% is from watercourses (Rimmelin 1998).

	Surface (km^2)	Runoff ($m^3 s^{-1}$)	Drainage ($L s^{-1} km^{-2}$)	Population density (inhab km^{-2})	Inhabitants/ runoff (inhab $m^{-3} s$)
Porge (Arès)	221.6	3.63	18	310	17263
Cirès (Andernos)	48.7	0.63	13	445	34402
Renet (Lanton)	17.9	0.61	34	43	1283
Lanton (Lanton)	36.1	0.28	8	43	5562
Milieu (Audenge)	21.3	0.63	19	63	3313
Ponteils (Audenge)	23.3	0.23	10	63	6414
Tagon (Biganos)	29.6	0.67	23	113	4939
Leyre (Biganos)	2141.4	18.16	8	113	13360
Landes (Gujan-Mestras)	116.6	0.52	4	315	70703
Total	2656.5	25.34	137	1510	157239

Table 1. General characteristics of the nine studied watercourses in the Arcachon lagoon catchment. The Leyre average runoff was calculated from daily runoffs that were measured between the sampling period by the French institute of regional environment (DIREN). The Porge, Cirès, Lanton, Ponteils and Landes runoffs have been computed using the average of the measured runoffs from 1989 to 1993 (Auby et al., 1994). Other stream runoffs have been estimated from watershed areas, assuming that the surface/runoff ratio equals that of the Leyre catchment.

In total, the catchment is typical of lowlands, with a surface area of 4138 km^2 and slopes below 0.25%. It is relatively homogenous topographically, climatically (isohyets between 900 and 1000 mm) and geologically (Auby et al. 1994). Maritime pine forests occupy 84% of the catchment, with growth on the sandy soil of Pleistocene origin named *Sable des Landes* (Trichet et al. 1997). These soils are typical for podsols that occur on coarse, poor, siliceous parent materials (on periglacial sand deposits) under temperate humid climates (Lundström et al. 2000). These podsols are characterised by high acidity (pH typically between 4 and 5) low inorganic nutrient availability, and high carbon content that can reach 50 g per kg soil (Jolivet et al. 2007). Although mainly silicated, some Miocene-carbonated outcrops can be observed locally in this sandy catchment, particularly along the Leyre River (Folliot et al. 1993). Also, in the Ponteils catchment, the carbonate precipitates that are used by the landfill of the city of Audenge, closed since 2008, can be found inside soils (Canton et al. 2010).

The Sables des Landes contains a free and continuous water table covering more than 4000 km^2, close to the Arcachon lagoon. With a variable thickness of between 10 and 130 m, the water table is usually located very close to the surface in which the regime determines three main Landes types (Righi and Wilbert 1984). The hygrophilous lande occupies the major part of the Landes catchment, with a superficial water table below 1 m; the mesophilous lande, present in the middle and low watercourse valleys, is characterised by a strong water table amplitude of up to 2 m,

creating flooding and drying periods; and finally, an important water table with a downward pull occurs on the edge of the streams up to 3 m, thus characterising the xerophilous lande.

The area has been massively drained and forested with pine trees (*Pinus pinaster*) following the imperial decree of 1857, and currently pine forest is the major surface cover (84% of the area, Fig. 1B). Intensive farming of corn and other vegetables is now prevalent in areas from 130 to 280 km^2, which have replaced traditional farming area as well as forest (Auby et al. 1994).

2.2. Sampling strategy

Different watercourse types were sampled in this study, including the Leyre River with the highest runoff (18.2 $m^3 s^{-1}$, representing 80% of the total freshwater inputs), two canals with a particular water regime and several streams with very small runoffs (annual average below 0.7 $m^3 s^{-1}$). Nine rivers from the north to the south were sampled at their outlet into the lagoon during one year, from February 2008 to February 2009 (Fig. 1A; Table 1). These nine main watercourses have been chosen for this carbon study because they cover an area spanning from the north to the south, representing about 90% of the total catchment area and nearly the entire freshwater input into the lagoon. The streams present the highest drainages--in general above 10 L s^{-1} km^{-2}--due to their small watershed surface, and the north and south of the Arcachon catchment show the most important population densities, above 100 inhab km^{-2}. Consequently, these watersheds with high inhabitants to runoff ratios are subjected to more anthropogenic pressures, primarily through urban rainwater discharge, as most of the domestic load is being treated.

The Renet, Ponteils and Tagon streams and the Leyre River were sampled every two weeks, whereas the Porge and Landes canals and the Cirès, Milieu and Lanton streams were sampled every four weeks. In addition, a longitudinal sampling was carried out in October 2008 along the Leyre River to study the longitudinal variations in carbon and its associated parameters in this watershed (Fig. 1B). During the study, all carbon forms (organic, inorganic, particulate and dissolved forms, and isotopic ratios) were characterised, along with other parameters, in the nine rivers of the Arcachon lagoon watershed (Figs. 2 and 3; Tables 2 and 3).

2.3. Field techniques

In the field, the conductivity and temperature of the watercourses were measured with a portable probe, Cond340i, and the pH was measured using a combined electrode (Metrohm) quickly after sampling. The subsurface water was sampled and then filtered back to the laboratory the same day to measure levels of SPM, POC, δ^{13}C-POC, C/N and Chl *a*. The filtered water was then used for a total alkalinity (TA) analysis.

Dissolved organic carbon (DOC) samples were obtained after a water filtration in the field through pre-combusted GF/F filters (porosity of 0.7 µm) in decontaminated Pyrex vials (25 ml) and acidified with HCL 37%. The DOC filtrates were stored at 4°C before analysis at the laboratory.

Water required to measure the stable isotope composition of the dissolved inorganic carbon (δ^{13}C-DIC) was obtained by overfilling 100 ml glass headspace vials, setting the vials and then poisoning the sample with $HgCl_2$ solution to avoid bacterial activity. The samples were stored in the dark before analysis.

The CO_2 partial pressure (pCO_2) in river waters was directly measured by a homemade portable equilibrator system that was used in the field (following Frankignoulle et al. 2001). An Infra Red Gas Analyzer (LI-COR®, LI-820) was used to measure the pCO_2 in dry air that was equilibrated with freshwater. The LI-820® was calibrated at the laboratory one day before the field experiment using two gas standards of 0 and 2959±59 ppmv. The equilibrator consists of a Plexiglas cylinder (height: 30 cm, diameter: 8 cm) that is filled with marbles to increase the exchange surface area. The system works as a closed system: water, through a portable peristaltic pump (Masterflex®, 1 L min^{-1}), runs from the top to the bottom of the equilibrator, and air is pumped upwards (1 L min^{-1}). The pCO_2 of air equilibrates with the pCO_2 of water and is then measured by the LI-COR® after being dried by a Dierite grain tube. After 7 min. the pCO_2 is constant and the entire equilibration between the air and water is achieved; then, measurements are recorded with the datalogger LI-1400®.

2.4. Laboratory analyses

The water for SPM and POC measurements was filtered through pre-weighed and pre-combusted Whatman GF/F glassfibre filters (0.7 µm of porosity). The filters were then dried at 60°C and stored in the dark; subsequently, the SPM was determined by the weight difference. POC was measured using the same filter; the filters were acidified in crucibles with 2N HCL to remove carbonates and were then dried at 60°C (Etcheber et al. 2007). The POC content was measured by combustion using a LECO CS 125 analyser. The POC in mg L^{-1} and POC in % (of SPM) were then calculated. The uncertainty was ± 0.05% of SPM.

The DOC concentrations were measured with a SHIMADZU TOC 5000 analyser, which in principle is based on thermal oxidation after a DIC removal step (Sharp 1993; Cauwet 1994). The precision is better than 2%.

The water for Chl *a* measurement was filtered through GF/F filters, which were stored in the dark at -80°C until analysis. Pigments were extracted with 90% acetone, and the fluorescence was measured before and after acidification (Yentsch and Menzel 1963; Strickland and Parsons 1972).

The total alkalinity (TA) was measured by titration with HCl 0.1 N on 100 ml filtered samples and was calculated by a Gran function linearisation (Gran 1952) between pH 4.2 and pH 3. The reproducibility between the measures was better than ± 5 µmol L^{-1}.

The water for the measurement of δ^{13}C-POC and the C/N ratio was filtered through pre-combusted GF/F filters. The filters were dried and stored in pre-cleaned glass vials; prior to the analysis, the filters were decarbonated using HCl 12 N and dried overnight (Lorrain et al. 2003). The measurements were performed by coupling an elemental analyser (EA; Carlo Erba NC2500) to an Isotope Ratio Mass Spectrometer (IRMS; Micromass Isoprime). The carbon isotope ratio is expressed in the delta notation (δ^{13}C) relative to Pee Dee Belemnite. The δ^{13}C-POC levels were calibrated against the lab standards of Acetanilide (-26‰), Glycine (-45.2‰), Caseine (-23.3‰) and Bassin (-17.55‰), which were themselves calibrated against certified standards (IAEA-CH6, -10.45‰; IAEA-CH7, -32.15‰; and USGS24, -16.05‰). The C/N ratio was calibrated against certified acetanilide. The reproducibility of the δ^{13}C-POC levels and the C/N ratio was better than ± 0.2‰ and ± 0.2, respectively.

The δ^{13}C-DIC measurements were made following Gillikin and Bouillon (2007). In 100 ml vials that were filled to the top, a headspace was first created with Helium gas to obtain a volume of approximately 20% of the total volume of the vial. Then, 0.3 ml of warm 85% phosphoric acid was added to transform the carbonate forms into CO_2. To ensure gas equilibration, the vials were shaken and placed upside down for 1.5 h. The samples were measured using the above-mentioned EA-IRMS by injecting 3 mL of the CO_2 gas that was contained in each vial headspace through an injection port that was mounted before the water trap of the EA. δ^{13}C-DIC was calibrated against a homemade standard (45 mg of Na_2CO_3 were dissolved in a vial, flushed with He gas flow, with 3 ml of H_3PO_4) that had been calibrated against a certified standard (NBS19, -1.96‰) using a dual-inlet IRMS (Micromass Isoprime). The isotopic value of the standard Na_2CO_3 found was -4.5 ± 0.2‰. Finally, the equation of Miyajima et al. (1995) was applied to correct for the partitioning of the CO_2 between the headspace and the water phase and to calculate the δ^{13}C of the total DIC. The repeatability was approximately ± 0.1‰ between samples.

The DIC concentration was calculated from the pCO_2 and TA measurements (in addition to the water temperature) by resolving inorganic carbon system equations using dissociation constants from Mehrbach et al. (1973). The excess CO_2, defined as the quantity of DIC that was theoretically transferred as CO_2 to the atmosphere after water-air equilibration, was calculated as

the difference between in situ DIC and a theoretical DIC at the atmospheric equilibrium, following Abril et al. (2000).

The GraphPad Prism 5 and Xlstat softwares were used for statistical analysis. The Shapiro-Wilk test was used to test the normality of the data, followed by the Kruskal-Wallis test (in the case of nonparametric data) for analysis of variance (ANOVA) and the Dunn's multiple comparison test (post-test).

3. Results

3.1. Organic carbon distribution in the nine rivers flowing to the Arcachon lagoon

The average organic carbon and associated parameters, as well as their seasonal patterns, are presented in Table 2 and Figure 2 for each river. The water temperature, with an average of 12.9 ± 0.5°C, showed a typical annual trend with values ranging from 3.5°C during winter to 19.6°C during the summer period, with both canals showing the highest temperatures. The water conductivity varied little in all of the rivers throughout the year (near 205 ± 31 µS cm^{-1}), with the exception of the Porge canal, where conductivity can reach 4420 µS cm^{-1} (salinity of 1.9) depending on the tidal rhythm during the sampling day; in fact, the canal links the Lacanau lake to the lagoon in the North (Fig. 1).

The Leyre runoff (Fig. 2) during the sampling period presented a hydrological regime that is typically observed in south-western France (Pardé 1956). It consisted of short flooding periods in the spring (*ca*. 30 $m^3 s^{-1}$) related to important precipitations, then a low water flow throughout the summer period and finally, in the late autumn and winter, river runoff maxima reaching up to 100 $m^3 s^{-1}$. The SPM (Figs. 2A, B and C) did not show any clear seasonal pattern and was low during the year, generally below 20 mg L^{-1}. The average was 8.4 ± 3.4 mg L^{-1}; the lowest values were found in the Landes canal (2.7 ± 1.1 mg L^{-1}), and the highest values were found in the other canal and the streams (near 10 mg L^{-1} on average). In addition, some high values were measured during flood events (in the Leyre River, day 336 with 16.4 mg L^{-1}; Fig. 3C). Similarly, the values of POC concentrations were weak in these poorly turbid waters of the lowland regions, from 0.7 ± 0.3 mg L^{-1} in the Landes canal to only 2.49 ± 2.2 mg L^{-1} in the Tagon stream (Table 2). Nevertheless, the POC content (% of SPM) was high throughout the year, varying from about 16% (in the Leyre River) to 24% (in the Porge canal), with maxima in late autumn/winter and spring (Figs. 2D, E and F). δ^{13}C-POC was somewhat constant throughout the year without any clear trend. The average value of -28.59‰ is typical of terrestrial C_3 plants (Mook and Tan 1991). Also, the C/N ratios did not show any clear seasonal pattern, with values ranging between 12 ± 0.9 in the Landes

canal and 19.9 ± 2.2 in the Lanton stream (Figs. 2G to 2L; Table 2). Chl *a* was low in the Arcachon lagoon catchment rivers throughout the year, with an average of 1.3 ± 1.4 µg L^{-1}. The lowest values, below 1 µg L^{-1}, were found in streams, such as the Cirès or Ponteils, even if higher values were observed in the other watercourses, particularly in the Porge canal, with a bloom of 17.5 µg L^{-1} occurring on day 197 (Fig. 2M). As a consequence, the mean POC/Chl *a* ratios were always high--ranging from 580 to 4200 in the Landes canal and the Milieu stream, respectively--but exhibited large differences between the seasons, reflecting the annual pattern of the Chl *a* concentration (Table 2).

The DOC in the nine rivers presented an annual average of 6.6 ± 2.2 mg L^{-1} (Figs. 2P, Q and R; Table 2), with the highest values of up to 8.0 mg L^{-1} in the Porge canal and the Tagon and Ponteils streams, and the lowest values between 4.2 and 5.8 mg L^{-1} in the other watercourses. Furthermore, the DOC concentration showed a seasonal pattern during the sampling year, with significant differences (ANOVA, p-value: 0.0074) between the summer and the winter or spring, where the highest values were measured (Figs. 2P, Q and R). The TOC concentration ranged between 5.7 ± 1.1 and 13.3 ± 2.1 mg L^{-1} in the Landes and Porge canals, respectively (annual average of 8.2 ± 2.6 mg L^{-1}). The DOC/POC ratio ranged between 2 and 8, showing the predominance of DOC to POC in these lowland rivers (Table 2).

	T (°C)	Conductivity ($\mu S\ cm^{-1}$)	SPM ($mg\ L^{-1}$)	POC ($mg\ L^{-1}$)	DOC ($mg\ L^{-1}$)	TOC ($mg\ L^{-1}$)	DOC/POC	POC/Chl *a*	δ^{13}C-POC (‰)	C/N
Porge	**13.3**	**1113**	**12.0**	**2.425**	**10.9**	**13.29**	**4.5**	**753**	**-28.1**	**15.3**
	5.0	*1166*	*7.2*	*1.1*	*1.7*	*2.1*		*578.3*	*2.0*	*3.8*
	(3.5~19.2)	(230~4420)	(2.6~26.6)	(1.055~4.191)	(8.03~12.98)	(9.583~16.31)		(60~2252)	(-33.6~-25.9)	(11~24)
Cirès	**12.2**	**203**	**5.1**	**1.158**	**5.8**	**6.98**	**5.0**	**3438**	**-28.4**	**18.9**
	2.4	*27*	*1.0*	*0.3*	*1.2*	*1.4*		*2394*	*0.2*	*1.1*
	(6.5~16.1)	(162~253)	(3.8~7.8)	(0.622~1.821)	(4.031~8.087)	(4.653~9.66)		(1361~8846)	(-28.6~-28.1)	(17~21)
Renet	**12.9**	**201**	**10.4**	**1.728**	**5.5**	**7.19**	**3.2**	**3825**	**-28.6**	**19.6**
	2.4	*28*	*16.9*	*2.8*	*1.1*	*3.1*		*3156*	*0.4*	*1.9*
	(6.6~16.6)	(178~277)	(3~82.9)	(0.137~13.43)	(4.075~9.853)	(4.919~18.82)		(460~12137)	(-29.4~-28)	(16~23)
Lanton	**12.5**	**176**	**11.2**	**2.289**	**5.2**	**7.51**	**2.3**	**4140**	**-28.7**	**19.9**
	2.8	*8*	*7.9*	*1.7*	*1.5*	*2.7*		*2530*	*0.4*	*2.2*
	(5.8~16.7)	(161~193)	(4.8~35.1)	(0.948~7.31)	(3.17~7.416)	(4.591~14.73)		(647~8169)	(-29.1~-28.0)	(17~23)
Milieu	**12.7**	**270**	**6.5**	**1.506**	**4.2**	**5.74**	**3.8**	**4221**	**-28.1**	**17.3**
	3.5	*34*	*4.1*	*1.2*	*1.1*	*2.0*		*4004*	*0.9*	*1.7*
	(4.2~17.5)	(215~321)	(1.7~18)	(0.14~4.639)	(2.379~5.785)	(2.706~9.639)		(685~15218)	(-28.9~-26.5)	(13~19)
Ponteils	**12.8**	**221**	**6.5**	**1.328**	**8.0**	**9.34**	**6.0**	**2244**	**-28.4**	**16.2**
	3.3	*69*	*5.6*	*1.2*	*1.5*	*1.8*		*1779*	*0.6*	*2.4*
	(5.1~18.6)	(138~325)	(1.6~26.3)	(0.047~6.038)	(5.702~11.8)	(6.386~13.48)		(193~6062)	(-29.2~-26.9)	(11~22)
Tagon	**12.6**	**205**	**12.8**	**2.485**	**8.3**	**10.78**	**3.6**	**2359**	**-29.0**	**17.0**
	3.8	*17*	*9.5*	*2.2*	*2.9*	*5.3*		*1631*	*0.5*	*2.6*
	(3.8~18.6)	(172~258)	(3.5~50.3)	(0.114~11.67)	(3.095~12.7)	(5.585~24.37)		(143~6062)	(-30.2~-28.3)	(12~21)
Leyre	**12.7**	**170**	**8.7**	**1.320**	**5.5**	**6.82**	**4.2**	**1748**	**-28.7**	**14.4**
	4.2	*15*	*5.7*	*0.9*	*1.8*	*1.9*		*1146*	*0.5*	*1.3*
	(3.8~18.6)	(151~195)	(2.3~26.4)	(0.161~4.245)	(2.736~10.13)	(4.333~10.65)		(109~5121)	(-29.5~-27.7)	(12~17)
Landes	**14.1**	**195**	**2.7**	**0.650**	**5.0**	**5.68**	**7.7**	**581**	**-29.2**	**12.0**
	4.6	*21*	*1.1*	*0.3*	*0.9*	*1.1*		*230*	*0.4*	*0.9*
	(4.6~19.6)	(156~233)	(1.3~4.5)	(0.126~1.121)	(3.282~6.499)	(3.408~7.612)		(109~894)	(-29.8~-28.6)	(11~13)

Table 2. Organic carbon and associated physical and chemical parameters in the nine rivers entering the Arcachon lagoon; average (bold), standard deviation (in italic) and range (between brackets). T: temperature; SPM: suspended particulate matter; POC: particulate organic carbon; DOC: dissolved organic carbon; TOC: total organic carbon; Chl *a*: Chlorophyll *a*; δ^{13}C-POC: particulate organic carbon isotopic ratio and C/N: carbon/nitrogen ratio of particulate organic matter.

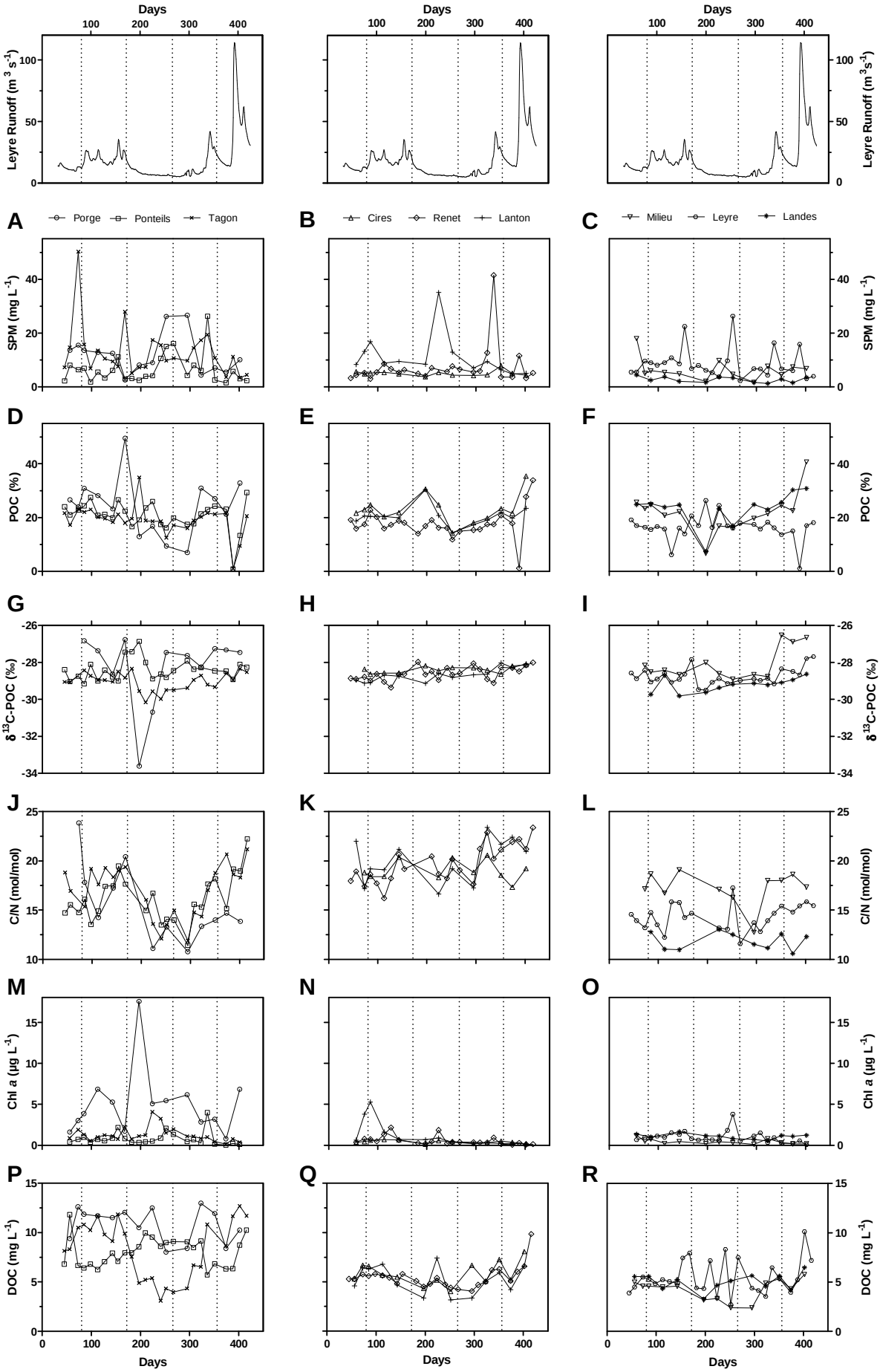
Days
Leyre Runoff (m 3 s-1)
A
Porge
Ponteils
Tagon
B
Cires
Renet
Lanton
C
Milieu
Leyre
Landes
SPM (mg L-1)
D
E
F
POC (%)
G
H
I
δ13C-POC (‰)
J
K
L
C/N (mol/mol)
M
N
O
Chl a (µg L-1)
P
Q
R
DOC (mg L-1)

Figure 2. Seasonal variations in the organic matter and its associated parameters in the nine studied rivers. A, B, and C: suspended particulate matter (SPM); D, E, and F: particulate organic carbon (POC, % of SPM); G, H, and I: stable isotope of POC (δ^{13}C-POC); J, K, and L: C/N ratio of particulate organic matter; M, N, and O: Chlorophyll *a* (Chl *a*) and P, Q, and R: dissolved organic carbon (DOC). Panels show the daily discharge of the Leyre River. Day 0 is January 1st, 2008.

3.2. Inorganic carbon distribution in the nine rivers flowing to the Arcachon lagoon

The observed inorganic carbon parameters in the nine watercourses are summarised in Table 3, and their seasonal patterns are shown in Figure 3. The DIC is the sum of CO_2^* (aqueous CO_2 and carbonic acid H_2CO_3), bicarbonate (HCO_3^-) and carbonate (CO_3^{2-}) ions. In this sandy catchment, the pH that was measured in the nine rivers averaged 6.55 ± 0.25 and ranged between 6.09 and 7.03 (data not shown). These values are in the lower end of the range that is typical of river values (6 - 8.4; Meybeck 1983). As a consequence of this acidic characteristic of the river waters, the DIC exists mostly in the HCO_3^- and CO_2^* forms (300 ± 134 and 189 ± 78 µmol L^{-1}, respectively; Table 3). The part of DIC that is represented by TA, with a mean of 300 ± 135 µmol L^{-1}, was almost entirely bicarbonate ions; the carbonate ion concentrations were close to zero for this pH range.

Overall, the DIC parameters showed a clear seasonal pattern, with significant differences between the winter and summer period (ANOVA, p-value: < 0.005) in the nine rivers. In fact, the river pCO_2 (Figs. 3A, B and C), with most minimum values during the winter months approaching 1000 - 2000 ppmv, increased in the spring to reach maximum values during the summer and autumn (up to 10000 ppmv in the Ponteils stream) (Table 3). The TA in the river water also followed this seasonal trend to a lesser extent, with the lowest values (approximately 100 µmol L^{-1}) measured during the winter months and the highest values reaching close to 1000 µmol L^{-1} in some watercourses during the summer months (the Ponteils and Tagon streams). In every instance, the rivers flowing to the Arcachon lagoon, with an average of 3922 ± 1645 ppmv, were always net sources of CO_2 to the atmosphere throughout the sampled year. As a consequence, the excess CO_2 (Figs. 3G, H and I; Table 3) reflected this seasonal pattern, with minima observed in the winter (near 100 µmol L^{-1} in the Leyre River) and maxima observed in the summer/autumn periods (nearly 500 µmol L^{-1}in the Ponteils stream), when the difference between the water pCO_2 and the atmospheric value was the highest.

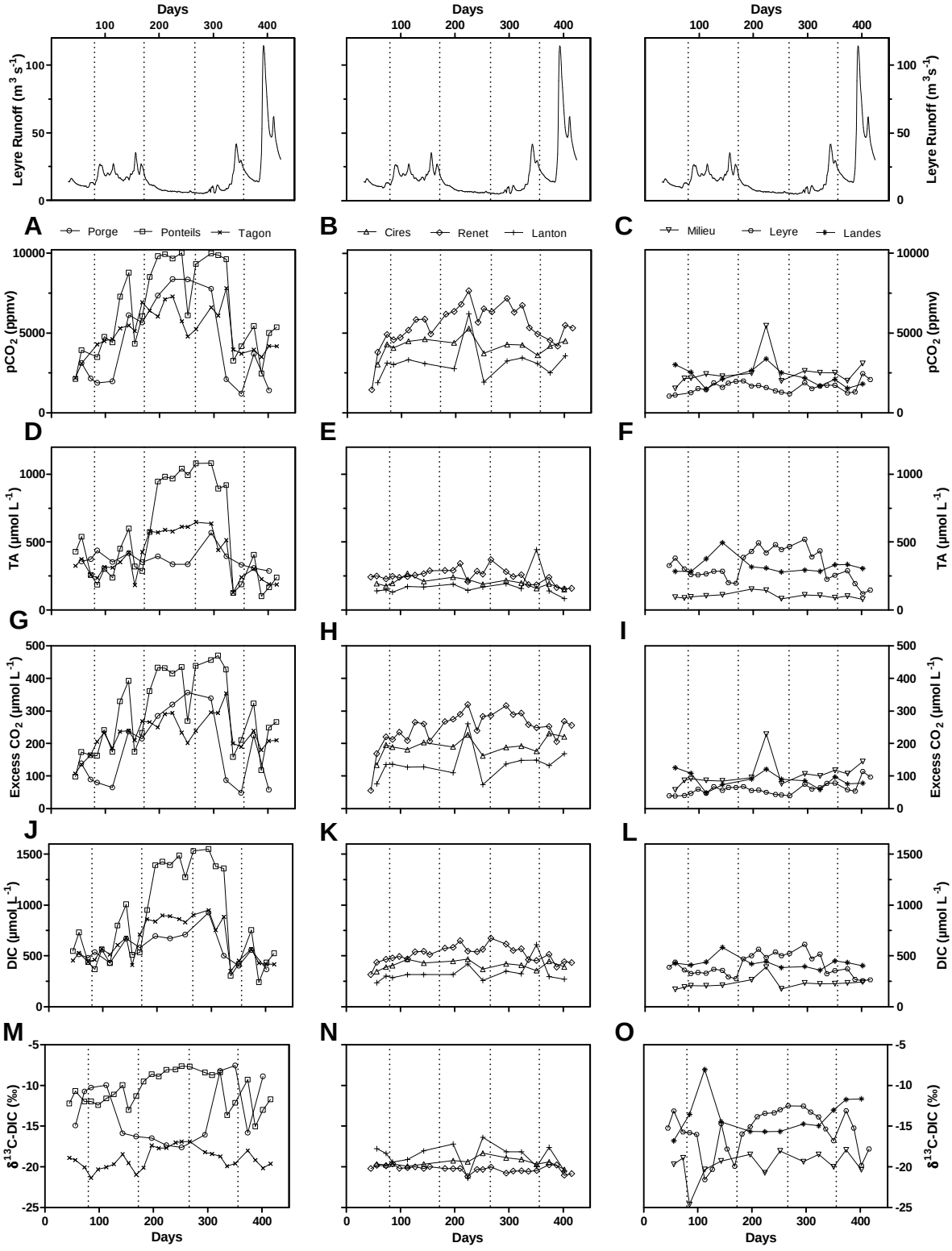

Figure 3. Seasonal variations in the inorganic carbon and its associated parameters in the nine studied rivers. A, B, and C: partial pressure of carbon dioxide (pCO_2); D, E, and F: total alkalinity (TA); G, H, and I: excess of carbon dioxide (Excess CO_2); J, K, and L: dissolved inorganic carbon (DIC) and M, N, and O: stable isotope of DIC (δ^{13}C-DIC). Panels show the daily discharge of the Leyre River. Day 0 is January 1st, 2008.

	pCO_2 (ppmv)	TA ($\mu mol\ L^{-1}$)	Excess CO_2 ($\mu mol\ L^{-1}$)	DIC ($\mu mol\ L^{-1}$)	$\delta^{13}C$-DIC (‰)
Porge	**4364**	**374.4**	**181.6**	**573.9**	**-13.3**
	2775	*69.5*	*113.5*	*148.3*	*3.8*
	(1192~8380)	(286~569)	(48~357)	(366~924)	(-17.6~-7.5)
Cirès	**4212**	**201.1**	**191.2**	**411.3**	**-19.5**
	544.7	*31.8*	*26.5*	*40.0*	*0.5*
	(3020~5280)	(151~268)	(133~231)	(347~467)	(-20.3~-18.3)
Renet	**5479**	**247.5**	**247.3**	**513.2**	**-20.3**
	1279	*52.4*	*54.4*	*80.8*	*0.4*
	(1437~7653)	(154~370)	(56~320)	(317~674)	(-21.2~-19.6)
Lanton	**3167**	**175**	**136.9**	**330.8**	**-18.6**
	1057	*85.6*	*45.8*	*95.7*	*1.4*
	(1889~6220)	(83~444)	(73~260)	(236~612)	(-21.4~-16.4)
Milieu	**2554**	**104.3**	**106.4**	**229.5**	**-19.7**
	949.8	*22.2*	*42.5*	*55.1*	*1.7*
	(1529~5460)	(78~153)	(57~229)	(170~390)	(-24.6~-17.9)
Ponteils	**6546**	**550.4**	**292.4**	**859.3**	**-10.6**
	2742	*351.4*	*121.3*	*454.9*	*2.1*
	(2116~10012)	(101~1082)	(98~470)	(240~1550)	(-15.0~-7.6)
Tagon	**5125**	**394.6**	**228.1**	**640.7**	**-19.0**
	1425	*167.6*	*54.0*	*200.7*	*1.3*
	(2188~7809)	(128~648)	(108~354)	(349~949)	(-21.4~-16.9)
Leyre	**1604**	**325**	**59.96**	**403.6**	**-15.6**
	338.7	*113.9*	*18.0*	*104.0*	*2.6*
	(1046~2453)	(120~520)	(38~114)	(255~612)	(-21.6~-12.5)
Landes	**2250**	**324.1**	**87.58**	**429.4**	**-13.8**
	590.6	*60.8*	*23.0*	*55.2*	*2.4*
	(1485~3382)	(279~495)	(48~125)	(359~583)	(-16.8~-8.0)

Table 3. Observed inorganic carbon parameters in the nine rivers entering the Arcachon lagoon; average (bold), standard deviation (in italic) and range (between brackets). pCO_2: partial pressure of carbon dioxide; TA: total alkalinity; DIC: dissolved inorganic carbon and $\delta^{13}C$-DIC: dissolved inorganic carbon isotopic ratio.

The nine rivers exhibited significant differences in their DIC parameters. In particular, the DIC values of the Milieu, Leyre and Landes rivers were generally well below these of the Porge, Ponteils or Tagon watercourses (Fig. 3; Table 3). Indeed, the pCO_2 and excess CO_2 values in these three rivers were almost always below 4000 ppmv and 150 $\mu mol\ L^{-1}$, respectively, throughout the year. Strong differences (at least twofold) in the water TA were also recorded between the Ponteils and Tagon streams and the Milieu and Lanton streams (Table 3). With regard to the DIC concentrations, the $\delta^{13}C$-DIC that was measured in the nine rivers showed significant differences between the watercourses (Fig. 3M, N and O; Table 3). In the Cirès, Renet, Milieu, Lanton and

Tagon streams, δ^{13}C-DIC values near -20‰ were measured throughout the year, and a few clear seasonal patterns were observed, with more depleted and enriched values measured during the winter/spring and summer/fall months, respectively, ranging from -24.6 to -16.4‰ in these watercourses. In the Ponteils stream, the same pattern was clearly observed but with much more ^{13}C-enriched values throughout the year, ranging from -15.0 to -7.6‰ during the winter/spring and the summer periods, respectively, with a mean of -10.6‰ (Table 3). The intermediate situation was observed in the Leyre River, with values ranging from -21.6 to -12.5‰ during the winter/spring and summer/fall months, respectively. Finally, an opposite seasonal trend was recorded in both the canals with more ^{13}C-depleted values during the summer and autumn months (values close to -17.0‰) and, to the contrary, more enriched values measured during the winter months (values close to -8.0‰).

3.3. Longitudinal carbon variations along the Leyre River

Figure 4 presents the longitudinal variations of all of the carbon and associated parameters along the Leyre River continuum in early October 2008. The organic carbon parameters (Figs. 4A, C, E, G and I) that were measured from the outlet of the river to 65 km upstream were in the range of those that were measured in the other sampled watercourses. The SPM and POC concentrations were between 1.33 and 7.38 mg L^{-1} and between 0.27 and 1.31 mg L^{-1}, respectively, with no differences along the river. The POC (% of SPM) was nearly constant from the outlet to 40 km upstream (values close to 16%) and then increased up to 20%, especially in the Petite Leyre (Figs. 1B and 4C). The DOC showed fairly constant values of between 1.7 and 3.1 mg L^{-1}, with the exception of a high value of 4 mg L^{-1} downstream, close to the outlet of the Leyre. Finally, the δ^{13}C-POC was roughly constant along the Leyre River (Fig. 4I), with values of -28.9 ± 0.6‰ as in the other rivers of the Arcachon lagoon catchment. The C/N ratios were 12.3 ± 1.2, and the Chl *a* was below 1 µg L^{-1} (data not shown).

In contrast, the DIC parameters showed more contrasting longitudinal variations along the Leyre River (Figs. 4B, D, F, H and J). Indeed, the water pCO_2 declined downstream from the source (*ca.* 4000 ppmv) to the outlet (*ca.* 1000 ppmv), although a higher water pCO_2 value (*ca.* 2500 ppmv) was recorded very close to the river outlet. The TA presented constant values (near 400 µmol L^{-1}) from the outlet to 36 km upstream, but local variations were recorded upstream (Fig. 4F). Consequently, these variations were also found in the DIC concentrations, which ranged from 180 to 722 µmol L^{-1}. Finally, the δ^{13}C-DIC showed a clear spatial trend, with more ^{13}C-enriched values close to the outlet, evolving from -20.48 to -12.17‰.

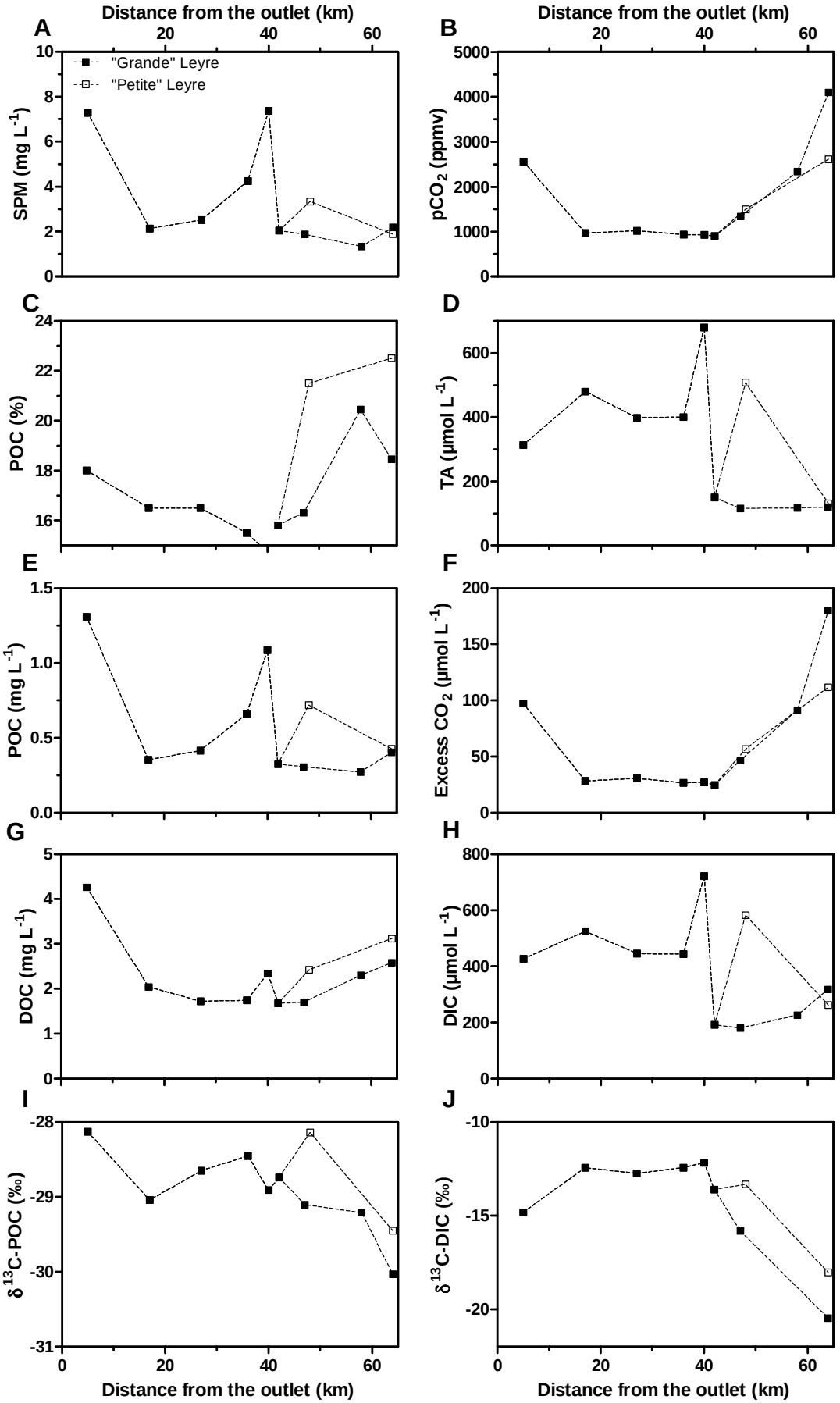
A
B
C
D
E
F
G
H
I
J
"Grande" Leyre
"Petite" Leyre
SPM (mg L-1)
pCO2 (ppmv)
POC (%)
TA (µmol L-1)
POC (mg L-1)
Excess CO2 (µmol L-1)
DOC (mg L-1)
DIC (µmol L-1)
δ13C-POC (‰)
δ13C-DIC (‰)
Distance from the outlet (km)
Distance from the outlet (km)
Distance from the outlet (km)
Distance from the outlet (km)

Figure 4. Variations in the carbon and its associated parameters along the Leyre River continuum on the 2nd and 3rd of October, 2008. A: suspended particulate matter (SPM); B: partial pressure of carbon dioxide (pCO_2); C: particulate organic carbon (POC, % of SPM); D: total alkalinity (TA); E: particulate organic carbon (POC); F: excess of carbon dioxide (excess CO_2); G: dissolved organic carbon (DOC); H: dissolved inorganic carbon (DIC); I: stable isotope of POC (δ^{13}C-POC) and J: stable isotope of DIC (δ^{13}C-DIC). Open squares represent the "Petite Leyre" (east) and dark squares the "Grande Leyre" (west) after 42 fm from the outlet (Fig. 1).

4. Discussion

4.1. Similarities and differences among the nine rivers

In general, the nine rivers that were sampled around the Arcachon lagoon show common carbon characteristics because of the uniformity of this catchment: low SPM and POC concentrations that were associated with a high contribution of POC within the SPM, a low Chl *a* concentration, high POC/SPM and C/N ratios, very negative levels of δ^{13}C-POC, a high DOC concentration, and a low TA that was associated with a high pCO_2. This condition of low SPM and POC concentrations associated with a high contribution of POC within the SPM is typical of lowland regions and is due to weak erosion rates that lead to clear waters (low turbidity) (Meybeck 1982; Meybeck 1993). The POC in the nine rivers is allochthonous and originates from soil and terrestrial C_3 plants. Indeed, C/N values of higher than 12 are typical of higher plants (Bordovskiy 1965), and δ^{13}C-POC values of -27 to -30‰ are typical of terrestrial C_3 plants (Mook and Tan 1991). In addition, the overall low Chl *a* concentration and high POC/Chl *a* ratio indicate the low contribution of phytoplankton to POC. Indeed, phytoplankton generally exhibits a POC/Chl *a* ratio ranging between 20 and 140, and it is generally accepted that phytoplankton-dominated POM has a POC/Chl *a* ratio that is lower than 200 (Savoye et al. 2003 and references therein). In the nine sampled rivers, the mean POC/Chl *a* ratio was 2590 ± 1396. Photosynthesis is likely limited by hydrological factors as shown in the rivers of eastern England by Neal et al. (2006); e.g., the Leyre River shows the highest runoffs and a low water residence time. Additionally, these waters, with their low pH and low nutrient concentrations (especially phosphate) represent unusual habitats for phytoplankton growth, as has been shown in peatlands (Greenwood and Lowe 2006). On the contrary, the omnipresence of acidic podsols with high organic carbon content (Righi and Wilbert 1984; Trichet et al. 1997; Jolivet et al. 2007) leads to important DOC concentrations in the nine sampled rivers, as has been found in boreal wetlands and temperate peatlands (Agren et al. 2007; Billett et al. 2006). Aitkenhead et al. (1999) have shown that DOC fluxes appear to strongly reflect the size of the soil organic carbon pool in the catchment. Although the podsolisation process typically results in the net retention of DOC, mature podsols can be a net DOC source to

rivers (Aitkenhead and McDowell 2000). Furthermore, this DOC originates from high molecular mass (HMM) compounds as humic acids (terrestrial plant detritus), which are much more recalcitrant and are thus found in river waters (Vestin et al. 2008). Additionally, streams that drain lowland (<700 m) catchments have higher DOC concentrations than those that drain upland catchments (Aitkenhead et al. 1999). Furthermore, with the predominance of silicate rocks in this catchment, the nine watercourses are acidic and generally present low TA values throughout the year, which is typical of rivers draining sandstone watersheds (Meybeck 1987). The entirety of the rivers flowing to the Arcachon lagoon is oversaturated in CO_2 throughout the year, thus representing a source of CO_2 to the atmosphere. In catchments such as the Arcachon watershed, where a preponderance of small streams is found, the chemistry is more strongly influenced by aquatic-terrestrial connections (Jones and Mulholland 1998; Jones et al. 2003). Consequently, the CO_2 that is attributable to instream biotic processes is typically minor in these rivers, indicating that the major source of CO_2 originates from root and bacterial respiration in soils and from groundwater discharge (Castelle and Galloway 1990; Piñol and Avila 1992; Kling et al. 1992). Furthermore, the extremely negative δ^{13}C-DIC values and low Chl *a* concentrations generally confirm that the instream primary production is low in these types of rivers, as has already been shown in other watercourses, such as peatland streams (Dawson et al. 2001).

In spite of the general common characteristics of the carbon parameters, differences between the nine rivers were investigated by performing a principal component analysis (PCA; Fig. 5) where the nine rivers are distributed functions to eight variables. Six of these variables represent the measured parameters showing the greatest variations throughout the year (the δ^{13}C-DIC, TA, DOC, pCO_2, POC and C/N ratio), and two represent characteristics of river watersheds (inhabitant/runoff ratio and drainage). First, an important contrast is observed in the very negative δ^{13}C-DIC (below -18‰), low TA (in general below 250 µmol L^{-1}) and very high C/N ratios (above 17 mol mol^{-1}) that were measured in the Cirès, Renet, Lanton, Milieu and Tagon streams as compared to the others. The high C/N ratio indicates that the POM is mainly of higher plant origin (Bordovskiy 1965).

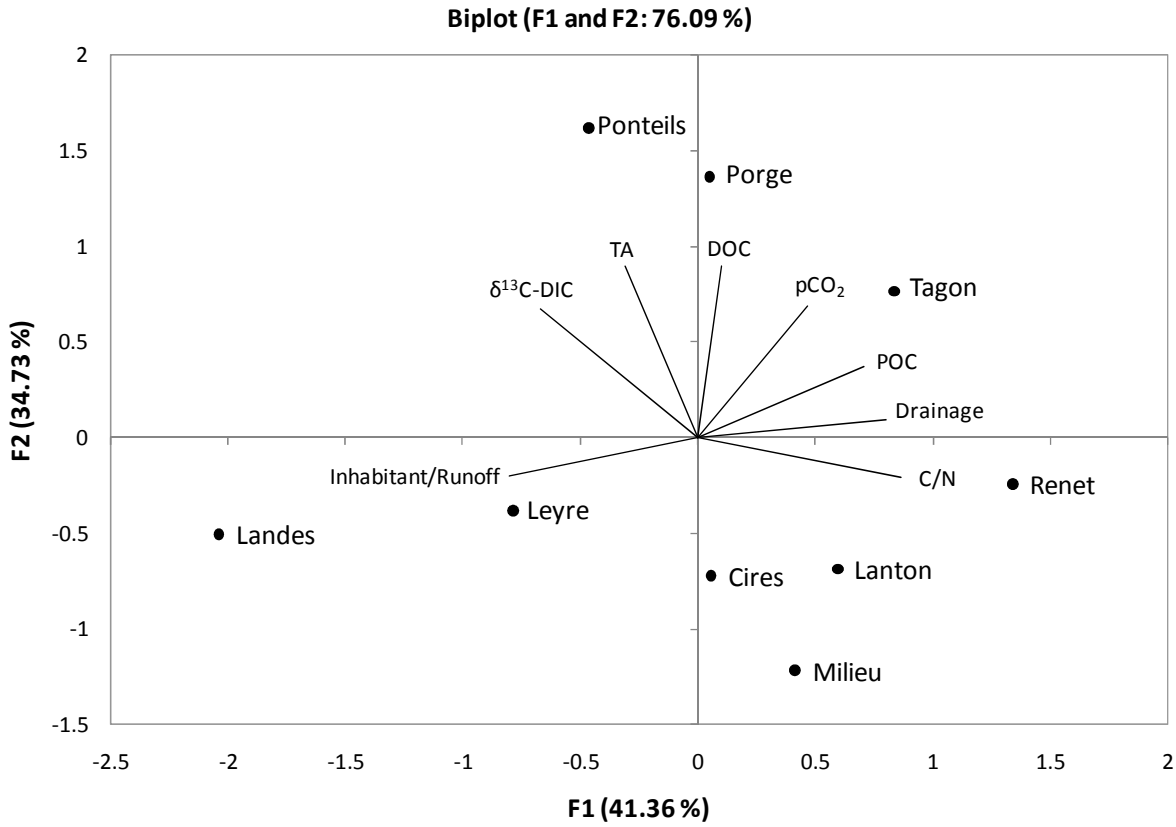

Figure 5. Loadings plot of the principal component analysis PCA total variance percentage =76.09%. The graph shows the distribution of the nine sampled rivers, nine observations functions to the eight measured factors (8 variables) as well as the correlations between the variables. Only eight variables were used here, as the redundancy of several variables hid the total explained variance; i.e., the inhabitant/runoff ratio (inhab m^{-3} s), stable isotope ^{13}C of DIC ($\delta^{13}C$-DIC, ‰), total alkalinity (TA, µmol L^{-1}), DOC (mg L^{-1}), pCO_2 (ppmv), POC (mg L^{-1}), drainage (L s^{-1} Km^{-2}) and C/N ratio. Variables that are situated along the same directional axis correlate positively with each other (TA/$\delta^{13}C$-DIC, POC/Drainage); variables that are situated at opposite ends of the plot correlate negatively with each other (e.g., POC/inhabitant/runoff, C/N/$\delta^{13}C$-DIC); variables that are situated in the centre of the plot are poorly correlated and are poor predictors. The horizontal axis explains 41.36% of the variability and the vertical axis, 34.73%; thus, the representation of the variables on these two axes is of good quality.

The low δ^{13}C-DIC associated with a low TA indicates that, in these rivers, the CO_2 originating from soil respiration and terrestrial plant decomposition largely predominates. In fact, in a system where the soil CO_2 is primarily derived from the decomposition of C_3 plant organic matter, the CO_2 produced has a δ^{13}C-CO_2 value that is close to the initial substrate, with means of -30 to -24‰ (Vogel 1993). Furthermore, in these watersheds, the erosion rates are weak and in general only silicate rocks are affected because of the absence of carbonate rocks. This leads to strongly depleted δ^{13}C-DIC and weak TA values. Indeed, assuming that monolithic silicate rivers have a TA of 125 µmol L^{-1} and monolithic carbonate rivers have a TA of 3195 µmol L^{-1}, according to Meybeck (1987), the carbonate contribution to rock weathering does not exceed 5% in these five rivers of the Arcachon lagoon catchment. Consequently for silicate weathering, bicarbonate ions originate solely from soil CO_2, and the associated δ^{13}C-DIC value reflects that of the soil CO_2, close to -20‰ (Amiotte-Suchet et al. 1999). On the contrary, in the four other rivers, i.e., the Porge, Ponteils, Leyre and Landes, the δ^{13}C-DIC values are much more ^{13}C-enriched (less negative), with values that are generally above -15‰ and the TA values are higher than the former four rivers, with values that are typically above 300 µmol L^{-1}. For example, in the Ponteils stream, the heaviest δ^{13}C-DIC values that were measured in the Arcachon lagoon catchment are likely explained by a greater presence of carbonates in this watershed, which is attested to by the strong TA values, as both measured parameters are positively correlated (Fig. 5). For carbonate rock weathering, one half of the bicarbonates originate from the mineral itself and the other from soil CO_2, leading to more ^{13}C-enriched δ^{13}C-DIC values (Jin et al. 2009). In addition, in the Porge canal, the contribution of marine waters from the lagoon, with a δ^{13}C-DIC value close to 0‰, could explain these enriched δ^{13}C-DIC values that were measured in the canal as well as the high TA values. Indeed, high conductivities were measured during some of the sampling days and were related to high tide in the lagoon. Furthermore, the phytoplankton biomass can develop to significant concentrations in the Lacanau lake to the north and the Sanguinet lake to the south, which are linked to the Porge and Landes canals, respectively, and can then be transported into canals by dominant flows, as has already been shown in the rivers of eastern England by Neal et al. (2006). This could also lead to more ^{13}C-enriched DIC in both canals, photosynthesis modifying the δ^{13}C-DIC, and aquatic photoautotroph utilising $^{12}CO_2$ as a carbon source at a faster rate than $^{13}CO_2$ (Parker et al. 2005).

Another contrast is observed in the Ponteils, Porge, Tagon and Renet watercourses, where DOC and pCO_2 are particularly high in comparison to the others. In fact, high DOC concentrations particularly here decomposable compounds found in the soil solution and groundwater, constitute

an appropriate substrate for bacterial mineralisation, leading to large amounts of CO_2 in the rivers in turn (Sobek 2005). Nevertheless, the highest DOC values measured in these rivers (the Porge canal) may be the result of anthropogenic disturbance and the effect of land use modification on the DOC concentrations (Aitkenhead et al. 1999). Finally, in this ACP, high inhabitant/runoff ratios and low drainage values, correlated with low POC concentrations, differentiate the Leyre River and the Landes canal from the other watercourses and explain a soil contribution to POC concentrations rather than anthropogenic pressures, as was shown by Abril et al. (2002) in the Zenne River.

4.2. Temporal carbon variations during the hydrological cycle

Seasonal variations of carbon parameters in the nine flowing rivers of the Arcachon lagoon catchment were investigated. In particular, the role of water runoff was scrutinised.

4.2.1. Organic carbon dynamics

In the Leyre River, where runoff data are available, the SPM concentrations, and to a lesser extent the POC concentrations, roughly increase with runoff until *ca.* 20 m^3 s^{-1} and then decrease (Figs. 6A and E), whereas the δ^{13}C-POC increases until reaching a plateau at the highest runoffs (Fig. 6I). Two processes seem to be involved: until *ca.* 20 m^3 s^{-1}, an increase in the runoff leads to an increase in the SPM and POC concentrations because of greater soil erosion (e.g., Hope et al. 1997), and then, when the runoff peaks, this material is exported downstream and replaced by another one, likely litter that was immersed during the flood period (e.g., Veyssy et al. 1999) as is suggested by the shift in δ^{13}C-POC (Fig. 6I).

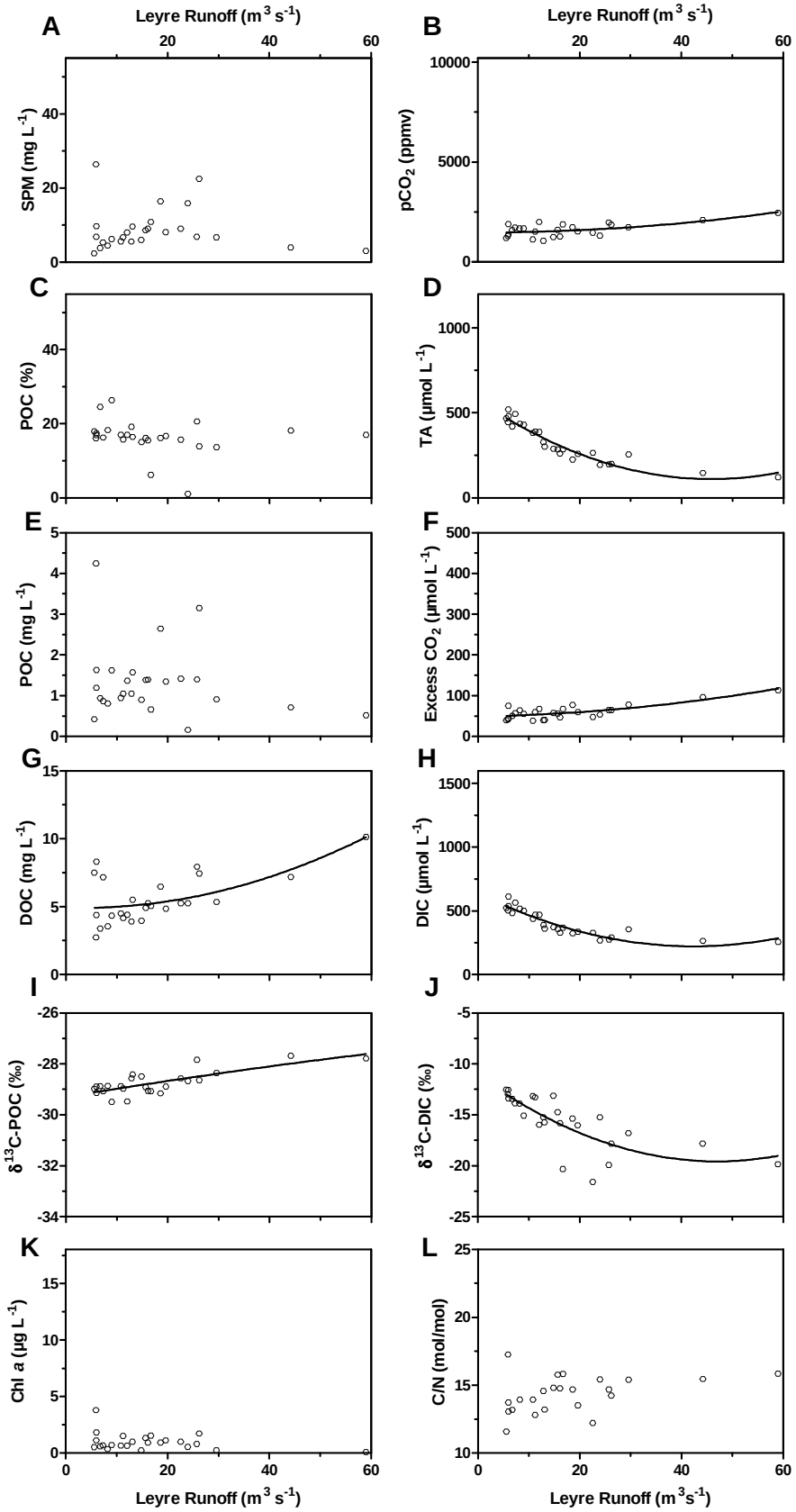
A
Leyre Runoff (m 3 s-1)
SPM (mg L-1)
B
pCO2 (ppmv)
C
POC (%)
D
TA (µmol L-1)
E
POC (mg L-1)
F
Excess CO2 (µmol L-1)
G
DOC (mg L-1)
H
DIC (µmol L-1)
I
δ13C-POC (‰)
J
δ13C-DIC (‰)
K
Chl a (µg L-1)
L
C/N (mol/mol)

Figure 6. A: suspended particulate matter (SPM); B: partial pressure of carbon dioxide (pCO_2); C: particulate organic carbon (POC, % of SPM); D: total alkalinity (TA); E: particulate organic carbon (POC); F: excess of carbon dioxide (excess CO_2); G: dissolved organic carbon (DOC); H: dissolved inorganic carbon (DIC); I: stable isotope of POC (δ^{13}C-POC); J: stable isotope of DIC (δ^{13}C-DIC); K: chlorophyll *a* (Chl *a*) and L: carbon/nitrogen ratio of organic matter (C/N ratio) versus the water runoff in the Leyre River.

DOC concentrations in the Arcachon rivers show significant differences (p-value: 0.0074) with higher DOC values between the late autumn/winter/spring period, and weaker concentrations in the summer months. In the Leyre River, this is illustrated by the significant positive correlation (p-value: 0.0015) between the DOC concentration and the runoff (Fig. 6G). This flushing effect has been verified in many temperate zone studies (Tranvik and Janson 2002; Mulholland 2003). Indeed, it leads to a dominant soil and plant organic matter source of riverine DOC (Mantoura and Woodward 1983; Aitkenhead et al. 1999). The DOC is derived partly from the degradation of biota and from roots and mycorrhiza exudates and is characterised by a low molecular mass (LMM) and is highly decomposable (Lundström et al. 2000; Vann Hees et al. 2005). In the Arcachon watershed, this LMM DOC, in contrast to the more recalcitrant DOC compounds with high molecular masses (HMM), is mineralised in the soil within a few days and is thus not measured in rivers, although it leads to important river CO_2 concentrations. Also, a contribution of simple DOC from the hyporheic zone, i.e., deposited detritus that was covered with sediments before it could decompose, represents a primary source for stream biota (Schindler and Krabbenhoft 1998). In the Arcachon lagoon catchment, all of these origins and processes are involved. The significant positive correlation (p-value: 0.0004) found between the pCO_2 and DOC concentrations (Fig. 7A), particularly in the Lanton, Ponteils and Leyre Rivers, illustrates the contribution of simple DOC compounds from the hyporheic zone to the river DOC. Additionally, a positive correlation between the C/N ratio and the DOC has been found in the Tagon (p-value: < 0.0001) and Milieu (p-value: 0.0233) streams (Fig. 7B), suggesting a contribution of refractory soil to DOC compounds, as HMM compounds have higher C/N ratios (Aitkenhead and McDowell 2000). In any case, the highly terrestrial decomposable DOC has a weak impact in terms of organic carbon transport to the lagoon but plays a central role in CO_2 degassing into the atmosphere, which refers to the “gas conduit” notion that was formulated by Kling et al. (1991) for arctic lakes and streams.

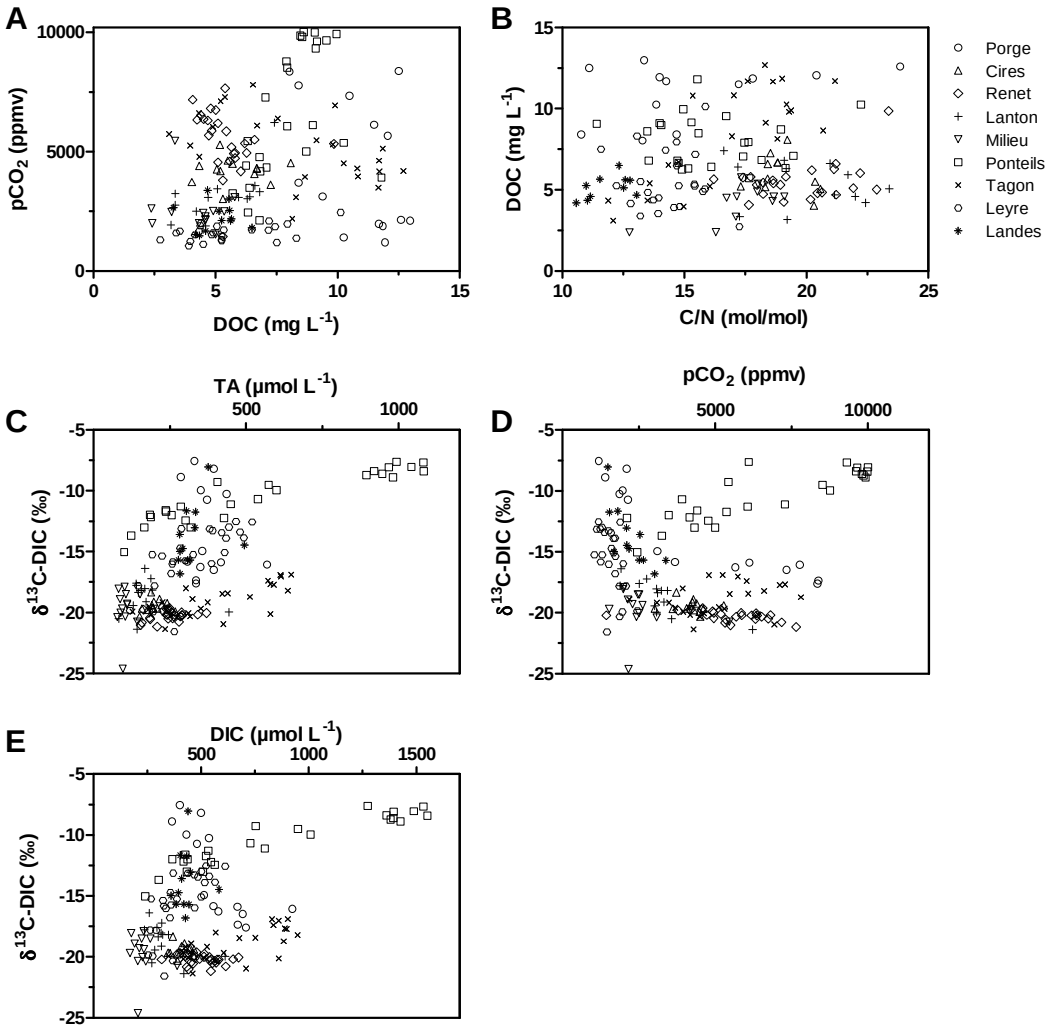

Figure 7. Carbon cross-parameter plots for the nine sampled rivers. A: the partial pressure of CO_2 versus the dissolved organic carbon (pCO_2/DOC); B: the dissolved organic carbon versus the C/N ratio of organic matter (DOC/C/N); C: the stable isotope of DIC versus the total alkalinity (δ^{13}C-DIC/TA); D: the stable isotope of DIC versus the partial pressure of CO_2 (δ^{13}C-DIC/pCO_2) and E: the stable isotope of DIC versus the dissolved inorganic carbon (δ^{13}C-DIC/DIC).

4.2.2. Inorganic carbon dynamics

Generally, the organic carbon parameters measured in the nine rivers show a relative temporal stability throughout the year due to the predominance of a constant terrestrial source for the river waters, leading to slow processes with more "buffered" reactions. In contrast, the DIC parameters show clear, strong, seasonal contrasts; this is particularly true of those dealing with CO_2 transfer through the soil, groundwater, river or atmosphere (pCO_2, Excess CO_2, DIC, and δ^{13}C-DIC), as well as of those dealing with chemical alteration (TA). The DIC in river waters has three main sources: soil CO_2, bedrock and soil minerals through carbonate and silicate dissolution and atmospheric CO_2 exchange at the air/water interface (Yang et al. 1996). In the Leyre catchment, all of the DIC parameters show a clear correlation with the water runoff (Fig. 6). Indeed, the TA decreases with runoff (Fig. 6D). During high flow periods, the streamflow is a mixture of three different runoffs: surface runoff, subsurface or hypodermic runoff and groundwater flow (Probst 1985). The decrease in the TA with high flows is attributable to the dilution of HCO_3^- ions by surface and subsurface flows, as was shown by Probst (1986) in the Girou River (France). In addition, strong seasonal variations were measured in almost all rivers, with a higher TA in the summer, autumn and groundwater discharge periods or during effluent conditions when carbonate-enriched groundwater drains river surface waters (Hynes 1983; Sophocleous 2002). Also, under low runoff, the groundwater residence time is increased and accumulates rock-weathering products; consequently, during discharge periods, DIC-enriched groundwater fuels river water with DIC (Jones and Mulholland 1998). In the Ponteils stream, strong values are also explained by better hydraulic permeability of the aquiferous material (Rimmelin et al. 1998) and by the presence of carbonate precipitates that were used by the landfill to bury domestic wastes inside soils which subsequently impacted the aquifer and, in turn, the stream (Canton et al. 2010). The decrease in DIC concentrations with runoff is also found in the Leyre River (Fig. 6H). In contrast, pCO_2 increases with runoff in the Leyre River, with consequently higher values during winter periods. The CO_2 in this river is generally weaker than it is in the streams throughout the year and is less influenced by terrestrial-aquatic connections. In the case of the Leyre River, however, the positive correlation between both parameters (p-value: 0.0011) may be explained by this influence. In fact, CO_2 can originate from the increased heterotrophic metabolism of organic matter that is transported from terrestrial ecosystems in winter; i.e., falling leaves or plant detritus on the edge of the river that are immersed during flood events and then in situ mineralised (Finlay 2003). The negative correlations between δ^{13}C-DIC and runoff (Fig. 6J) and pCO_2 in the Leyre River (Fig. 7D) strengthen this idea of a higher mineralisation rate during flood events, respiration of the soil and litter that is dominated by C_3 plants leading to more ^{13}C-depleted δ^{13}C-DIC values.

In contrast to the Leyre River, in the other streams where water runoff is not available, the pCO_2 is significantly associated with higher values during the summer (June–October) than during the fall and winter (November–February). In small streams, CO_2 sources are different: large CO_2 inputs from the soil and groundwater occur during low-flow periods, which are also enhanced by a longer residence time of the water in soils and in the groundwater. Amiotte-Suchet et al. (1999) suggest that in summer, the rate of soil organic matter oxidation is high, inducing high pCO_2 in soils and preventing atmospheric CO_2 from penetrating the soil. Additionally, in all of the streams except for the Ponteils, the δ^{13}C-DIC values were negatively correlated with the pCO_2 (Fig. 7D) because of the higher carbon dioxide production by the mineralisation of the soil and/or litter of C_3 plant origin. In contrast, in the winter and early spring, the CO_2 in the river decreases due to the predominance of superficial flow, a minor contribution of groundwater to surface water (influent condition) and a lower water residence time in the soils and groundwater. The excess CO_2 levels that were measured in the Arcachon catchment streams were consistently larger than those that were measured in larger watercourses (the Leyre or the Landes canal). This result is in agreement with Genereux and Hemond (1992), who showed that small streams tend to emit large amounts of CO_2 per unit area in turbulent conditions. Nevertheless, these values are largely below those that were found by Abril et al. (2000) concerning rivers flowing into the Scheldt estuary. The excess CO_2 levels found in Arcachon streams could be related to oxygen depletion but also to the root respiration of superior plants in the soils or anaerobic bacterial metabolism in the water, sediments and soils (Hamilton et al. 1995). This result is supported by the seasonal variation parallelism that exists between the river pCO_2 and excess CO_2 levels that were observed in the nine rivers (Figs. 3A, B, and C and G, H, and I, respectively). Generally, in all of the Arcachon streams, even if the δ^{13}C-DIC values decreased significantly with the CO_2 partial pressures, during summer periods when the water pCO_2 is high, the δ^{13}C-DIC tends to be heavier. The first possible explanation for this observation is that the air/water exchange might be enhanced during low flow periods because of a longer residence time of the water in the stream (Amiotte-Suchet et al. 1999). This would in turn lead to higher δ^{13}C-DIC values but also to pCO_2 values that stay high at this period, as the difference between the air and water pCO_2 is initially (before gas exchange) very important (Polsenaere and Abril, submitted). The second possible explanation is the contribution of carbonate-enriched groundwater during the summer months to the surface water, particularly in streams showing the strongest TA variations during the year, as in the Leyre River. Indeed, a strong positive correlation between the δ^{13}C-DIC and TA (p-value: < 0.0001) is always notable in the nine rivers of the Arcachon catchment (Fig. 7C). To a larger extent, in the Ponteils stream, the greater presence of anthropogenic and natural carbonate in the groundwater actually leads to the

only significant positive correlation (p-value: < 0.0001) between the δ^{13}C-DIC values and the pCO_2 in the Arcachon catchment. This correlation shows the strong influence of carbonate on the δ^{13}C-DIC, which in the Ponteils stream prevails on the influence of mineralisation. As a consequence, the Ponteils δ^{13}C-DIC values reflect those that are found in a carbonate-dominated watershed (Aucour et al. 1999; Barth et al. 2003; Kanduč et al. 2007). The influence of carbonates on the δ^{13}C-DIC is also seen in the longitudinal variations in the DIC parameters along the Leyre River. In fact, the presence of numerous Miocene carbonated outcrops in this watershed (Folliot et al. 1993) leads to locally high TA and δ^{13}C-DIC values. Finally, in both canals, the more ^{13}C-depleted δ^{13}C-DIC values that were measured during the summer/autumn periods and the negative δ^{13}C-DIC/pCO_2 correlation are likely explained by a higher mineralisation rate during the low-flow period. During the winter, the inputs of water with higher δ^{13}C-DIC values from the lakes to the north and south of both canals could also explain the winter trend (Atekwana and Krishnamurthy 1998).

4.3. Watershed carbon export and degassing

4.3.1. The relative importance of POC, DOC and DIC in land carbon export through rivers

Meybeck (1993) reported a carbon budget that was carried to the ocean by temperate rivers of 19.4, 20.3 and 60.3% for DOC, POC and DIC, respectively, and proportions of 37:18:45 for DOC:POC:DIC in global rivers, representing a total flux to the oceans that was estimated to be 0.542 Gt C yr^{-1}. When inland aquatic systems are included in the global models, it is usually only for the passive transport of carbon through the riverine pipe. Nevertheless, a large part of the carbon that is lost from terrestrial systems degasses as CO_2 from the inland water surface to the atmosphere and does not reach the ocean (Cole et al. 2007; Ciais et al. 2008). Cole et al. (2007) suggest that, of the at least 1.9 Pg C yr^{-1} that is received by inland waters from land, 40% is returned as CO_2 to the atmosphere, 12% is sequestered in sediments and the remaining 48% is transported to the ocean. The revision of this "active pipe" hypothesis, advanced by Cole et al. (2007) and by Tranvik et al. (2009), increased the total amount of organic carbon that was imported to inland waters from the terrestrial environment to 2.9 Pg C yr^{-1}, of which 48% is the degassing of CO_2 (from instream, soil and groundwater respiration), 21% is buried in sediments and 31% reaches the ocean. Table 4 presents the carbon export rates from different catchments in temperate to boreal zones along with the relative importance of POC, DOC and DIC exports and the importance of CO_2 degassing from water to the atmosphere in carbon budgets. In temperate catchments, the export of organic carbon (DOC + POC) generally predominates that of inorganic

carbon; this has been shown in forested rivers in Japan (Kawasaki 2002; Okazaki 2001) with 0.76-2.61 t C km^{-2} yr^{-1}, in the rivers of England and Wales (Worrall et al. 2007) with 5.3-3.18 t C km^{-2} yr^{-1} and in the peatland streams of Scotland (Billett et al. 2004; Dawson et al. 2004) with 28.3±5.7 and 12.3-31.2 t C km^{-2} yr^{-1}, respectively. This same pattern is also observed in boreal peatland streams, where the majority of the DOC is exported due to the large amounts of organic carbon that is stoked in these soils (Rantakari et al. 2010; Wallin et al. 2010; Jonsson et al. 2007). In boreal lakes, in contrast, the export of DIC can predominate, as was illustrated by Finlay et al. (2009) in a eutrophic lake (Canada) with 56% DIC export, and also by Abril et al. (2000), who reported 61% DIC export in temperate rivers of the Scheldt estuary due to much heterotrophic activity and acidification from nitrification, enhancing the CO_2 production. Nevertheless, in many cases, the portion of the DIC that is exported by river waters can largely be underestimated if the CO_2 degassing to the atmosphere is not taken into account in the inland carbon budget, as was shown in the temperate rivers of England and Wales (Worrall et al. 2007), in boreal peatland streams (Rantakari et al. 2010) and in boreal lakes (Sobek et al. 2006), where CO_2 degassing represented 40, 73 and 42% of the DIC export, respectively (Table 4). Dawson et al. (2004) also showed the importance of CO_2 degassing, as was illustrated by a decrease in the CO_2-C flux:HCO_3-C flux ratio. Similarly, a study by Billett et al. (2004) reported a computed total flux of 30.4 ± 6.2 t C km^{-2} yr^{-1} in a lowland peatland system, with the CO_2 degassing representing an additional 4.6 t C km^{-2} yr^{-1}, thus increasing the overall carbon flux from the peatlands.

Site characteristics	Carbon Export rates	TOC Export	POC Export	DOC Export	DIC Export	Excess CO_2	DIC $_{equilibrium}$	CO_2 degassing	References
temperate lowland rivers (France)	**2.01-35.05**	**0.83-8.54** *36*	**0.10-1.64** *7*	**0.73-7.9** *29*	**0.68-6.21** *21*	**0.13-3.13** *8*	**0.55-3.08** *13*	**0.49-19.4** *43*	This study
temperate rivers (Japan)	**1-3.55**			**0.76-2.61** *74*	**0.24-0.94** *26*				Okazaki (2001); Kawasaki (2002)
temperate rivers (England & Wales)	**9.00-11.97**	**5.3-7.18** *60*	**1.93-2.62** *25*	**3.37-4.56** *35*		**2.07-2.88** *24*		**4.19** *40*	Worrall et al. (2007)
temperate groundwaters (UK)						**1.4-2.9**			Worrall and Lancaster (2005)
temperate mountain rivers (France)			**5.3**						Coynel et al. (2005)
temperate rivers (Belgium)	**8.61-38.03**	**2.84-11.33** *36*	**2.18-17.44** *27*	**0.66-3.89** *9*	**5.75-16.85** *61*	**0.59-1.37** *6*	**5.16-15.48** *55*		Abril et al. (2000)
temperate lowland peatland streams (Scotland)	**30.4±6.2**	**28.3±5.7** *93*			**2.1±0.5** *7*			**4.6**	Billett et al. (2004)
temperate peatland streams (NE Scotland)	**12.6-32.9**	**12.3-31.2** *95*	**0.8-9.7** *23*	**11.5-21.5** *72*		**0.294-1.73** *5*			Dawson et al. (2004)
boreal peatland streams (Finland)	**7.97-64.2**	**2.3-14.8** *24*			**0.87-1.4** *3*			**4.8-48** *73*	Rantakari et al. (2010)
boreal peatland streams (nothern Sweden)	**3.68**			**2.98** *81*	**0.7±0.09** *19*				Wallin et al. (2010)
boreal peatland streams (nothern Sweden)	**3.9-5.2**			**3.1-4.1** *80*	**0.8-1.1** *20*				Jonsson et al. (2007)
boreal peatland streams (nothern Sweden)								**2.9±0.1** *30*	Oquist et al. (2009)
boreal lake Frisksjon (Sweden)		*34*			*5*			*42*	Sobek et al. (2006)
boreal eutrophic Katepwa lake (Canada)		*14*	*1*	*13*	*56*			*2*	Finlay et al. (2009)
equatorial streams (eastern Amazonia)								**2.0-4.0**	Davidson et al. (1010)

Table 4. Synthesis of carbon export rates from different catchments, with the relative importance of POC export, DOC export, DIC export (DIC at equilibrium and the excess of CO_2) and CO_2 degassing to carbon budgets. Values in bold are expressed in t C km^{-2} yr^{-1}, and values in italics are expressed in %.

4.3.2. Carbon export fluxes in the Arcachon lagoon catchment

Adding together the nine studied rivers, the total carbon export from the Arcachon lagoon watershed is estimated to be 15871 t C yr^{-1} and normalised by the surface area to an export rate of 115.49 t C km^{-2} yr^{-1}, with the CO_2 degassing to the atmosphere at 5376 t C yr^{-1} and 49.83 t C km^{-2} yr^{-1} (43%), respectively (Table 5). Of this total carbon export per year, the Leyre River accounts for more than 65%, with 10446 t C yr^{-1} (Table 5). On average, the carbon export rate of this catchment is estimated to be between 2.01 to 35.05 t C km^{-2} yr^{-1}, which is within the range of values that have been found for other temperate or boreal catchments, with proportions of 7:29:21 (8:13) for POC:DOC:DIC (excess CO_2:$DIC_{equilibrium}$) (Tables 4 And 5). The POC export, due to the low erosion rates in this lowland watershed, ranged between 0.1 and 1.64 t C km^{-2} yr^{-1} (7% of the total export rate, Table 5). These values are slightly below the range that was found by Worrall et al. (2007) in the rivers of England and Wales or by Dawson et al. (2004) in the peatland streams of Scotland (Table 4). In any case, the POC exports of the studied watercourses are far below those that were found by Coynel et al. (2005) in the mountainous rivers flowing to the bay of Biscay (at least 5.3 t C km^{-2} yr^{-1}) because of the higher erosion rates in such systems.

The DOC fluxes present a mean of 3.7 t C km^{-2} yr^{-1}, with the minimum at 0.73 in the Landes canal and the maximum at 7.9 t C km^{-2} yr^{-1} in the Tagon stream (Tables 4 and 5), and represent a significant part (29%) of the total carbon export of the Arcachon lagoon catchment (Tables 4 and 5). These fluxes approach the data that was reported for a forested catchment in central Japan (0.76-2.61 t C km^{-2} yr^{-1}; Kawasaki et al. 2005) but are below the values that were found in streams draining peatland in temperate or boreal zones because of the larger amounts of organic carbon that is stocked in these soils (Rantakari et al. 2010; Jonsson et al. 2007; Billett et al. 2004; Dawson et al. 2004). The DIC export rate also represents a large part of the Arcachon Carbon budget (21% without accounting for the CO_2 degassing portion, Tables 4 and 5) and ranges from 0.68 to 6.21 t C km^{-2} yr^{-1}, which is similar to the values that were reported for peatland catchment rivers in temperate and boreal zones (Billett et al. 2004; Wallin et al. 2010; Jonsson et al. 2007). The excess CO_2 for the whole catchment is 8% and is on the same order of magnitude as the POC export to the lagoon and the value reported by Abril et al. (2000) for rivers flowing to the Scheldt estuary (Tables 4 and 5). Also, the excess CO_2 exports (0.13-3.13 t C km^{-2} yr^{-1}) are within the range of values that were found by Worrall et al. (2007) in the rivers of England and Wales, by Worrall and

Lancaster (2005) for groundwater excess CO_2 in the United Kingdom and by Dawson et al. (2004) in peatland streams (Table 4).

	ORGANIC CARBON			INORGANIC CARBON			
	TOC	POC	DOC	DIC	Excess CO_2	DIC $_{equilibrium}$	CO_2 Degassing
	C EXPORT						C DEGASSING
Porge	**1658**	**306**	**1352**	**780**	**226**	**554**	**171***
	7.48	*1.38*	*6.10*	*3.52*	*1.02*	*2.50*	0.77*
Cirès	**149**	**25**	**124**	**97**	**47**	**50**	**362**
	3.06	*0.51*	*2.55*	*1.99*	*0.97*	*1.03*	7.4
Renet	**144**	**29**	**115**	**111**	**56**	**55**	**348**
	8.06	*1.62*	*6.44*	*6.21*	*3.13*	*3.08*	19.4
Lanton	**63**	**15**	**48**	**35**	**15**	**20**	**99**
	1.74	*0.42*	*1.33*	*0.97*	*0.42*	*0.55*	2.74
Milieu	**128**	**35**	**93**	**54**	**26**	**28**	**94**
	6.00	*1.64*	*4.36*	*2.53*	*1.22*	*1.31*	4.41
Ponteils	**66**	**9**	**57**	**59**	**23**	**36**	**108***
	2.83	*0.39*	*2.45*	*2.53*	*0.99*	*1.54*	4.65*
Tagon	**275**	**44**	**231**	**143**	**56**	**87**	**242**
	9.28	*1.48*	*7.79*	*4.82*	*1.89*	*2.94*	8.17
Leyre	**4096**	**667**	**3429**	**2455**	**470**	**1985**	**3895**
	1.91	*0.31*	*1.60*	*1.15*	*0.22*	*0.93*	1.8
Landes	**97**	**12**	**85**	**85**	**16**	**68**	**57***
	0.83	*0.10*	*0.73*	*0.73*	*0.14*	*0.58*	0.486*
TOTAL ($t\ C\ Yr^{-1}$)	**6676**	**1142**	**5534**	**3819**	**935**	**2883**	**5376**
TOTAL ($t\ C\ km^{-2}\ Yr^{-1}$)	*41.20*	*7.86*	*33.34*	*24.46*	*9.99*	*14.46*	49.83
Percentage (%)	**36**	**7**	**29**	**21**	**8**	**13**	**43**

Table 5. Watershed carbon export, export rates and CO_2 degassing; carbon export in $t\ C\ yr^{-1}$ (bold) and carbon export rates in $t\ C\ km^{-2}\ yr^{-1}$ (italic). The CO_2 degassing was calculated using the StreamCO$_2$-DEGAS model, based on the pCO_2, total alkalinity and δ^{13}C-DIC (Polsenaere and Abril, submitted). (*) CO_2 Degassing for the Porge, Ponteils and the Landes watercourses were estimated using K_{600} values that were set to 5, 10 and 5 $cm\ h^{-1}$, respectively. $DIC_{equilibrium}$ is computed as a theoretical DIC concentration in a river at atmospheric equilibrium (Abril et al. 2000).

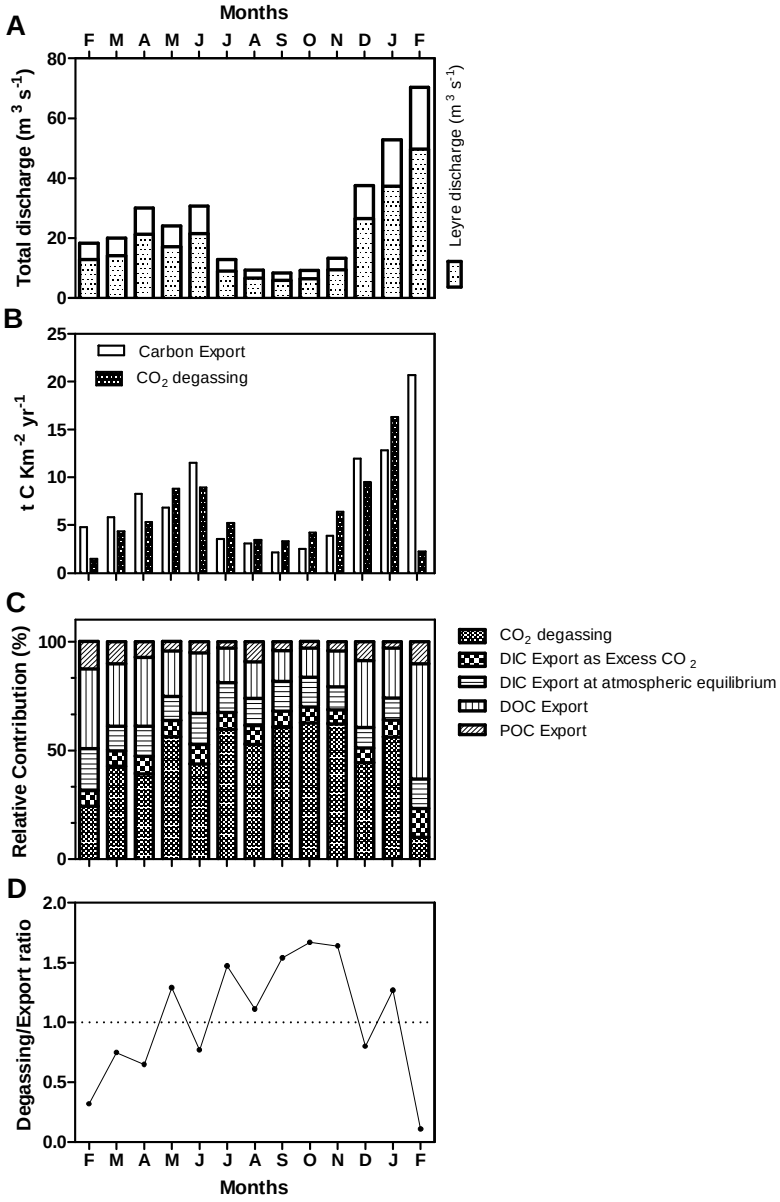

Figure 8. Seasonal variations in the watershed carbon export rates and CO_2 degassing. A: the monthly river discharges to the lagoon, with the part represented by the Leyre River; B: the mean carbon export rate to the lagoon and CO_2 degassing from the rivers to the atmosphere; C: the relative contribution of degassing (CO_2 degassing), dissolved inorganic carbon (excess CO_2 and DIC at atmospheric equilibrium), dissolved organic carbon (DOC) and particulate organic carbon (POC) to the carbon export to the lagoon and D: the CO_2 degassing/carbon export ratio (degassing/export).

The carbon export budget of the Arcachon lagoon watershed has been computed using the monthly averages for carbon concentrations and river runoffs (Fig. 8A). Daily runoff values were available solely for the Leyre River; thus, those for the other watercourses have been normalised using the surface/runoff relationship between the Leyre and the other catchments. Consequently, even if each river was sampled every two weeks, the carbon exports could be underestimated. In fact, very precise flux estimations require suitable hydrological monitoring and sampling frequency, particularly to clearly characterise flood events (Meybeck et al. 2001; Coynel et al. 2005). Furthermore, monitoring carbon fluxes, particularly CO_2 fluxes, at the outlets of the rivers does not take into account the processes that are involved in CO_2 evasion or production prior to the measured point and thus leads to significant underestimation of total carbon loss and export to the ocean (Worrall and Landcaster, 2005; Worrall et al., 2007; Wallin et al. 2010). This has been confirmed in the Leyre catchment, where the measured water pCO_2 levels declined downstream (Fig. 4B). This suggests that CO_2 degassing occurs along the Arcachon rivers, likely due to a reduction in the groundwater inputs downstream, as was shown elsewhere by Dawson et al. (1995), or to the fact that the degassing of CO_2 that is loaded in headwaters predominates over the emission of CO_2 that is loaded during transit, as was illustrated by Teodoru et al. (2009) in Canadian boreal rivers.

In this manner, a model that is based on mass-balance equations has been developed to assess the integrated CO_2 losses or degassing (DIC exchange and CO_2 degassing) from the Arcachon rivers to the atmosphere by using only the water pCO_2, TA and δ^{13}C-DIC (Polsenaere and Abril, submitted). Moreover, the StreamCO_2-DEGAS model allows for the calculation of the integrated gas transfer velocity K_{600} on the Arcachon rivers where the model is applicable; the K_{600} values are site-specific and relatively unknown in small streams, leading to large uncertainties in the computation of CO_2 fluxes from the water to the atmosphere (Genereux and Hemond 1992; Wanninkhof et al. 1992). Thus applying an averaged calculated K_{600}, it is possible to estimate the CO_2 degassing to the atmosphere from the other Arcachon rivers (Table 4). The K_{600} values that were derived from the CO_2-DEGAS between 7 ± 5 and 21 ± 9 cm h^{-1} in the Leyre River and the Tagon stream, respectively (Polsenaere and Abril, submitted), are within the range of those that have been found elsewhere (Wanninkhof et al. 1990; Raymond and Cole 2001), allowing us to validate the model. In each river of the Arcachon lagoon, the CO_2 degassing represents a significant part of the carbon budget, ranging from 0.5 to 19.4 t C km^{-2} yr^{-1} (Table 4 and 5). This estimated CO_2 degassing range is close to those that have been computed in other studies in temperate, boreal peatlands (Billett et al. 2004; Rantakari et al. 2010; Oquist et al. 2009) and in equatorial streams (Davidson et al. 2010), with 4.6, 4.8 - 48, 2.9 ± 0.1 and 2.0 - 4.0 t C km^{-2} yr^{-1},

respectively (Table 4). Adding together the calculated CO_2 degassing for the nine rivers flowing to the Arcachon lagoon, the total carbon export from this lowland watershed is increased by a factor of two (from 65.66 to 115.49 t C km^{-2} yr^{-1}, Table 5). Also, the DIC export is multiplied by a factor of three, leading to a total DIC export of 75 t C km^{-2} yr^{-1} instead of 25 t C km^{-2} yr^{-1}. Therefore, for the total carbon export by the nine rivers, 29% of the DOC, 7% of the POC and 21% of the DIC is transported to the Arcachon lagoon, with 43% degassing as CO_2 to the atmosphere before reaching the lagoon (on the 64% of DIC export in these rivers; Table 5). These percentages are very close to those that were found in the compilations of Cole et al. (2007) and Tranvik et al. (2009) (40 and 48%, respectively), and they are also close to those found elsewhere in temperate or boreal catchments (Table 4). Moreover, during the sampling year, the CO_2 degassing from the nine rivers was similar to or larger than the carbon export (POC, DOC and DIC) to the Arcachon lagoon, as was suggested elsewhere by the recent data compilations named above. This is particularly true from the late spring to the late autumn, when the river waters have the highest oversaturation rates (Fig. 8B). In any case, the CO_2 degassing is greater than or equal to the DOC export rate throughout the year, with the exception of February, when the DOC concentrations in the river waters are the largest and the CO_2 concentrations are the lowest, leading to a large drop of CO_2 degassing (Fig. 8B and C). Consequently, the Degassing/Export ratio is high in this catchment during the year, as shown in Figure 8D.

The total carbon export from the nine rivers to the lagoon is of great importance in the understanding of the carbon cycle of the Arcachon lagoon, representing a significant carbon input of 10494 t C yr^{-1} to the basin, with 5376 t C yr^{-1} being degassed as CO_2 to the atmosphere before entering the lagoon. Nevertheless, each carbon form exported has only a weak influence on the ecological functioning of the lagoon. Indeed, the POC export (1142 t C yr^{-1}) is low compared to the primary production of the eelgrass *Zostera noltii* (17800 t C yr^{-1}; Auby and Labourg 1996) and to the phytoplankton primary production of the lagoon (17920 t C yr^{-1}; Glé et al. 2008). Additionally, Dang et al. (2009) have shown that riverine particulate organic matter contributes weakly to the diet of primary consumers, such as the clams in the Arcachon lagoon (below 15%). The riverine DOC, which has a higher value than that found in the lagoon, can fuel the aquatic trophic chain through microbial degradation, but its impact is weak due to the dilution of these riverine inputs by the oceanic waters of the lagoon. The same result can be stated for DIC export, where the riverine concentrations are low in comparison to the oceanic water DIC due to higher TA values. However, the total loss of carbon from the watershed to the Arcachon lagoon, estimated to 115.5 g C m^{-2} yr^{-1}, with 50 g C m^{-2} yr^{-1} as CO_2 degassing to the atmosphere, represents a significant part (i.e. 1/3) of the carbon uptake by the land. Indeed, the carbon fixation

by the maritime pine forest of Landes Gascony is estimated to be 345 g C m^{-2} yr^{-1} on average on the last ten years from 1996 to 2006 (EUROFLUX site of the Bray, 44°43'33.24" N, 0°46'33.72" W) (Loustau, personal communication).

5. Conclusion

During this one-year study, nine rivers draining into the Arcachon lagoon presented contrasting characteristics in their carbon dynamics, particularly between two canals, streams and a larger river. These differences could be linked to their drainage characteristics; i.e., their flow regimes, location around the lagoon and their physical parameters (surface and depth). Nevertheless, due to the uniformity of the catchment, similar trends (seasonal variations and carbon speciation) can be drawn for all of the watercourses. POC represented the smallest contribution to the overall carbon flux in this uniform and flat lowland catchment due to low erosion rates, with the highest concentrations being reached after flood events. In contrast, the presence of enriched organic carbon soils (podsols) led to an important quantity of allochthonous DOC in the surface waters. Finally, along with the allochthonous organic matter and large CO_2 input from groundwater and soils, all of the watercourses were found to be oversaturated in CO_2 when compared to the atmosphere throughout the year by a factor ranging from 2 to 20, according to the season. Autochthonous organic matter was found to poorly contribute to POC composition, as shown by a generally low Chlorophyll *a* concentration and high POC/Chl *a* ratio and by an isotope composition of the POC that is characteristic of C_3 terrestrial plants. Finally, the presence of the "Sables des Landes" formation and the nearly complete absence of carbonate rocks led to acidic water and low alkalinity values in the rivers, with the exception of locally enriched carbonate groundwater discharge or domestic activities. Consequently, a large amount of CO_2 was lost to the atmosphere by river continuums. Such a flux must be taken into account when dealing with carbon export budgets at the ecosystem scale because it is usually subject to large uncertainties. Additionally, the majority of these rivers (88% and more than 80% of the total watershed surface and runoff, respectively) were sampled accurately to constrain at best the carbon exports to the Arcachon lagoon, although more available data (daily stream runoffs) and a better sampling frequency will allow for increased knowledge of carbon exports to the Arcachon lagoon.

Acknowledgements

We would like to express our thanks to the people that contributed to field sampling and laboratory analyses. This paper is a contribution to the PNEC-Littoral Atlantique and ANR PROTIDAL projects.

CHAPITRE III.

ECHANGES DE CO_2 ATMOSPHERIQUE DANS LA LAGUNE D'ARCACHON

PARTIE III.1. TURBULENT FLUX MEASUREMENTS BY EDDY CORRELATION OVER A TEMPERATE INTERTIDAL FLAT IN SOUTHWESTERN FRANCE [10]

PARTIE III.2. SPATIAL AND TEMPORAL CO_2 EXCHANGE MEASURED BY EDDY CORRELATION OVER A TEMPERATE INTERTIDAL FLAT AND THEIR RELATIONSHIPS TO NET ECOSYSTEM PRODUCTION [11]

[10] Turbulent flux measurements by Eddy Correlation over a temperate intertidal flat in southwestern France, Polsenaere P., Lamaud E., Bretel P., Bonnefond J.-M., Delille B., Detandt G., Loustau D. and G. Abril, Submitted to ***Journal of Geophysical Research*** (anglais corrigé par American Journal Experts).

[11] Spatial and temporal CO_2 exchange measured by eddy correlation over a temperate intertidal flat and their relationships to net ecosystem production, Polsenaere P., Lamaud E., Bonnefond, J.-M, Lafon V., Bretel, P., Delille, B., Deborde J., Loustau, D. and G. Abril, Submitted to ***Biogeosciences*** (anglais corrigé par American Journal Experts).

III. ECHANGES DE CO_2 ATMOSPHERIQUE DANS LA LAGUNE D'ARCACHON

III.1. TURBULENT FLUX MEASUREMENTS BY EDDY CORRELATION OVER A TEMPERATE INTERTIDAL FLAT IN SOUTHWESTERN FRANCE

Résumé

Des mesures de vitesse de friction, de flux de chaleurs latentes et sensibles ainsi que de flux de dioxyde de carbone entre l'atmosphère et un platier intertidal vaseux, situé dans le sud-ouest de la France, ont été réalisées en utilisant la technique micrométéorologique d'Eddy Covariance (EC). Cette technique de mesure de flux turbulents est encore peu utilisée en zone intertidale. La méthodologie et les résultats sont discutés dans ce travail, en utilisant une série temporelle d'une semaine obtenue entre le 1er et le 7 juillet 2008 dans la lagune d'Arcachon. En particulier, les rythmes diurnes et tidaux, i.e. marée basse le jour, marée basse la nuit, marée haute le jour et marée haute la nuit (mesures en continu sur ces quatre cas différents) influencent fortement les échanges turbulents. Les cospectres moyens des flux de chaleurs et de CO_2 sont généralement bien définis. Ceci permet en partie de valider la méthodologie d'EC utilisée dans cette étude, i.e., celle d'Aubinet et al. (2000) du projet EUROFLUX, appliquée à la zone intertidale. Les pics maximaux dans le domaine des basses fréquences (BF) observés dans les cospectres montrent que les grands tourbillons prédominent dans le transport des échanges turbulents. Cette contribution des BF est attribuée aux conditions atmosphériques instables qui caractérisent la lagune la plupart du temps. En effet, sur les quatre cas mesurés, 71% des données correspondant à des valeurs de Z/L, l'index de stabilité atmosphérique de Monin-Obukhov, inférieures à -0.04. La vitesse de friction (u^*) est mesurée entre 0.04 et 0.66 m s^{-1} pendant la semaine. Les régressions linéaires significatives entre u^* et la vitesse du vent ont montré que la rugosité de surface de la lagune est très faible (les ratios u^*/u sont proches de 0.033) avec aucune différence claire entre le cas de marée basse et celui de marée haute. Les flux de chaleur latente (LE) dominent sur les flux de chaleur sensible (H) avec des rapports de Bowen toujours inférieurs à 1. Les flux de H, entre -16.5 et 126.6 W m^{-2} semblent plutôt contrôlés par les gradients de températures entre l'air et l'eau ou les sédiments. Les flux de LE, entre 5.5 et 684.7 W m^{-2}, sont clairement corrélés au vent durant les quatre cas, et aux radiations pendant la journée, en raison des forts taux d'évaporation de l'eau et de la vase. Le platier se comporte comme une faible source de CO_2 vers l'atmosphère

avec des flux verticaux mesurés entre -6 et 12 $\mu mol\, m^{-2}\, s^{-1}$. Néanmoins, à marée basse le jour, la lagune se comporte comme un puits de CO_2 du fait de l'activité photosynthétique des communautés benthiques (en majorité des herbiers de *Zostera noltii*). Pendant la nuit, en raison de la respiration des communautés benthiques et pélagiques, et quelquefois pendant le jour, de phénomènes physiques de déstockage, la lagune émet vers l'atmosphère de grandes quantités de CO_2 vers l'atmosphère. Les contrôles physiques et biologiques sur les flux turbulents, observés pendant la semaine de mesure, sont précisément discutés dans cet article. La validation de la technique d'EC et les flux turbulents obtenus dans la lagune d'Arcachon laissent envisager des perspectives intéressantes quant aux connaissances sur le fonctionnement d'une lagune intertidale de la zone côtière d'un point de vue biogéochimique et écologique.

Abstract

Measurements of friction velocity, sensible heat, latent heat and carbon dioxide flux were performed over a temperate intertidal mud flat located in southwestern France using the micrometeorological Eddy Correlation (EC) technique. Few studies have addressed turbulent fluxes using EC over intertidal areas such as the Arcachon lagoon. This paper presents methods and results for a one-week time series recorded between July 1st and 7th, 2008. Rhythmic tidal and diurnal cases, including low tide / day, low tide / night, high tide / day and high tide / night, greatly influenced turbulent exchanges. Averaged power cospectra of sensible heat, latent heat and carbon dioxide flux were generally well shaped, which partly validates the EC methodology used in this study. Specifically, this study adapted the Aubinet et al. (2000) method from EUROFLUX to the intertidal area. Maximum frequency peaks were observed in the low frequency (LF) domains of cospectra and show that rather large eddies dominate turbulent exchange transport. The observed low frequencies are attributed to unstable conditions that commonly occur in the Arcachon flat. In fact, 71% of Monin-Obhukov stability parameter (Z/L) values were less than -0.04. Friction velocities (u^*) ranged between 0.04 and 0.66 m s^{-1} during the week. The linear regressions computed between u^* and wind speed showed that the roughness of the lagoon was very weak (u^*/u ratio close to 0.033) and that there were no clear differences between low and high tides. The latent heat flux (LE) clearly dominated over H during the week, and the Bowen ratio was always below unity. H fluxes ranged from -16.5 to 126.6 W m^{-2} and were apparently linked to air or water / sediment temperature gradients in the lagoon. LE fluxes, which ranged from 5.5 to 684.7 W

m^{-2}, were clearly correlated with both wind stress and photosynthetically active radiation (PAR) during the day due to intensive evaporation of mud and water. The flat acted as a small source of CO_2 to the atmosphere with CO_2 fluxes ranging from -6 to 12 µmol m^{-2} s^{-1}. Nevertheless, at daytime low tide, the tidal flat acted as a sink for CO_2 due to high rates of photosynthesis in benthic communities (mostly by *Zostera noltii* eelgrass). As a result of both nighttime respiration by the benthic and pelagic ecosystems and occasional daytime destocking, the lagoon degassed large amounts of CO_2 to the atmosphere. This paper discusses the various physical and biological controls on turbulent fluxes that were observed during the week. By validating the EC technique and describing the turbulent fluxes observed in the Arcachon lagoon, this study provides a means for improving our understanding of tidal flat ecosystems.

1. Introduction

The coastal zone is a transition area between land and open ocean. It receives considerable amounts of nutrients and organic matter from the land, exchanges large amounts of matter and energy with the open ocean and constitutes one of the most biogeochemically active areas of the biosphere (Gattuso et al., 1998; Gazeau et al., 2004; Borges et al., 2005). Despite the fact that the fluxes of carbon and nutrients are disproportionately high in coastal zones relative to the coastal surface area, which equals approximately 7% of that of the ocean, the coastal zone has only recently been included in global carbon budgeting efforts (Smith and Hollibaugh, 1993; Borges, 2005). Intensive exchanges of CO_2 between the atmosphere and the coastal environment are expected, and these fluxes are significant for global carbon budgets (Borges et al., 2006). Moreover, the coastal zone is highly sensitive to climate change, and one of the greatest challenges for understanding estuarine ecosystem processes is accurately estimating the carbon budget (Yan et al., 2008).

Various studies show that the present net global ocean CO_2 uptake is 1.5-2.0 Pg C yr^{-1}, which corresponds to about 25% of industrial emissions (Takahashi et al., 2002). Similarly, Borges et al. (2006) showed that the European continental shelves are significant sinks for atmospheric CO_2 and absorb 68.1 Tg C yr^{-1}. This sink is equivalent to that reported for the European terrestrial biosphere (grasslands, croplands, peatlands and forests) of 66.1 Tg C yr^{-1} (Janssens et al., 2005). In addition to marginal seas, the coastal zone includes estuaries, lagoons, salt marshes and tidal mud flats. As a consequence of this heterogeneity, combined with scarce data and unreliable surface area estimates, current estimates of the CO_2 flux from near-shore ecosystems are prone to large uncertainties (Borges et al., 2006). For example, estuaries act as sources of CO_2 to the atmosphere due to the degradation of riverine organic carbon (Frankignoulle et al., 1998; Abril et al., 2002). Borges et al. (2006), at the European scale, reported CO_2 release from inner estuaries of about 67.0 Tg C yr^{-1}. This emission would almost fully balance the sink of atmospheric CO_2 computed for continental shelves, although the value is probably an over-estimate due to the type of estuaries used in its compilation, which were mostly macrotidal estuaries with higher aqueous CO_2 concentrations, and due to discrepancies in estuary surface area estimates.

CO_2 fluxes between the atmosphere and coastal systems are usually computed from the partial pressure of CO_2 (pCO_2) measured in water by equilibrators (Frankignoulle et al., 2003;

Borges et al., 2006; Takahashi et al., 2009) or calculated indirectly from carbonate equilibrium constants based on measurements of water temperature, salinity, pH and dissolved inorganic carbon (DIC) (Weiss, 1974; Cai and Wang, 1998). CO_2 fluxes are then calculated using the equation $F = \alpha K \Delta pCO_2$, where α is the CO_2 solubility coefficient, K is the gas transfer velocity that quantifies the rate at which the gas crosses the air/water interface and ΔpCO_2 is the difference between aqueous and gaseous pCO_2. CO_2 exchanges in coastal systems are also computed at the air/water interface using floating chambers (Frankignoulle et al., 1998) or between the air and intertidal sediment at low tide using benthic chambers (Migné et al., 2002). From these studies, it appears that these methods provide insights into the processes that control CO_2 fluxes but sometimes fail to describe the large temporal and spatial variability of the system. Also, CO_2 flux computation can be subject to large uncertainties due to difficulties in accurately assessing gas transfer velocity (Raymond and Cole, 2001). In the coastal zone, K is potentially controlled by wind speed, the size and shape of the ecosystem, water current velocity and its direction relative to the wind and water depth and turbidity (Wanninkhof and McGillis, 1999; Zappa et al., 2003; Borges et al., 2004; Calleja et al., 2008; Abril et al., 2009). Methods for determining K have numerous problems. The floating chamber method has been suspected to artificially enhance CO_2 exchange across the air/water interface (Raymond and Cole, 2001); gas tracer injections are scarce and integrate K values over time scales longer than the tidal rhythm; and low-tide benthic chambers are affected by the heterogeneity and patchiness of the intertidal sediment habitat at various spatial and temporal scales (Migné et al., 2004). Surface heating during low tide could also interfere with metabolic processes on tidal flats.

Contrary to pCO_2-based flux calculations and chamber methods, micro-meteorological measurements and especially the Eddy Correlation technique (EC) seem particularly appropriate for CO_2 flux computations in these heterogeneous and dynamic systems (Vesala et al., 2006; Kathilankal et al., 2008; Zemmelink et al., 2009). In recent years, the EC technique has emerged as an alternative method for continuously assessing CO_2 exchange rates across the atmosphere-vegetation interface by measuring the covariance between fluctuations in the vertical wind velocity and CO_2 mixing ratio at very high frequencies and at the ecosystem scale (Aubinet et al., 2000; Baldocchi, 2003). The EC method is non-invasive, and it provides direct and continuous measurements of net carbon dioxide exchange for a whole ecosystem. The area sampled by this technique, referred to as the method footprint, ranges between a hundred meters and several kilometers depending on measurement height, surface roughness and atmospheric stability. Moreover, EC is capable of measuring

ecosystem CO_2 exchanges across a spectrum of time scales ranging from hours to years (Baldocchi, 1988). Particularly in coastal zones, EC can provide insights into the relationship between ecosystem gas exchange and environmental factors on time scales that are short enough to resolve short-term (diurnal and seasonal) variability in these highly dynamic systems (Zemmelink et al., 2009). For intertidal areas, EC facilitates the comparison of fluxes in the presence and absence of water (Houghton and Woodwell, 1980; Kathilankal et al., 2008; Zemmelink et al., 2009). However, the method also has limitations; it is applicable only under certain turbulent conditions that may not always occur over flat surfaces with potentially modest roughness. For this reason, the EC method requires important qualitative and quantitative analyses as well as corrections based on the physical and theoretical backgrounds underlying the method (Baldocchi et al., 1988).

Few studies have reported EC measurements for continental and coastal aquatic systems in general or for CO_2 fluxes at the air/water and air/sediment interfaces for intertidal systems in particular. Anderson et al. (1999) have used this method to estimate air/water CO_2 fluxes over a small woodland lake in Minnesota, USA, as did Vesala et al. (2006) over a boreal lake in southern Finland for a full open-water period. Morison et al. (2000) used EC to characterize the productivity of C_4 aquatic grass in a tropical Amazonian floodplain, and Guérin et al. (2007) similarly assessed a tropical reservoir in French Guinea. Eugster et al. (2003) estimated CO_2 exchanges by the EC method on Arctic Alaskan and mid-latitude Swiss lakes. Rocha and Goulden (2008) have shown large inter-annual CO_2 and energy exchange variability with the EC technique in a freshwater marsh in southern California. Houghton and Woodwell (1980) and Kathilankal et al. (2008) studied tidal influence on carbon exchanges in salt marshes in the USA, and Zemmelink et al. (2009) applied the EC technique to the intertidal Wadden Sea estuary in Europe.

In this paper, we present one week of EC measurements of momentum, latent heat, sensible heat and carbon dioxide flux over a temperate intertidal flat in the Arcachon lagoon, which is located in southwestern France. This paper attempts to first describe and validate the EC technique for this specific environment, in which fluxes occur alternately between air and sediments as well as between air and water, and to then analyze the physical and biological factors that drive these fluxes under both conditions.

2. Materials and Methods

2.1. Experimental Site Description

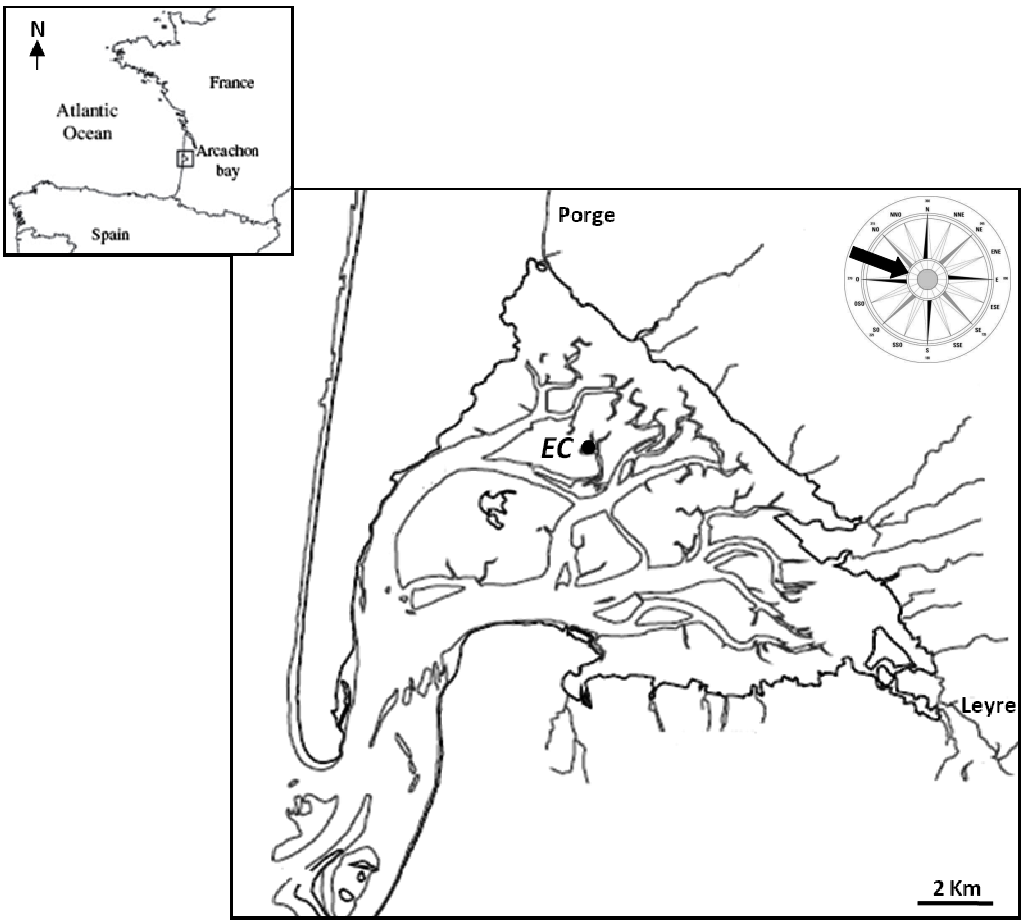

Figure 1. View of the Arcachon lagoon showing the subtidal zone (channels) and the intertidal mud flat area. The location of the eddy correlation (EC) system is shown. The black arrow indicates the prevailing winds measured during the week (from the west-northwest, 270-315°).

The Arcachon lagoon is a temperate intertidal flat with a surface area of 174 km^2 that is located on the southwestern Atlantic coast of France (44°40'N, 01°10'W). This triangularly shaped bay is enclosed by the coastal plain of Landes Gascony and communicates with the Atlantic ocean through an 8-km narrow channel (Figure 1). Its mean depth is 4.6 m. The shallow lagoon experiences semi-diurnal tides with amplitudes varying from 0.8 to 4.6 m (Plus et al., 2008). During a tidal cycle, it exchanges approximately 264 x 10^6 m^3 and 492 x 10^6 m^3 of water with the ocean for average neap and spring tides, respectively. The lagoon also receives freshwater, but to a lesser extent. The annual input of freshwater is 1.25 x 10^9 m^3

(1.8×10^6 m^3 at each tidal cycle), of which 8% is groundwater, 13% is rainfall and 79% is delivered by watercourses (Rimmelin, 1998). The Arcachon watershed includes several watercourses that drain into the lagoon: 17 small streams, 2 canals running north and south and one river, the Leyre, in its southeastern corner. The Leyre represents 73% of the total freshwater flow to the lagoon, and the Porge (northern) canal contributes 24% (Manaud et al., 1997; De Wit et al., 2005; Plus et al., 2008). Water temperatures in the bay range from 6°C in the winter to 22.5°C in the summer; water salinity varies from 22 to 35 PSU as freshwater inputs vary throughout the year.

The Arcachon lagoon surface can be divided in two main parts: the channels, with a maximum depth of 25 m and a surface area of 57 km^2, and shallower channels extending from the main channels, which cover a large intertidal zone of 117 km^2 (Figure 1). Approximately 60% (70 km^2) of the intertidal mud flat is colonized by the aquatic angiosperm *Zostera noltii,* which makes the Arcachon lagoon the most important eelgrass meadow in Europe with an estimated production ranging from 127 to 181 g C m^{-2} yr^{-1} (Auby, 1991). The microphytobenthic communities in the flat also represent a significant proportion of benthic production, which is estimated at between 104 and 114 g C m^{-2} yr^{-1} (Auby, 1991; personal communication). Together, these two categories of benthic primary production represent more than half of the total primary production of the lagoon (Auby, 1991). Near the channels and particularly in the subtidal zone, a more limited extent of *Zostera marina* eelgrass meadow covers 4% of the lagoon surface. About 18,000 tons of Japanese oysters (*Crassostrea gigas)* are also produced in this area each year.

An EC system was moored in the central part of the Arcachon flat (44°42'59.15"N, 01°08'36.96"W) in an intertidal area characterized by *Zostera noltii* eelgrass meadow in July 2008 (Figure 1). Root system growth begins at the end of the winter and maximum amounts of biomass are achieved in the spring. The leaf growth period begins in the spring, and leaves reach maximum biomass in the summer (Auby and Labourg, 1996). During the experiment, the zone was repeatedly exposed to air for four hours and submerged for nine hours. Due to tides, the relative sensor height measurement (Z), which describes the difference between the fixed sensor height and the water level, ranged from 5.50 m at low tide to 2.80 m at high tide (Figure 2).

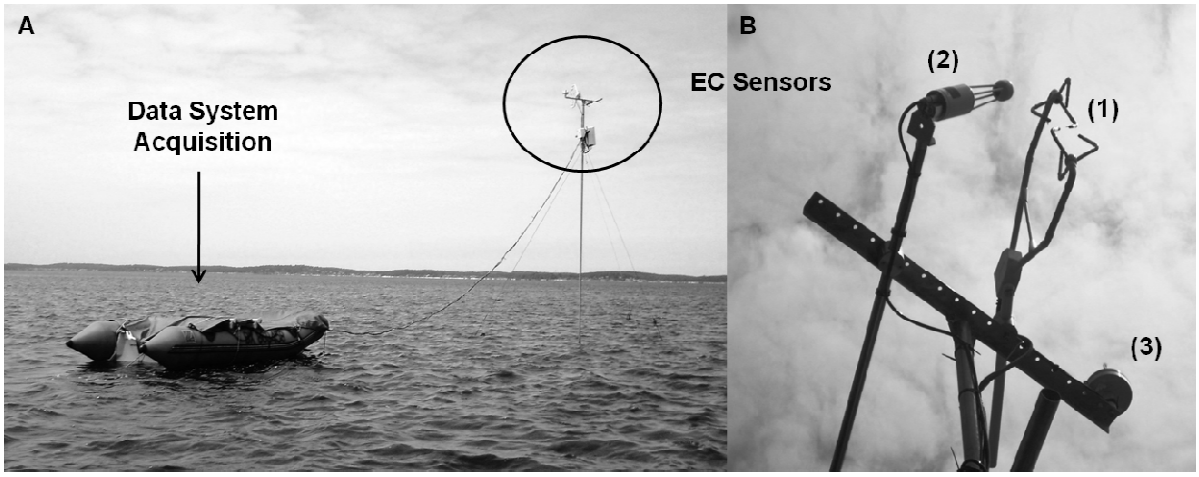

Figure 2. The eddy correlation system in the Arcachon lagoon. A. General view of the measurement system showing the sensors mounted on the mast and the data acquisition system *Campbell CR3000* in the inflatable dinghy. B. Sensors: (1) sonic anemometer *CSAT3*, (2) infrared gas analyzer *LI-7500* and (3) quantum sensor *SKP215*. Sensor height was 5.50 m above the water surface at low tide and 2.80 m at high tide.

2.2. Turbulent flux by the EC technique

The atmosphere contains turbulent motions (eddies) due to the buoyancy and shear of vertically moving air (Aubinet et al., 2000) that transport trace gases, such as CO_2 (Baldocchi, 2003). The EC technique measures turbulent eddies to determine the net fluxes moving vertically across the ecosystem/atmosphere interface.

The mean turbulent flux of the parameter c in the vertical direction (F_c) is expressed as the covariance between the fluctuations in the vertical wind velocity (w) and the parameter density or concentration (ρ_c) as (Moncrieff et al., 1997):

$$F_c = \overline{w'\rho_c'} \quad (1)$$

where the overbar represents a temporal average (for ten minutes in this case) and primes denote the instantaneous turbulence fluctuations in contrast to their temporal average (e.g., $w' = w - \overline{w}$ and $\rho_c' = \rho_c - \overline{\rho_c}$, Reynolds, 1895).

Then, carbon dioxide (F_c), sensible heat (H) and latent (LE) heat fluxes can be defined as:

$$F_c = \overline{w'c'} \quad (2)$$

$$H = \rho C_p \overline{w'T'} \quad (3)$$

$$LE = L\overline{w'q'} \quad (4)$$

where c is CO_2 concentration, ρ is the density of dry air, C_p is the specific heat of the air at a constant pressure, T is the temperature, L is the latent heat of vaporization of water, and q is the H_2O concentration. CO_2 and sensible heat fluxes are directed upward when values of F_c and H are positive and downward when these values are negative.

The friction velocity (u^*, m s^{-1}) can be computed as:

$$u^* = \sqrt{\overline{-w'u'}} \quad (5)$$

where u is the horizontal component of wind.

Finally, the Monin-Obhukov stability index (Z/L) for characterizing atmospheric conditions can be expressed as:

$$\frac{Z}{L} = \frac{Z K g \left(-H / T C_p \right)}{\rho u^{*3}} \quad (6)$$

where Z is the relative sensor height measurement, L is the Monin-Obukhov length, K is the Von-Karman constant and g is the gravitational acceleration.

2.3. Turbulent flux measurement system in the Arcachon lagoon

Fluxes of CO_2 (µmol m^{-2} s^{-1}), latent heat, sensible heat (watt m^{-2}) and friction velocity (m s^{-1}) were measured in the intertidal flat (Figure 2) between July 1 and 7, 2008, using an EC system. The system utilized a sonic anemometer (model *CSAT3, Campbell Scientific Inc.*, Logan, UT) to measure the three components of wind speed (m s^{-1}) and sonic temperature (°C). An infrared gas analyzer (model *LI-7500, Licor Inc.*, Lincoln, NE) measured CO_2 and H_2O concentrations (mmol m^{-3}) in addition to atmospheric pressure (kPa). Analog output signals from these fast-response instruments were sampled and digitized at a rate of 20 Hz. These two main EC sensors were separated by 0.25 m. A filtered silicon quantum sensor (*SKP215, Skype Instruments*, Llandrindod Wells, UK) was used to measure photosynthetically active radiation (PAR, µmol m^{-2} s^{-1}) every minute (Figure 2A). The sensors were mounted on a mast that was driven into the mud and fixed by three wires to keep it vertical and minimize vibrations that could bias EC flux measurements (Figure 2B). Data were transmitted by a waterproof cable to a central acquisition system (model *CR3000, Campbell Scientific Inc.*, Logan, UT), which was located on an anchored inflatable dinghy and protected by a tide pool. The entire system was powered by rechargeable lead batteries (12 volts, 100 amps by hour), which were replaced every four days.

2.4. Data processing: computations and corrections

Raw data were processed following the Aubinet et al. (2000) method. This method was originally developed in the context of the EUROFLUX project for net carbon and water exchanges in forests and was modified for application to the intertidal zone. One modification involved incorporating the variations in relative measurement height caused by tides. Fluxes were also computed with a shorter averaging period than usual (10 rather than 30 min) to capture the quick transitions between low and high tides.

The *EdiRe* software from the University of Edinburgh (Scotland) was selected for this study because it includes all of the necessary options for processing EC data (Mauder et al., 2008). Data processing involved nine steps. (1) Spikes were removed from anemometer and gas analyzer data using a threshold based on the standard deviation of the difference between consecutive data points. After (2) modifying units and applying statistical operations, (3) coordinates were rotated to align with the streamlines of the ten-minute averages. Two rotations were made around the z- and y-axes. (4) Linear trends were removed from the sonic temperature, H_2O and CO_2 channels to eliminate low-frequency effects. (5) Time-lag values were determined for the H_2O and CO_2 channels using a cross-correlation procedure that finds the maximum absolute correlation within a time lag window of $-1 \leq \tau \leq 1$ s for each ten-minute segment of raw data. (6) Mean values, turbulent fluxes and characteristic parameters, including the Monin-Obhukov stability index (Z/L), were computed and (7) high-frequency corrections were made to account for losses due to sensor time responses, sensor spatial separation and digital sampling. All of these frequency corrections were applied through transfer functions based on Kaimal-Moore's cospectral models (Kaimal et al., 1972; Moore, 1986). (8) To account for the effects of fluctuations in temperature and water vapor on the measured fluctuations in CO_2 and H_2O (Webb et al., 1980), data were corrected by the Webb-Pearman-Leuning method. For CO_2 flux (F_c) in an open-path infrared gas analyzer, the relevant equation is:

$$F_c = \overline{w'c'} + \mu\frac{\bar{c}}{\bar{\rho}}\overline{w'q'} + (1+\mu\sigma)\frac{\bar{c}}{\bar{T}}\overline{w'T'} \qquad (7)$$

where μ is the ratio of the molecular weights of dry air and water vapor and σ is the ratio of the densities of water vapor and dry air. (9) Finally, statistical tests (steady-state and integral turbulence characteristics tests) were used to verify the quality of the data.

During the study, the fetch around the mast was at least 1,000 m at low tide and larger at high tide in all wind directions (Figure 1). Therefore, we can assume that all measured fluxes

originated from the intertidal area because these distances generally exceed the EC measurement footprint. It is commonly assumed that the Z:fetch ratio must be lower than 1:100 for unstable atmospheric conditions and lower than 1:300 for stable atmospheric conditions (Leclerc and Thurtell, 1990; Hsieh et al., 2000). With Z equal to 5.50 m at low tide, the system required a minimum fetch of 550 m for unstable conditions and 1650 m for stable conditions. Our fetch distance of at least 1000 m fulfils this criterion most of the time for stable conditions and all of the time for unstable conditions, which are more frequent.

When Z is high (low tide), it is possible that our ten-minute averaging time fails to capture low-frequency (LF) contributions to turbulent fluxes, which correspond to large eddies. Alternatively, when Z is low (high tide), the sensors may not be fast enough to capture high-frequency (HF) contributions that correspond to small eddies. Of course, the position of the cospectra and consequently the likelihood of missing these patterns depend on wind speed. This effect of wind speed has the opposite effect from that of Z; it shifts toward LF patterns when the wind speed decreases and vice versa. However, because the flat is fairly smooth, the wind speed gradient between 5.50 and 2.80 m height is weak, especially during unstable conditions.

2.5. Cospectral analysis

In parallel with the data processing described above, cospectral analysis was conducted to quantify the frequency distribution of the covariance of the raw signals (w-c, w-q, w-T) (Figure 6).

First, the cospectra of the raw data were computed with the *EdiRe* software for each of the ten-minute samples. Power cospectra between the vertical wind velocity and carbon dioxide concentration, water vapor concentration and temperature were normalized by the product of the standard deviation of w and carbon dioxide (c), water vapor (q) and temperature (T), respectively. Normalization facilitates quantification of the efficacy of vertical transfer of the relevant parameter. Finally, cospectra were presented in semi-log scale according to the normalized frequency, n, defined as:

$$n = fZ/u \quad (8)$$

where f denotes the natural frequency (Hz), Z is the relative sensor measurement height and u is the wind speed (m s^{-1}).

Figure 6A presents the median-averaged cospectra of all ten-minute samples from the daytime low tide sequence for July 5, 2008, 12:00 to 14:00 GMT. Similarly, Figures 6B and

6C present median-averaged cospectra for the nighttime low tide sequence from July 6, 2008, 23:00 to 01:00 GMT and for the daytime high tide sequence from July 6, 17:00 to 19:00 GMT. Sufficient continuous data for this analysis were not available for the nighttime high tide case.

Finally, ideal cospectra from Kaimal and Finnigan (1994) were plotted to analyze the position of the cospectra obtained in our experiment. This procedure can identify possible losses at low or high frequencies due to the arrangement of the EC system or meteorological conditions (see 2.4).

2.6. Data quality control

The removal of errant processed data is important for obtaining reliable turbulent flux measurements from the eddy correlation technique. Potential causes of bias or error include instrument malfunctions, processing/mathematical artefacts, ambient conditions that are not conducive to the EC method (non-stationary periods, convergence, and divergence), heavy precipitation (particularly for the open-path gas analyzer) or a measurement footprint larger than the zone of interest (Burba and Anderson, 2005). Steady-state conditions were tested with coupled signals: (u, w), (v, w), (w, T), (w, c) and (w, q). Standard deviations and covariances of the specified signals were computed on short time intervals of one minute, and these values were compared to those computed from the chosen time interval of ten minutes. Only steady-state data (from periods with differences of less than 30%) were retained according to Foken and Wichura (1996). A second statistical test (Foken et al., 1991, 1997) was used to verify EC data quality based on the integral turbulence characteristics of wind components and temperature. Values of σ_w/u^* and σ_T/T^* were computed (where σ is the standard deviation of the specified signals) and compared to their parameterized values for various ranges of stability (Z/L). Only data with at least a 50% match were retained. Using these two statistical tests, retained EC data for the Arcachon lagoon study are considered "high quality data" and have a general flag from 1 to 3 following the 2nd QA/QC Workshop for Eddy Covariance Measurements (18-19 January 2004, Italy; Foken, 2003).

Figure 3 shows the turbulent flux data (H, LE and F_c) before and after quality processing. In total, 17%, 9% and 8% of CO_2, latent heat and sensible heat fluxes were discarded, respectively.

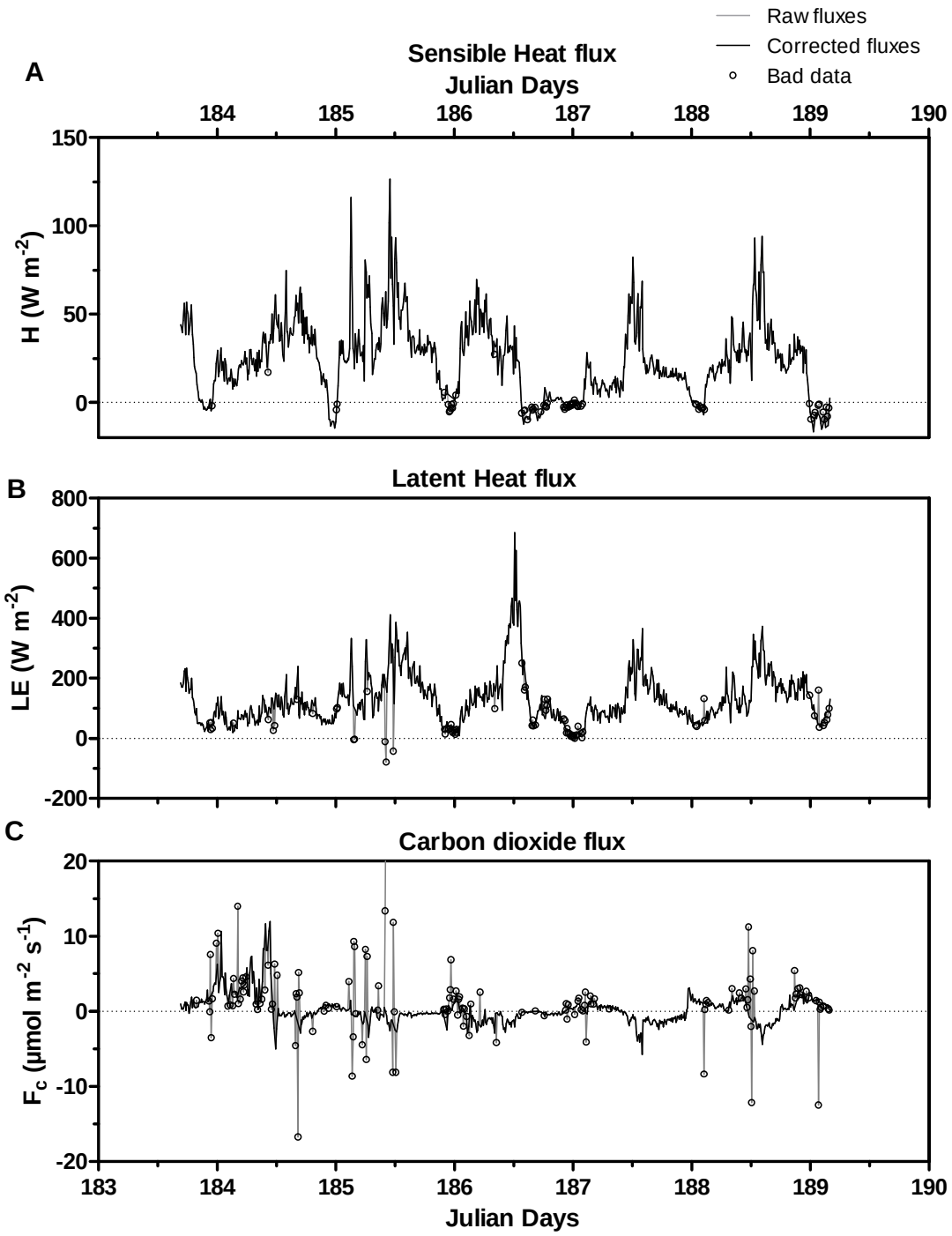

Figure 3. Turbulent fluxes obtained by EC before and after data quality processing. A: Sensible heat flux (H), B: latent heat flux (LE) and C: Carbon dioxide flux (F_c). Only 8%, 9% and 17% of H, LE and F_c data, respectively, were discarded to obtain high-quality flux results. Some of the raw data are not shown in C (above 40 µmol m^{-2} s^{-1}, day 185) to more clearly show F_c variations.

3. Results and Discussion

Diurnal and tidal rhythms engender distinctive conditions in the Arcachon tidal flat that are useful for describing ecosystem function. In the following sections, we refer to these cases as daytime low tide (LT/Day), nighttime low tide (LT/Night), daytime high tide (HT/Day) and nighttime high tide (HT/Night).

3.1. Characteristics of the study period in the Arcachon lagoon

3.1.1. Environmental conditions

Table 1 and Figure 4 present meteorological parameters measured between July 1 (day 183, 16:40 GMT) and July 7, 2008 (day 189, 04:00 GMT). Variable meteorological conditions were encountered during the week. Water height averaged 0.93 ± 0.91 m (Table 1) and ranged from 0 m at low tide to a maximum of 2.65 m at high tide on day 186 (Figure 4). Air exposure typically lasted four hours and immersion lasted nine hours. Sunlight was roughly synchronized with low tide during the deployment. The first day was heavily clouded, with PAR values below about 500 µmol m^{-2} s^{-1} at midday (Figure 4A). Days 185 and 186 were sunny with intermittent clouds, and PAR values reached approximately 2000 µmol m^{-2} s^{-1} at midday. The two last days (187 and 188) were characterized by intermediate conditions and had PAR values of approximately 1250 µmol m^{-2} s^{-1} at midday.

Air temperatures fluctuated around a mean value of 19.8 ± 1.7°C according to the diurnal rhythm and ranged between 15.5°C and 25°C (Figure 4B, Table 1). However, strong, rapid variations were observed particularly with wind direction changes. For instance, during ebb tide on day 186, the air temperature increased from 15.5°C to 24.9°C when the wind direction shifted from the east-southeast (90-135°) to the south-southwest (180-225°) (Figures 4B and F).

Concentrations of CO_2 and H_2O in the air also showed large diurnal and tidal variations, ranging between 349 and 421 ppmv and between 7.15 and 14.8 g m^{-3}, respectively (Table 1). Minimum air CO_2 concentrations of about 350 ppmv were observed during LT/Day, and maximum values of up to 410 ppmv were recorded during LT/Night (Figure 4C). As for air temperature, dramatic changes in H_2O concentration were observed on day 186 with wind direction changes. During LT/Day, H_2O concentration dropped from 11 to 8 g m^{-3} as the temperature increased with the change of wind direction described above (Figure 4F). As the tide rose and air temperature decreased at dusk, the H_2O concentration in the air increased and remained at approximately 12 g m^{-3} until day 187 (Figure 4D).

Environmental parameters	Low Tide / Day	Low Tide / Night	High Tide / Day	High Tide / Night	Average
PAR ($\mu mol\ m^{-2}\ s^{-1}$)	**1102 ± 613** (23 ~ 2185)	(0 ~ 15)	**562 ± 524** (21 ~ 2020)	(0 ~ 19)	**425 ± 570** (0 ~ 2185)
h (m)			**1.5 ± 0.8** (0.1 ~ 2.6)	**1.1 ± 0.7** (0.1 ~ 2.5)	**0.9 ± 0.9** (0 ~ 2.6)
T_a (°C)	**20.6 ± 1.9** (17.6 ~ 24.9)	**19.2 ± 1.2** (15.7 ~ 21.7)	**19.8 ± 1.8** (15.9 ~ 24.6)	**19.5 ± 1.7** (15.5 ~ 22.8)	**19.8 ± 1.7** (15.5 ~ 24.9)
P_a (hP_a)	**1014 ± 2** (1009 ~ 1016)	**1013 ± 2** (1011 ~ 1018)	**1013 ± 2** (1010 ~ 1017)	**1013 ± 2** (1009 ~ 1018)	**1013 ± 2** (1009 ~ 1018)
CO_2 (ppmv)	**376 ± 7** (349 ~ 403)	**382 ± 10** (369 ~ 413)	**378 ± 6** (365 ~ 407)	**383 ± 10** (372 ~ 421)	**380 ± 8** (349 ~ 421)
H_20 ($g\ m^{-3}$)	**10.3 ± 1.2** (7.3 ~ 13.2)	**10.9 ± 1.3** (8.6 ~ 12.8)	**10.5 ± 1.3** (8.0 ~ 14.8)	**10.6 ± 1.4** (7.1 ~ 14.0)	**10.6 ± 1.3** (7.1 ~ 14.8)
e (kP_a)	**1.4 ± 0.2** (1.0 ~ 7.8)	**1.5 ± 0.2** (1.2 ~ 1.8)	**1.4 ± 0.2** (1.1 ~ 2.0)	**1.4 ± 0.2** (1.0 ~ 1.9)	**1.4 ± 0.2** (1.0 ~ 2.0)
Wind speed ($m\ s^{-1}$)	**5.3 ± 1.3** (1.4 ~ 8.5)	**3.9 ± 1.7** (0.6 ~ 7.9)	**4.8 ± 1.6** (1.3 ~ 8.4)	**4.2 ± 1.9** (0.9 ~ 10.0)	**4.6 ± 1.7** (0.6 ~ 10.0)

Table 1. Environmental parameters in the Arcachon lagoon between July 1 and 7, 2008 are classified according tidal and diurnal rhythms (low tide / day, low tide / night, high tide / day and high tide / night). PAR: photosynthetically active radiation; h: water height; T_a: air temperature; P_a: air pressure; CO_2 and H_2O: carbon dioxide and water concentrations in the atmosphere; e: water vapor pressure in the atmosphere.
A threshold PAR value of 20 µmol m^{-2} s^{-1} was used to distinguish day and night; high tide conditions were defined as having non-zero water depths. Four PAR values above 2200 µmol m^{-2} s^{-1} were not included in the average PAR calculations because they are unrealistic and attributed to quantum sensor noise.

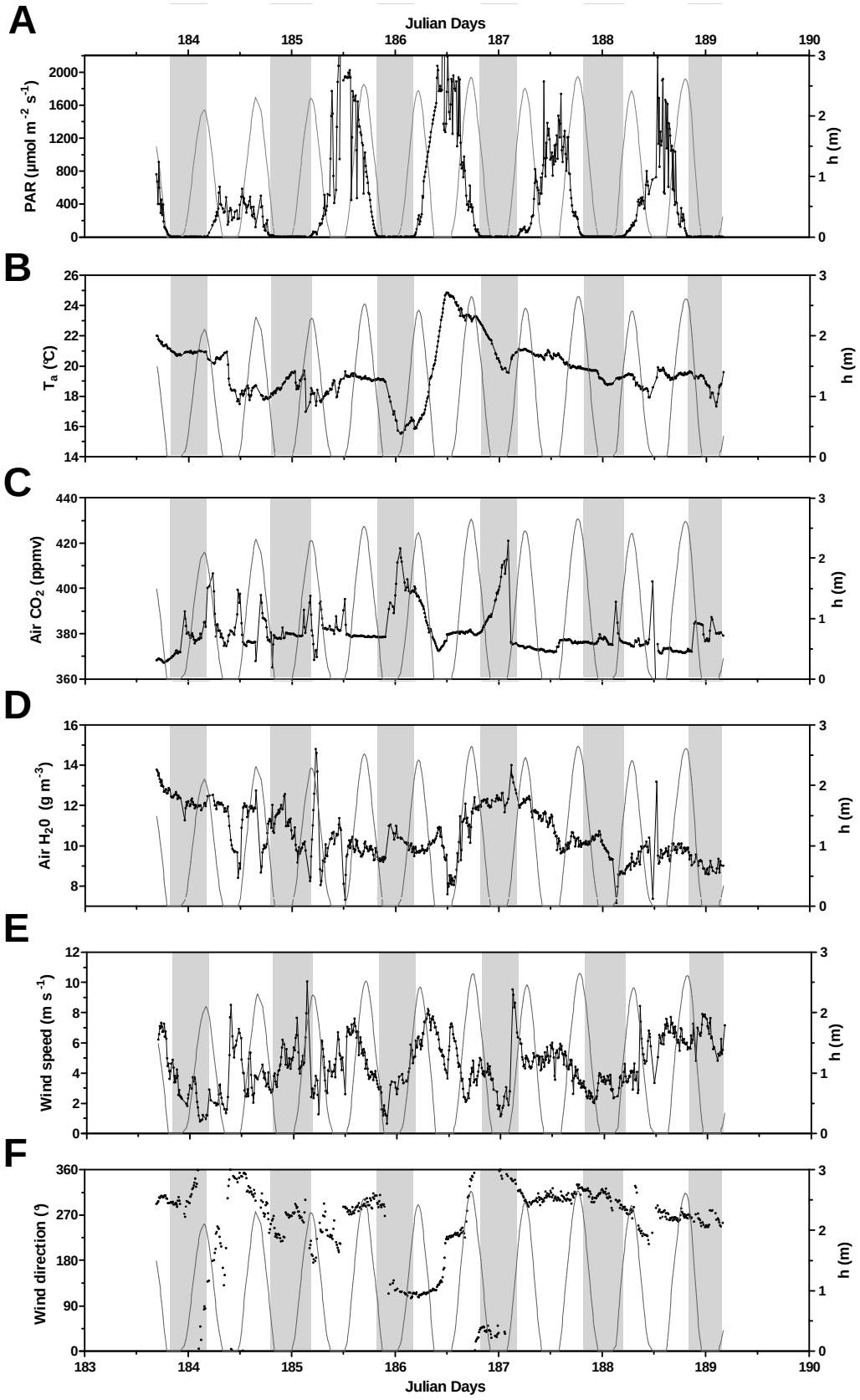
A
Julian Days
PAR (µmol m-2 s-1)
h (m)
B
Ta (°C)
h (m)
C
Air CO2 (ppmv)
h (m)
D
Air H20 (g m-3)
h (m)
E
Wind speed (m s-1)
h (m)
F
Wind direction (°)
h (m)
Julian Days

Figure 4. Environmental parameters measured in the Arcachon lagoon between July 1, 16:40 (GMT) and July 7, 2008, 04:00 (GMT). A: Photosynthetically active radiation (PAR) and water height (h); B: air temperature (T_a); C: carbon dioxide concentration in the air (CO_2); D: water vapor concentration in the air (H_2O); E: wind speed and F: wind direction. Data for day 183 (July 1, 2008) are squares, and grey bands represent night periods. A PAR value of 20 µmol m^{-2} s^{-1} was used to distinguish daytime and nighttime periods, and high tide periods are defined as having non-zero water depths. In A, four PAR data points above 2200 µmol m^{-2} s^{-1} are off-scale and are attributed to quantum sensor noise.

Wind speeds underwent large, rapid variations throughout the study period, ranging from 0.6 to 10.0 m s^{-1} (Figure 4E) with a mean value of 4.6 ± 1.7 m s^{-1} (Table 1). Winds most frequently (40% of the time) flowed from the west-northwest (270-315°), and other wind modes flowed from the west-southwest and north-northwest (225-270° and 315-360°, respectively) (Figure 4F). In the Arcachon lagoon, the prevailing winds generally blow from the west, but northerlies are dominant during the spring and summer (Manaud et al., 1997). During LT/Day 184, a sudden increase in wind speed from approximately 1.5 to 8.5 m s^{-1} occurred concomitant with an upwind direction change from the west-southwest (225-270°) to the north-northwest (315-360°) (Figures 4E and F).

3.1.2. Temporal variations in EC turbulent fluxes

Figure 5 presents temporal variations in the turbulent fluxes between the atmosphere and the Arcachon lagoon. The friction velocity (u^*), which is computed from the momentum flux, was weak throughout the experiment; its mean value was 0.21 ± 0.09 m s^{-1} (Table 2), and it generally ranged between 0.1 and 0.3 m s^{-1} (Figure 5B). Values of u^* were similar or slightly higher than those observed over lakes (Vesala et al., 2006) and bare soil (Stella et al., 2011). The lowest u^* values were generally measured during the night (LT/Night and HT/Night), and the highest values were recorded during LT/Day and to a lesser extent at high tide (Figure 5B). During LT/Day 184, notably high u^* values of around 0.6 m s^{-1} occurred (Figure 5B) simultaneously with the same changes in wind speed and direction that are described above (Figures 4E and F).

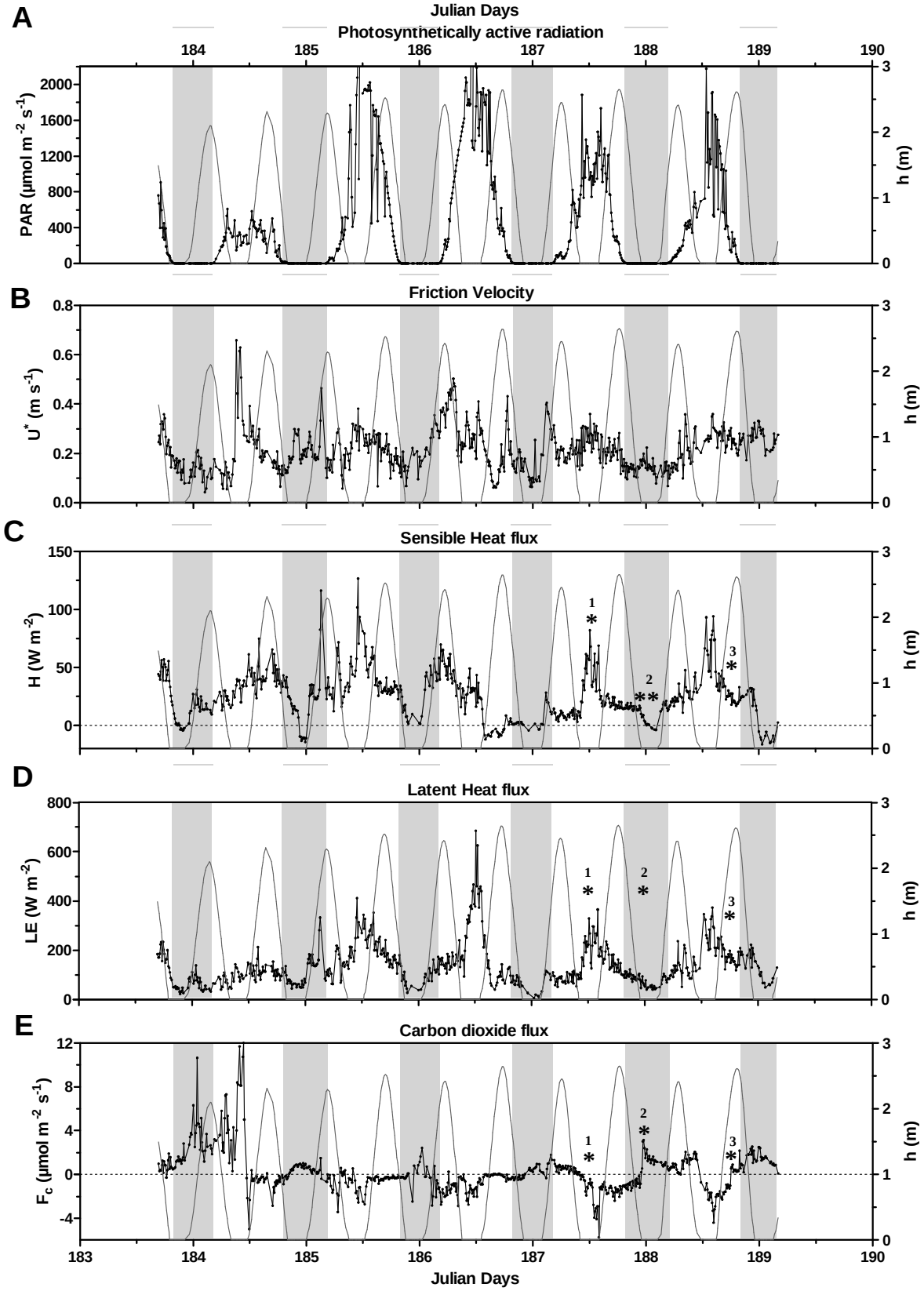
A
Julian Days
Photosynthetically active radiation
PAR (µmol m-2 s-1)
h (m)
B
Friction Velocity
U* (m s-1)
h (m)
C
Sensible Heat flux
H (W m-2)
h (m)
D
Latent Heat flux
LE (W m-2)
h (m)
E
Carbon dioxide flux
Fc (µmol m-2 s-1)
h (m)
Julian Days

Figure 5. Turbulent fluxes measured by EC in the Arcachon lagoon during July 1-7, 2008. A: Photosynthetically active radiation (PAR); B: friction velocity (u^*); C: sensible heat flux (H); D: latent heat flux (LE) and E: carbon dioxide flux (F_c). Data for day 183 (July 1, 2008) are squares, and grey bands represent night periods. The ***** identify periods during which spectral and cospectral analyses were made (Figure 6): Low Tide / Day, 12:00 to 14:00 GMT (05/07/2008), Low Tide / Night, 23:00 to 01:00 GMT (06/07/2008) and High Tide / Day, 17:00 to 19:00 GMT (06/07/2008). A PAR value of 20 µmol m^{-2} s^{-1} was used to distinguish daytime and nighttime periods, and high tide periods were defined as having non-zero water depths.

	Low Tide / Day	**Low Tide / Night**	**High Tide / Day**	**High Tide / Night**	**Average**
u^* (m s^{-1})	**0.3 ± 0.1** (0.1 ~ 0.7)	**0.2 ± 0.1** (0.1 ~ 0.3)	**0.2 ± 0.1** (0.1 ~ 0.5)	**0.2 ± 0.1** (0.0 ~ 0.5)	**0.2 ± 0.1** (0.0 ~ 0.7)
H (W m^{-2})	**43.8 ± 22.6** (6.7 ~ 126.6)	**2.5 ± 11.0** (-16.5 ~ 32.7)	**28.5 ± 17.6** (-12.1 ~ 74.9)	**22.7 ± 18.0** (-14.1 ~ 116.2)	**26.0 ± 20.8** (-16.5 ~ 126.6)
LE (W m^{-2})	**235.3 ± 124.5** (44.9 ~ 684.7)	**62.4 ± 31.5** (5.5 ~ 184.5)	**148.8 ± 64.3** (40.7 ~ 458.2)	**104.5 ± 51.2** (32.9 ~ 332.4)	**141 ± 86.3** (5.5 ~ 684.7)
F_c (µmol m^{-2} s^{-1})	**-0.3 ± 3.3** (-5.7 ~ 12)	**0.9 ± 0.8** (-2.5 ~ 3.1)	**-0.2 ± 1.4** (-5.0 ~ 7.3)	**0.7 ± 1.9** (-2.8 ~ 10.6)	**0.1 ± 1.9** (-5.7 ~ 12.0)
Z/L	**-0.17 ± 0.14** (-0.84 ~ -0.01)	**-0.02 ± 0.23** (-1.5 ~ 0.47)	**-0.15 ± 0.25** (-1.76 ~ 0.56)	**-0.23 ± 0.26** (-1.25 ~ 0.08)	**-0.15 ± 0.25** (-1.76 ~ 0.56)

Table 2. Indices and fluxes measured by EC in the Arcachon lagoon from July 1-7, 2008 are classified according tidal and diurnal periods (low tide / day, low tide / night, high tide / day and high tide / night). u^*: Friction velocity; H: sensible heat flux; LE: latent heat flux; F_c: carbon dioxide flux and Z/L: Monin-Obhukov stability parameter for the atmosphere. Positive fluxes are from the basin to the atmosphere and negative fluxes are from the atmosphere to the basin. Averages ± SD are in bold and ranges are between brackets. A PAR value of 20 µmol m^{-2} s^{-1} was used to distinguish daytime and nighttime periods, and high tide was defined as having non-zero water depths.

Fluxes of H and LE averaged 26.0 ± 20.8 W m^{-2} and 141.0 ± 86.3 W m^{-2} (Table 2), respectively. Trends were similar throughout the week (Figures 5C and D). Heat fluxes were significantly different during the four cases ($p<0.05$). H and LE exchanges between the lagoon and the atmosphere followed the diurnal cycle with, in average, minimum values measured during nighttime LT and HT (Figures 5C and D, Table 2). Maximum mean values were reached at midday. Based on meteorological parameters, an interesting heat flux pattern occurred on day 186: a strong LE peak (around 600 W m^{-2}) was observed during low tide (Figure 5D) that corresponded precisely to the observed increase in air temperature and decrease in H_2O concentration that are associated with the change in wind direction from the east-southeast to the south-southwest (Figure 4). High evapotranspiration rates were further enhanced by a rapid drop in air pressure (from 1016 to 1012 hPa) at this time (temporal variations not shown, Table 1). As the tide rose, it moved cold waters over the warm mud sediments at the same time that evening air temperature decreased. As the H_2O concentration increased, the LE flux was reduced. At the same time, H fluxes from the atmosphere to the water became negative because the air became warmer than the surface water (Figures 4 and 5). Latent heat fluxes were clearly larger than sensible heat fluxes throughout the experiment. The Bowen ratio (H/LE) was generally below 0.5 except during HT/Day, when its value was 0.89. This finding is in agreement with results by Vesala et al. (2006) over a boreal lake in Southern Finland. Days 185 and 186 showed contrasting heat flux trends; relative to H, LE was particularly high on day 186. The opposite condition occurred on the previous day, when H fluxes increased to more than 100 W m^{-2} while LE remained near 300 W m^{-2} (Figures 5C and D).

H flux and friction velocity (u^*) define atmospheric stability in the Arcachon lagoon. The tidal flat was generally characterized by unstable conditions (i.e., a negative mean Monin-Obhukov stability index, Z/L) even at night (Table 2). Overall, 71% of the data set was characterized by Z/L values of less than -0.04. Of the remainder, 15% had Z/L values between -0.04 and zero, indicating neutral conditions, and 13% had positive values, indicating stable conditions (Kader et al., 1990). During unstable conditions, large convective turbulent structures developed and supported large turbulent exchanges. During LT/Day, unstable conditions in the lagoon had strongly negative Z/L values of -0.17 ± 0.14. These atmospheric conditions resulted from fairly low u^* values and strong positive H fluxes (warm air moving upward). The strongly positive H fluxes are more diagnostic of this case than the u^* effect. During HT/Day and HT/Night, Z/L values for unstable conditions averaged -0.15 ± 0.25 and -0.23 ± 0.26 (Table 2). H fluxes were positive but demonstrated smaller variations than in the

previous case therefore u^* had a greater influence on atmospheric conditions during these cases. In contrast, the LT/Night case experienced greater stability. Its near-neutral conditions were characterized by significantly ($p<0.05$) less negative Z/L values than the others (-0.02 ± 0.23, Table 2). The LT/Night case was associated with weakly positive or even negative H fluxes (Table 2).

CO_2 fluxes between the lagoon and the atmosphere were generally weak during the study period; the values mostly ranged between -4.0 and 2.0 µmol m^{-2} s^{-1} (Figure 5E). CO_2 exchanges at both the air/water and the air/sediment interfaces responded significantly ($p<0.05$) to the tidal and the diurnal cycles and were also affected by weather conditions (Figure 5E). A large amount of CO_2 was emitted to the atmosphere during the cloudy, unstable period at the beginning of the experiment regardless of the regular cycles. Specifically, a peak CO_2 flux (12.0 µmol m^{-2} s^{-1}) occurred during low tide on day 184, concurrent with the previously discussed changes in friction velocity and wind direction (Figures 5E and 4). During subsequent LT/Day cases, CO_2 flux values were generally negative and averaged -0.3 ± 3.3 µmol m^{-2} s^{-1} (Table 2). A CO_2 sink of approximately 2.0 µmol m^{-2} s^{-1} was observed on days 185 and 186 (Figure 5E); there were no clear differences between the two days despite their different heat flux trends (Figures 5C and D). On the two following days, slightly larger CO_2 sinks (approximately 3.0 µmol m^{-2} s^{-1}) were measured. These sinks were balanced by releases of CO_2 to the atmosphere during LT/Night (averaging 0.9 ± 0.8 µmol m^{-2} s^{-1}). During nights 185/186 and 187/188, CO_2 degassing was 2.0 µmol m^{-2} s^{-1} (Figure 5E). During incoming and high tides, CO_2 uptake by the lagoon and CO_2 degassing to the atmosphere were reduced by 35% and 21%, respectively (Table 2). For example, on night 187/188, CO_2 degassing decreased from 1.1 µmol m^{-2} s^{-1} at low tide to 0.8 µmol m^{-2} s^{-1} one hour later, after the tide had risen by only 35 cm (Figure 5E).

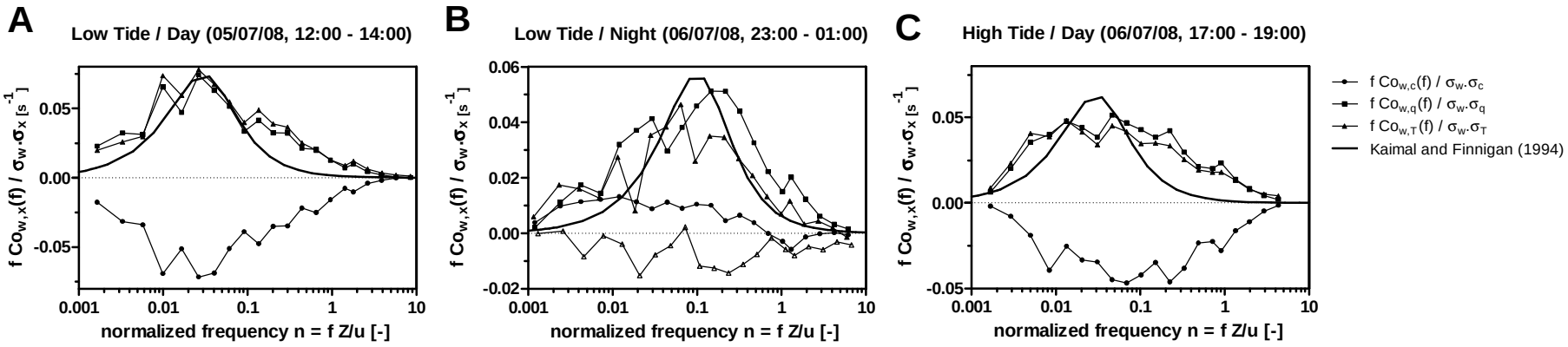

Figure 6. Power cospectra (semi-log graphs) obtained during EC flux measurement in the Arcachon lagoon are classified according diurnal and tidal rhythms (Low Tide / Day, Low Tide / Night and High Tide / Day). A: Carbon dioxide (CO_2), B: latent heat (LE) and C: sensible heat (H) flux cospectra were median-averaged for the following periods: A: Low Tide / Day, 12:00 to 14:00 GMT (05/07/2008), B: Low Tide / Night, 23:00 to 01:00 GMT (06/07/2008) and C: High Tide / Day, 17:00 to 19:00 GMT (06/07/2008) (see ***** in Figure 5). The High Tide / Night case is not shown because very few data matched this sequence. Cospectra from Kaimal and Finningan (1994) centered according to their Z/L values are presented for comparison. In the Low Tide / Night case, the H cospectrum has been separated into two median-averaged cospectra from 23:00 to 00:00 (positive H cospectrum) and from 00:00 to 01:00 (negative H cospectrum) that correspond to positive and negative H flux values (Figure 5). Positive cospectra represent fluxes from the lagoon to the atmosphere and negative cospectra represent fluxes from the atmosphere to the lagoon.

3.2. Cospectral analysis

Figure 6 presents the averaged and normalized cospectra obtained during LT/Day, LT/Night and HT/Day periods (see 2.5.). The shapes and the trends observed in the CO_2 (w_c), latent heat (w_q) and sensible heat (w_T) flux cospectra show interesting patterns. In the three cases, all cospectra appeared well defined and similar in the HF domain (Figures 6A, B and C). They close at the characteristic normalized frequency limit of ten and no HF cut-offs were observed in w_c and w_q compared to w_T. In contrast, Eugster et al. (2003), using a closed-path gas analyzer in their EC set up over a midlatitude Swiss lake, observed HF losses in CO_2 and H_2O cospectra. The results obtained in the case of the Arcachon lagoon, using an open-path gas analyzer, show for the three cases that no HF losses occurred in the CO_2 and H_2O flux measurements using a sensor response of 20 Hz, and that EC fluxes in the HF domain were well quantified. These results show that the relative sensor height Z was adequate to measure all small eddies even during high tide when Z was minimized (see 2.4).

Because unstable conditions dominated during the LT/Day and HT/Day cases (Table 2), the fluxes were dominated by large scale convective turbulence structures, which shifted the cospectra toward lower frequencies than in LT/Night case as observed elsewhere by Kaimal and Finnigan (1994) and Sahlée et al. (2008). In the LT/Day and HT/Day cases, the cospectra matched fairly well with ideal cospectra from Kaimal and Finnigan (1994), whose maxima were centered on normalized frequencies near 0.03 for unstable conditions. During LT/Day, the predominance of unstable conditions along with a maximum measurement height, explain the slight LF losses observed in Figure 6A. This led to an underestimation of all fluxes by about 10%.

In LT/Night case, less unstable or near-neutral atmospheric conditions were recorded (Table 2). In consequence, all cospectra close in the LF domain (Figure 6B). They match roughly with the position of the theoretical cospectra centered on normalized frequencies close to 0.1 in the case of Z/L values near zero (Kaimal and Finnigan, 1994). Nevertheless, the w_c cospectra, which is positive in this case due to respiration fluxes, is slightly displaced toward lower frequencies (Figure 6B) compared to the others (w_q and w_T). This finding may arise from the spatial heterogeneity that characterizes the flat during LT/Night because *Zostera noltii* seagrass meadows are distributed patchily over the sediment. In their study on EC fluxes between the atmosphere and a Swiss lake, Eugster et al. (2003) observed LF contributions from land-based respiration in their w_c cospectra. Mahrt et al. (2001) showed

that spatial variations in the case of moisture surface flux induced a shift toward larger scales. In our study, this LF shift was not encountered in the w_q cospectra for LT/Night due to homogeneous evaporation from the uniform sediments; the aquatic plant transpiration was zero at night due to stomatal closure.

In conclusion, a frequency sensor response of 20 Hz and an averaging time of ten minutes appear to effectively balance the need to integrate low-frequency signals with the need to detect the quick flux variations that characterize these dynamic, heterogeneous systems due to the effects of tidal rhythms.

3.3. Flux comparison and physical / biological controls on turbulent exchanges in the Arcachon lagoon

3.3.1. Comparison with other systems

For the last few years, the EC technique has been used to estimate turbulent exchanges over aquatic environments ranging from oceans to tidal lakes and marshes. Kondo and Tsukamoto (2007) measured CO_2 fluxes over the equatorial Indian Ocean that ranged from -2.1 to 2.1 µmol m^{-2} s^{-1}. Vesala et al. (2006) measured turbulent fluxes over a boreal lake for a full open-water period and found ranges of 0.1 to 0.3 m s^{-1}, -20 to 40 W m^{-2}, 0 to 100 W m^{-2} and -1 to 5 µmol m^{-2} s^{-1} for the friction velocity (u^*), sensible heat (H), latent heat (LE) and carbon dioxide (F_c) fluxes, respectively. In a freshwater marsh in southern California, Rocha and Goulden (2008) estimated fluxes of -200 to 600 W m^{-2}, 0 to 450 W m^{-2} and -30 to 10 µmol m^{-2} s^{-1} for H, LE and F_c, respectively. For the Amazon floodplain, Morison et al. (2000) found CO_2 and latent heat fluxes ranging from -60 to 20 µmol m^{-2} s^{-1} and from 0 to 10 mmol m^{-2} s^{-1}, respectively. In a tidally influenced environment, a salt marsh in Virginia (USA), Kathilankal et al. (2008) estimated turbulent fluxes that ranged from -50 to 200 W m^{-2} for H, from 0 to 600 W m^{-2} for LE and from -8 to 4 µmol m^{-2} s^{-1} for F_c. Zemmelink et al. (2009) found springtime carbon dioxide fluxes of +/- 10 µmol m^{-2} s^{-1} over the intertidal Wadden Sea estuary.

In comparison with these results, the EC deployment in the Arcachon tidal flat found values of u^*, H, LE and F_c that ranged from 0.04 to 0.66 m s^{-1}, from -16.5 to 126.6 W m^{-2}, from 5.5 to 684.7 W m^{-2} and from -5.7 to 12 µmol m^{-2} s^{-1}, respectively. These results are generally higher than those obtained over oceans or lakes (Eugster et al., 2003), but they are rather low relative to salt and freshwater marshes (Houghton and Woodwell, 1980; Rocha and Goulden, 2008) as well as temperate and tropical estuaries (Frankignoulle, 1998; Morison et al., 2000), with the exception of LE.

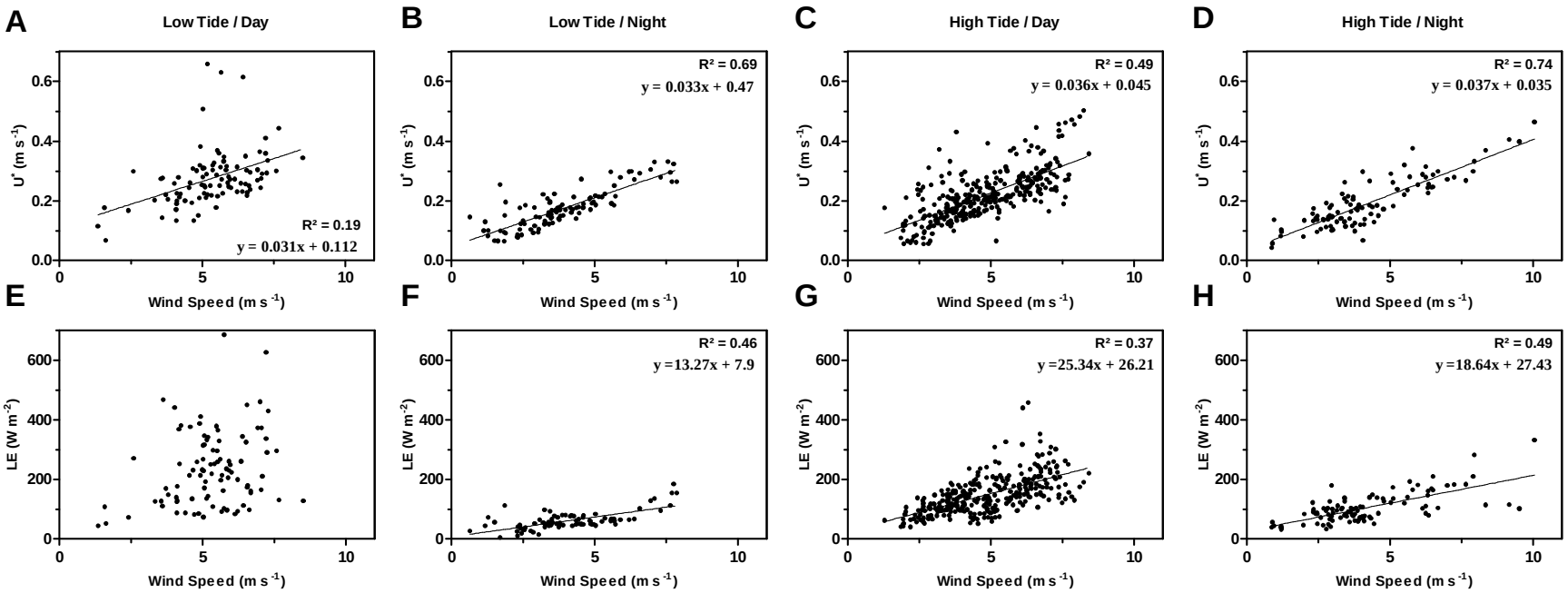

Figure 7. Influence of wind speed on EC-measured turbulent fluxes during the four periods in the Arcachon lagoon. A, B, C and D: friction velocity (u^*); E, F, G and H: latent heat flux (LE). A PAR value of 20 µmol m^{-2} s^{-1} was used to distinguish daytime and nighttime periods, and high tide periods were defined as having non-zero water depths. P values for all of the linear regressions are significant (<0.0001).

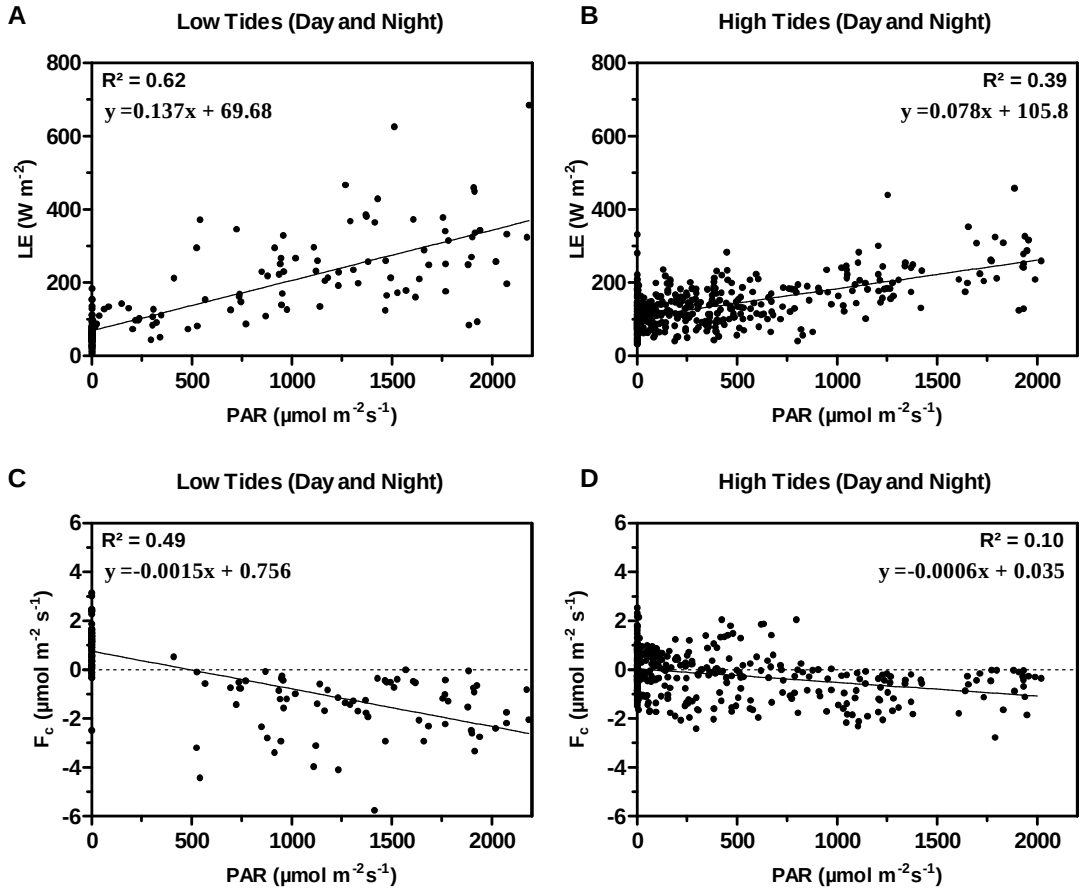

Figure 8. Influence of photosynthetically active radiation (PAR) on EC turbulent fluxes at low and high tides in the lagoon. A and B: latent heat (LE); C and D: carbon dioxide (F_c). A and C: low tides; B and D: high tides. F_c values at night are presented to demonstrate the variations in ecosystem respiration. F_c values obtained during the beginning of the experiment (days 183 and 184) are attributed to destocking rather than biological degassing (respiration) and were discarded (Figure 5). Also, four PAR data points (>2200 µmol m^{-2} s^{-1}) have been excluded from linear regressions of F_c and LE on PAR because they are unrealistic and likely represent quantum sensor noise. P values for the linear regressions are significant (<0.0001). A PAR value of 20 µmol m^{-2} s^{-1} was used to distinguish daytime and nighttime periods, and high tide periods are defined as having non-zero water depths.

3.3.2. Physical / biological controls on turbulent fluxes in the Arcachon lagoon

The flux characterization of the four lagoon conditions demonstrates the large effects of both tidal and diurnal rhythms on turbulent exchanges with the atmosphere. Significant ($p<0.05$) variations were observed in flux parameters among the four cases. The physical and biological controls involved in these different situations are depicted in Figures 7 and 8 and discussed in the following sections.

Physical controls

Friction velocity and surface roughness

Significant linear regressions were computed between friction velocity (u^*) and wind speed (Figures 7A, B, C and D). Linear regressions with u^* were found to be significant for all four cases, and the best regression models exist for nighttime periods, especially LT/Night periods, which have only slightly unstable or near-neutral conditions (Figures 7B and D). The linear relationship between the friction velocity and the wind speed was initially established theoretically according to the logarithmic wind profile equation under neutral stability conditions (Sutton, 1953; Elliott, 1958). Small slope values (u^*/u) were 0.031 and 0.037 at LT and HT, respectively, and indicate that the surface roughness of the Arcachon lagoon is remarkably low (Figure 7). Values of u^*/u were lower than those measured over bare soils in agricultural land (approximately 0.066) (Stella et al., 2011). Interestingly, roughness is slightly higher during high tide, likely due to shear induced by high waves near the water surface.

CO_2 destocking and degassing

During the study period, interesting physical processes were measured by the EC method at both LT and HT. For instance, for LT/Day on day 184, a major release of CO_2 to the atmosphere occurred (12 µmol m^{-2} s^{-1}) (Figure 5E). This phenomenon coincided with sudden increases in friction velocity (Figure 5B) and wind speed and with a change in wind direction from the west-southwest to the north-northwest (Figures 4E and F), as previously seen. These EC measurements probably highlight a destocking event that occurred with the onset of turbulence. In any case, based on the peak intensities of the flux values, the event could correspond to a biological activity like community respiration (CR). Besides, during both HT/Night and HT/Day periods on day 184, a large quantity of CO_2 was emitted to the atmosphere; flux values were higher than 10 and 7 µmol m^{-2} s^{-1} during night and day,

respectively (Figure 5E). This release could be attributed to a shift in water CO_2 concentrations resulting from sediment resuspension and the mixing of CO_2–enriched bottom waters with CO_2 –depleted surface waters. Over Arctic and Swiss lakes, Eugster et al. (2003) found that periods of convective mixing water were associated with larger CO_2 fluxes that were generally from the water to the atmosphere.

LE fluxes and evaporative effect predominance

LE fluxes result from physical evaporation and biological transpiration, which are often difficult to distinguish within an ecosystem. In this study, LE flux showed a significant relationship with wind speed, especially during LT/Night and HT/Night (Figures 7F and H). According to the Penman-Monteith equation (Monteith and Unsworth, 1990), LE fluxes are controlled by two main factors: net radiation and the vapor pressure deficit of the air. At night, LE was controlled only by the second factor (the air stripping effect) and, logically, better correlations with wind speed were obtained. During the day, the effect of radiation was dominant and led to weaker linear regressions with wind speed (Figures 7E and G).

Significant regressions between LE fluxes and PAR were found during the day at both low and high tides (Figures 8A and B). During LT/Day, the mud sediment receives high PAR and can reach more than 40°C (Blanchet, 2004), especially just after the "Jusant" flow, when the intertidal area has emerged but is still wet. High rates of evaporation occur, enhanced by wind increases or pressure drops (Figure 5D). During HT/Day, LE responds to solar radiation; it is enhanced as the water is warmed under high PAR. This phenomenon has previously been quantified in the Amazon floodplain at both low and high tides (Morison et al., 2000). Water temperatures in July 2008 were warm: temperatures between 21°C and 23.5°C were measured during a 24-hour cycle on July 2-3, 2008 (data not shown).

During the day, it was difficult to evaluate the relative contributions of evaporation and transpiration. In both cases, carbon dioxide exchanges were weaker than concurrent latent heat fluxes (Figures 5D and E; Table 2). As a consequence, evaporation can be assumed to prevail over transpiration. The water use efficiency (WUE) of 0.2 measured in the Arcachon lagoon was much lower than values reported in forested ecosystems or croplands near 5.0 and 10.0 respectively (Stella et al., 2009). Additional evidence of the dominance of evaporation in the lagoon is the particularly high LE flux measured during LT/Day 186 (Figure 5D). On days 185 and 186, the same CO_2 uptake was measured at low tide (Figure 5E), but the LE flux was

lower on day 185. Therefore, this result was attributed to physical evaporation rather than biological transpiration.

The water column: a diffusive barrier to turbulent fluxes

The tide clearly induced decreases in both CO_2 release at night (by approximately 21%) and CO_2 uptake during the day (by approximately 35%) (Table 2, Figure 5E). Similar results were found by Houghton and Woodwell (1980) in a salt marsh and by Heilman et al. (1999) in a marsh in Texas (USA). Kathilankal et al. (2008) found a similar level of CO_2 uptake reduction (46 ± 26%) over a salt marsh. The tide could act as a barrier to diffusion, reducing fluxes either from the lagoon to the atmosphere or vice versa. During high tide, CO_2 from benthic and pelagic respiration could be only slowly emitted to the atmosphere through the water layer; much of the CO_2 could also be dissolved in seawater and exported with the tide. These pathways for CO_2 release from intertidal systems to adjacent creeks and bays have previously been described in tidal wetlands (Cai et al., 2003; Borges et al., 2003).

Biological controls

LT CO_2 flux variations

Except on day 184, the first day of the study, negative CO_2 fluxes were consistently observed during LT/Day cases (Figure 5E). Furthermore, the CO_2 concentrations measured by the EC system gas analyzer were significantly ($p < 0.05$) lower than concentrations measured during the other three cases indicating systematic CO_2 sinks. This CO_2 uptake is probably explained primarily by photosynthetic activity of the marine angiosperm *Zostera noltii*, which was particularly common around the EC mast. In the lagoon, seagrass reaches maximum levels of biomass and density in the summer (June-September) and minimum levels in the winter (Auby and Labourg, 1996). It has generally been shown that rates of photosynthesis by *Zostera noltii* are higher at low tide owing to sediment depressions. The depressions can retain sufficient water for leaf hydration and rapid air-water CO_2 diffusion (Silva et al., 2005). Benthic primary production in the lagoon may also be supported by epiphyte microphytobenthic communities (Auby, 1991). In contrast, during LT/Night cases, positive CO_2 fluxes largely corresponded to total ecosystem respiration (Figure 8C, data plotted in y axis).

Figure 8C clearly shows positive F_c values at night and negative F_c values at day. However, poor negative correlations were observed between F_c and PAR during LT/Day. This result is

inconsistent with the significant negative correlations found by Morison et al. (2000) in the Amazon floodplain and earlier by Houghton and Woodwell (1980) in a salt marsh near New York (USA). A clear pattern exists between F_c and PAR as suggested by the regressions found in Figure 8C and by the temporal variations observed in Figure 5E. However, poor correlations were observed at LT/Day (Figure 8C) because the strongest CO_2 uptake rates did not coincide with maximum PAR values (e.g., compare day 185 to day 187, Figure 5E). Under particular high PAR (midday), *Zostera noltii* seagrass may experience water stress leading to lower rates of photosynthesis (Leuschner et al., 1998). In the *Zostera noltii* meadows of Ria Formosa, a coastal lagoon in Portugal, Silva et al. (2005) found that angiosperms could use photo-inhibitory mechanisms to down-regulate photosynthesis by dissipating excess irradiance as heat. Seagrasses could then be expected to protect themselves by lowering their CO_2 uptake during periods of maximum PAR. Down-regulation probably occurred during LT/Day 185, when reduced CO_2 uptake and enhanced H fluxes were observed; the inverse situation was observed during LT/Day 187 (Figures 5C and E).

HT CO_2 flux variations

To a lesser extent than for the LT/Day case, CO_2 sinks were observed during HT/Day (Figure 5E). HT/Day sinks could be attributed to pelagic primary production by blooming phytoplankton, especially small and non-siliceous cells that are well adapted to the low-nutrient concentrations that characterize the summer season (Glé et al., 2007). As for LT/Day cases, but to a greater extend, no clear correlations were found between F_c and PAR values during HT/Day cases (Figure 8D). This result could potentially be due to variations in photosynthetic efficiency and especially to a decrease in production activity. Indeed, diffusion of CO_2 from the water column to the plant is more difficult under HT/Day conditions even if *Zostera noltii* eelgrasses continue to photosynthesize at reduced rates during high tide (Figure 8D). This result was also found by Kathilankal et al. (2008) for *Spartina alterniflora* plants.

4. Summary and conclusion

Few studies have used EC to address turbulent fluxes over coastal systems; the current study of the Arcachon lagoon is one of the first to study systems that are influenced by tidal rhythms and that experience rapid variations in water height that affect turbulent exchanges. In this paper, the field deployment and data processing methods detailed for the EC technique produce high-quality vertical flux data for energy, heat and CO_2. The measured turbulent exchanges were evaluated in terms of temporal variations and turbulence analysis and demonstrate the effective adaptation of the EC technique to the tidal flat environment. Indeed, averaged cospectra of sensible heat, latent heat and carbon dioxide flux were generally found similar and well shaped during each case. Maximum frequency peaks were observed in the low frequency domains of cospectra due to unstable atmospheric conditions that occur in the tidal flat. Moreover, significant linear regressions were computed between u^* and u, LE and u, and LE and PAR values. It shows that physical and biological ecosystem processes in the Arcachon lagoon were found to correspond well to variations in turbulent flux. Other correlations have been observed between F_c and PAR values which indorse this fact. Nevertheless, these latter correlations were weaker because F_c flux and PAR data were treated as a whole without taking into account the spatial and temporal heterogeneity of the lagoon. In this way, a work in progress uses four data sets obtained in two contrasted sites and three different seasons in the lagoon. In particular, a data treatment done to the EC CO_2 fluxes by sectors of wind direction using satellite images of the flat appears very interesting in the understanding of the ecological functioning of these highly heterogeneous and dynamic zones.

Acknowledgments

This study was supported by the ANR project PROTIDAL coordinated by Pierre Anschutz and also by the Aquitaine region that has financed the EC system. This study would not exist without the help of all co-authors of this paper. We are really grateful to Jonathan Deborde and Georges Oggian, for their help for the EC deployment in field.

III.2. SPATIAL AND TEMPORAL CO_2 EXCHANGE MEASURED BY EDDY CORRELATION OVER A TEMPERATE INTERTIDAL FLAT AND THEIR RELATIONSHIPS TO NET ECOSYSTEM PRODUCTION

Résumé

Des mesures de flux verticaux de dioxyde de carbone entre l'atmosphère et un platier vaseux intertidal tempéré, localisé dans le sud-ouest de la France, ont été menées en utilisant la technique d'Eddy Covariance (EC). Des mesures originales ont été obtenues dans deux sites contrastés de la lagune d'Arcachon pendant quatre périodes et trois saisons différentes (automne 2007, été 2008, automne 2008 et printemps 2009). Dans cet article, les variations spatio-temporelles, observées dans les échanges de CO_2 aux échelles diurne, tidale et saisonnière, sont présentées et discutées. Des images satellites de la lagune à marée basse le jour ont été utilisées afin de mettre en relation l'échange net de l'écosystème avec l'occupation du platier par les producteurs primaires, en particulier par les herbiers de *Zostera noltii*. Les flux de CO_2 pendant les quatre déploiements montrent d'importantes variations spatio-temporelles, la lagune passant rapidement d'un statut de puits à celui de source de CO_2. Les flux de CO_2 montrent en général des valeurs négatives (influx) et positives (efflux) faibles, entre -13 et 19 µmol m^{-2} s^{-1} au maximum. Les conditions de marée basse la journée sont toujours caractérisées par un pompage de CO_2 atmosphérique. Au contraire, pendant l'immersion et durant la marée basse la nuit, les flux de CO_2 sont soit positifs ou négatifs ou proches de zéro, selon la saison et la station mesurées. A l'automne 2007, à la station la plus interne de la lagune, avec un herbier inégal de *Zostera noltii* (couverture estimée à 22 ± 14% dans les secteurs de vents mesurés), l'influx de CO_2 est de -1.7 ± 1.7 µmol m^{-2} s^{-1} à marée basse le jour et l'efflux de 2.7 ± 3.7 µmol m^{-2} s^{-1} à marée basse la nuit. Une production primaire brute de 4.4 µmol m^{-2} s^{-1} pendant l'émersion peut être attribuée aux communautés microphytobenthiques en majorité. Pendant l'immersion, la colonne d'eau est source de CO_2 vers l'atmosphère, ce qui suggère une hétérotrophie et une importante remise en suspension du microphytobenthos. A l'été et l'automne 2008, à la station centrale présentant un herbier dense de Zostère naine (92 ± 10%), les assimilations de CO_2 sont de -1.5 ± 1.2 et -0.9 ± 1.7 µmol m^{-2} s^{-1} à marée basse le jour, respectivement. Les efflux nocturnes de CO_2 sont de 1.0 ± 0.9 et 0.2 ± 1.1 µmol m^{-2} s^{-1}, résultant en une production primaire brute pendant l'émersion de 2.5 et 1.1 µmol m^{-2} s^{-1} respectivement, que l'on peut attribuer en majorité aux herbiers. A la même station en avril 2009, avant que *Zostera noltii* ne commence à croître, le pompage de

CO_2 à marée basse le jour est le plus fort (-2.7 ± 2.0 µmol m^{-2} s^{-1}) et probablement attribué au microphytobenthos, dominant la production nette de l'écosystème dans ce cas. Les relations entre l'échange net de l'écosystème et les radiations, classées par direction de vent, sont en général négatives lorsque *Zostera noltii* prédomine, et positives lorsque l'angiosperme est moins représentée, ces dernières suggérant des processus de photoacclimatation par le microphytobenthos, tels que des migrations verticales à l'intérieur du sédiment. Des influx de CO_2 sont aussi observés pendant l'immersion à la station centrale au printemps et au début de l'automne, et sont apparemment liés aux blooms phytoplanctoniques se développant à l'entrée de la lagune, faisant suite à l'advection de masses d'eau appauvries en CO_2. Bien que des données hivernales soient nécessaires afin de quantifier précisément le budget de CO_2 de la lagune d'Arcachon, nos résultats suggèrent que ce platier tidal contribue faiblement au budget de CO_2 de l'océan côtier.

Abstract

Measurements of carbon dioxide fluxes were performed over a temperate intertidal mudflat in southwestern France using the micrometeorological Eddy Correlation (EC) technique. EC measurements were carried out in two contrasting sites of the Arcachon lagoon during four periods and in three different seasons (autumn 2007, summer 2008, autumn 2008 and spring 2009). In this paper, spatial and temporal variations in vertical CO_2 exchanges at the diurnal, tidal and seasonal scales are presented and discussed. In addition, satellite images of the tidal flat at low tide were used to link the net ecosystem exchange (NEE) with the occupation of the mudflat by primary producers, particularly by *Zostera noltii* meadows. CO_2 fluxes during the four deployments showed important spatial and temporal variations, with the lagoon rapidly shifting from a sink to a source of CO_2. CO_2 fluxes showed generally low negative (influx) and positive (efflux) values and ranged from -13 to 19 µmol m^{-2} s^{-1} at maximum. Low tide and daytime conditions were always characterised by an uptake of atmospheric CO_2. In contrast, during immersion and during low tide at night, CO_2 fluxes where positive, negative or close to zero, depending on the season and the site. During the autumn of 2007, at the innermost station with a patchy *Zostera noltii* bed (cover of 22 ± 14% in the wind direction of measurements), CO_2 influx was -1.7 ± 1.7 µmol m^{-2} s^{-1} at low tide during the day, and the efflux was 2.7 ± 3.7 µmol m^{-2} s^{-1} at low tide during the night. A gross primary production (GPP) of 4.4 µmol m^{-2} s^{-1} during emersion could be attributed mostly to microphytobenthic communities. During immersion, the water was a source of CO_2 to the atmosphere, suggesting strong heterotrophy or resuspension of microphytobenthic cells. During the summer and

autumn of 2008, at the central station with a dense eelgrass bed (92 ± 10%), CO_2 uptakes at low tide during the day were -1.5 ± 1.2 and -0.9 ± 1.7 µmol m^{-2} s^{-1}, respectively. Nighttime effluxes of CO_2 were 1.0 ± 0.9 and 0.2 ± 1.1 µmol m^{-2} s^{-1} in summer and autumn, respectively, resulting in a GPP during emersion of 2.5 and 1.1 µmol m^{-2} s^{-1}, respectively, attributed primarily to the seagrass community. At the same station in April 2009, before *Zostera noltii* started to grow, the CO_2 uptake at low tide during the day was the highest (-2.7 ± 2.0 µmol m^{-2} s^{-1}) and could be attributed to microphytobenthos dominance on NEP in this case. NEE versus PAR relationships for data ranked by wind directions were generally negative where and when *Zostera noltii* was dominant and positive when this community was minor. The latter relationship suggests important processes of photo-acclimatisation by the microphytobenthos, such as migration through the sediment. Influxes of CO_2 were also observed during immersion at the central station in spring and early autumn and were apparently related to phytoplankton blooms occurring at the mouth of the lagoon, followed by the advection of CO_2-depleted water with the tide. Although winter data would be necessary to determine a precise CO_2 budget for the lagoon, our results suggest that tidal flat ecosystems are a modest contributor to the CO_2 budget of the coastal ocean.

1. Introduction

The coastal zone is defined as the ocean area on the continental shelf with a depth of less than 200 m, including all estuarine areas to the upstream limit of tidal influence. The coastal zone receives considerable amounts of nutrients and organic matter from the land, exchanges matter and energy with the open ocean (Borges, 2005) and thus constitutes one of the most biogeochemically active areas of the biosphere (Gattuso et al., 1998; Borges et al., 2005). In the coastal ocean, shallow depth favours light penetration in a large part of the water column and allows for a strong coupling between pelagic and benthic processes. These characteristics make the coastal zone very active in terms of CO_2 exchange, with atmosphere, benthic and pelagic primary production and respiration (Gazeau et al., 2004; Borges et al., 2006). The coastal zone covers approximately 7% of the surface of the global ocean; despite its relatively modest surface area, this zone accounts for 14–30% of all oceanic primary production, 80% of organic matter burial and 90% of sedimentary mineralisation (Mantoura et al., 1991; Pernetta and Milliman, 1995). In addition, continental shelves act as a net sink of CO_2 of -0.21 ± 0.36 PgC yr^{-1} – i.e., 15% of the open ocean sink – whereas near-shore estuarine environments emit +0.27 ± 0.23 PgC yr^{-1} to the atmosphere (Laruelle et al., 2010). This active but heterogeneous region of the ocean has recently begun to be taken into account in global carbon budgeting efforts (Frankignoulle et al., 1998; Borges, 2005).

The ability of an ecosystem to consume CO_2 and produce organic matter is governed to a large extent by its net ecosystem production (NEP), defined either as the rate of net organic carbon burial and export or as the difference between ecosystem-level gross primary production (GPP) and community respiration (CR) (Smith and Hollibaugh, 1993; Gattuso et al. 1998). GPP represents the C fixation by autotrophic organisms, and CR represents the respiration of all organisms, both autotrophic and heterotrophic. Both GPP and CR are summed per unit ground or water area over time (Chapin et al., 2006). Autotrophic ecosystems have GPP greater than their CR and are net producers of organic C that can be accumulated in the system or exported outside of the system. Heterotrophic ecosystems have GPP lower than their CR and are net consumers of organic C supplied by an external source (Odum, 1956). GPP and CR are processes that also consume and release, on a short timescale, inorganic C in an ecosystem. In a terrestrial system, GPP directly consumes atmospheric CO_2, and CR releases CO_2 directly to the atmosphere. Thus, the net ecosystem exchange (NEE), defined as the net vertical CO_2 exchange between the ecosystem and the atmosphere, is

generally approximated by NEP in many terrestrial ecosystems over short timescales (Baldocchi, 2003). In contrast, in aquatic systems, GPP consumes dissolved inorganic carbon and reduces the concentration of CO_2 in the water. This reduction of CO_2 generates a diffusion gradient that causes CO_2 to enter the water from the atmosphere (Chapin et al., 2006). CR in aquatic systems releases CO_2 to the water, where it dissociates into bicarbonate and carbonate ions, generating a water–air CO_2 gradient that tends to emit CO_2 to the atmosphere. Because water–air diffusion is a slow process in comparison with GPP and CR and also compared to lateral water movements, NEE and NEP can be very different over short timescales in aquatic systems (Gattuso et al., 1998; Borges et al., 2006). For instance, a system that receives large amounts of CO_2-saturated water can be autotrophic but also a source of atmospheric CO_2. In addition, a system that receives large amounts of allochthonous organic matter can be heterotrophic but serve as a sink of atmospheric CO_2 if waters are strongly stratified and if the surface layer in contact with the atmosphere becomes net autotrophic. Finally, in aquatic systems, carbonate precipitation and dissolution are additional processes that affect CO_2 concentration: dissolution raises it, whereas precipitation decreases it. For instance, a significant release of CO_2 to waters as a result of carbonate precipitation by invasive benthic macrofauna has been reported in San Francisco Bay (Chauvaud et al., 2003). Inversely, a significant reduction of CO_2 degassing resulting from carbonate dissolution has been reported in a turbid, eutrophic and heterotrophic estuary (Abril et al., 2003).

In the coastal zone, NEP and GPP show important variations both spatially and temporally, depending on a large suite of environmental factors, mainly light and nutrient availability and organic matter loads. Open shelves are net autotrophic and serve as CO_2 sinks (Gazeau et al., 2004; Borges, 2005). Estuaries are generally heterotrophic and are a CO_2 source because of the large inputs of labile organic matter from rivers that fuel CR, while GPP is limited in estuaries by light availability (Smith and Hollibaugh, 1993; Frankignoulle et al., 1998; Borges, 2005). Shallow coastal environments colonised with seagrass meadows are generally net autotrophic, with a GPP estimated at 224.9 ± 11.1 mmol C m^{-2} d^{-1} (Duarte et al. 2010). The intertidal area of the coastal zone also has particular properties with respect to NEP and CO_2 fluxes. First, benthic GPP can be greatly enhanced at low tide because of the increased availability of light and high temperature (Parsons et al., 1984; Hubas et al., 2006). During emersion, benthic NEP is equivalent to NEE. However, during immersion, planktonic and benthic NEP do not necessary correspond to NEE, as a substantial advection of metabolic

carbon can occur. Indeed, outwelling of CO_2 supersaturated waters with the tide have been described in salt marsh and mangrove ecosystems (Borges et al., 2003; Wang and Cai, 2004).

CO_2 fluxes at the water–air interface can be measured directly using floating chambers (Frankignoulle et al., 1998) or calculated from water partial pressure of CO_2 (pCO_2) measurements and a given gas transfer velocity. However, CO_2 flux computations can be subject to large uncertainties because of the difficulty in accurately assessing the gas transfer velocity (Raymond and Cole, 2001; Vachon et al., 2010). Similarly, the floating chamber method has been suspected to artificially enhance the CO_2 exchange across the air–water interface (Raymond and Cole, 2001). CO_2 fluxes at the air–sediment interface at low tide can be assessed by deploying benthic chambers (Migné et al., 2002), but this method suffers from variability of intertidal sediment habitat resulting from patchiness at all timescales and from spatial patchiness, in particular (Migné et al., 2004). Additionally, surface heating during low tide can also interfere with metabolic processes in tidal flats. Micrometeorological measurements, especially the Eddy Correlation technique (EC), show potential, as CO_2 fluxes across heterogeneous intertidal areas can be obtained with the same technique, at high tide and low tide (Houghton and Woodwell, 1980; Kathilankal et al., 2008; Zemmelink et al., 2009). In addition, the EC method is non-invasive and provides direct and continuous measurements of the net carbon dioxide exchange of a whole ecosystem across a spectrum of time scales from hours to years (Baldocchi, 1988; Aubinet et al., 2000; Baldocchi, 2003). Applying the EC in the coastal zone appears to be a very promising technique, as the method can provide flux data on timescales short enough to resolve the temporal variability induced by the tidal, diurnal and seasonal cycles. However, the method can also have limitations and requires important qualitative and quantitative analyses and corrections because of its physical and theoretical background (Baldocchi et al., 1988; Polsenaere et al., submitted). In intertidal ecosystems, EC measurements present the great advantage of providing precise CO_2 fluxes at the air/water interface during immersion and at the air/sediment interface during emersion. In salt marshes, the EC technique has shown substantial changes in fluxes throughout the tidal cycle (Houghton and Woodwell, 1980; Kathilankal et al., 2008). Likewise, Zemmelink et al. (2009) used the EC technique over the intertidal Wadden Sea mudflat in Europe and observed a CO_2 sink, particularly at low tide and during the day.

On four occasions between 2007 and 2009, we employed an EC system in a lagoon dominated by an intertidal mudflat in south-western France. In a previous paper, (Polsenaere et al. submitted), we presented the methodological aspects of this work and discussed the

validity of computed fluxes obtained by EC. In this paper, we present results on the continuous CO_2 fluxes obtained during four different periods over two intertidal areas of the Arcachon lagoon. The main focuses of this paper are (1) to describe and characterise the temporal and spatial variations of CO_2 exchanges occurring in the lagoon during the day and night and during emersion and immersion; (2) to understand the CO_2 flux dynamic in the Arcachon lagoon in relation to the components of NEP (benthic and planktonic GPP and CR) – we focus more specifically on the low tide/day period, during which we could relate CO_2 fluxes to the tidal flat occupation by *Zostera noltii* eelgrass meadows; and (3) to evaluate the CO_2 budget of the lagoon and compare this budget to fluxes reported in other coastal systems.

2. Materials and Methods

2.1. Study site

The Arcachon lagoon is a temperate intertidal flat of 174 km^2 on the southwestern Atlantic coast of France (44°40'N, 01°10'W). This triangle-shaped bay is enclosed by the coastal plain of Landes, Gascony, and communicates with the Atlantic Ocean through a narrow channel 8 km in length (Fig. 1.). With a mean depth of 4.6 m, this shallow lagoon presents semi-diurnal tides with amplitudes varying from 0.8 to 4.6 m (Plus et al., 2008). During a tidal cycle, the lagoon exchanges approximately 264 10^6 m^3 and 492 10^6 m^3 of water with the ocean during average neap and spring tides, respectively. The lagoon also receives freshwater, but to a lesser extent, with an annual input of 1.25 10^9 m^3 (1.8 10^6 m^3 at each tidal cycle), of which 8% is from groundwater, 13% is from rainfall and 79% is from rivers and small streams (Rimmelin, 1998). The Leyre River in the southeastern corner of the lagoon represents 73% of the total freshwater flows (Manaud et al., 1997; De Wit et al., 2005). Water temperatures in the bay vary from 6°C in winter to 22.5°C in summer, and water salinity varies from 22 to 35 PSU according to freshwater input variations during the year.

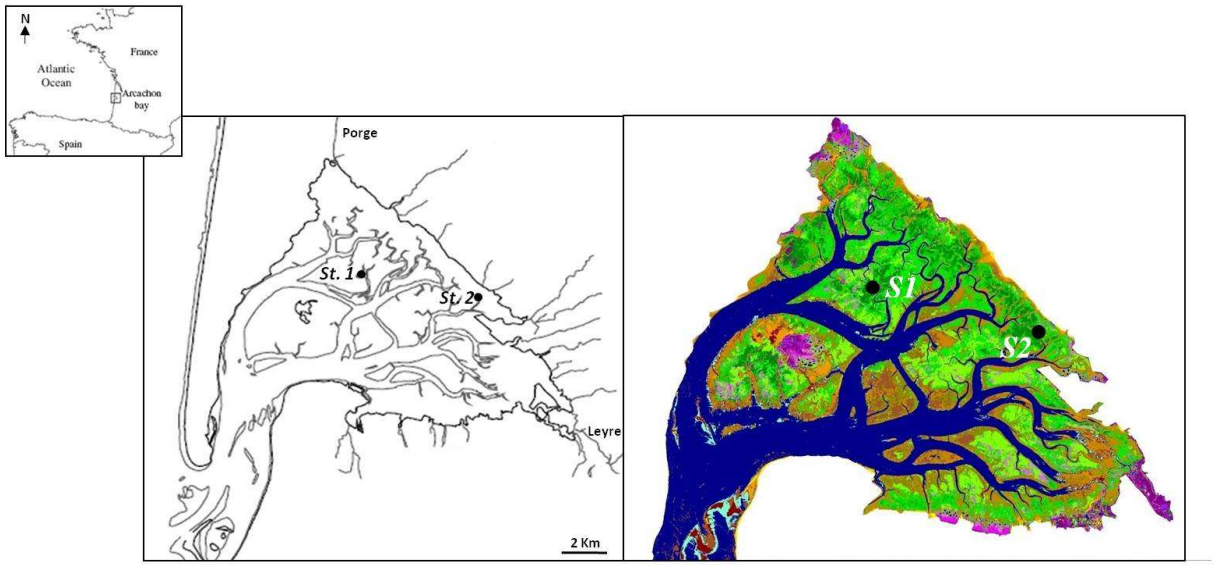

Fig. 1. Localisation and the Eddy Correlation (EC) experimental sites. A: the Arcachon lagoon with the subtidal zone (channels, in white) and the intertidal mudflat area (in grey); B: the two EC sites: Station 1 (44°42'59.15"N, 01°08'36.96"W) and Station 2 (44°42'19.96"N, 01°04'01.35"W). The *Zostera noltii* seagrass meadow is derived from the SPOT satellite image of the 22/06/2005; it represents 60% of the intertidal area (shades of green show the differences in seagrass density).

The Arcachon lagoon surface is composed of 57 km^2 of channels, with a maximum depth of 25 m, which drain a large muddy tidal flat of 117 km^2. At two different intertidal sites of the mudflat (Fig. 1), an EC measurement system was deployed on four occasions and during the spring, summer and autumn seasons. A first deployment was made in the inner part of the lagoon at Station 2 (N 44°42'19.96", W 01°04'01.35") in September–October 2007. The three other deployments were carried out at the central station in the lagoon at Station 1 (N 44°42'59.15", W 01°08'36.96") in July 2008, September–October 2008 and in April 2009. During the four experiments, throughout the tidal cycle, the tidal flat was emerged for approximately four hours and immersed for approximately nine hours.

2.2. CO_2 fluxes measured by EC in the Arcachon lagoon

2.2.1. Theory behind the EC technique

The atmosphere contains turbulence (eddies) caused by buoyancy and shear (Aubinet et al., 2000) of upward and downward moving air that transports trace gases such as CO_2 (Baldocchi, 2003). The EC technique allows for the measurement of these turbulent eddies to determine the net flux of any scalar movement vertically across the ecosystem/atmosphere interface.

The mean turbulent flux of the scalar c in the vertical direction (F_c) is expressed as the covariance between the fluctuations in the vertical wind velocity (w) and the scalar density or concentration (ρ_c) (Moncrieff et al., 1997) as

$$F_c = \overline{w'\rho_c'} \quad (1)$$

where the overbar represents a temporal average (i.e., 10 min were used in the case of the Arcachon lagoon), and primes denote the instantaneous turbulent fluctuations relative to their temporal average (e.g., $w' = w - \overline{w}$ and $\rho_c' = \rho_c - \overline{\rho_c}$, Reynolds, 1895).

Carbon dioxide fluxes (F_c) can be then defined as

$$F_c = \overline{w'c'} \quad (2)$$

where F_c is expressed in µmol m^{-2} s^{-1}, w is expressed in m s^{-1} and c (the CO_2 concentration) in µmol m^{-3}. CO_2 fluxes are directed upward when F_c values are positive and downward when corresponding values are negative.

2.2.2. Turbulent flux measurement system in the Arcachon lagoon

Fluxes of CO_2 were measured using an EC system deployed four times in two intertidal flat sites: from the 30th of September at 11:35 to the 3rd of October 2007 at 08:55 (GMT) at Station 2 (Fig. 1); and from the 1st at 16:40 to the 7th of July 2008 at 04:00 (GMT), from the 25th of September at 15:10 to the 17th of October 2008 at 01:10 (GMT) and from the 1st at 16:30 to the 13th of April 2009 at 22:50 (GMT) at Station 1, for a total of 4, 7, 20 and 13 days, respectively.

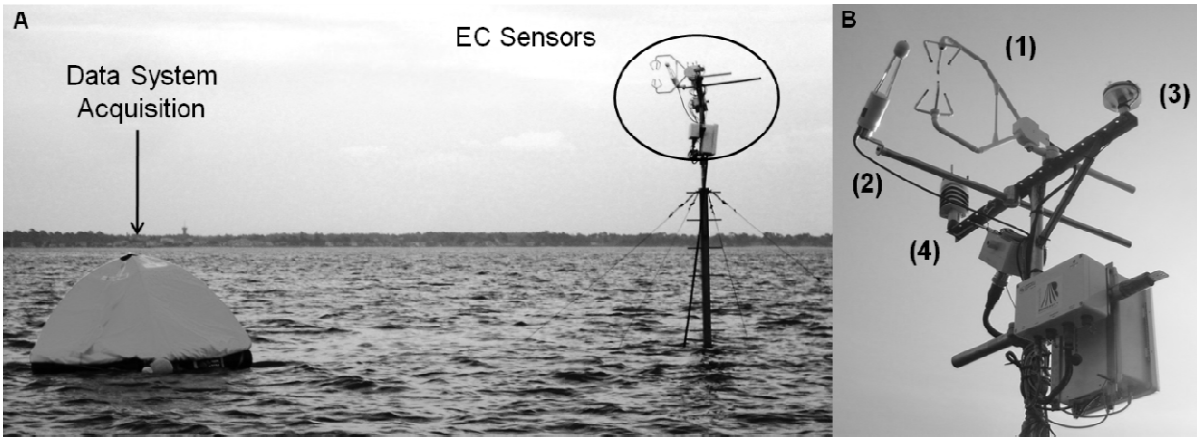

Fig. 2. The Eddy Correlation system deployed in the Arcachon lagoon in April 2009. A: general view of the system measurement showing the sensors mounted on the mast and the data system acquisition *Campbell CR3000* in the lifeboat; B: the sensors: (1) the sonic anemometer *CSAT3*, (2) the infra red gas analyser *LI-7500*, (3) the quantum sensor *SKP215* and (4) the meteorological station (*Vaisala WXT510*). The measurement heights were 4.20, 5.50, 7.0 and 5.0 m in September–October 2007, July 2008, September–October 2008 and April 2009, respectively.

Our EC system (Fig. 2) was fixed to a mast and consisted of a sonic anemometer (model *CSAT3*, *Campbell Scientific Inc.*, Logan, UT) to measure the three wind speed components (m s^{-1}), as well as the sonic temperature (°C), and an infra-red gas analyser (model *LI-7500*, *Licor Inc.*, Lincoln, NE) that measured CO_2 and H_2O concentrations (mmol m^{-3}) and atmospheric pressure (kPa). Analogue output signals from these fast-response instruments were sampled and digitised at the rate of 20 Hz. With these two main EC sensors separated by a distance of 0.25 m, a filtered silicon quantum sensor (*SKP215*, *Skype Instruments*, Llandrindod Wells, UK) was used to measure photosynthetically active radiation (PAR, µmol m^{-2} s^{-1}) every minute (Fig. 2B). Additionally, a meteorological transmitter (model *WXT510*, *Vaisala Inc.*, Finland*)* was set up in September–October 2008 and April 2009. This transmitter provided additional wind speed and direction measurements that could be compared with data from the sonic anemometer and other weather parameters: air temperature, pressure, humidity, and the amount, intensity and duration of rainfall events. The sensors were mounted on a mast inserted in the mud and secured by three wires to keep it vertical and to limit vibrations that could bias EC flux measurements (Fig. 2A). Data were recorded by a central acquisition system (model *CR3000*, *Campbell Scientific Inc.*, Logan, UT) (connected to the sensors with a waterproof cable) located in an anchored inflatable raft and protected by a tide pool. The

entire system was powered by rechargeable lead batteries (12 volts, 100 amperes per hour) and replaced every four days.

The equipment used was similar for the four deployments except during September–October 2007, when a different sonic anemometer (model *Windmaster, Gill Instr.*, UK) was used, as well as a different sample frequency for both EC sensors, i.e., 10 Hz. Also during this deployment, the PAR was not directly measured at the EC station but at the Cap Ferret meteorological station (N 44°37'54", W 01°14'54"). Global radiation (J cm^{-2}) hourly data were first obtained and then converted to W m^{-2} and to µmol m^{-2} s^{-1}, assuming a factor of 2 from W m^{-2} to µmol m^{-2} s^{-1}, to homogenise PAR units between the four deployments. The sensors for the four field setups were mounted at maximum heights (during low tide) of 4.20, 5.50, 7.0 and 5.0 m in September–October 2007, July 2008, September–October 2008 and April 2009, respectively.

2.2.3. Data processing and quality control

Raw data were processed following the Aubinet et al. (2000) methodology developed in the context of the EUROFLUX project for net carbon and water exchanges of forests and modified to be applied to intertidal areas. The first important adaptation of the forest-based methodology to the case of the Arcachon mudflat was to adjust for variations in the relative measurement height with the tidal rhythms, which must be included in EC data computations and corrections. Secondly, fluxes were computed with a shorter averaging period (10 min) than usually used (30 min) to detect the quick transitions from low tide to high tide and vice versa. A detailed description of the data processing used here is given in Polsenaere et al. (submitted). To summarise, data were processed using the EdiRe software from the University of Edinburg (Scotland) by applying the following steps: (1) spike removal in anemometer or gas analyser data; (2) unit modifications and statistical operations; (3) coordinating rotation to align coordinate system with the stream lines of the 10 min. averages; (4) linear de-trending of sonic temperature, H_2O and CO_2 channels; (5) determining time lag values for H_2O and CO_2 channels using a cross-correlation procedure; (6) computing mean values, turbulent fluxes and characteristic parameters, e.g., the Monin–Obhukov stability index Z/L; (7) high-frequency corrections via transfer functions based on Kaimal–Moore's co-spectral models (Kaimal et al., 1972; Moore, 1986); and (8) performing a Webb–Pearman–Leuning correction to account for the effects of fluctuations of temperature and water vapour on measured fluctuations in CO_2 and H_2O (Webb et al., 1980).

In parallel to frequency corrections, a cospectral analysis was carried out for each period to quantify the distribution by frequency of the covariance of the raw measured signals. In particular, the power cospectra between the vertical wind velocity and carbon dioxide were computed and analysed as detailed in Polsenaere et al. (submitted).

According to data quality control protocols, incorrect processed data must be removed to obtain reliable CO_2 flux measurements. Several factors can lead to bias or errors, i.e., instrument malfunctions, processing/mathematical artefacts, ambient conditions not satisfying the EC methodology (non-stationary periods, convergence, divergence), heavy precipitation – particularly for open-path gas analyser – or a measurement footprint larger than the fetch of interest (Burba and Anderson, 2005). An adapted procedure developed for the Arcachon lagoon study is presented in Polsenaere et al. (submitted). Two main statistical tests were used: (1) the steady-state test was applied to pairs of specified signals, particularly to w and c in this study. Standard deviations and covariances of w and c were computed on short time intervals of 1 min, and these values were compared to those computed on the chosen time run of 10 min, following Foken and Wichura (1996). Only data corresponding to a difference lower than 30% (periods defined as steady-state conditions) were retained. (2) The statistical test was based on the integral turbulence characteristics of wind components and temperature, according to Foken et al. (1991, 1997). The σ_w/u^* and σ_T/T^* ratios of the data signals (where σ is the standard deviation of the specified signals) were computed and compared to their parameterised values according to different ranges of stability (Z/L parameter). Only data matching with a difference of less than 50% were retained. Using these two statistical tests, the retained EC data for the Arcachon lagoon corresponded to "high-quality data" with a general flag from 1 to 3, according to Foken (2003). In the end, 73%, 83%, 83% and 87% of CO_2 flux data were retained for the September–October 2007, July 2008, September–October 2008 and April 2009 periods, respectively.

2.3. Eelgrass retrieval from satellite data

The fetch around the mast always ranged between at least 1000 m at Station 1 and 700 m at Station 2 at low tide in all the wind directions (Fig. 1.). Thus, we can assume that all measured fluxes were from the intertidal area of interest, the fetch being generally larger than the footprint of the measurements. Indeed, the relative maximum sensor height at low tide was 4.20 m at Station 2 and ranged between 5 and 7 m at Station 1; it is generally accepted

that the relative height:footprint ratio must be 1:100 and 1:300 for unstable and stable atmospheric conditions, respectively (Leclerc and Thurtell, 1990; Hsieh et al., 2000). In the following, we therefore assume that the footprint of our measurement was close to 1 km.

To relate the temporal and spatial variations in the measured for NEE with the distribution of vegetation on the mudflat, satellite images at low tide during the day were analysed. The occupation of the *Zostera noltii* eelgrass meadows was quantified within a circle of 1 km radius centred on the EC mast for both sites. Each circle was then divided into eight sectors corresponding to different wind directions: 0–45°: north–northeast, 45–90°: east–northeast, 90–135°: east–southeast, 135–180°: south–southeast, 180–225°: south–southwest, 225–270°: west–southwest, 270–315°: west–northwest and 315–360°: north–northwest wind directions. Satellite images from SPOT were processed using the methodology based on the normalised vegetation index (Barillé et al., 2010). With the exception of the very low eelgrass densities that can be confused with microphytobenthos, the seagrass meadow surfaces can be assessed and the associated cover density can be derived from these images. This approach has been applied to the retrieval of the meadows at Arcachon. For this purpose, images from the CNES/Kalideos database were used. Georeferenced images were downloaded and calibrated using field reflectance data. Finally, channel surfaces, oyster farms, and salt marshes were masked, before calculating the vegetation index on a pixel basis. The eelgrass position and density were deduced from the 2D mapped index. A dataset of 36 GPS observations collected during autumn 2009 were compared to a SPOT map derived from an image acquired 8/09/2009. The results show that ground-truthing corroborated the map in approximately 90% of the cases. This test validates this mapping approach that was applied to the five satellite images used in this study.

In all, we analysed five images corresponding to the lagoon at low tide during the day. The first was recorded on 13/09/2007, precisely matching with the EC deployment carried out in autumn 2007 at Station 2 in the back of the lagoon. The second image, recorded on 17/10/2008, matched the deployment made in autumn 2008 at Station 1 in the centre of the lagoon. The third image, recorded at the same station and at the same season the next year, on 08/09/2009, was solely used to describe the inter-annual change of the seagrass meadow. Finally, no image precisely matched the deployment from spring 2009 at Station 1, with the closest matching image recorded on 24/06/2009. A fifth image, recorded the next year at Station 1 on 14/04/2010, was also analysed. The latter two images provided insights on the possible changes of the meadow during the spring period.

F_c (µmol m^{-2} s^{-1})	**Low Tide/Day**	**Low Tide/Night**	**High Tide/Day**	**High Tide/Night**	**Average F_c**	**Daily F_c**
September/October 2007 (Station 2)	**-1.7 ± 1.70** (-10.0 ~ 0.9)	**2.7 ± 3.7** (0.2 ~ 18.6)	**0.4 ± 1.1** (-2.4 ~ 3.9)	**1.9 ± 2.4** (-0.4 ~ 13.3)	**0.8 ± 2.7** (-10.0 ~ 18.6)	**0.5 ± 0.4** (0.1 ~ 1.0)
July 2008 (Station 1)	**-0.31 ± 3.29** (-5.75 ~ 12.00)	**0.9 ± 0.8** (-2.5 ~ 3.1)	**-0.2 ± 1.4** (-5.0 ~ 7.3)	**0.7 ± 1.9** (-2.8 ~ 10.6)	**0.1 ± 1.9** (-5.7 ~ 12.0)	**0.1 ± 0.9** (0.8 ~ 3.1)
September/October 2008 (Station 1)	**-0.7 ± 2.3** (-10.8 ~ 14.3)	**0.2 ± 1.1** (-7.1 ~ 5.3)	**-0.14 ± 0.66** (-5.91 ~ 3.43)	**-0.27 ± 1.32** (-7.49 ~ 4.51)	**-0.23 ± 1.44** (-10.77 ~ 14.30)	**-0.23 ± 0.68** (-1.19 ~ 1.20)
April 2009 (Station 1)	**-2.7 ± 2.0** (-11.7 ~ 0.6)	**-1.3 ± 1.4**[*] (-6.2 ~ 1.9)	**-1.7 ± 1.4** (-8.7 ~ 2.6)	**-3.2 ± 2.4** (-13.1 ~ 0.4)	**-2.4 ± 2.1** (-13.1 ~ 2.6)	**-2.4 ± 0.9** (-4.2 ~ -0.8)

Table 1. Carbon dioxide fluxes (F_c) measured in the Arcachon lagoon in September/October 2007 at Station 2 and July 2008, September/October 2008 and April 2009 at Station 1 (see Fig. 1). Negative fluxes represent sinks of CO_2 and positive fluxes represent sources of CO_2 to the atmosphere by convention. A PAR threshold of 20 µmol m^{-2} s^{-1} has been chosen to separate day and night cases and high tide cases corresponding to zero-water heights (low tide cases). [*] Negative F_c data corresponding to very short periods of low tide/night and very fast changes in CO_2 fluxes in April 2009 (Days 94 and 96, Fig. 6E) were excluded from the average, as they were potentially affected by flooded areas.

3. Results

Because diurnal and tidal rhythms largely controlled the CO_2 fluxes, the following results refer to the four distinct cases generated by these two cycles: emersion around low tide during the day (LT/Day), emersion at night (LT/Night), immersion around high tide during the day (HT/Day) and immersion at night (HT/Night). The dynamics of the NEE in relation to the environmental parameters are described for each EC measurement as presented in Table 1 and Figures 3, 4, 5 and 6.

3.1. Autumn 2007 at Station 2

Over the three days of measurements in September–October 2007 at Station 2, the Arcachon lagoon acted as a source of CO_2 to the atmosphere, with an average of 0.8 ± 2.7 µmol m^{-2} s^{-1} and fluxes ranging from -10.0 to 18.6 µmol m^{-2} s^{-1} (Table 2, Fig. 3E). However, at low tide during sunny afternoons with PAR values reaching more than 1000 µmol m^{-2} s^{-1} at midday (Fig. 3A), strong CO_2 uptakes (CO_2 sinks) were systematically observed, as seen on Days 273 and 274, with values close to 6 and 10 µmol m^{-2} s^{-1}, respectively (Fig. 3E). In contrast, during nighttime at low tide, the lagoon emitted large quantities of CO_2 to the atmosphere, acting as a CO_2 source (2.7 ± 3.7 µmol m^{-2} s^{-1} on average, Table 1), as measured between Days 273 and 274 and between Days 275 and 276, with values largely above 10 µmol m^{-2} s^{-1} (Fig. 3E). The CO_2 uptake observed at LT/Day 275 was weak, reaching only 2 µmol m^{-2} s^{-1}, compared to that observed on preceding days (Fig. 3E); this change corresponded to the occurrence of a mass of relatively hot air (approaching 24°C, Fig. 3B) concomitant with a change in wind direction from the east–southeast (90–135°) to south–southwest (180–225°) (Fig. 3D) sectors and with a higher speed, above 5 m s^{-1} (Fig. 3C).

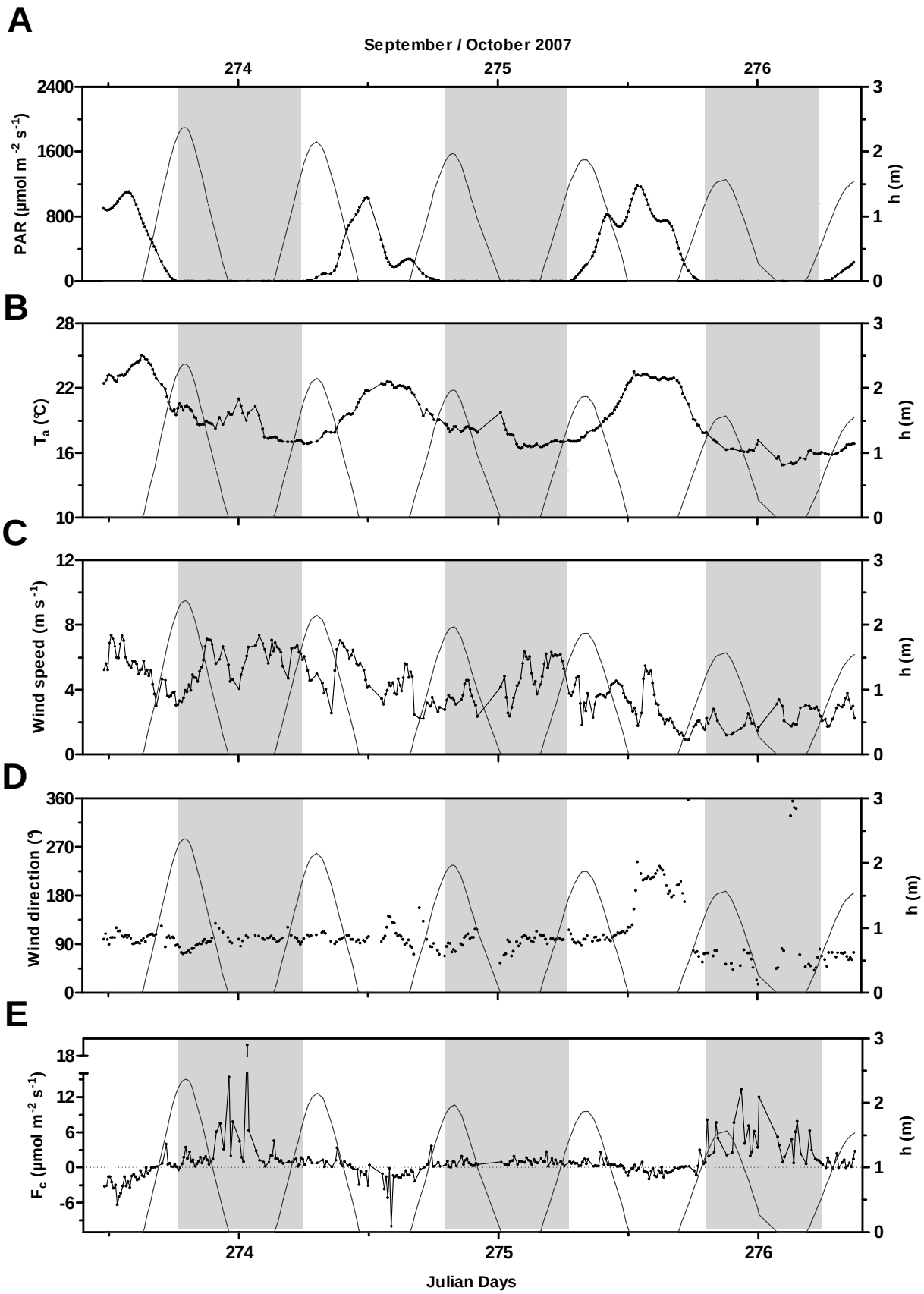
A
September / October 2007
274
275
276
2400
1600
800
0
PAR (µmol m -2 s-1)
3
2
1
0
h (m)
B
28
22
16
10
Ta (°C)
C
12
8
4
0
Wind speed (m s -1)
D
360
270
180
90
0
Wind direction (°)
E
18
12
6
0
-6
Fc (µmol m -2 s-1)
Julian Days

Fig. 3. Environmental parameters and carbon dioxide fluxes measured during the EC deployment in the Arcachon lagoon (St. 2) from the 30th of September at 11:35 to the 3rd of October 2007 at 08:55 (GMT). A: photosynthetically active radiation (µmol m^{-2} s^{-1}) and water height (m); B: temperature of the air (°C); C: wind speed (m s^{-1}); D: wind direction (°) and E: carbon dioxide fluxes (µmol m^{-2} s^{-1}). Negative fluxes represent sinks of CO_2, and positive fluxes represent sources of CO_2 to the atmosphere by convention. Day 273 squares with the 30th of September 2007. A PAR threshold of 20 µmol m^{-2} s^{-1} was chosen to separate day and night cases, and high tide cases correspond to zero-water heights (low tide cases). PAR data have been transformed in µmol m^{-2} s^{-1} from global radiation data in W m^{-2}, assuming a factor of 2 from global radiation to PAR values. A specific range for F_c (panel E) was chosen for a better visualisation of CO_2-flux variations.

3.2. Summer 2008 at Station 1

In July 2008, at Station 1, the Arcachon lagoon showed weaker CO_2 exchanges than in autumn 2007 at Station 2, acting on average as a small source of CO_2 to the atmosphere over the week (0.1 ± 1.9 µmol m^{-2} s^{-1}), with CO_2 fluxes ranging generally from -5.75 to 2 µmol m^{-2} s^{-1} (Fig. 4E, Table 1). During summer 2008 at LT/Day, high CO_2 uptakes were measured, reaching values of -5 µmol m^{-2} s^{-1}, as observed during Day 187 (Fig. 4E). These CO_2 sinks occurred particularly during sunny days, with PAR values close to 1500 µmol m^{-2} s^{-1} at midday, and were roughly synchronised with low tides (from Days 185 to 188, Fig. 4A). PAR values measured during this season showed variable but intense radiations above 2000 µmol m^{-2} s^{-1} at midday (Days 185 and 186, Fig. 4A). At LT/Night, CO_2 emissions to the atmosphere were measured, with CO_2 flux values generally above 2 µmol m^{-2} s^{-1} (Fig. 4E). At the beginning of the measurement (Days 183 and 184), this classical scheme of CO_2 uptake at LT/Day and CO_2 degassing at LT/Night was perturbed and replaced by a strong CO_2 source to the atmosphere, also at LT/Day, reaching 12 µmol m^{-2} s^{-1} (Fig. 4E). During this event, PAR values were below 500 µmol m^{-2} s^{-1} at midday (Fig. 4A), and a particular mass of air coming from the south–southwest wind sector (180–225°) changed in speed, reaching 8 m s^{-1}, and in direction (Figs. 4C and D).

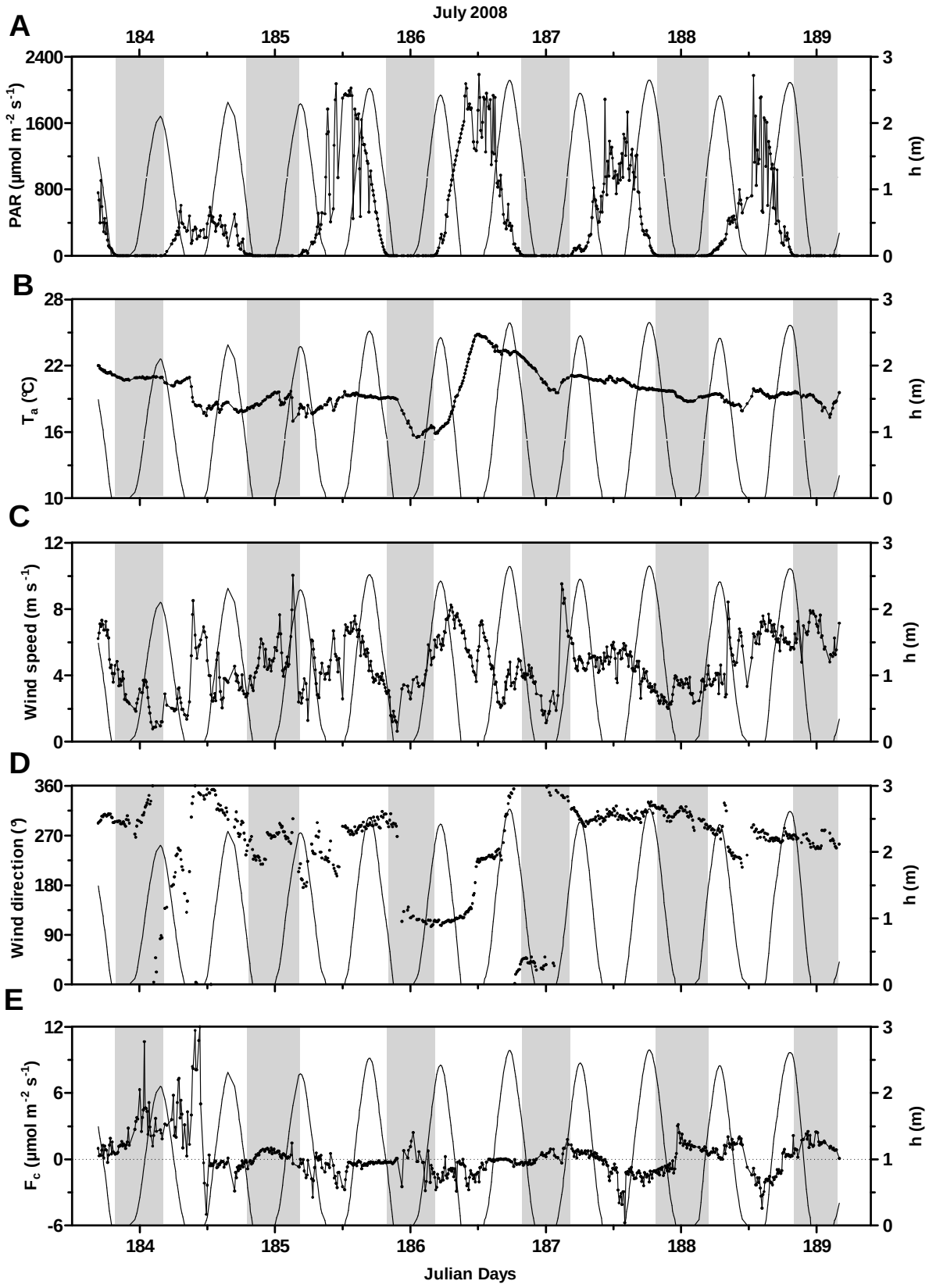
July 2008
A
B
C
D
E
PAR (µmol m-2 s-1)
Ta (°C)
Wind speed (m s-1)
Wind direction (°)
Fc (µmol m-2 s-1)
h (m)
Julian Days

Fig. 4. Environmental parameters and carbon dioxide fluxes measured during the EC deployment in the Arcachon lagoon (St. 1) from the 1st of July at 16:40 to the 7th of July 2008 at 04:00 (GMT). A: photosynthetically active radiation PAR (µmol m^{-2} s^{-1}) and water height (m); B: temperature of the air (°C); C: wind speed (m s^{-1}); D: wind speed (°) and E: carbon dioxide fluxes (µmol m^{-2} s^{-1}). Negative fluxes represent sinks of CO_2, and positive fluxes represent sources of CO_2 to the atmosphere by convention. Day 183 squares with the 1st July 2008 and grey bands represent night periods. A PAR threshold of 20 µmol m^{-2} s^{-1} was chosen to separate day and night cases, and high tide cases correspond to zero-water heights (low tide cases). Notice that four PAR data above 2200 µmol m^{-2} s^{-1} are not shown, with the chosen scale corresponding to non-realistic data due to quantum sensor noise. A specific range for F_c (panel E) was chosen for a better visualisation of CO_2 flux variations.

3.3. Autumn 2008 at Station 1

Contrary to the previous measurements, in September–October 2008 at Station 1, the Arcachon lagoon was a sink of CO_2 over the twenty days, with an average uptake of 0.2 ± 1.4 µmol m^{-2} s^{-1} and the CO_2 fluxes ranging generally from -5.0 to 3.0 µmol m^{-2} s^{-1} (Table 1). During this deployment, medium CO_2 sinks were measured at LT/Day, with values generally close to 5 µmol m^{-2} s^{-1} (i.e., Days 287 and 289), whereas weak CO_2 sources were found at LT/Night below 3 µmol m^{-2} s^{-1} (i.e., Days 286 and 288) (Fig. 5E). The PAR values were typical for the season, with some values close to 1250 µmol m^{-2} s^{-1} being measured at midday during sunny days. The PAR values were slightly higher than those measured during the same season in 2007 at Station 2, probably because of the presence of clouds during the three days of measurement. At Station 1, PAR values observed at midday decreased over the twenty days of measurement, from 1500 µmol m^{-2} s^{-1} to 1300 µmol m^{-2} s^{-1}, i.e., at a rate of -10 µmol m^{-2} s^{-1} each day (Fig. 5A). As noted in the previous measurements, reductions in CO_2 influxes at LT/Day and in CO_2 effluxes at LT/Night with immersion were observed. Indeed, during Day 276, the CO_2 flux shifted in less than one hour from -1.5 µmol m^{-2} s^{-1} at LT to -0.7 µmol m^{-2} s^{-1} with 30 cm of water, whereas the PAR remained high and constant (Fig. 5E). During flood tide on Night 279/280, CO_2 degassing decreased from 1.0 to 0.2 µmol m^{-2} s^{-1} in less than one hour after the tidal flat immersion. Contrary to September–October 2007 at Station 2 and July 2008 at Station 1, CO_2 influxes were measured at HT/Night (-0.3 ± 1.3 µmol m^{-2} s^{-1} on average, Table 1), as found during Night 282/283, with values reaching -7 µmol m^{-2} s^{-1} (Fig. 5E). In addition, a strong CO_2 emission of 14 µmol m^{-2} s^{-1} was observed at LT/Day (Day 279) immediately after a sudden and concomitant increase in air temperature and wind speed (Figs. 5B and C) and a switch in wind direction to the 180–225° sector (Fig. 5D).

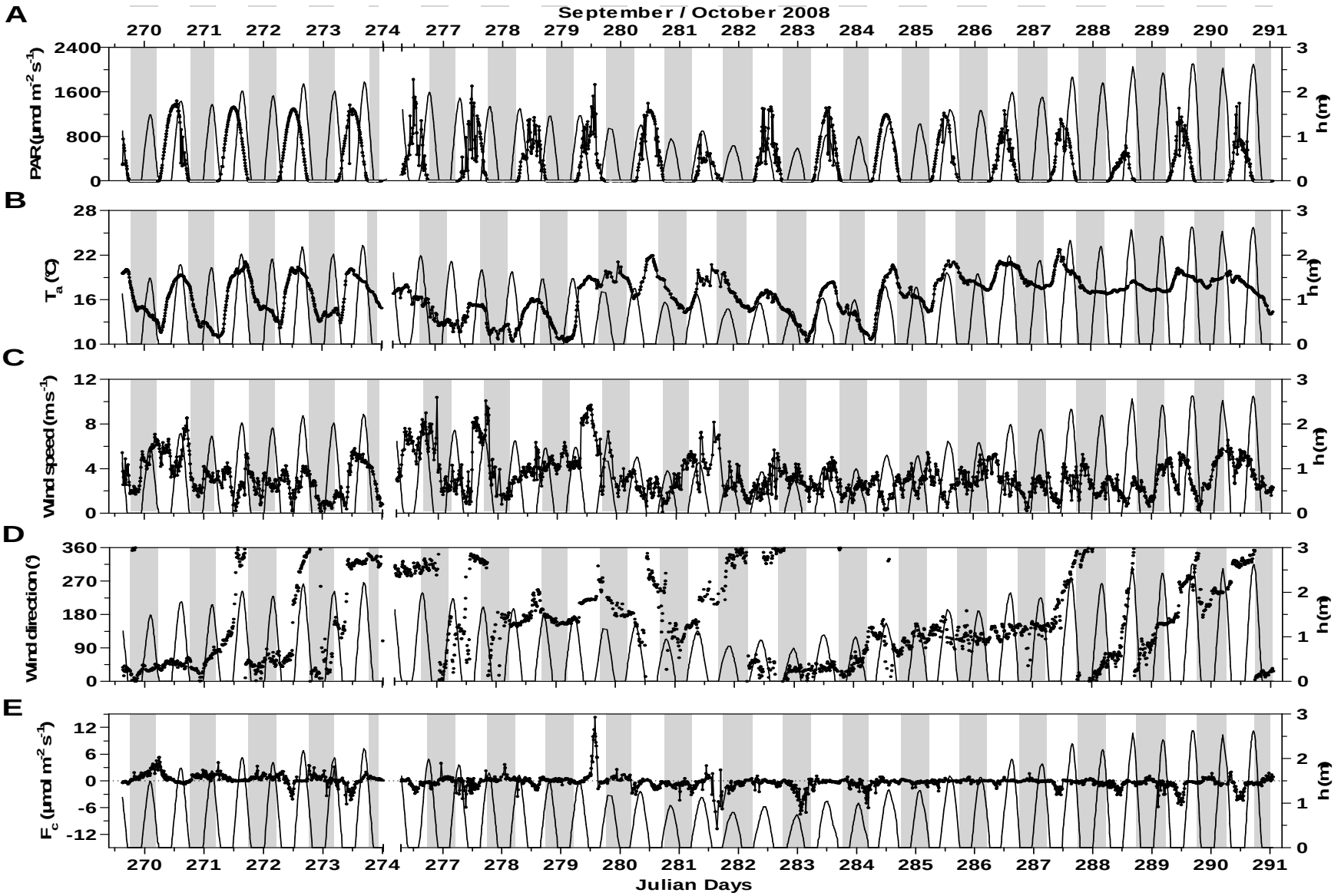
A
September / October 2008
PAR(µmol m-2 s-1)
h(m)
B
Ta (°C)
C
Wind speed (m s-1)
D
Wind direction (°)
E
Fc (µmol m-2 s-1)
Julian Days

Fig. 5. Environmental parameters and carbon dioxide fluxes measured during the EC deployment in the Arcachon lagoon (St. 1) from the 25th of September at 15:10 to the 17th of October 2008 at 01:10 (GMT). A: photosynthetically active radiation PAR (µmol m^{-2} s^{-1}) and water height (m); B: temperature of the air (°C); C: wind speed (m s^{-1}); D: wind direction (°) and E: carbon dioxide fluxes (µmol m^{-2} s^{-1}). Negative fluxes represent sinks of CO_2, and positive fluxes represent sources of CO_2 to the atmosphere by convention. Day 269 squares with the 25th of September 2008, and grey bands represent night periods. Data between the 30th of September (00:10) and the 2nd October 2008 (07:10) could not be measured due to technical problems during the deployment. A PAR threshold of 20 µmol m^{-2} s^{-1} was chosen to separate day and night cases, and high tide cases correspond to zero-water heights (low tide cases). A specific range for F_c (panel E) was chosen for a better visualisation of CO_2 flux variations.

3.4. Spring 2009 at Station 1

In April 2009, the strongest CO_2 sink was measured in the Arcachon lagoon, with -2.4 µmol m^{-2} s^{-1} on average and CO_2 fluxes ranging from -13 to 3 µmol m^{-2} s^{-1} over the thirteen days of measurement (Table 1). No clear pattern was observed, in contrast to the previous measurements, with the CO_2 fluxes always negative regardless of the diurnal or the tidal phase (Fig. 6E). Nevertheless, the largest sinks of CO_2 also occurred at LT/Day (i.e., Days 93 and 103), and fluxes were close to zero or positive as soon as night fell, in particular at low tide (i.e., Nights 98/99 and 100/101) (Fig. 6E). At LT/Day during Days 95 and 96, weaker CO_2 influxes corresponded to cold masses of air close to 13°C with low wind speeds near 1 m s^{-1} and wind directions from the south–southeast (135–180°) (Figs. 6B, C, D and E). In contrast to the three previous measurement periods, when LT/Night cases always corresponded to CO_2 releases to the atmosphere due to benthic respiration, in April 2009, CO_2 fluxes at LT/Night were either null or negative (Table 1 and Fig. 6E). In fact, these negative fluxes occurred during very short periods of LT/Night, at the end (Day 94) or at the beginning (Days 94/95 and 95/96) of the night and immediately after or before immersion (Fig. 6E). In conditions of well-established LT/Night conditions (Days 92, 97, 98, 100 and 101), CO_2 fluxes were null.

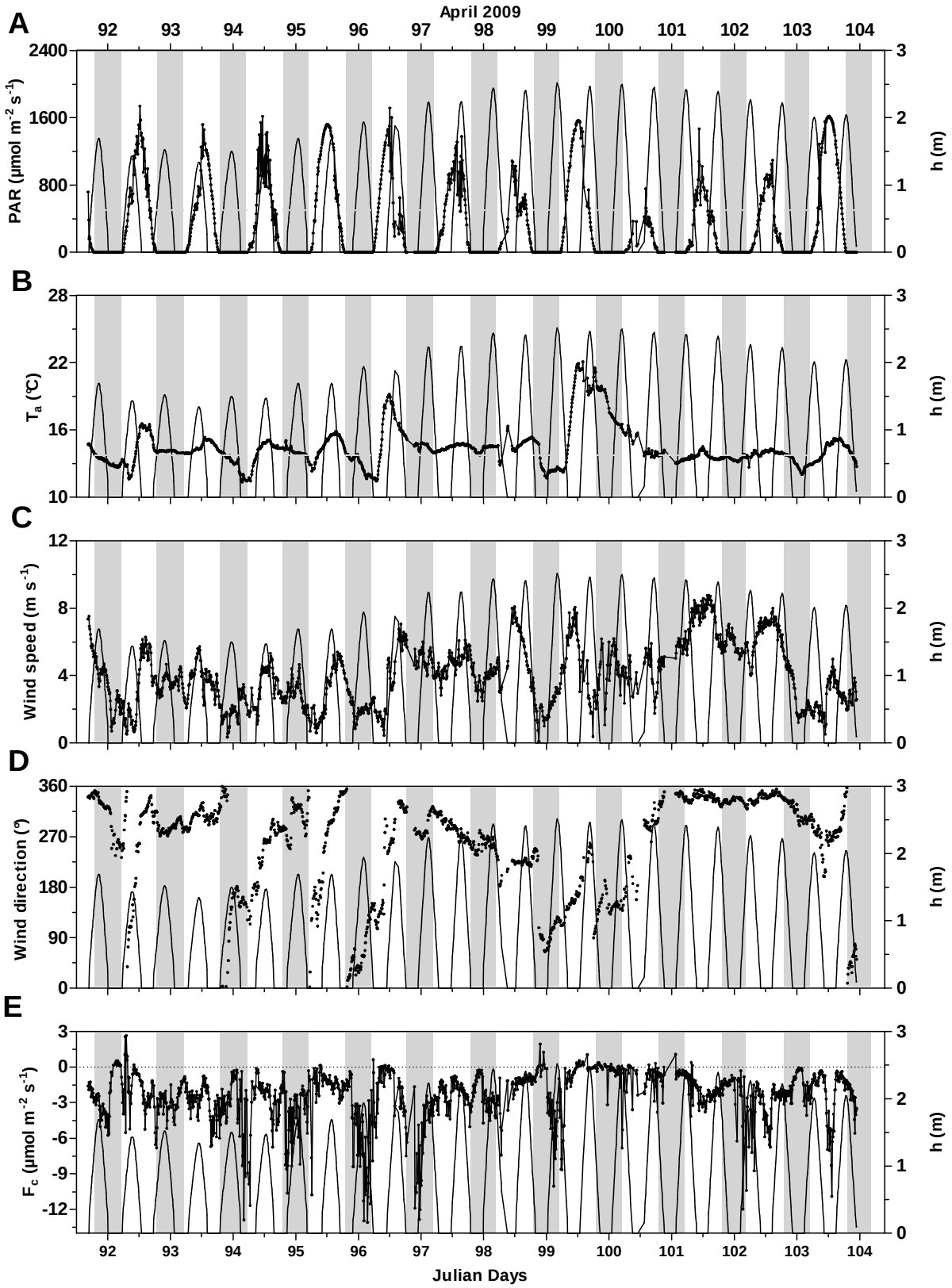
A
April 2009
92 93 94 95 96 97 98 99 100 101 102 103 104
PAR (µmol m-2 s-1)
2400
1600
800
0
h (m)
3 2 1 0
B
Ta (°C)
28
22
16
10
C
Wind speed (m s-1)
12
8
4
0
D
Wind direction (°)
360
270
180
90
0
E
Fc (µmol m-2 s-1)
3
0
-3
-6
-9
-12
Julian Days

Fig. 6. Environmental parameters and carbon dioxide fluxes measured during the EC deployment in the Arcachon lagoon (St. 1) from the 01st of April at 16:30 to the 13th of April 2009 at 22:50 (GMT). A: photosynthetically active radiation PAR (µmol m^{-2} s^{-1}) and water height (m); B: temperature of the air (°C); C: wind speed (m s^{-1}); D: wind direction (°) and E: carbon dioxide fluxes (µmol m^{-2} s^{-1}). Negative fluxes represent sinks of CO_2, and positive fluxes represent sources of CO_2 to the atmosphere by convention. Day 91 squares with the 1rst April 2009 and grey bands represent night periods. A PAR threshold of 20 µmol m^{-2} s^{-1} was chosen to separate day and night cases, and high tide cases correspond to zero-water heights (low tide cases). A specific range for F_c (panel E) was chosen for a better visualisation of CO_2 flux variations.

3.5. Wind direction, CO_2 fluxes and *Zostera noltii* cover

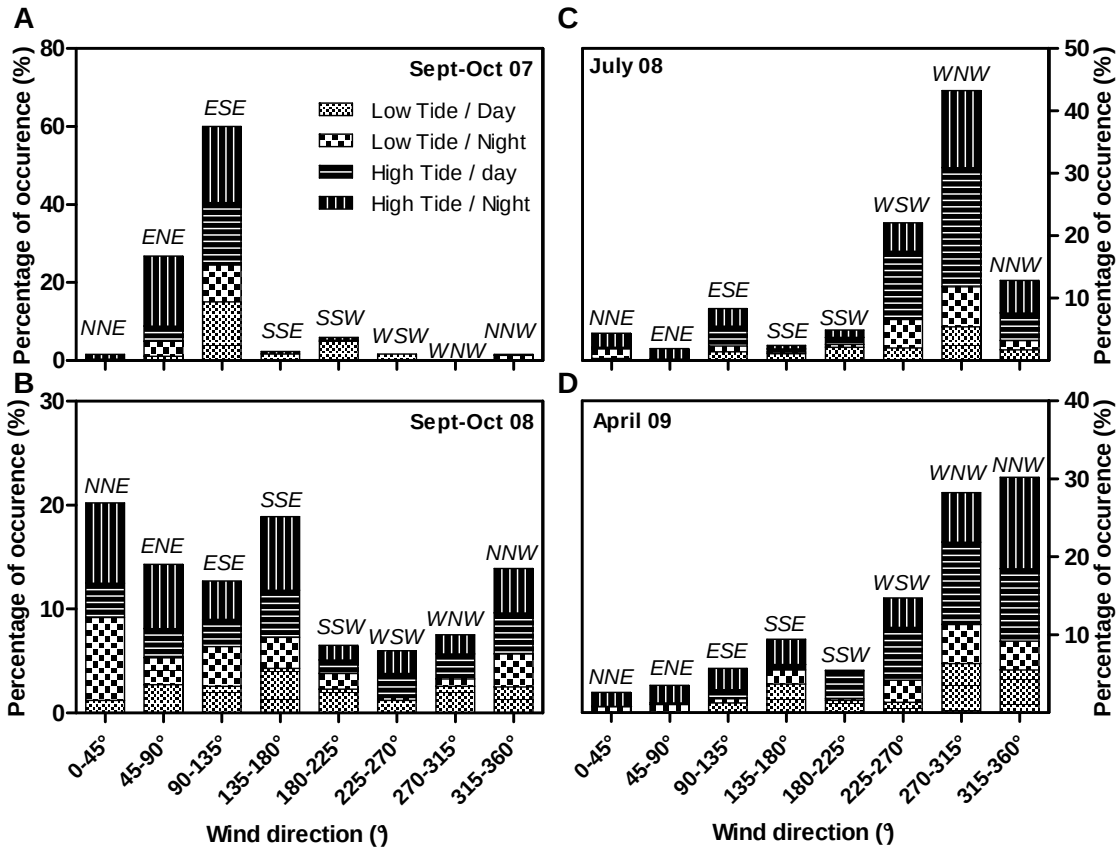

Fig. 7. The wind directions during the four EC measurements in the Arcachon lagoon by percentage of occurrence and functions to the tidal and diurnal rhythms (low tide/day, low tide/night, high tide/day and high tide/night). A: 30/09 to 03/10 2007 (St. 2), B: 25/09 to 17/10 2008 (St. 1), C: 01 to 07/07 2008 (St. 1) and D: 01 to 13/04 2009 (St. 1). NNE: north–northeast; ENE: east–northeast, ESE: east–southeast, SSE: south–southeast; SSW: south–southwest; WSW: west–southwest; WNW: west–northwest and NNW: north–northwest wind directions.

Figure 7 presents the occurrence of prevailing winds per sector for each period. Wind directions varied temporally according to the season and also spatially according to the station. In September–October 2007 at Station 2, the prevailing winds blew mostly from the east–southeast and east–northeast, with 60% and 27% of occurrence, respectively (Fig. 7A). In autumn 2008 at Station 1, no wind direction clearly prevailed; the north–northeast (0–45°) and south–southeast (135–180°) sectors both accounted for 20% of the wind, and the 180–315° sector accounted for less than 10% (Fig. 7B). During July 2008 and April 2009 at Station 1, wind direction also changed often, but consistent prevailing winds occurred from the 225–315° and the 270–360° sectors. Consequently, winds from the west–northwest were mostly observed during both seasons, reaching more than 40% in summer 2008 and 30% of occurrence in spring 2008 (Figs. 7C, D).

The analyses of satellite images of the lagoon at LT/Day in relation to the percentage of EC measurements for each period are presented in Table 2. In autumn 2007 at Station 2, seagrass cover was generally low, ranging between 4% and 51% from the south–southwest and east–southeast wind sectors, respectively (Table 2). More than 60% of the CO_2 flux data corresponded to the highest *Zostera noltii* cover (27% from the east–southeast sector) and the more negative averaged CO_2 flux (-2.1 ± 1.4 µmol m^{-2} s^{-1}, Table 2). Inversely, more than 20% of the data matched the lowest seagrass cover (4% from the south–southwest sector) and one of the least negative averaged CO_2 fluxes (-0.7 ± 0.6 µmol m^{-2} s^{-1}, Table 2). In summer 2008 at Station 1, where no satellite image was available, almost 50% of F_c data were measured from the west–northwest sector, with a flux of -2.0 ± 1.4 µmol m^{-2} s^{-1} on average (Table 2). In autumn 2008 at the same station, higher *Zostera noltii* covers were measured than during the same season in 2007 at Station 2, with values ranging between 70% (south–southeast) and 99% (west–northwest) (Table 2). A total of 21% and 17% of flux data (-0.9 ± 1.0 and -0.7 ± 1.3 µmol m^{-2} s^{-1} on average) corresponded to covers of 70% (south–southeast) and 93% (east–northeast), respectively. The next year, in autumn 2009, exactly the same percentage of *Zostera noltii* cover was observed (92 ± 10% in average), between 69 and 99% (Table 2). These results are in particular in accordance with the study of Auby and Labourg (1996), who showed that seagrass generally reaches maximum densities of biomass in summer–autumn in the Arcachon lagoon. In spring 2009 at Station 1, where no images matched precisely with the EC deployment, approximately 30% of F_c data corresponded to the west–northwest and north–northwest wind sectors, with average fluxes of -3.0 ± 1.5 and -3.1 ± 1.2 µmol m^{-2} s^{-1}, respectively (Table 2). The analysis of the image recorded on April 2010 (14/04), the year

after the EC deployment, showed very low seagrass cover, below 5%, regardless of wind direction (data not shown). In fact, seagrass leaves only begin to grow in spring, showing rather low above-ground biomass, and the minimum values are observed in winter, with a root system (rhizome) persisting throughout the year (Duarte, 1989; Auby and Labourg, 1996; Vermaat and Verhagen, 1996). The image recorded on 24/06/2009 at Station 1 showed slightly lower seagrass cover than in late summer–autumn (range: 62–97%) but higher than that measured previously, in early spring 2010. However, this image, obtained two months after the EC deployment carried out in April 2009, may represent the evolution of the meadow over the spring period in terms of ecological processes. The image could then be used to link the CO_2 fluxes and the seagrass cover measured in this period at Station 1. In particular, the more negative CO_2 flux (-4.5 ± 2.6 µmol m^{-2} s^{-1}, in average) measured in April 2009 corresponded to the highest *Zostera noltii* cover (97%) observed in June 2009 from the west–southwest sector of wind direction (Table 2). Inversely, the less negative CO_2 fluxes (-1.0 ± 1.6 µmol m^{-2} s^{-1}, in average) corresponded to the lowest seagrass cover (62%) from the south–southeast wind sector (Table 2).

		NNE 0–45°	**ENE 45–90°**	**ESE 90–135°**	**SSE 135–180°**	**SSW 180–225°**	**WSW 225–270°**	**WNW 270–315°**	**NNW 315–360°**
Station 2 Autumn 2007	***Zostera noltii* cover (13/09/2007)**	**19%**	**25%**	**27%**	**17%**	**4%**	**14%**	**15%**	**51%**
	F_c (µmol m^{-2} s^{-1})		**-0.9 ± 0.7**	**-2.1 ± 1.4**	**-2.1 ± 4.4**	**-0.7 ± 0.6**	**-0.7 ± 0.7**		
	Percentage of F_c data		4%	61%	7%	21%	7%		
Station 1 Summer 2008	**F_c (µmol m^{-2} s^{-1})**			**-1.1 ± 0.9**	**-1.4 ± 0.3**	**-1.4 ± 0.6**	**-0.9 ± 0.9**	**-2.0 ± 1.4**	**-0.7 ± 0.2**
	Percentage of F_c data			11%	6%	14%	18%	47%	4%
Station 1 Autumn 2008	***Zostera noltii* cover (17/10/2008)**	**98%**	**93%**	**86%**	**70%**	**95%**	**99%**	**99%**	**98%**
	***Zostera noltii* cover (08/09/2009)**	**97%**	**95%**	**87%**	**69%**	**94%**	**98%**	**99%**	**98%**
	F_c (µmol m^{-2} s^{-1})	**-0.5 ± 1.5**	**-0.7 ± 1.3**	**-0.1 ± 0.9**	**-0.9 ± 1.0**	**-1.5 ± 2.6**	**-2.2 ± 2.0**	**-2.0 ± 1.1**	**-1.5 ± 1.2**
	Percentage of F_c data	9%	17%	14%	21%	9%	6%	12%	12%
Station 1 Spring 2009	***Zostera noltii* cover (24/06/2009)**	**90%**	**89%**	**74%**	**62%**	**94%**	**97%**	**96%**	**94%**
	F_c (µmol m^{-2} s^{-1})			**-3.8 ± 3.6**	**-1.0 ± 1.6**	**-1.6 ± 1.0**	**-4.5 ± 2.6**	**-3.0 ± 1.5**	**-3.1 ± 1.2**
	Percentage of F_c data			6%	19%	8%	7%	32%	28%

Table 2. Relationships between the *Zostera noltii* cover from the satellite image analyses and the measured CO_2 fluxes from the Arcachon lagoon, at low tide during the day, according to sectors of wind direction. 0–45°: north–northeast, 45–90°: east–northeast, 90–135°: east–southeast, 135–180°: south–southeast, 180–225°: south–southwest; 225–270°: west–southwest, 270–315°: west–northwest, 315–360°: north–northwest wind directions. Notice that F_c values obtained in July 2008 during the beginning of the experiment (Days 183, 184) and in September–October 2008 (Day 279) have been discarded for calculations, representing destocking but not biological degassing by respiration (Figures 5F and 6F).

4. Discussion

4.1. Spatial and temporal variations of NEE in relation to the NEP of the Arcachon lagoon

4.1.1. Relationship between low tide CO_2 fluxes and the distribution of *Zostera noltii* meadows

Zostera noltii Hornem. is a common intertidal seagrass of the European and African coasts distributed from Norway to Mauritania (Den Hartog, 1970). It constitutes an important and highly productive component of the benthic environment in these near-shore soft-bottom ecosystems (McRoy and McMillan, 1977). In the Arcachon lagoon, *Zostera noltii* beds are particularly extensive, colonising the major part of the intertidal area (60%, i.e., 70 km^2) between -1.9 m and +0.8 m relative to local Mean Sea Level (Amanieu, 1967).

With regard to satellite images, a significant spatial difference in *Zostera noltii* cover was observed at Stations 2 and 1 during the same season in autumn 2007 and 2008 (Table 2). Even if late summer coincides with maximum in *Zostera noltii* biomass, in September–October 2007 in the inner part of the lagoon, the percentage of occupation by the seagrass was only 22 ± 14% on average. In contrast, in September–October 2008 in the middle of the lagoon at Station 1, the cover of *Zostera noltii* was much more important, with a mean of 92 ± 10% (Table 2). This spatial distribution is in strong agreement with the extent of the *Zostera noltii* seagrass beds in 2007 in the lagoon reported by Plus et al. (2010).

	***Zostera noltii* cover (%)**	**NEP (µmol m^{-2} s^{-1})**	**CR (µmol m^{-2} s^{-1})**	**GPP (µmol m^{-2} s^{-1})**
September/October 2007 (Station 2)	**22 ± 14**	**1.7 ± 1.7**	**2.7 ± 3.7**	**4.4**
July 2008 (Station 1)		**1.5 ± 1.2**	**1.0 ± 0.9**	**2.5**
September/October 2008 (Station 1)	**92 ± 10**	**0.9 ± 1.7**	**0.2 ± 1.1**	**1.1**

Table 3. Comparison of NEP components at low tide for the autumn season at the two stations and in summer at Station 1. NEP was assumed as NEE at low tide during daytime, CR was assumed as NEE at low tide during the night, and GPP was assumed as the sum of NEP and CR. Notice that F_c values obtained in July 2008 during the beginning of the experiment (Days 183, 184) and in September-October 2008 (Day 279) have been discarded for calculations, representing destocking but not biological degassing by respiration (Figures 5F and 6F). The GPP and CR calculations for the spring 2009 period at Station 1 were not possible because of the slight negative averaged flux value obtained at low tide/night.

For the low tide conditions, we assumed that benthic CR was equivalent to NEE at night (Rocha and Goulden, 2008), and benthic NEP was equivalent to NEE averaged over the daytime. GPP at low tide can be calculated as the NEE during the day plus the NEE at night, as presented in Table 3. In autumn 2007 at Station 2 with a low *Zostera noltii* density, a particularly high GPP of 4.4 µmol m^{-2} s^{-1} was calculated, the CR showing the highest value, with 2.7 ± 3.7 µmol m^{-2} s^{-1}, resulting in an NEP of 1.7 ± 1.7 µmol m^{-2} s^{-1} (Table 3). In contrast, in autumn 2008 at Station 1 with a high *Zostera noltii* density, a slightly low GPP of 1.09 µmol m^{-2} s^{-1} was found, the CR being moderate, equal to 0.2 ± 1.1 µmol m^{-2} s^{-1}, resulting in an NEP of 0.9 ± 1.7 µmol m^{-2} s^{-1} (Table 3). In parallel, at both stations, rapid changes in CO_2 fluxes (NEP) were observed in relation to wind direction and seagrass cover; the most negative (the highest NEP) and the least negative (the lowest NEP) CO_2 fluxes matched the highest and the lowest seagrass cover, respectively (Table 2). These results indicate that *Zostera noltii* appears to greatly control the NEP (GPP and CR) in autumn at Station 1 where the cover is high, but only partly controls the NEP at Station 2, where the cover is low. In contrast, microphytobenthos communities appear to significantly contribute to the GPP at Station 2 in autumn, where *Zostera noltii* meadow cover is low. The production of these communities in the lagoon is estimated to be between 104 and 114 g C m^{-2} yr^{-1}, of the same order as the production of *Zostera noltii* (Auby, 1991). Such high GPP by microphytobenthos at low tide in intertidal mudflats has already been reported by Guarini (1998) in the Marennes-Oléron basin (France), by Migné et al. (2004) in the Bay of Somme (eastern English Channel, France), by Spilmont et al. (2006) in the mudflat of the Seine Estuary (English Channel, France), and by Hubas et al. (2006) in the intertidal bay of Roscoff Aber. In addition, in

September–October 2007 at Station 2, the highest CR (LT/Night) is probably accounted for by the intense grazing of meiofauna and macrofauna on microphytobenthos, the latter being easily and rapidly transferred toward superior benthic heterotrophic components in intertidal areas (Middelburg et al., 2000; Spilmont et al., 2006). Our results suggest the occurrence of two superimposed metabolic carbon cycles in the lagoon, functioning at different timescales: a rapid C cycling (high GPP and CR), ensured by microphytobenthic communities at Station 2 (tide or week scales), and a slow C cycle (low GPP and CR), ensured by the seagrass meadows at Station 1 (seasonal scale).

GPP and CR calculations could not be performed for the data obtained in April 2009 (Station 1), as discussed previously; CO_2 fluxes over the mudflat were null or slightly negative at LT/Night and could not be attributed to benthic CR at low tide. In the unvegetated tidal flat of the Wadden Sea at the same season, Zemmelink et al. (2009) reported null and negative CO_2 fluxes with both EC and chamber techniques. Several processes could partly explain these fluxes in the Arcachon mudflat during this season, when the *Zostera noltii* cover was low and is generally dominated by microphytobenthic GPP, as shown by Spilmont et al. (2006) in the Seine Estuary (France). First, microphytobenthic cells can migrate down to deeper layers of the sediment at night as protection against grazing by deposit-feeders (Blanchard et al., 2001); thus, respiration would not release CO_2 to the atmosphere but deeper into the sediments. Second, CO_2 generated by benthic respiration could be almost entirely involved in the dissolution of carbonate shells and not released to the atmosphere, as occurred for instance in a Mediterranean seagrass meadow (*Posidonia oceanica*) in winter (Barrón et al. 2006).

Concerning seasonal variations at Station 1, in July 2008, the values of GPP (2.5 µmol m^{-2} s^{-1}) and CR (1.0 ± 0.9 µmol m^{-2} s^{-1}) were similar to those obtained in September–October 2008, resulting in an NEP of 1.5 ± 1.2 µmol m^{-2} s^{-1} (Table 3). This result suggests that at Station 1 during the summer season, the predominance of *Zostera noltii* on the NEP (GPP and CR) was similar to that noticed during the early autumn at the same station. In spring 2009, a stronger NEP (-2.7 ± 2.0 µmol m^{-2} s^{-1}, Table 2) was measured at LT/Day in comparison to the NEP values measured in summer-autumn 2008. In addition, as in autumn 2007 at Station 2, in April 2009 at Station 1, rapid changes in CO_2 fluxes were measured, with wind direction and *Zostera noltii* cover obtained in June 2009; in particular, the more negative (the strongest NEP) and less negative (lowest NEP) CO_2 fluxes matched the highest and lowest seagrass cover (Table 2). This finding suggests that *Zostera noltii* partly controls the NEP at Station 1 during the spring season. In

contrast, the NEP, and more specifically the GPP, is probably driven by microphytobenthos communities during early spring at Station 1, where *Zostera noltii* cover is still low as its growth period is just starting. During each spring season, the mud sediments of the intertidal area of the Arcachon lagoon are notably the location of strong microphytobenthic biomasses; they produce a brown biofilm above the sediment surface and present an intense photosynthetic activity.

The changes in the relative importance of these two main primary producers at Station 1 throughout the year do not indicate clearly significant differences in the benthic production of the Arcachon lagoon. This result is in opposition to the study of Hubas et al. (2006), who showed in bare sediments in the bay of Morlaix that only one primary producer strongly contributed to community production. In contrast, the present study is in agreement with the study of Ouisse et al. (2010) in the same bay, who observed a changing importance of primary producers (*Zostera noltii*, associated epiphytes and benthic microalgae) over the course of the year, resulting in a relatively constant rate of production at the community scale.

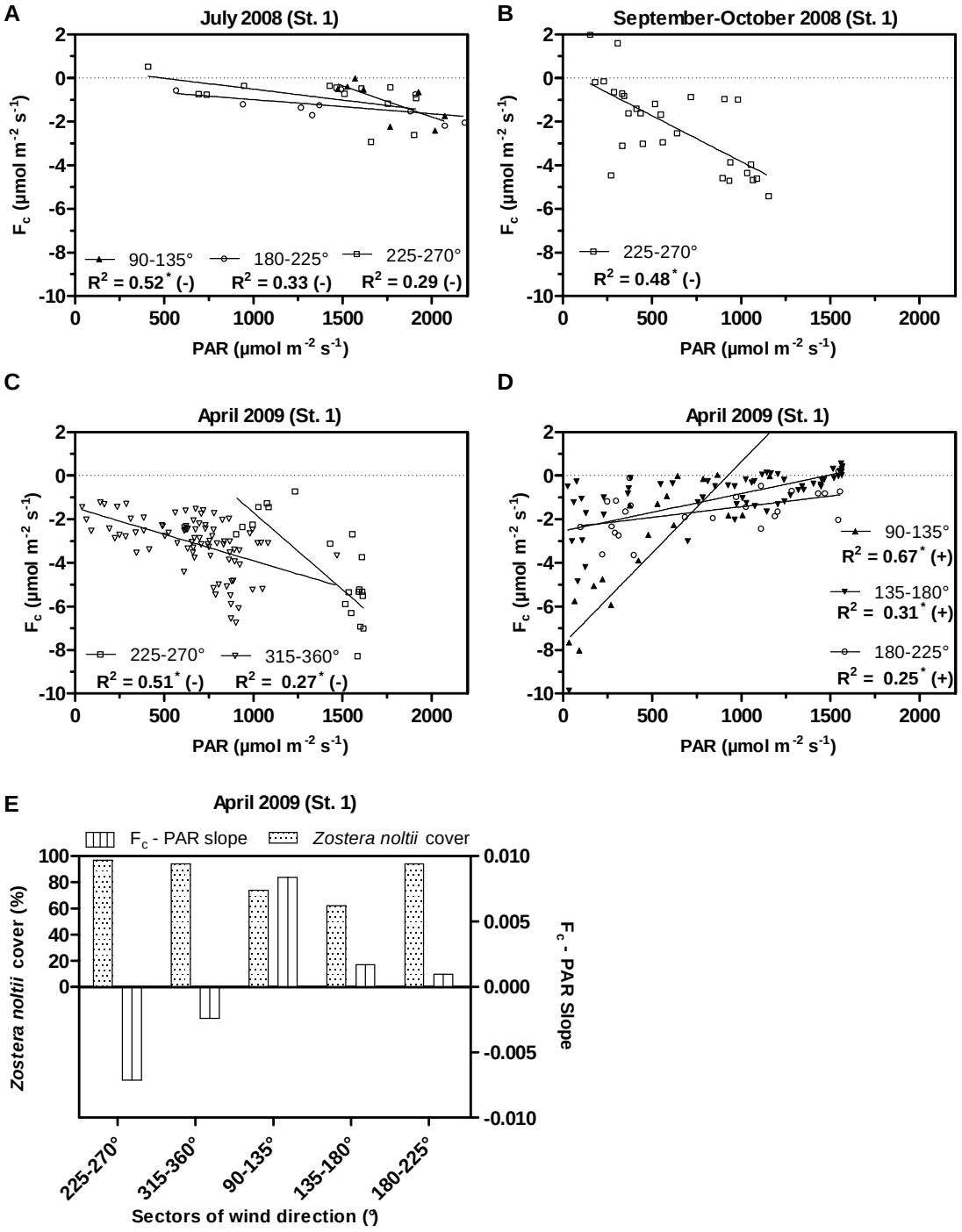
A
July 2008 (St. 1)
F_c (µmol m^-2 s^-1)
PAR (µmol m^-2 s^-1)
90-135°
180-225°
225-270°
R² = 0.52* (-)
R² = 0.33 (-)
R² = 0.29 (-)
B
September-October 2008 (St. 1)
225-270°
R² = 0.48* (-)
C
April 2009 (St. 1)
225-270°
315-360°
R² = 0.51* (-)
R² = 0.27* (-)
D
April 2009 (St. 1)
90-135°
R² = 0.67* (+)
135-180°
R² = 0.31* (+)
180-225°
R² = 0.25* (+)
E
April 2009 (St. 1)
F_c - PAR slope
Zostera noltii cover
Zostera noltii cover (%)
F_c - PAR Slope
225-270°
315-360°
90-135°
135-180°
180-225°
Sectors of wind direction (°)

Fig. 8. P/I linear regressions obtained at low tide during the day in the Arcachon lagoon according to wind directions; A: July 2008 (Station 1); **-0.003x + 3.91** (90–135°); **-0.0006x – 0.34** (180–225°); **-0.001x + 0.50** (225–270°). B: September–October 2008 (Station 1); **-0.004x + 0.38** (225–270°). C and D: April 2009 (Station 1); **-0.007x + 5.40** (225–270°); **-0.002x – 1.47** (315–360°); **0.008x – 7.73** (90–135°); **0.002x – 2.54** (135–180°); **0.001x – 2.40** (180–225°). E: F_c-PAR slopes (C and D) versus *Zostera noltii* covers in April 2009. F_c: Carbon dioxide fluxes; PAR: photosynthetically active radiation; 0–45°: north–northeast; 45–90°: east–northeast, 90–135°: east–southeast, 135–180°: south–southeast, 180–225°: south–southwest; 225–270°: west–southwest; 270–315°: west–northwest and 315–360°: north–northwest wind directions. Notice that F_c values obtained in July 2008 corresponding to PAR values above 2200 µmol m^{-2} s^{-1} have not been taken into account for correlations, these PAR values correspond to non-realistic data due to quantum sensor noise. Additionally, F_c values obtained in July 2008 during the beginning of the experiment (days 183, 184) and in September–October 2008 (day 279) have been discarded representing destocking but not biological degassing by respiration (Figures 5F and 6F). PAR data in September–October 2007 have been transformed in µmol m^{-2} s^{-1} from global radiation data in W m^{-2} assuming a factor 2 from global radiation to PAR values. * denotes the significance of the linear regressions (p values below 0.05).

To clarify and complete our analysis about the control of the CO_2 fluxes in the tidal flat at LT/Day, P–I relations ranked by wind direction and *Zostera noltii* cover were analysed (Fig. 8). In September–October 2007 at Station 2, no correlation between NEE and PAR was found. Additionally, in July 2008 at Station 1, no clear patterns were observed, as discussed in Polsenaere et al. (submitted). However, when data were classified according to sectors of wind direction, negative NEE vs. PAR linear regressions were found, particularly from the east–southeast wind direction (90–135°) and two others showing a similar shape, from the south–southwest (180–225°) and the west–southwest (225–270°) wind directions (Fig. 8A). Contrasts in *Zostera noltii* densities between the 90–135° and 180–270° sectors in July 2008 at Station 1, could explain the differences observed by the EC technique. In September–October 2008 at the same station, a similar NEE–PAR relation (Fig. 8B) was observed for the west–southwest direction, matching the strongest CO_2 uptake and the most extensive seagrass meadow (Table 2). Such negative correlations have been observed with EC by Morison et al. (2000) for the C_4 aquatic grass *Echinochloa polystachya* of the Amazon and by Kathilankal et al. (2008) for the *Spartina alterniflora* in a salt marsh on the eastern coast of Virginia. Using benthic incubations, Silva et al. (2005) obtained the same results for *Zostera noltii* meadows in the intertidal flats of the Ria Formosa lagoon in Portugal. These negative correlations between NEE and PAR (or positive correlations between CO_2 uptake by the vegetated community and the intensity of available light) suggest an optimal adaptation of the plants to environmental conditions, such as temperature, humidity and light.

In April 2009 at Station 1, negative linear regressions were measured from the west–southwest (225–270°) and north–northwest wind directions (315–360°), matching the highest seagrass cover observed in June 2009 (Fig. 8C and Table 2). Nevertheless, positive relations were also obtained for three continuous wind direction sectors covering 90–135°, which notably matched the lowest *Zostera noltii* cover (Fig. 8D and Table 2). This result is in opposition to other studies carried out in intertidal mudflats, which systematically reported negative correlations between CO_2 fluxes and irradiance (Guarini, 1998; Migné et al., 2004; Spilmont et al., 2006; Migné et al., 2007). During this spring period, microphytobenthic communities, generally diatoms in the majority, are known to dominate benthic GPP in the lagoon, forming dense mats on the mudflat (Auby, personal communication). Even, microphytobenthic cells living as epiphytes on young *Zostera noltii* leaves could represent a significant part of the benthic GPP, especially in winter and early spring, as shown by Ouisse et al. (2010) in an intertidal *Zostera noltii* bed (Western English Channel, France). The lack of correlation between NEE and air temperature for these three wind directions suggest that CR is not stimulated by surface heating. Photoinhibition of photosynthesis may also occur, but this mechanism has been observed primarily in laboratory and rarely in field conditions (Blanchard and Cariou-Le Gall, 1994; Guarini, 2000). Finally, it has been shown that microphytobenthic cells can migrate vertically through the sediments to protect them in response to long periods of light exposure at LT/Day as behavioural process of photo-acclimatisation (Blanchard et al., 2004; Serôdio et al., 2008). In consequence, this last hypothesis may explain the positive NEE–PAR correlations obtained in April 2009. Figure 8E presents the processes implied at this period with negative and positive NEE–PAR slopes associated with the highest and the lowest *Zostera noltii* covers, respectively. These results may confirm the previous concept of the concomitant presence of young *Zostera noltii* leaves together with microphytobenthic epiphytes and microphytobenthic mats on sediments in spring 2009 at Station 1.

4.1.2. Diurnal and tidal changes in NEE during the different seasons

Throughout the diurnal and tidal cycles, variations in NEE were large, with the lagoon often rapidly shifting from source to sink. For instance, at Station 1 in July 2008 on Day 184 and daytime, NEE rapidly dropped from 12.0 µmol m^{-2} s^{-1} at low tide to -5.0 µmol m^{-2} s^{-1} as soon as the water submerged the flat. Inversely, at night, between Days 187 and 188, the CO_2 flux was -0.8 µmol m^{-2} s^{-1} at the end of the immersion and rose to 3.0 µmol m^{-2} s^{-1} at the beginning of emersion (Fig. 4E). There are a number of processes that can induce these rapid changes in NEE, including benthic and planktonic GPP and CR, advection with water movements and air–water gas

exchange. Although in the intertidal Wadden Sea, Zemmelink et al. (2009) found little dependency of CO_2 fluxes on the tide, this was not the case in the Arcachon lagoon. The effect of rising tide on CO_2 exchange was first reported by Houghton and Woodwell (1980) in a salt marsh. Kathilankal et al. (2008) reported a 46% reduction in CO_2 uptake during emersion. In these salt marsh systems, part of the vegetation remains emerged even at high tide. In intertidal systems like the Arcachon lagoon or the Wadden Sea, at low tide, benthic GPP and CR are theoretically the two main drivers of NEE (i.e., NEP in this case), as discussed in the previous section. When the tide rises over the flat, benthic and planktonic communities contribute to GPP and CR, but their effect on NEE may not be immediate because water–air gas exchange is slow in comparison with the duration of the immersion. For instance, for typical conditions in coastal systems and a gas-transfer velocity of 10 cm h^{-1}, it takes 3.5 hours for pCO_2 to decrease from 600 to 500 ppmv with gas exchange, which corresponds to a CO_2 flux of ~1.2 µmol m^{-2} s^{-1}, comparable to what we observed here. Consequently, a negative water–air gradient can be created, for instance by phytoplankton at the mouth of the lagoon at low tide. When these undersaturated water masses enter the lagoon with the flood tide, a negative NEE would be observed, but it would be only partly the result of the NEP of the lagoon at high tide. Inversely, intense benthic and planktonic CR at high tide in the lagoon would not necessarily immediately generate an equivalent degassing of CO_2 to the atmosphere, with some of the CO_2 remaining in solution and being advected with the subsequent ebb tide. Such CO_2 outwelling from intertidal systems to adjacent creeks and bays has been observed in many tidal wetlands (Cai et al., 2003; Wang and Cai, 2004; Borges et al., 2003).

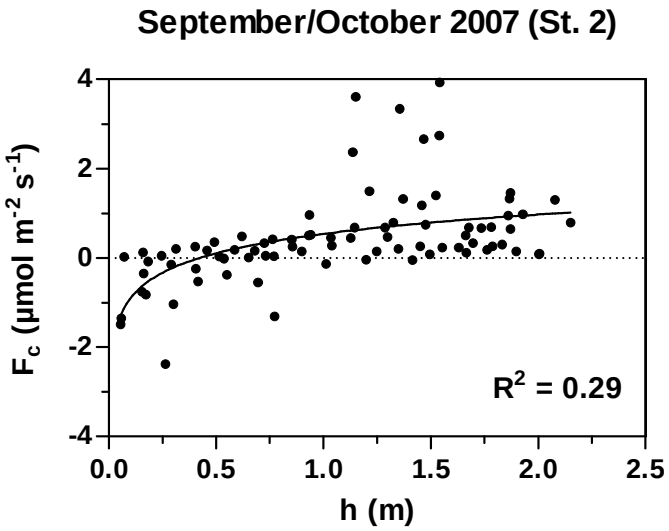

Fig. 9. Carbon dioxide fluxes (F_c) in September–October 2007 (**St. 2**) during immersion as a function of the water height (h). Beyond 50 cm, the lagoon changed from a sink of CO_2 into a source of CO_2 to the atmosphere.

The September 2007 measurements at Station 2 in the inner part of the lagoon provide a first and relatively simple scheme for conceptualising NEE dynamics in relation to NEP at the different phases of the day and the tide. During this experiment, we observed strong CO_2 uptake at LT/day but CO_2 degassing during all other cases (Figure 3E, Table 1). This suggests that at LT/day, the tidal flat was autotrophic, whereas it was heterotrophic during the night and during immersion. In addition, CO_2 degassing at LT/Night and HT/Night was significantly higher ($p<0.05$) than at HT/day, which suggests that in the daytime, benthic and planktonic GPP could significantly reduce CO_2 degassing. Benthic GPP by microphytobenthos is controlled by light availability (Parsons et al. 1984) and is believed to be light limited during immersion. However, the presence of microphytobenthos can significantly contribute to planktonic GPP at the beginning of the flood tide. Indeed, Guarini (1998) showed that a large part of microphytobenthic cells can be re-suspended with the flooding tide and largely contribute to the planktonic GPP during HT/Day periods. In September 2007 at Station 2, we found a significant positive correlation between CO_2 fluxes and water height (Fig. 9). Indeed, the lagoon clearly shifted from a sink of CO_2 at LT/day (Table 1) to a source of CO_2 to the atmosphere with the rising tide as soon as the water height reached 0.5 m. It is possible that during this transition phase the organic matter newly synthesised by the microphytobenthos, predominant at this station at low tide, fed the respiration of the water column during high tide. Such rapid carbon recycling between the benthic and planktonic compartments would explain the NEE patterns observed during this experiment.

At Station 1, in the centre of the lagoon, patterns of CO_2 fluxes were fundamentally different, as uptake of atmospheric CO_2 were also observed during immersion. This was the case during the day at the three periods of measurements and also during the night in September 2008 and in April 2009. In contrast, in July 2008, the lagoon was a source of CO_2 at HT/night, being a sink at HT/day (Table 1). Negative NEE during HT/night demonstrates the impact of planktonic GPP at the outlet of the lagoon, followed by advection of CO_2-depleted water masses with the flood tide. Indeed, the channel and subtidal areas of the lagoon are the sites of development of phytoplankton blooms in the lagoon dominated by large diatom cells leading to high primary production rates, particularly in early spring (Glé et al., 2007, 2008). In April 2009, the uptake of atmospheric CO_2 during immersion at Station 1 was nearly two times higher at night than during the day (Table 1), which reveals that the CO_2 depletion of the waters occurred a few hours before daytime, precisely when the water masses were at the mouth of the lagoon. On the contrary, the water present at daytime over the tidal flat absorbed less atmospheric CO_2, as it was present at the outlet of the lagoon during the night; this also suggests that during this spring period, GPP during immersion was lower in the lagoon than outside of the lagoon. Glé et al. (2007) showed that, in late winter–early spring (in 1999 and 2003) at each high tide during this season, oceanic blooms were advected into the lagoon, first in the external waters and second in the internal waters, with the intensity of this production being always higher in the external waters. In addition, in spring 2009 at Station 1, as previously discussed, microphytobenthic GPP was important during the LT/day period; we thus expected that, like in autumn 2007 at Station 2, the exudation of highly biodegradable compounds to the water would enhance CR during the following immersion phase (Guarini, 1998). However, we did not observe CO_2 degassing during this phase, but rather negative or slightly positive NEE. This suggests that at this season, the respired microphytobenthic GPP could participate in the decrease observed in the CO_2 uptake from LT/Day to HT/Day (Table 1) but that planktonic GPP dominates during the immersion phase at Station 1.

In July and September 2008, NEE during emersion at Station 1 showed different patterns. In September, NEE was slightly negative (~-0.2 µmol m^{-2} s^{-1}; Table 1) at both HT/day and HT/night, suggesting a predominant role of advection of CO_2-depleted waters from the mouth of the lagoon, as in April 2009. In contrast, in July 2008, the water in the lagoon was a sink of CO_2 at daytime but a source of CO_2 at night, meaning that advection phenomena were probably less important than metabolic processes in the lagoon at Station 1 (Table 1).

CO_2 uptake at LT/Day was systematically reduced at HT/Day during the four deployments (Fig. 5E and Table 1). CO_2 uptakes could be reduced by the lower photosynthetic activity of primary producers due to light limitation in the presence of water; this is especially true for *Zostera noltii* in the summer and autumn seasons in 2008 at Station 1, where the seagrass cover is maximal. However, Silva et al. (2005) noted that information on photosynthetic efficiency during air-exposed versus immersed conditions is inconsistent, suggesting that the key factor in CO_2 uptake by air-exposed *Zostera noltii* is the leaf water content (Silva et al., 2005). Leuschner et al. (1998) demonstrated a linear relationship between the leaf water content of the marine angiosperm and its net photosynthetic rate. In the Arcachon lagoon, the existence of depressions in the sediment at low tide probably allowed higher photosynthetic rates of the seagrass than during water immersion, as shown by Silva et al. (2005) in the Ria Formosa lagoon. Indeed, these depressions could retain a considerable amount of water, enough to maintain leaf hydration, and allow rapid air–water CO_2 diffusion. Nevertheless, even if CO_2 diffuses through water approximately 10000-fold more slowly than through air (Stumm and Morgan, 1996), carbon uptake continues during tidal flooding in the lagoon but at reduced rates, as shown by the CO_2 uptake generally still measured at this period for the four deployments (Table 1). In addition, the decrease in CO_2 uptake during the day, along with the CO_2 degassing to the atmosphere at night (Fig. 5E) with the tide, can also result from physical processes, with the water column acting as a diffusion barrier against gas exchange between the water and the atmosphere (Houghton and Woodwell, 1980; Kathilankal et al., 2008). Other examples of physical processes driving CO_2 fluxes were discussed in Polsenaere et al. (submitted), i.e., at Station 1, in July 2008 on Day 184 (Fig. 4E), and also in the present study in September–October 2008 on Day 279 (Fig. 5E). In both periods, a strong CO_2 degassing to the atmosphere was measured at LT/Day. The singular CO_2 degassing, too high and rapid to be explained by biological respiration, could be attributed to destocking processes linked to the onset of atmospheric turbulence (high wind speeds) occurring on some days, particularly in the morning or in the midday, after calm atmospheric conditions.

4.2. Tidal flats and the CO_2 budget of the coastal zone

Several studies have focused on CO_2 exchange with the atmosphere over coastal areas and have highlighted the dynamic and heterogeneity of these systems. Using pCO2-based-flux calculations, benthic chambers or EC techniques, CO_2 budgets in various coastal environments have been reported. Concerning coastal wetlands, the study of Heilman et al. (1999), with a conditional sampling technique, reported carbon exchanges between a freshwater marsh in Texas (United States) and the atmosphere, from -1.9 to 1.7 g C m^{-2} day^{-1}. Using the EC method over a freshwater marsh dominated by *Typha latifolia* L. in California (United States), Rocha and Goulden (2008) reported a carbon release of 0.4 g C m^{-2} day^{-1} averaged over five years of measurement between 1999 and 2003. In a salt marsh dominated by *Spartina alterniflora*, located on the eastern coast of Virginia (United States), Kathilankal et al. (2008) measured, using an EC system, a carbon assimilation of -0.7 g C m^{-2} day^{-1} averaged over the six months corresponding to the growing season. Houghton and Woodwell (1980) measured a net flow of carbon of -0.8 g C m^{-2} yr^{-1} from the atmosphere to the Flax Pond salt marsh, dominated by *Spartina alterniflora,* on the north shore of Long Island, New York (United States). Concerning tidal flats, Zemmelink et al. (2009) computed a carbon uptake from the atmosphere to an intertidal estuary of the Wadden Sea (Griend Island, Netherlands) of -1.9 g C m^{-2} day^{-1} averaged over 68 days of measurements during the spring period. Spilmont et al. (2006), using the benthic chamber technique, reported a low autotrophic carbon budget of -0.1 g C m^{-2} day^{-1} for the mudflat of the Seine estuary (English Channel, France). Finally, in the Bay of Somme (Eastern English Channel, France), Migné et al. (2004), using the same method, computed a heterotrophic carbon budget of 0.2 g C m^{-2} day^{-1} at maximum.

Because we do not have flux data for winter conditions, we will not attempt to provide a precise annual CO_2 budget for the Arcachon lagoon. However, the estimation given here takes into account the most productive seasons of the bay over three years, i.e., spring, summer and early autumn, as well as the spatial variations in CO_2 fluxes existing in the tidal flat, i.e., with measurements in two different stations. Thus, our data reveal that in spring, the lagoon represented a net sink of CO_2 of -2.5 g C m^{-2} day^{-1}, whereas in summer and early autumn, the lagoon either acted as a small source or sink of CO_2, with 0.1 and -0.2 ~ 0.8 g C m^{-2} day^{-1}, respectively. This carbon uptake is similar to or greater than those computed in the other tidal flats in France and in Netherlands (Migné et al., 2004; Spilmont et al., 2006; Zemmelink et al., 2009). Nevertheless, it remained low compared to other tidal systems, such as salt or freshwater marshes (Houghton and Woodwell, 1980; Rocha and Goulden, 2008) or temperate estuaries (Frankignoulle, 1998).

Even if annual fluxes of atmospheric CO_2 over lagoons are relatively weak, these latter remain sparsely characterised from a carbon budget perspective. In the last evaluation of carbon fluxes in the global ocean carried out by Laruelle et al. (2010), studies on carbon fluxes over lagoons account for only 10% of the global flux. However, the intertidal area represents 24% of the surface area of the estuarine environment surface. In addition, CO_2 fluxes in tidal flats and estuaries are greatly contrasting, with estuarine water emitting large amounts of CO_2, whereas the intertidal area absorbs CO_2 in small quantities. In consequence, separating tidal flats from the rest of estuarine systems would reduce the global CO_2 emission by near-shore estuarine environments computed by Laruelle et al. (2010).

Acknowledgments

This study was supported by the ANR project PROTIDAL coordinated by Pierre Anschutz and also by the Aquitaine region that has financed the EC system. We are grateful to Guillaume Detandt, Georges Oggian and Dominique Serça for their help for the EC deployment. We acknowledge the Kalideos teams for giving us access the satellite image database.

CHAPITRE IV.

SYNTHESE GENERALE ET PERSPECTIVES

IV. SYNTHESE GENERALE ET PERSPECTIVES

IV.1. Le budget de carbone de la lagune d'Arcachon : les apports de ce travail

Dans le contexte général d'une meilleure compréhension et quantification du cycle du carbone en zone côtière, ce travail s'est attaché au cas particulier des lagunes intertidales à l'interface terre-océan-atmosphère. Avec ses 60% de superficie intertidale, la lagune d'Arcachon, point de jonction entre les différents compartiments, benthique, pélagique et atmosphérique apparaît comme un site idéal. La figure 4.1 synthétise les différents flux de carbone quantifiés dans ce travail: les apports depuis le continent par les fleuves et les échanges printaniers et estivaux avec l'atmosphère en période d'immersion et d'émersion.

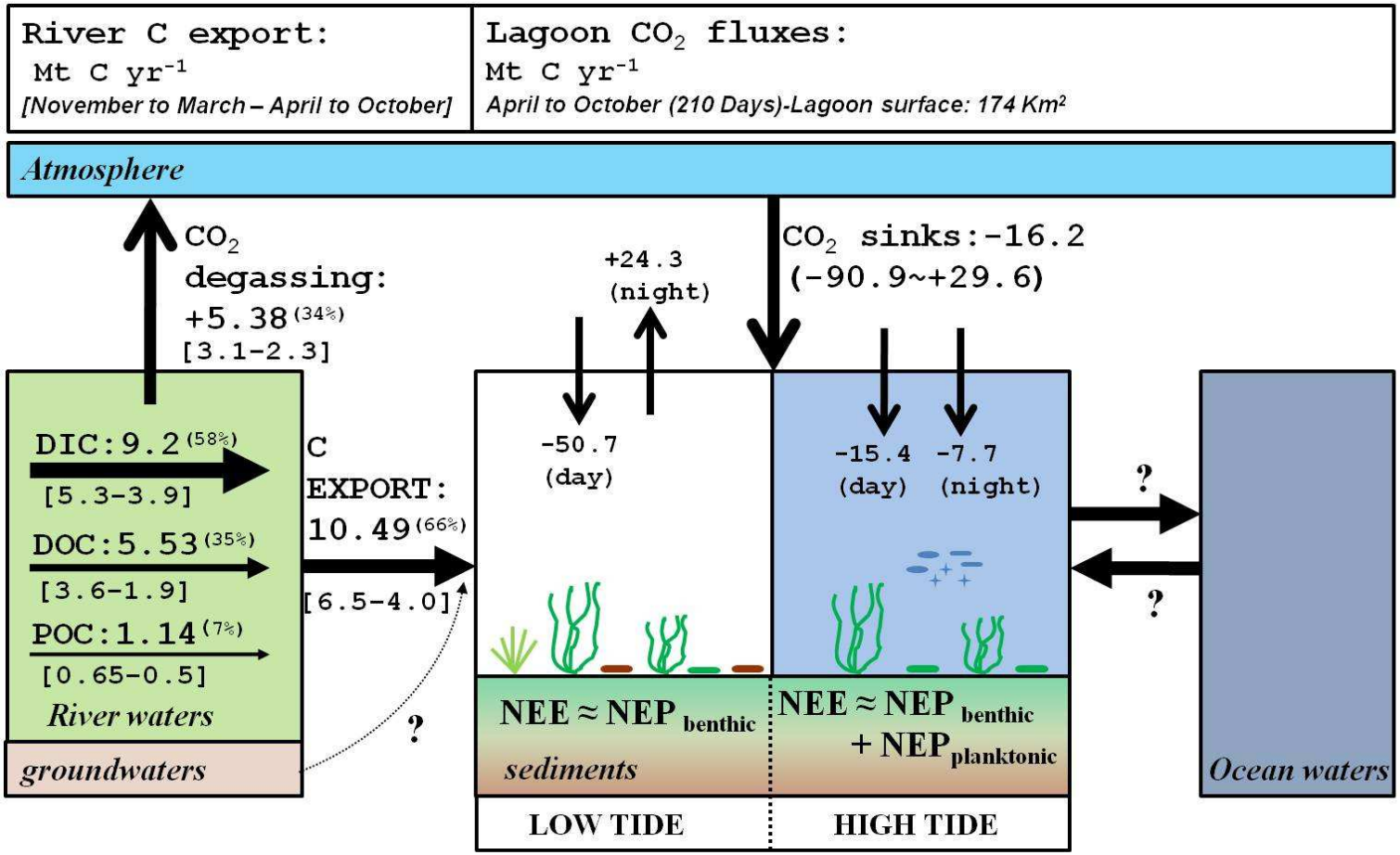

Figure 4.1. Estimation du budget de carbone de la lagune d'Arcachon. Les flux sont exprimés en milliers de tonnes de carbone par an (Mt C an^{-1}). Les apports par les rivières correspondent à un cycle hydrologique complet. Les chiffres indiqués correspondent au total annuel et aux deux périodes, hivernale (novembre 2008 - mars 2009) et estivale (mars-octobre 2009) ; les flux de CO_2 atmosphérique ont été obtenus à partir des mesures d'EC dans la lagune d'Arcachon sur la période d'avril à octobre (2007, 2008 et 2009) au cours des quatre déploiements. DIC: dissolved inorganic carbon; DOC: dissolved organic carbon; POC: particulate organic carbon; NEE: net ecosystem exchange and NEP: net ecosystem production.

IV.1.1. Les exports de carbone vers la lagune depuis les eaux de surface des rivières du bassin versant.

Notre suivi des rivières et ruisseaux est le premier travail focalisé sur les apports de carbone terrestre vers la lagune d'Arcachon. Ces dernières années, les travaux sur le bassin versant ont plutôt été centrés sur les nutriments azotés et phosphorés (Rimmelin et al., 1998 ; De Wit et al., 2001 ; Canton et al., 2010). Un important travail d'échantillonnage a permis d'étudier les dynamiques spatiales et saisonnières du carbone dans les eaux douces de rivière et d'en quantifier l'export de ses différentes formes à la lagune (Chapitre II). De plus, un modèle numérique (StreamCO_2-DEGAS) a permis d'évaluer la part du carbone dégazé sous forme de CO_2 depuis les eaux de surface, et n'atteignant jamais la lagune. Ce terme est largement significatif et représente 5.4 milliers de t C an^{-1}, soit 34% de l'export total (Figure 4.1). Ajouté à l'exportation vers la lagune estimée à 10.5 milliers de t C an^{-1} (soit 66%, Figure 4.1), il permet de quantifier la perte totale de carbone depuis le milieu terrestre vers le milieu aquatique, à savoir 15.9 milliers de t C an^{-1}. Quantifier cette perte est particulièrement utile pour boucler le bilan de carbone des écosystèmes terrestres, car elle constitue souvent une part significative de la quantité de carbone fixée sur terre. En effet, ramenée par unité de surface, la perte totale de carbone depuis le milieu terrestre vers le milieu aquatique est estimée dans cette étude à 115.5 g C m^{-2} an^{-1} (dégazage de CO_2 vers l'atmosphère : 49.8 g C m^{-2} an^{-1} et export total de carbone vers la lagune : 65.7 g C m^{-2} an^{-1}). Ce flux de carbone à travers le réseau hydrographique est très significatif si on le compare à la fixation de carbone par la forêt landaise (site EUROFLUX du Bray, 44°43'33.24″ N, 0°46'33.72″ W) estimée entre 57 g C m^{-2} an^{-1} (9.1 t C an^{-1}) en 2002 (Jarosz et al., 2008) et 575 g C m^{-2} an^{-1} (92 t C an^{-1}) en moyenne sur 1997 et 1998 (Berbigier et al., 2001)[12]. Il serait donc intéressant d'affiner le bilan de carbone de la forêt de pins maritimes couvrant le bassin versant en incluant nos données d'export de carbone à celles concernant les échanges de CO_2 entre les écosystèmes forestiers et l'atmosphère obtenus par l'équipe de l'INRA (Villenave d'Ornon). Nos données pourraient aussi alimenter un système d'information géographique pour mieux modéliser les flux d'eau et de carbone à l'échelle du bassin versant.

Par ailleurs, Il serait intéressant de préciser encore davantage la dynamique du carbone et particulièrement du CO_2 dissous, dans la zone de transition sol-nappe-rivière. Ceci permettrait

[12] La fixation de carbone par la forêt du Bray entre 1996 et 2006 est estimée à 3450 g C m^{-2} (INRA, Villenave d'Ornon)

de mieux contraindre l'état initial du modèle StreamCO_2-DEGAS et de le valider plus en détail. Un échantillonnage simultané d'eaux souterraines et des ruisseaux adjacents couplés à des mesures de pCO_2 et d'analyse de sols en deux ou trois points du bassin versant, permettrait de préciser les mécanismes de dégazage du CO_2 vers l'atmosphère. D'autre part, des mesures de respiration dans les sédiments et les eaux permettraient de mieux vérifier si cette composante est bien négligeable par rapport au transfert depuis les sols.

De par la stratégie d'échantillonnage adoptée et la formulation mathématique du dégazage de CO_2, une estimation la plus précise possible de l'export de carbone depuis le bassin versant vers la lagune d'Arcachon a été proposée. Cependant certains flux n'ont pu être caractérisés comme par exemple la contribution des eaux souterraines directement à la lagune (Figure 4.1). Du fait du très faible débit des nappes en comparaison des rivières, celle-ci est probablement négligeable comme c'est le cas pour l'azote (Rimmelin et al., 1998). L'apport total de carbone depuis les eaux de surface du bassin versant vers la lagune, estimé à 10.5 milliers de t C an^{-1} (sans le dégazage vers l'atmosphère, Figure 4.1), est très significatif, si on le compare par exemple à la production primaire nette des herbiers de *Zostera noltii* estimée entre 8.9 et 12.7 milliers de t C an^{-1} (Auby, 1991)[13]. Le devenir de ce matériel d'origine terrestre dans la lagune est inconnu et difficile à appréhender, du fait de la rapide dispersion et le mélange avec l'eau de mer en zone intertidale.

IV.1.2. Les échanges de CO_2 entre la lagune d'Arcachon et l'atmosphère

Une contribution majeure de ce travail concerne la mesure directe des flux verticaux de CO_2 entre la lagune et l'atmosphère, de manière continue à marée haute et à marée basse, et sa mise en relation avec la distribution de l'herbier de *Zostera noltii* (Chapitre III). Dans cet objectif, la technique de mesure de flux turbulents par Eddy Covariance (EC) a été appliquée pour la première fois dans ce type d'écosystème très dynamique et variable, cette dernière n'étant que très récemment et peu utilisée en zone côtière intertidale (Kanthilankal et al., 2008 ; Zemmelink et al., 2009). L'échange net de l'écosystème (NEE) a pu être ainsi caractérisé à un pas de temps court et à l'échelle de l'écosystème afin d'intégrer au maximum les variations spatio-temporelles d'une zone côtière hétérogène comme la lagune choisie pour ce travail.

[13] Les dernières estimations évaluent à la hausse la production nette des herbiers de *Zostera noltii* entre 45 et 75 milliers de t C an^{-1} (Auby, communication personnelle ; Ribando et al., en préparation).

Une première étape s'est centrée sur l'aspect méthodologique de la technique depuis son déploiement sur le terrain jusqu'à l'obtention de flux qualitatif et quantitatif (à l'aide de tests statistiques et d'analyse spectrale) et sa validation en zone intertidale. Sur la base des quatre sets de données obtenus dans cette étude, il semble qu'assez peu de données biaisées doivent être retirées, les critères de validité de la méthode étant respectés la plupart du temps. Ceci fût en particulier lié au choix d'une période d'intégration des flux de CO_2, de chaleurs sensible et latente et d'énergie, plus courte (10 min) que celle utilisée pour les écosystèmes terrestres (30 min), en adéquation avec la dynamique du rythme de la marée. Egalement, l'analyse spectrale a permis de mettre en évidence une bonne quantification de ces flux transportés dans l'atmosphère par les tourbillons de petite taille aux hautes fréquences grâce à un temps de scrutation des capteurs très élevé de 20 Hz. L'analyse a montré que, du fait des conditions d'instabilité atmosphérique prédominant dans la lagune, les flux transportés aux basses fréquences par les grands tourbillons étaient susceptibles d'être légèrement sous-estimés (d'environ 10%) lors des marées basses la journée, en particulier en Juillet 2008. Finalement, nous avons obtenu une bonne adéquation entre les flux de CO_2 et de chaleurs et les paramètres environnementaux et les contrôles biologiques, pour les quatre périodes caractéristiques. Ceci conforte les analyses mathématiques choisies et permet de valider la technique d'EC en zone intertidale.

La deuxième étape de ce travail a été d'étudier les échanges verticaux avec l'atmosphère, notamment les échanges de CO_2 (NEE) obtenus au cours des quatre situations caractéristiques (marée basse le jour, marée basse la nuit, marée haute le jour et marée haute la nuit) et de les mettre en relation avec l'ensemble de ces facteurs physiques et contrôles biologiques aux différentes échelles tidale, diurne, saisonnière et spatiale. Nos mesures ont concerné les périodes printanière, estivale et automnale (d'Avril à Octobre) grâce à quatre déploiements, ceux menés en hiver s'étant avérés trop difficiles d'un point de vue logistique. Les échanges verticaux de CO_2 avec l'atmosphère ont été caractérisés de manière continue avec la même technique sur trois saisons, trois ans et deux stations différentes. Il en ressort en moyenne un puits de CO_2 à marée basse le jour d'environ 51 milliers de t C an^{-1} quelque soit la saison, entre Avril et Octobre en relation avec l'activité photosynthétique des principaux producteurs primaires de la lagune (Figure 4.1). En particulier, les herbiers de *Zostera noltii* prédominent durant les mois d'été et d'automne à la Station 1 où l'herbier est bien développé alors que les communautés microphytbenthiques prédominent durant le mois d'Avril (printemps) à la

Station 1 où l'herbier commence seulement à pousser ainsi que durant le mois de septembre (été) à la Station 2 où l'herbier est très peu représenté. Une réponse différente de la photosynthèse à marée basse le jour entre les zones des herbiers et les zones de vase nue, a été observée. Quelque soit la saison et la station, les courbes NEE *vs* I sont en effet très différentes selon prédominance d'herbier de *Zostera noltii* (Juillet/Septembre 2008, Station 1) ou non (Avril 2009, Station 1 et Septembre 2007, Station 2). Les mesures de nuit à marée basse ont montré que la respiration benthique (CR) émettait vers l'atmosphère environ 24 milliers de t C an^{-1} (mesure effectuée à partir des données d'Avril à Octobre) en moyenne (Figure 4.1), le maximum étant mesuré à la station 2 en automne avec 103 milliers de t C an^{-1} où la vase nue et le microphytobenthos prédominent. A marée basse, des phénomènes de déstockage non biologique lié à la reprise de la turbulence, notamment à marée basse le jour, ont pu aussi être notés, augmentant les quantités de CO_2 émises à l'atmosphère (été-automne à la Station 1).

La mesure directe de flux de CO_2 pendant l'immersion a mis en évidence que l'eau agit comme une barrière diffusive réduisant les échanges, tant pour l'assimilation du CO_2 par les producteurs primaires le jour que pour le dégazage de CO_2 vers l'atmosphère la nuit. Des puits faibles de CO_2 ont été observés dans les deux situations le jour (Figure 4.1). En Avril 2009, à la Station 1, l'absorption de CO_2 par l'eau plus importante la nuit que le jour, a montré qu'il pouvait y avoir un décalage temporel entre l'activité photosynthétique et le pompage de CO_2. Dans le cas du bassin d'Arcachon, ce décalage est aussi spatial car la masse d'eau qui recouvre l'estran la nuit se trouve dans les passes le jour. Ce statut particulier dans ce dernier cas a pu s'expliquer par la lenteur des échanges verticaux de CO_2 avec l'atmosphère en comparaison avec la dynamique biologique pouvant générer des gradients de pCO_2 très rapides. Par conséquent, pendant l'immersion, le CO_2 est aussi importé ou exporté avec la marée sous forme dissoute.

Au final, ce travail a montré la dynamique extrême des flux de carbone en milieu intertidal, avec des flux qui changent fréquemment de signe en fonction de la marée et de l'ensoleillement. De plus, nous avons pu estimer que pendant la période printanière et estivale, la lagune se comporte comme un puits faible de CO_2 d'environ 16 milliers de t C, d'Avril à Octobre (Figure 4.1). Enfin, nos mesures supportent l'hypothèse d'une photosynthèse benthique principalement active le jour à marée basse, et qui alimente ensuite la respiration de la colonne d'eau à marée haute.

IV.1.3. Les flux métaboliques de la lagune d'Arcachon

Les données de flux de CO_2 atmosphérique mesurées dans la lagune d'Arcachon au cours des quatre cas caractéristiques ont permis d'apporter des précisions sur les flux métaboliques benthique et pélagique des trois principaux producteurs primaires de la lagune, i.e. les herbiers de *Zostera noltii*, les communautés microphytobenthiques et phytoplanctoniques. En particulier, concernant les flux benthiques, cette étude a mis clairement en évidence deux cycles métaboliques superposés fonctionnant à des échelles de temps différents ; (1) un cycle rapide du microphytobenthos à échelle de temps court de l'ordre de la marée ou de la semaine et s'accompagnant très probablement d'une exportation de carbone liée à des mises en suspension ; (2) un cycle plus lent de l'herbier, à échelle de temps annuel. Ces deux producteurs primaires ont alors des fonctions métaboliques, écologiques et trophiques différentes qui doivent être précisées.

Les données de marée basse et marée haute, le jour et la nuit, de Juillet et Septembre-Octobre 2008 mesurées à la Station 1 et de Septembre-Octobre 2007 à la Station 2 ont été utilisées pour calculer les différents termes de production benthique et pélagique (NCP, NPP, GPP) ainsi que ceux liés à la respiration (CR, AR, HR). Ces termes ont aussi été confrontés à ceux déjà existant dans la littérature et obtenus par d'autres méthodes. Les données d'Avril 2009 mesurées à la Station 1 n'ont pu être utilisées du fait d'un léger puits de CO_2 aussi à marée basse la nuit, probablement lié à des phénomènes de photo-acclimatation du microphytobenthos ou peut-être de dissolution de carbonates. Le Tableau 4.1 et la Figure 4.2 présentent et synthétisent les différents flux obtenus.

g C m^{-2} day^{-1} ($Mt\ C\ yr^{-1}$)	**Primary producers**	**NCP**	**NPP**	**GPP**	**CR**	**Methods**	**References**
LOW TIDE - BENTHIC METABOLISM	***Zostera noltii***		**0.34-0.49** (8.88-12.71)			**Biomasses** (Dry Weight)	**Auby**, 1991
		0.5		**1.22**	**0.72**	**Benthic chambers** CO_2 fluxes	**Davoult et al.** (unpublished data) from 2005 to 2007 (March, May and September)
		1.25		**1.86**	**0.61**	**Eddy Correlation** CO_2 fluxes	**this study** (Station 1, LT in July and September 2008)
	Microphytobenthos			**0.09-0.22** (4.93-12.27) **0.29-0.32** (16.13-17.62)		**Chlorophylle *a*** concentrations	**Auby**, 1991 **Auby** (unpublished data)
		1.31		**1.58**	**0.27**	**Benthic chambers** CO_2 fluxes	**Davoult et al.** (unpublished data) from 2005 to 2007 (in March, May and September)
		1.72		**4.55**	**2.83**	**Eddy Correlation** CO_2 fluxes	**this study** (Station 2, in September-October 2007)
HIGH TIDE - BENTHIC & PELAGIC METABOLISM	**Phytoplankton**		**0.25** (16.07)			^{14}**C** short incubations at incident light	**Glé et al.**, 2008 (year 2003)
		0.21		**0.98**	**0.78**	**Eddy Correlation** CO_2 fluxes	**this study** (Station 1, HT in July 2008)

Tableau 4.1. Estimation des principales composantes du métabolisme intertidal de la lagune d'Arcachon – synthèse et comparaisons des données obtenues dans la littérature et à partir de cette étude (en g C m^{-2} $jour^{-1}$ (Mt C an^{-1})) (voir aussi **Figure 4.1**). Limitations de chaque méthode dans les estimations de production : Biomasses (poids secs) : NPP apparente, méthode peu standardisée, sous-estimations possibles ; Chambres benthiques : variations spatiales (et temporelles) mal intégrées, sur- ou sous-estimations possibles ; Chlorophylle *a* : renouvellement des populations lié à la remise en suspension non pris en compte, sous-estimations; ^{14}C : GPP ou NPP suivant le temps d'incubations, mesures potentielles à la lumière incidente, surestimations possibles et EC : traitement de données, précision sur le footprint, exactitude et connaissances des flux mesurés, sur- ou sous-estimations. NCP: net community production; NPP: net primary production; GPP: gross primary production and CR: community respiration. Il en ressort des estimations très comparables entre les différentes études/méthodes pour les herbiers de *Zostera noltii* et les communautés phytoplanctoniques mais pas pour la GPP et la CR du compartiment microphytobenthique. Concernant ce dernier, la différence entre la GPP obtenue d'après Auby (1991, communication personnelle) et d'après cette étude (ou celle de Davoult et al., communication personnelle) est très probablement due à une exportation importante des communautés microphytobenthiques lors de l'immersion. Le terme de NCP, équivalent à celui de NEP, a plutôt été choisi ici, celui-ci se rapportant directement aux différentes communautés de producteurs primaires.

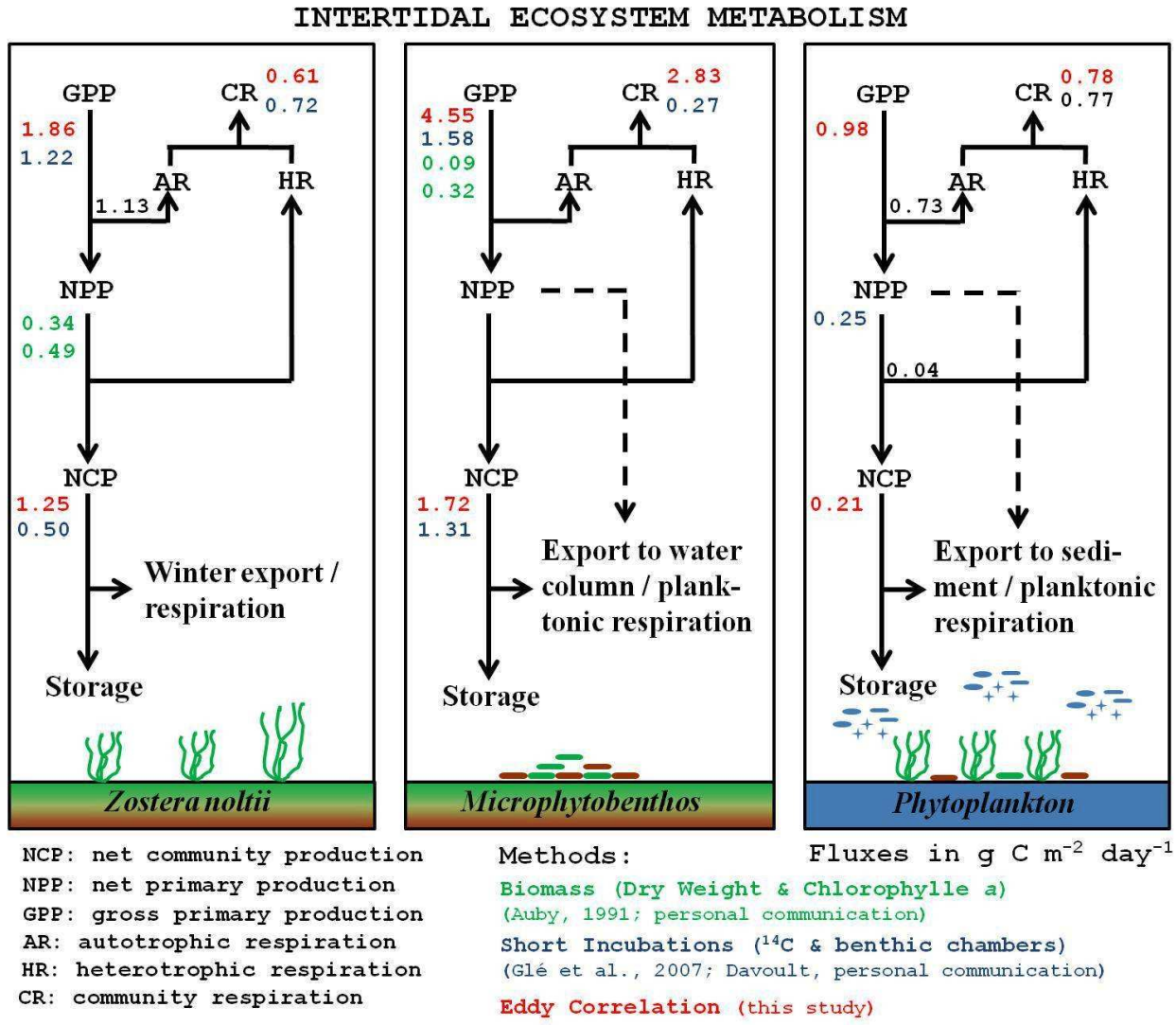

Figure 4.2. Estimation du métabolisme de l'écosystème intertidal de la lagune d'Arcachon en séparant les trois principaux producteurs primaires. Les flux sont exprimés en g C m^{-2} $jour^{-1}$. Les méthodes utilisées ainsi que les différentes estimations obtenues sont présentées dans le **Tableau 4.1**. Les chiffres en noir ont été déduits à partir des valeurs existantes, mesurées et/ou calculées (« residuals »).

Concernant les herbiers de *Zostera noltii*, les mesures d'EC menées en Juillet et Septembre-Octobre 2008 à la station 1 ont permis d'estimer la NCP (ou NEP) à marée basse à 1.25 g C m^{-2} $jour^{-1}$, en moyenne. Cette valeur, bien que plus élevée, reste comparable à celles obtenues par chambre benthique sur une station représentative de l'herbier de *Zostera noltii* dans la lagune avec 0.50 g C m^{-2} $jour^{-1}$, en moyenne (Davoult et al., communication personnelle) (Figure 4.2 et Tableau 4.1). Cette différence peut s'expliquer par les mesures de mars 2005 réalisées avec les chambres benthiques, donnant une NCP proche de 0.52 g C m^{-2} $jour^{-1}$, prenant ainsi en compte la période hivernale où l'herbier est très peu représenté. Une deuxième explication se trouve aussi dans les valeurs faibles de NCP obtenues en mai 2006 par les chambres, de l'ordre de 0.17 g C m^{-2} $jour^{-1}$ en moyenne, alors que l'herbier est déjà développé. Ces valeurs de NCP sont également comparables à celle donnée par Auby (1991) estimée entre 0.34 et 0.49 g C m^{-2} $jour^{-1}$, et basée sur des mesures de biomasses qui ne donnent cependant qu'une estimation de la NPP apparente[14]. En effet, les biomasses ne permettent pas d'estimer le terme de respiration et peuvent être associées à des erreurs dues à la consommation par les herbivores et surtout à la chute naturelle des feuilles (Garrigue, 1987). Enfin, les valeurs calculées de GPP et de CR à partir des mesures par chambres benthiques et EC révèlent des résultats très similaires de 1.22-1.86 et 0.72-0.61 g C m^{-2} $jour^{-1}$ respectivement (Figure 4.2 et Tableau 4.1).

Les flux métaboliques au sein du compartiment microphytobenthique, très mal documentés dans la lagune, montrent au contraire d'importantes différences entre les méthodes, en particulier sur l'estimation de la GPP (Tableau 4.1 et Figure 4.2). Les mesures d'EC en Septembre-Octobre 2007 à la Station 2 donnent une GPP estimée à 4.55 g C m^{-2} $jour^{-1}$, très largement supérieure à celle estimée par Auby (1991 ; communication personnelle) entre 0.09 et 0.32 g C m^{-2} $jour^{-1}$, à partir de biomasses moyennes en mg Chl *a* m^{-2} an^{-1} (de Jong et al., 1994). Il est en effet très approximatif de calculer des productions à partir de biomasses microphytobenthiques car celles-ci ne rendent pas compte du renouvellement des populations lié à la remise en suspension des sédiments de surface, cette dernière étant très difficile à appréhender (Guarini, 1998). Ces différences entre ces deux estimations de la GPP microphytobenthique suggèrent un export important et rapide de ces communautés vers la colonne d'eau pouvant alimenter la respiration planctonique ou encore contribuer à la production primaire planctonique pélagique (Guarini, 1998). Egalement, bien que les mesures par EC en Station 2 et par chambres benthiques sur des vases nues conduisent à des NCP similaires de 1.72 et 1.31 g C m^{-2} $jour^{-1}$ respectivement, une différence d'un facteur proche

[14] Les dernières valeurs de NCP estimées par des mesures de marquage sur les herbiers, entre 0.2 et 1.5 g C m^{-2} $jour^{-1}$ (Ribando et al. (en préparation), sont encore plus cohérentes avec les valeurs mesurées par Eddy Covariance dans cette étude.

de 3 est observée entre les valeurs de GPP, celle-ci étant liée surtout au terme de CR, qui semble très différent entre les chambres et la technique d'EC à la même station (Tableau 4.1 et Figure 4.2).

Finalement, en ce qui concerne les flux métaboliques à la fois pélagique et benthique à marée haute, cette étude permet d'apporter là aussi des précisions en particulier sur le compartiment phytoplanctonique dans le bassin d'Arcachon. Les mesures d'EC menées en Juillet 2008 à marée haute à la Station 1 donnent une NCP totale (pélagique et benthique) estimée à 0.21 g C m^{-2} $jour^{-1}$ ainsi qu'une GPP et une CR de 0.98 et 0.78 g C m^{-2} $jour^{-1}$ respectivement (Tableau 4.1 et Figure 4.2). Cette NCP est relativement proche de la NPP phytoplanctonique estimée par Glé et al. (2008) à hauteur de 0.25 g C m^{-2} $jour^{-1}$. Cette dernière estimation basée sur la mesure du taux d'assimilation du ^{14}C au bout de 24 heures environ, peut être affectée par certains biais, d'abord parce qu'elle fait l'hypothèse d'une NPP homogène à marée haute et à marée basse dans les chenaux, et que la lumière disponible *in situ* est la même que celle dans le microcosme où ont été faites les incubations. Ensuite, la mesure d'assimilation du ^{14}C se situe plutôt entre la GPP et la NPP (Marra, 2009). Enfin, la NCP obtenue par EC est très dépendante des processus d'advection des masses d'eau avec la marée et de délai d'équilibration du CO_2 entre l'air et l'eau. De plus, elle intègre aussi la production benthique, même si l'on suppose que la lumière est fortement atténuée pendant l'immersion. Enfin, le terme de respiration planctonique reste très approximatif, du fait du manque de mesures dans l'eau du bassin d'Arcachon.

Si les herbiers de *Zostera noltii* sont maintenant suivis depuis un certain nombre d'années dans la lagune, notamment par des mesures annuelles de biomasses sur le terrain et des cartographies réalisées à partir de photographies aériennes ou plus récemment par des estimations de densités de couvert à partir d'images satellites (Auby, 1991 ; Auby and Labourg, 1996 ; Auby et al., 2009 ; Plus et al., 2010 ; Lafon, communication personnelle), il n'en va pas de même des communautés microphytobenthiques. Et pourtant celles-ci jouent un rôle majeure dans la NCP benthique des écosystèmes intertidaux (Migné et al., 2002 ; Migné et al., 2004, Hubas et al., 2006) en particulier de la lagune d'Arcachon (Auby, 1991). Il pourrait être envisagé davantage de mesures, notamment une étude spatio-temporelle des flux par EC en parallèle de chambres benthiques, d'analyse de biomasse chlorophyllienne dans les sédiments, et de mesures de respiration benthique et planctonique (cf. différence entre les CR estimées par chambres benthiques et par EC). Ceci permettrait de connaître leur dynamique de production au même titre que celle des herbiers ou encore des populations phytoplanctoniques. Il serait alors possible grâce à des mesures simultanées par chambres benthiques et par EC (1) d'affiner les relations entre flux de CO_2 et

dynamique et contribution des différents compartiments à la NCP et (2) de comparer les deux techniques afin de mieux quantifier et qualifier les flux mesurés. Les mesures simultanées de flux par EC et chambres benthiques ont été réalisées dans la lagune d'Arcachon lors du dernier chantier PNEC en septembre-octobre 2007 mais mériteraient d'être poussées plus loin. Enfin, afin de préciser les termes de NCP, GPP et CR benthiques pendant l'immersion, il serait intéressant de coupler aux mesures de flux de CO_2 atmosphérique par EC, des mesures de flux d'O_2 par Eddy Covariance sous-marine à l'interface eau-sédiment (Berg et al., 2003). Un projet de post-doctorat financé en partie par l'équipe ECOBIOC permettra de mettre en place très prochainement cette méthode dans la lagune d'Arcachon afin d'obtenir des flux quantitatifs et qualitatifs d'oxygène à cette interface sur des superficies de l'ordre d'une dizaine de mètres carrés, et qui pourront être comparés aux flux eau-air obtenue par notre méthode atmosphérique.

IV.2. Les inconnues subsistant dans le cycle du carbone de la lagune d'Arcachon

Les résultats obtenus par ce travail de thèse permettent de mettre aussi en évidence un certain nombre d'inconnues qui subsistent dans notre compréhension du cycle de carbone en zone intertidale. Il est en effet nécessaire d'approfondir nos connaissances de certains flux métaboliques et trophiques, afin de proposer un modèle de fonctionnement écologique et biogéochimique du bassin d'Arcachon.

IV.2.1. Les échanges atmosphériques hivernaux et le devenir de la biomasse de l'herbier

Les mesures de flux de CO_2 par EC n'ont été réalisées que durant les saisons printanière, estivale et début automnale (d'Avril à Octobre). L'intensité et la direction des flux en période hivernale restent en réalité inconnues. Puisque nos mesures se situent dans la période principale de croissance de l'herbier de zostère, nous devons nous interroger sur le devenir de ce matériel en période hivernale (Figure 4.2). En effet, durant cette saison (fin automne-hiver), la biomasse foliaire de l'herbier de *Zostera noltii* diminue alors que le rhizome et les racines persistent dans les premiers centimètres de sédiment jusqu'à la reprise de croissance principale au cours du printemps et de l'été (Auby and Labourg, 1996). Les populations hivernantes de Bernaches cravant et de cygnes, seules consommatrices significatives de *Zostera noltii* dans la lagune, ne broutent pas plus de 2% de la production annuelle totale des herbiers (Auby, 1991 ; Auby et al., 2009). Les herbiers peuvent aussi être directement consommés à l'intérieur de la lagune par certains invertébrés

comme l'isopode *Idotea chelipes* abondant dans le bassin mais cette consommation reste limitée (Auby and Labourg, 1996). Si une partie de ce matériel (production épigée surtout), difficilement quantifiable, est exportée depuis la lagune vers l'océan, où des feuilles de *Zostera noltii* ont pu être retrouvées à l'entrée de la lagune ou sur les plages environnantes, la majorité de ce matériel végétal est probablement recyclé ou stocké à l'intérieur de la lagune (Auby and Labourg, 1996). Les feuilles de *Zostera noltii* peuvent soit être entraînées par les courants et se retrouver dans tous les milieux de la lagune plus ou moins fractionnées, soit s'accumuler dans les sédiments de l'herbier (Auby, 1991). Une expérience *in situ*, menée en période estivale par Auby (1991), a montré que la décomposition de ce matériel végétal est plus rapide à l'intérieur du sédiment anoxique de l'herbier, grâce à la présence de bactéries sulfato-réductrices, qu'en situation intertidale lorsque les feuilles sont entrainées par les courants et alternativement déposées sur les estrans et reprises par la marée. Ainsi, des dégazages de CO_2 vers l'atmosphère pourraient se produire à marée basse et conduire à un statut hétérotrophe de la lagune en hiver. Cette même expérience, réalisée en période hivernale, à des températures basses, permettrait de valider cette hypothèse.

Les études isotopiques des détritus de phanérogame dans les échelons trophiques supérieurs des systèmes côtiers et précisément de la lagune (Thayer et al., 1978, Dang et al., 2009), indiquent que la majeure partie de la matière organique des herbiers serait plutôt dégradée très lentement et stockée dans les sédiments du bassin. Il a par exemple été montré que les sédiments de la lagune sont composés à 24 ± 7% de zostères dégradées (feuilles) au tout début du printemps (Avril), lorsque l'herbier est encore très peu développé, ce qui suggère un stockage et une accumulation dans les sédiments (Dubois, communication personnelle). De plus, Duarte et Cebrián (1996) ont montré qu'en général une large fraction (81.4% en moyenne) de la production de phanérogames marines n'était pas consommée par les organismes herbivores. Les tissus de zostère, ayant des rapports C:N:P forts, sont en effet considérés comme réfractaires et se décomposent très lentement (Duarte et al., 2010). Une fraction significative de la GPP de ces herbiers pourrait donc ne pas être utilisée par les hétérotrophes tendant à rendre ce type d'écosystème autotrophe et puits de CO_2 (Duarte and Cebrián ; Gattuso et al., 1998). Ceci mérite d'être confirmé par des mesures d'EC en hiver, pour vérifier si la dégradation du matériel issu de l'herbier ne génère pas de fort dégazage de CO_2 vers l'atmosphère. Les NEP faibles mais positives mesurées par chambres benthiques en présence d'herbiers dans la baie de Morlaix (entre 0.46 et 1.8 g C m^{-2} $jour^{-1}$ pendant un cycle annuel complet, Ouisse et al., 2010) ainsi que celles mesurées dans la lagune d'Arcachon en Mars 2005 (proches de 0.52 g C m^{-2} $jour^{-1}$, Davoult et al., communication personnelle) suggère en effet que les dégazages hivernaux sont modestes et que la lagune pourrait être nette autotrophe.

La mise en place de mesures automatisées de flux par EC atmosphérique (CO_2) et sous marine (O_2) permettrait de préciser l'importance relative des productions planctonique et benthique et de la production benthique en phase immergée et émergée. Pour cela, la mise en place d'une station pérenne alimentée par énergie solaire et où seraient mesurées continuellement les flux métaboliques et les paramètres physiques et physico-chimiques de l'eau serait d'une grande utilité. Un tel outil permettrait d'affiner le budget de carbone de la lagune et de caractériser son comportement puits ou source de carbone vis-à-vis de l'atmosphère aux différentes échelles tidales, saisonnières et annuelles, grâce aux séries temporelles obtenues. L'avantage des mesures réalisées ainsi lors de cette étude a été de prendre en compte dans un premier temps la variabilité spatiale des flux et surtout de vérifier et de contrôler les aspects qualitatif et quantitatif des mesures sur des périodes ponctuelles permettant de le faire. Le succès de cette étude incite à continuer vers davantage d'instrumentation *in situ*, qui permettra d'accéder aux divers compartiments du métabolisme de l'écosystème.

IV.2.2. Problématique liée à l'évolution à long terme de l'herbier de *Zostera noltii*

Le bassin d'Arcachon contient le plus grand herbier d'Europe de Zostère naine, qui couvre 60% de sa zone intertidale. Cependant une étude récente a montré que la surface des herbiers à Zostère tendait à diminuer et de manière accélérée depuis ces dernières années. Plus et al. (2010) ont montré que depuis 20 ans (1988-2008) l'espace occupé par les herbiers de *Zostera noltii* et de *Zostera marina* avait régressé respectivement de 33 et 74% soit une baisse estimée à 22.8 et 2.7 km^2, en accélération depuis 2005 pour *Zostera noltii*. Les raisons de cette régression sont encore mal comprises. Aucun signe de changement environnemental ne peut pour le moment expliquer cette régression. Cependant, certaines hypothèses ont été avancées comme les activités de dragage dans la lagune augmentant les matières en suspension et limitant la pénétration de la lumière dans la colonne d'eau ; la présence du protiste pathogène *Labyrinthula zosterae* qui fut responsable dans les années 1930 de la quasi-disparition des herbiers du bassin ; la présence de molécules herbicides liée aux activités agricole, urbaine ou nautique.

Les raisons expliquant cette régression peuvent en effet être multiples mais témoignent toutes globalement d'une tendance à l'instabilité et à la vulnérabilité du bassin d'Arcachon. Il a aussi été montré que cette régression ne s'effectuait pas de manière uniforme dans toute la lagune, le secteur Est étant davantage touché que les parties Ouest et Nord (Auby et al., 2009 ; Plus et al., 2010). Dans ce contexte et à la vue des premiers résultats obtenus entre flux verticaux de CO_2

mesurés et couvertures des herbiers par images satellites, il serait envisageable de suivre, en particulier aux échelles saisonnière et annuelle, ces populations ainsi que les processus impliqués dans cette évolution à long terme dans le bassin d'Arcachon. L'étude couplée image satellite/EC en simultané sur trois déploiements a permis de clairement discriminer la présence ou non de l'herbier de *Zostera noltii* suivant la station étudiée dans le bassin. Ainsi, toute variation saisonnière ou interannuelle, de couvert d'herbier se répercuterait sur l'intensité et la direction des flux verticaux de CO_2 mesurés par EC, ainsi que sur l'allure des courbes P/I. Il deviendrait alors possible d'identifier très précisément dans le temps, les périodes (semaines) de croissance maximales de l'herbier et à quelles conditions environnementales elles correspondent.

IV.2.3. La respiration planctonique dans la lagune d'Arcachon

Nous avons vu que la respiration planctonique dans la lagune d'Arcachon est très mal connue du fait de l'absence de mesure. En particulier, le couplage entre les processus benthiques et pélagiques reste à préciser. Celui-ci se caractérise par la remise en suspension et l'exsudation du microphytobenthos à marée montante, ce qui alimente la respiration de la colonne d'eau. Néanmoins, ce processus est probablement très hétérogène temporellement et spatialement et donc difficile à quantifier. Des mesures de respiration (par la méthode Winkler) à différentes phases de la marée devraient être envisagées pour combler ce manque. En effet, l'évolution de la pCO_2 dans l'eau mesurée en Mai 2006 avec un équilibrateur pendant 24h dans un chenal situé au fond de la lagune, a clairement permis de montrer ce couplage benthos-pelagos (Figure 4.3).

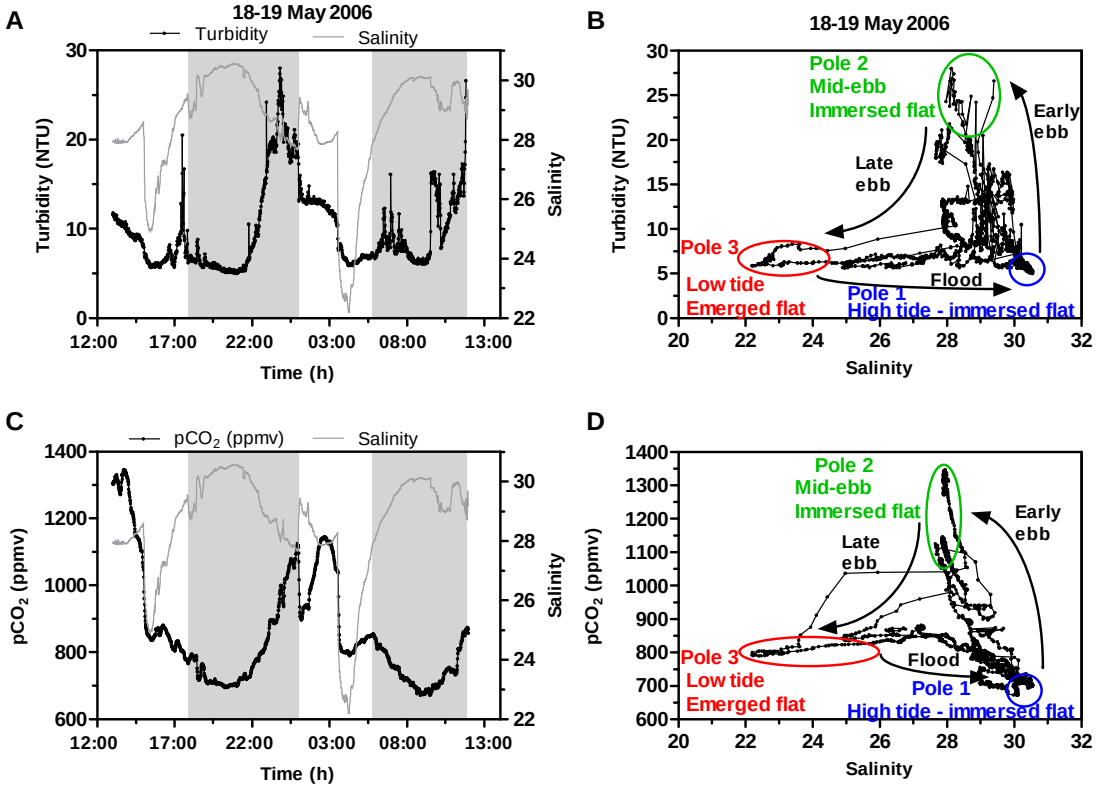

Figure 4.3. A et C: Evolution de la salinité, de la turbidité et de la pCO_2 dans un chenal du fond du bassin d'Arcachon (en face de Cassy) au cours de 24 heures (deux cycles de marée) réalisé en Mai 2006. Les bandes blanches indiquent que l'estran est découvert et les bandes noires qu'il est recouvert par la marée. B et D: Relation turbidité / salinité et pCO_2 / salinité au cours du même cycle (Abril, communication personnelle).

A ce moment, la pCO_2 se distribuait selon un mélange de 3 pôles (Figure 4.3.D): (1) des eaux "marines" de plus forte salinité et dominantes à marée haute, peu turbides et avec une pCO_2 de l'ordre de 700 ppmv ; (2) des eaux "intermédiaires" de salinité de l'ordre de 28 et très enrichies en matières en suspension (MES) (Figure 4.3.B) et en CO_2, présentes à mi-marée de jusant lorsque l'estran est encore recouvert ; (3) des eaux "de chenal", plus dessalées et influencées par les apports d'eau douce (ici la rivière Renet), dominantes à marée basse, lorsque l'estran est découvert depuis plus d'une heure. Ces données suggèrent que le sédiment de l'estran intertidal est source de carbone pour les masses d'eau qui viennent le recouvrir. Les données obtenues par EC au cours de cette étude permettent de valider cette interprétation pour la zone interne du bassin : en Septembre-Octobre 2007 à la Station 2 (proche du chenal dans lequel ce cycle de 24 heures a été réalisé en 2006), nous avons pu observer un puits significatif à marée basse la journée assuré par l'activité photosynthétique microphytobenthique, la lagune passant alors, à marée montante (après environ 50 cm d'eau), à un statut net source de CO_2 vers l'atmosphère (Chapitre II, Partie 2). Ces résultats permettent de proposer un schéma conceptuel de fonctionnement de l'écosystème basé sur une production primaire très importante à marée basse (microphytobenthos) lorsque la lumière est la plus disponible, puis sur un transfert vers la colonne d'eau soit sous forme de CO_2 produit de la respiration benthique, soit sous forme de matière organique (exsudats de microphytobenthos) qui est ensuite minéralisée par les organismes hétérotrophes dans la colonne d'eau. Dans un tel schéma de couplage benthos-pélagos, le sédiment serait autotrophe et la colonne d'eau hétérotrophe. Il ne semble pas cependant qu'il soit prédominant dans la zone plus centrale du bassin en été, où nous avons observé de flux de CO_2 négatifs même pendant l'immersion

IV.2.4. Dynamique des masses d'eaux de la lagune et échanges avec l'océan

Pour fermer le bilan de carbone de la lagune il serait aussi nécessaire de quantifier les échanges avec l'océan. Pour cela une étude détaillée de la distribution du CO_2 et des autres formes du carbone dans les eaux du bassin, en fonction des composantes hydrodynamiques de ce système serait très intéressante. Les mesures de flux verticaux de CO_2 par EC pourraient être couplées avec des acquisitions de pCO_2 (équilibrateur) dans les eaux de la lagune à différents points et pas de temps afin (1) de caractériser l'hétérogénéité spatiale et temporelle des masses d'eau d'un point de vue du carbone (2) de préciser l'influence des facteurs environnementaux, physique et biologique sur les pCO_2 des eaux de la lagune et les échanges avec l'atmosphère (3) de mieux comprendre les relations entre flux et gradients de pCO_2 en relation avec les processus physiques tels que le temps de résidence, la stratification ou le mélange des masses d'eau et la NEP et (4) d'estimer les

vitesses de transfert gazeux K_{600} dans le bassin, vitesse sujette à de très grandes incertitudes et très dépendante des caractéristiques du site de mesure. Il serait ensuite possible de coupler un modèle hydrodynamique tel que MARS (Plus et al., 2007 ; 2008) avec un module biogéochimique afin de reproduire ces observations. Les calculs de volumes oscillants, de flux résiduels aux frontières de la lagune ou encore de temps de renouvellement des masses d'eau, en relation avec les forçages physiques tel que le vent ou l'impact des rivières permettraient de quantifier les quantités de carbone entrant ou sortant au cours d'un cycle de marée. Par ailleurs, des cycles de mesure au niveau des passes pourraient être envisagés afin de mieux contraindre les échanges avec les masses d'eau océanique.

REFERENCES BIBLIOGRAPHIQUES

REFERENCES BIBLIOGRAPHIQUES

A, B, C

Abril, G., Etcheber, H., Borges, A.V. and Frankignoulle, M.: Excess atmospheric carbon dioxide transported by rivers into the Scheldt estuary, Comptes Rendus de l'Académie des Sciences Série II Fascicule A- Sciences de la Terre et des Planètes, 330(11), 761-768, 2000.

Abril, G., Nogueira, M., Etcheber, H., Cabeçadas, G., Lemaire, E. and Brogueira, M.J. : Behaviour of organic carbon in nine contrasting European estuaries, Estuarine, Coastal and Shelf Science 54, 241-262, 2002.

Abril, G., Etcheber, H., Delille, B., Frankignoulle, M. and Borges, A.V.: Carbonate dissolution in the turbid and eutrophic Loire estuary. Marine Ecology, Progress Series. 259, 129-138, 2003.

Abril, G., Commarieu M.-V., Sottolichio, A., Bretel, P. and Guérin, F.: Turbidity limits gas exchange in a large macrotidal estuary, Estuarine, Coastal and Shelf Science, 83, 342-348, 2009.

Abril, G.: Comment on: "Underwater measurements of carbon dioxide evolution in marine plant communities: A new method" by J. Silva et al. Estuarine, Coastal and Shelf Science, 82, 357-360, 2009.

Admiraal, W.: The ecology of estuarine sediment-inhabitant diatoms, in: Progress in Physiological Research, Round F.E., Chapman D.J. (ed.), 3, 269-322, 1984.

Ågren, A., Jansson, M., Ivarsson, H., Bishop, K. and Seibert, J.: Seasonal and runoff-related changes in total organic carbon concentrations in the River Öre, Northern Sweden, Aquat. Sci., 70, 21-29, 2007.

Aitkenhead, J.A., Hope, D. and Billett, M.F.: The relationship between dissolved organic carbon in stream water and soil organic carbon pools at different spatial scales, Hydrol. Process., 13, 1289-1302, 1999.

Aitkenhead, J.A. and McDowell, W.H.: Soil C:N ratio as a predictor of annual riverine DOC flux at local and global scales, Glob. Biogeochem. Cycles, 14, 127-138, 2000.

Amanieu, M.: Recherches écologiques sur la faune des plages abritées et des étangs saumâtres de la région d'Arcachon, PhD Thesis, Université Bordeaux 1, 1-234, 1967.

Amiotte-Suchet, P., Aubert, D., Probst, J.L., Gauthier-Lafaye, F., Probst, A., Andreux, F. and Viville, D.: $\delta^{13}C$ pattern of dissolved inorganic carbon in a small granitic catchment: the strengbach case study (Vosges mountains, France), Chemical Geology, 159, 129-145, 1999.

Amundson, R.G. and Davidson, E.A.: Carbon dioxide and nitrogenous gases in the soil atmosphere, J. Geochem. Explor., 38, 13-41, 1990.

Amundson, R., Stern, L., Baisden, T. and Wang, Y.: The isotopic composition of soil and soil-respired CO_2, Geoderma, 82, 83-114, 1999.

Anderson, D.E. et al.: Estimating lake-atmosphere CO_2 exchange, Limnology and Oceanography, 44, 988-1001, 1999.

Atekwana, E.A. and Krishnamurthy, R.V.: Seasonal variations of dissolved inorganic carbon and $\delta^{13}C$ of surface water: application of a modified gas evolution technique, Jour. of Hydrol., 205, 265-278, 1998.

Aubinet, M. et al.: Estimates of the annual net carbon and water exchange of forests: the EUROFLUX methodology, Advances in ecological research, 30, 115-175, 2000.

Auby, I.: Contribution à l'étude des herbiers de *Zostera noltii* dans le bassin d'Arcachon, thèse de doctorat, Université Bordeaux 1, 234 p., 1991.

Auby, I., Manaud, F., Maurer, D. and Trut, G. *:* Etude de la prolifération des algues vertes dans le bassin d'Arcachon, Rapport IFREMER - CEMAGREF - SSA - SABARC, 1-163, 1994.

Auby, I. and P.J. Labourg: Seasonal dynamics of Zostera noltii Hornem in Bay of Arcachon (France), Journal of Sea Research, 35, 269-277, 1996.

Auby, I., Trut, G., Plus, M. and Vignon, A.: Suivi stationnel des herbiers de zostères (*Zostera noltii* et *Zostera marina*) de la Masse d'eau côtière FRFC06 -Arcachon amont-District Hydrographique Adour-Garonne- 2007, Ifremer, RST /LER/AR/09-001, 1-40, 2009.

Aucour, A.M., Sheppard, S.M.F., Guyomar, O. And Wattelet, J.: Use of ^{13}C to trace origin and cycling of inorganic carbon in the Rhône river system, Chem. Geol., 159, 87-105, 1999.

Baldocchi, D.D., Hincks, B.B. and Meyers T.P.: Measuring biosphere-atmosphere exchanges of biologically related gases with micrometeorological methods, Ecology, 5, 1331-1340, 1988.

Baldocchi, D.D.: Assessing the eddy covariance technique for evaluating carbon dioxide exchange rates of ecosystems: past, present and future, Global Change Biology, 9, 479-492, 2003.

Barillé, L., Robin, M., Harin, N., Bargain, A. and Launeau, P.: Increase in seagrass distribution at Bourgneuf Bay (France) detected by spatial remote sensing, Aquatic Botany, 92, 185-194, 2010.

Barnola, J.M., Anklin, M., Porcheron, J., Raynaud, D., Schwander, J. and Stauffer, B.: CO_2 evolution during the last millennium as recorded by Antarctic and Greenland ice, Tellus Series B-Chemical and Physical Meteorology, 47, 264-272, 1995.

Barrón, C., Duarte, C.M., Frankignoulle, M. and Borges A. V.: Organic carbon metabolism and carbonate dynamics in a Mediterranean seagrass (*Posidonia oceanica*) meadow, Estuaries and Coasts, 29, 417-426, 2006.

Barth, J.A.C., Cronin, A.A., Dunlop, J. and Kalin, R.M.: Influence of carbonates on the riverine carbon cycle in an anthropogenically dominated catchment basin: evidence from major elements and stable carbon isotopes in the Lagan River N Ireland, Chemical Geology 200, 203-216, 2003.

Battin, T.J., Kaplan, L.A., Findlay, S., Hopkinson, C.S., Marti, E., Packman, A.I., Newbold, J.D. and Sabater, F.: Biophysical controls on organic carbon fluxes in fluvial networks, Nature Geoscience, 1, 95-100, 2008.

Beauvais, S.: Etude des Particules Exopolymériques Transparentes (TEP) en milieu marin. Dynamique et rôle dans le cycle du Carbone, Thèsede doctorat, Université Paris VI, 256pp., 2003.

Berbigier, P., Bonnefond, J. M., and Mellmann, P.: CO_2 and water vapour fluxes for 2 years above Euroflux forest site, Agr. Forest. Meteorol., 108, 183–197, 2001.

Berg, P., Roy, H., Janssen, F., Meyer, V., Jorgensen, B., Huettel, M. and de Beer, D.: Oxygen uptake by aquatic sediments measured with a novel non-invasive eddy-correlation technique, Mar. Ecol. Prog. Ser. 261: 75-83, 2003.

Bianchi, T.S, Filley, T., Dria, K. and Hatcher, P.G.: Temporal variability in sources of dissolved organic carbon in the lower Mississippi river, Geochimica et Cosmochimica Acta, 5, 959-967, 2004.

Billett, M.F., Palmer, S.M., Hope, D., Deacon, C., Storeton-West, R., Hargreaves, K.J., Flechard, C. and Fowler, D.: Linking land-atmosphere-stream carbon fluxes. Global Biogeo. Cycles, 18, gb1024, doi:10.1029/2003 gb002058, 2004.

Billett, M.F., Deacon, C.M., Palmer, S.M., Dawson, J.J.C. and Hope, D.: Connecting organic carbon in stream water and soils in a peatland catchment. J. of Geophys. Resear., 111, 1-13, 2006.

Billett, M.F. and Moore, T.R.: Supersaturation and evasion of CO_2 and CH_4 in surface waters at Mer Bleue peatland, Canada, Hydrological Processes, 22, 2044-2054, 2008.

Blanchard, G.F. and Cariou-Le Gall, V.: Photosynthetic characteristics of microphytobenthos in Marennes-Oléron Bay, France: preliminary results, J. Exp. Mar. Biol. Ecol., 182, 1-14, 1994.

Blanchard, G.F., Guarini, J.M., Orvain, F. and Sauriau, P.G.: Dynamic behaviour of benthic microalgal biomassin intertidal mudflats, Journal of Experimental Marine Biology and Ecology, 264, 85-100, 2001.

Blanchard, G.F., Guarini, J.M., Dang, C. and Richard, P.: Characterizing and quantify photoinhibition in intertidal microphytobenthos, Journal of Phycology, 40, 692-696, 2004.

Blanchet, H.: Structure et fonctionnement des peuplements benthiques du bassin d'Arcachon, thèse de doctorat, Université Bordeaux 1, 226 p, 2004.

Blanchet, H, de Montaudouin, X., Lucas, A., and Chardy, P.: Heterogeneity of macrozoobenthic assemblages within a *Zostera noltii* seagrass bed: diversity, abundance, biomass and structurine factors, Estuarine, Coastal and Shelf Science, 61, 111-123, 2004.

Bordovskiy, O.K.: Acumulation and transformation of organic substance in marine sediments, Marine Geology, 3, 5-114, 1965.

Borges, A.V.: Do we have enough pieces of the jigsaw to integrate CO_2 fluxes in the coastal ocean?, Estuaries, 28, 3-27, 2005.

Borges, A.V., Delille, B. and Frankignoulle, M.: Budgeting sinks and sources of CO_2 in the coastal ocean: diversity of ecosystems counts, Geophysical Research Letters, 32, LI4601, 2005.

Borges, A.V., Schiettecatte, L.-S., Abril, G., Delille, B. and Gazeau, F.: Carbon dioxide in European coastal waters, Estuarine, Coastal and Self Science, 70, 375-387, 2006.

Borges, A.V., Delille, B., Schiettecatte, L.S., Gazeau, F., Abril, G. and Frankignoulle, M.: Gas transfer velocities of CO_2 in three european estuaries (Randers fjord, Scheldt and Thames), Limno. and Oceanogra., 49(5), 1630-1641, 2004.

Borges, A. V., Djenidi, S., Lacroix, G., Théate, J., Delille, B. and Frankignoulle M.: Atmospheric CO_2 flux from mangrove surrounding waters, Geophys. Res. Lett., 30(11), 1558, doi:10.1029/2003GL017143, 2003.

Borges, A.V., and Abril, G.: Carbon dioxide and methane dynamics in estuaries, In Treatise on Coastal and Estuarine Science, Volume 8 – Biogeochemistry, Elsevier, 2012.

Boucher, J.M.: Etude océanographique des chenaux du basin d'Arcachon, these d'état, Université Bordeaux 1, 300p., 1968.

Brussaard, C.P.D. et al.: Effects of grazing, sedimentation and phytoplankton cell lysis on the structure of a coastal pelagic food web, Mar. Ecol. Progr. Ser., 123, 259-271, 1995.

Burba, G. and Anderson, D.: Introduction to the Eddy Covariance method: General Guidelines and Conventional Workflow, Licor, Inc., 1-141, 2005.

Cai, W.-J., and Wang, Y.: The chemistry, fluxes, and sources of carbon dioxide in the estuarine waters of the Satilla and Altamaha River, Georgia , Limnol. Oceanogr., 43**,** 657-668, 1998.

Cai, W.-J., Wang, Z., and Wang, Y.: The role of marsh-dominated heterotrophic continental margins in transport of CO_2 between the atmosphere, the land-sea interface and the ocean, Geophysical Research Letters, 30, 1849, 2003.

Calleja, M.LI., Duarte, C.M., Prairie, Y.T., Agusti, S. and Herndl, G.J.: Evidence for surface organic matter modulation of air-sea CO_2 gas exchange, Biogeosciences, 5, 4209-4233, 2008.

Canton, M., Anschutz, P., Coynel, A., Polsenaere, P., Auby, I. and Poirier, D.: Nutrient export to an eastern Atlantic coastal zone: first modeling and nitrogen mass balance, Biogeochemistry, DOI 10.1007/s10533-010-9558-7, 2010.

Canton, M., Anschutz, P., Naudet, V., Molnar, N., Mouret, A., Francecshi, M., Naessens, F. and Poirier, D.: Impact of a solid waste disposal on nutrient dynamics in a sandy catchment, Journal of Contaminant Hydrology, 116, 1-15, 2010.

Castelle, A.J. and Galloway, J.N.: Carbon dioxide dynamics in acid forest soils in Shenandoah national park, Virginia, Soil Sci. Soc. Am. J., 54, 252-257, 1990.

Cauwet, G.: HTCO method for dissolved organic carbon analysis in seawater: influence of catalyst on blank estimation, Mar. Chem., 47, 55-64, 1994.

Cerling, T.E., Solomon, D.K., Quade, J. and Borman, J.R.: On the isotopic composition of carbon in soil carbon dioxide, Geochimica et Cosmochimica Acta, 55, 3403-3405, 1991.

Chapin III, F.S. et al.: Reconciling Carbon-cycle Concepts, Terminology, and Methods, Ecosystems, 9, 1041-1050, 2006.

Chauvaud, L., J.K. Thompson, J.E. Cloern, and Thouzeau, G.: Clams as CO_2 generators: The *Potamocorbula amurensis* example in San Francisco Bay, Limnology and Oceanography 48:2086-2092, 2003.

Chen, C.T.A. and Borges, A.V.: Reconciling opposing views on carbon cycling in the coastal ocean: continental shelves as sinks and near-shore ecosystems as sources of atmospheric CO_2, Deep-Sea Research II, 56, 578-590, 2009.

Ciais, P., Borges, A.V., Abril, G., Meybeck, M., Folberth, G., Hauglustaine, D. and Janssens, I.A.: The impact of lateral carbon fluxes on the european carbon balance, Biogeosciences 5, 1259-1271, 2008.

Clark, I.D. and Fritz, P.: Environmental isotopes in hydrogeology, CCR Press/Lewis Publishers, Boca Raton, Fl. 328, 1997.

Cole, J.J., Caraco, N.F., Kling, G.W. and Kratz, T.K.: Carbon dioxide supersaturation in the surface waters of lakes, Science, 265, 1568-70, 1994.

Cole, J.J. and Caraco, N.F.: Carbon in catchments: connecting terrestrial carbon losses with aquatic metabolism, Mar. Freshwat. Res. 52, 101-110, 2001.

Cole, J. J., Prairie, Y.T., Caraco N.F., Mcdowell, W.H., Tranvik, L.J., Striegl, R.G., Duarte, C.M., Kortelainen, P., Downing, J.A., Middleburg, J. and Melack, J.: Plumbing the global carbon cycle: integrating inland waters into the terrestrial carbon budget, Ecosystems 10, 171-184, 2007.

Cottet, M., de Montaudouin, X., Blanchet, H., and Lebleu, P. : *Spartina anglica* eradication experiment and in situ monitoring assess structuring strength of habitat complexity on marine macrofauna at high tidal level, Estuarine, Coastal and Shelf Science, 71, 629-640, 2007.

Coynel, A., Etcheber, H., Abril, G., Maneux, E., Dumas, J. and Hurtrez, J.H.: Contribution of small mountainous rivers to particulate organic carbon input in the Bay of Biscay, Biogeochemistry, 74, 151-171, 2005.

Curl, H.J. and McLeod, G.C.: The physiological ecology of a marine diatom, Skeletonema costatum (Grev.) Cleve, J. Marine Res., 19, 70-88, 1961.

Craig, H.: Carbon 13 in plants and the relationships between carbon 13 and 14 variations in nature, Journal of Geology, 62, 115-149, 1953.

D, E, F

Dang, C., Sauriau, P.G., Savoye, N., Caill-Milly, N. and others: Determination of diet in Manila clams by spatial analysis of stable isotopes, Mar. Ecol. Prog. Ser., 387, 167-177, 2009.

Davies, J.L.: A morphogenic approach to world shore-lines, Zeitschrift für Geomorphologie, 8, 127-142, 1964.

Davidson, G.R.: The stable isotopic composition and measurement of carbon in soil CO_2, Geochimica et Cosmochimica Acta, 59, 2485-2489, 1995.

Davidson, E.A., Figueiredo, R.O, Markewitz, D. and Aufdenkampe, A.K.: Dissolved CO_2 in small catchment streams of eastern Amazonia: A minor pathway of terrestrial carbon loss, Journal of Geophysical Research, 115, G04005, doi:10.1029/2009JG001202, 2010.

Dawson, J. J. C., Hope, D., Cresser, M.S. and Billett, M.F.: Downstream changes in free carbon-dioxide in an upland catchment from Northeastern Scotland, J. Environ. Qual., 24, 699-706, 1995.

Dawson, J.J.C., Billett, M.F. and Hope, D.: Diurnal variations in the carbon chemistry of two acidic peatland streams in north-east Scotland, Fresh. Biol., 46, 13091322, 2001.

Dawson, J.J.C., Billett, M.F., Hope, D., Palmer, S.M. and Deacon, C.M.: Sources and sinks of aquatic carbon in a peatland stream continuum, Biogeochem., 70, 71-92, 2004.

Deborde, J., Anschutz, P., Glé, C., Commarieu, M.V., Lecroart, P., Auby, I., Maurer, D. and Abril, G.: Sediment-Water exchanges at low tide in a mesotidal lagoon: the Arcachon Bay (France), Marine Chemistry, 109, 98-114, 2008.

Degens, E.T.: Biogeochemistry of stable carbon isotopes, In Eglington E. and Murphy M.T.J. (Eds) Organic Geochemistry, Berlin, Springer-Verlag, 304-329, 1969.

De Jong, D.J., Nienhuis, P.M. and Kater, B.J.: Microphytobenthos in the Oosterschelde estuary (The Netherlands), 1981-1990; consequences of a changed tidal regime, 282/283, 183-195, 1994.

Den Hartog, C.: The sea-grasses of the world, Verh. Kon. Ned. Akad. Wet. Afd. Natuurk., Reeks 2, 59(1), 1-275, 1970.

Denman, K.L. et al.: Couplings Between Changes in the Climate System and Biogeochemistry, In: Climate Change 2007: The Physical Science Basis. Contribution of Working Group I to the Fourth Assessment Report of the Intergovernmental Panel on Climate Change [Solomon, S., D. Qin, M. Manning, Z. Chen, M. Marquis, K.B. Averyt, M.Tignor and H.L. Miller (eds.)], Cambridge University Press, Cambridge, United Kingdom and New York, NY, USA, 500-587, 2007.

De Wit, R., Stal, L.J., Lomstein, B.A.H., Van Gemerden, H., Viaroli, P., Cecherelli, V.-H., Rodriguez-Valera, F., Bartoli, M., Giordani, G., Azzoni, R., Schaub, B., Welsh, D.: ROBUST: The ROle of BUffering capacities in STabilising coastal lagoon ecosystems, Continental Shelf Research, 21, 2021-2041, 2001.

De Wit, R., Leibreich, J., Vernier, F., Delmas, F., Beuffe, H., Maison, Ph., Chossat, J.C., Laplace-Treyture, C., Laplana, R., Clavé, V., Torre, M., Auby, I., Trut, G., Maurer, D. and P. Capdeville : Relationship between land-use in the agro-forestry system of les Landes, nitrogen loading to and risk of macro-algal blooming in the bassin d'Arcachon coastal lagoon (sw France), Estuarine, Coastal and Shelf Science, 62, 453-465, 2005.

Dinsmore, K. J. and Billett, M. F.: Continuous measurement and modeling of CO_2 losses from a peatland stream during stormflow events, Water Resources Research, 44: W12417, doi:10.1029/2008WR007284, 2008.

Duarte, C.M.: Temporal biomass variability and production/biomass relationships of seagrass communities, Mar. Ecol. Prog. Ser., 51, 269-276, 1989.

Duarte, C.M.: Submerged aquatic vegetation in relation to different regimes, Ophelia, 41, 87-112, 1995.

Duarte, C.M. and Cebrián, J.: The fate of marine autotrophic production, Limnol. Oceanogr., 41, 1758-1766, 1996.

Duarte, C.M. and Prairie, Y.T.: Prevalence of Heterotrophy and Atmospheric CO_2 Emissions from Aquatic Ecosystems, Ecosystems, 8, 862-870, 2005.

Duarte, C.M., Marbà, N., Gacia, E., Fourqurean, J.W., Beggins, J., Barrón, C. and Apostolaki, E.T.: Seagrass community metabolism: assessing the carbon sink capacity of seagrass meadows, Global Biogeochemical Cycles, 24, 1-8, 2010.

Dürr, H.H., Laruelle, G.G., van Kempen, C.M. Slomp, C.P., Meybeck, M. and Middelkoop, H.: World-wide typology of near-shore coastal systems: defining the estuarine filter of river inputs to the oceans, Estuaries Coasts, 34(3), 441-458, 2011.

Elliott, W.P.: The growth of the atmospheric internal boundary layer, Trans. Am. Geophys. Union, 39, 1-48, 1958.

Etcheber, H. : Biogéochimie de la matière organique en milieu estuarien: comportement, bilan, propriétés, PhD., Université Bordeaux 1, 1983.

Etcheber, H., Taillez, A., Abril, G., Garnier, J., Servais, P., Moatar, F. and Commarieu, M.V.: Particulate organic carbon in the estuarine turbidity maxima of the Gironde, Loire and Seine estuaries: origin and lability, Hydrobiologia, 588, 245-259, 2007.

Etheridge, D.M., Steele, L.P., Langenfelds, R.L., Francey, R.J., Barnola, J.M. and Morgan, V.I.: Natural and anthropogenic changes in atmospheric CO_2 over the last 1000 years from air in Antarctic ice and firn, Journal of Geophysical Research - Atmosphere, 101, 4115- 4128, 1996.

Eugster, W. Et al.: CO_2 exchange between air and water in an arctic Alaskan and midlatitude swiss lake: importance of convective mixing, Journal of Geophysical Research, 108, 7.1-7.14, 2003.

Finlay, J.C.: Controls of streamwater dissolved inorganic carbon dynamics in a forested watershed, Biogeochem., 62, 231-252, 2003.

Foken, T., Skeib, G. and S.H. Richter: Dependence of the integral turbulence characteristics on the stability of stratification and their use for Doppler- Sodar measurements, *Z.* Meteorol., 41, 311- 315, 1991.

Foken, T. and B. Wichura: Tools for quality assessment of surface-based flux measurements, Agricultural and Forest Meteorology, 78, 83-105, 1996.

Foken, T., Jegede, O.O., Weisensee, U., Richter, S.H., Handorf, D., Görsdorf, U., Vogel, G., Schubert, U., Kirzel, H.-J. and V. Thiermann : Results of the LINEX-96/2 Experiment., Deutscher Wetterdienst, Forschung und Entwicklung, Arbeitsergebnisse, 48, 75 pp, 1997.

Foken, T.: Angewandte Meteorologie, Mikrometeorologische Methoden, Springer, Heidelberg, 289 pp, 2003.

Folliot, M., Pujol, C., Cahuzac, B. and Alvinerie, J.: Nouvelles données sur le Miocène moyen marin de Gironde-Approche des paléoenvironnements, Ciencias da Terra, Lisboa 12, 117-131, 1993.

Frankignoulle, M.: Field measurements of CO_2 air-sea exchange, Limnol. Oceanogr., 33, 315-322, 1988.

Frankignoulle, M., Abril, G., Borges A.V., Bourge, I., Canon, C., Delille, B., Libert, E. and J. M. Théate: Carbon dioxide emission from European estuaries, Science, 282, 434-436, 1998.

Frankignoulle, M., Borges, A.V. and Biondo, R.: A new design of equilibrator to monitor carbon dioxide in highly dynamic and turbid environments, Water Res., 35, 344-1347, 2001.

Frankignoulle, M., Biondo, R., Théate, J.-M. and A.V. Borges : Carbon dioxide daily variations and atmospheric fluxes over the open waters of the Great Bahama Bank and Norman's Pond using a novel autonomous measuring system, Caribbean Journal of Science, 39, 257-264, 2003.

G, H

Gaillardet J., Dupré B., Louvat P. and Allègre C.J.: Global silicate weathering and CO_2 consumption rates deduced from the chemistry of large rivers. Chem. Geol. 159, 3-30, 1999.

Garrigue, C.: La production primaire benthique-Compilation bibliographique, Rapports Scientifiques et Techniques, Science de la mer, Biologie Marine, 43, 38pp., 1987.

Gattuso, J.-P., Frankignoulle, M. and Wollast, R.: Carbon and carbonate metabolism in coastal aquatic systems, Annual Review Ecology Systematics, 29, 405-433, 1998.

Gazeau, F, Smith, V., S., Gentili, B., Frankignoulle, M. and Gattuso, J.P.: The European coastal zone: characterization and first assessment of ecosystem metabolism, Estuarine, Coastal and Shelf Science, 60, 673-694, 2004.

Gazeau, F., Borges A.V., Barrón, C., Duarte, C.M., Iversen, N., Middelburg, J.J., Delille, B., Pizay, M.D., Frankignoulle, M. and Gattuso, J.P.: Net ecosystem metabolism in a micro-tidal estuary (Randers Fjord, Denmark): evaluation of methods and interannual variability, Marine Ecology-Progress Series, 301, 23-41, 2005a.

Gazeau, F., Duarte, C.M., Gattuso, J.P., Barrón, C., Navarro, N., Ruíz, S., Prairie, Y.T., Calleja, M., Delille, B., Frankignoulle, F. and Borges, A.V.: Whole-system metabolism and CO_2 fluxes in a Mediterranean Bay dominated by seagrass beds (Palma Bay, NW Mediterranean), Biogeosciences, 2, 87-96, 2005b.

Genereux, D.P. and Hemond, H.F.: Determination of gas-exchange rate constants for a small stream on Walker Branch watershed, Tennessee, Water Resources Research, 28, 2365-2374, 1992.

Gillikin, D.P. and Bouillon, S.: Determination of $\delta^{18}O$ of water and $\delta^{13}C$ of dissolved inorganic carbon using a simple modification of an elemental analyzer – isotope ratio mass spectrometer EA-IRMS: an evaluation, Rapid communications in Mass Spectrometry, 21, 1475-1478, 2007.

Glé, C., Amo, Y.D., Bec, B., Sautour, B., Froidefond, J.M., Gohin, F., Maurer, D., Plus, M., Laborde, P. and Chardy, P.: Typology of environmental conditions at the onset of winter phytoplankton blooms in a shallow macrotidal coastal ecosystem, Arcachon Bay (France), Journal of Plankton research, 29, 999-1014, 2007.

Glé, C., Amo, Y.D., Sautour, B., Laborde, P. and Chardy, P.: Variability of nutrients and phytoplankton primary production in a shallow macrotidal coastal ecosystem Arcachon Bay, France. Estuarine, Coastal and Shelf Science, 76, 642-656, 2008.

Gran, G.: Determination of the equivalence point in potentiometric titrations. Part II, Analyst, 77, 661-671, 1952.

Greenwood, J. L. and Lowe, R.L.: The effects of pH on a periphyton community in an acid wetland, USA, Hydrobiologia, 561, 71-82, 2006.

Guarini, J.M. : Modélisation de la dynamique du microphytobenthos des vasières intertidales du bassin de Marennes-Oléron, Thèse de Doctorat, Université Pierre et Marie Curie, 177 pp., 1998.

Guérin, F. et al.: Gas transfer velocities of CO_2 and CH_4 in atropical reservoir and its river downstream, Journal of Marine Systems, 66, 161-172, 2007.

Hamilton, S.K., Sippel, S.J. and Melack, J.M.: Oxygen depletion and carbon dioxide and methane production in waters of the Pantanal wetland of Brazil, Biogeochemistry, 30, 115-141, 1995.

Heilman, J.L. et al.: Tower-based conditional sampling for measuring ecosystem-scale carbon dioxide exchange in coastal wetlands, Estuaries, 22, 584-591, 1999.

Hollibaugh, J.T. and Azam, F.: Microbial degradation of dissolved proteins in seawater, Limnol. Oceanogr., 28, 1104-1116, 1983 .

Hope, D., Billet, M.F. and Cresser, M.S.: A review of the export of carbon in river water: fluxes and processes, Environ. Pollut., 84, 301-324, 1994.

Hope, D., Billett, M.F. and Cresser, M.C.: Exports of organic carbon in two river systems in NE Scotland, J. Hydrol., 193, 61-82, 1997.

Hope, D., Palmer, S.M., Billett, M.F. and Dawson, J.J.C.: Carbon dioxide and methane evasion from a temperate peatland stream, Limnol. Oceanogr., 4, 847-857, 2001.

Houghton, R.A. and Woodwell, G.M.: The Flax Pond ecosystem study: exchanges of CO_2 between a salt marsh and the atmosphere, Ecology, 61, 1434-1445, 1980.

Hsieh, C.I., Katul, G. and Chi, T.W.: An approximate analytical model for footprint estimation of scalar fluxes in thermally stratified atmospheric flows, Advances in Water Resources, 23,765-772, 2000.

Hubas, C., Davoult, D., Cariou, T. and Artigas, L. P.: Factors controlling benthic metabolism during low tide along a granulometric gradient in an intertidal bay (Roscoff Aber Bay, France). Marine Ecology Progress Series 316: 53–68, 2006.

Hynes, H.B.N.: The stream and its valley, Verh. Internat. Verein. Limnol., 19, 1-15, 1975.

Hynes, H.B.N.: Groundwater and stream limnology, Hydrobiologia, 100, 93-99, 1983.

J, K, L

Janssens et al.: The carbon budget of terrestrial ecosystems at country-scale-a European case study, Biogeosciences, 2, 15-26, 2005.

Jarosz, N., Brunet, Y., Lamaud, E., Irvine, M., Bonnefond, J. M., and Loustau, D.: Carbon dioxide and energy flux partitioning between the understorey and the overstorey of a maritime pine forest during a year with reduced soil water availability, Agr. Forest. Meteorol., 148, 1508-1523, 2008.

Jin, L., Ogrinc, N., Hamilton, S.K., Szramek, K., Kanduc, T. and Walter, L.M.: Inorganic carbon isotope systematics in soil profiles undergoing silicate and carbonate weathering (Southern Michigan, USA), Chemical Geology, 264, 139-153, 2009.

Johnson, M.S., Lehmann, J., Riha, S.J., Krusche, A.V., Richey, J.E., Ometto, J.P.H.B. and Couto, E.G.: CO_2 efflux from Amazonian headwater streams represents a significant fate for deep soil respiration, Geophysical Research Letters 35, L17401, doi:10.1029/2008GL034619, 2008.

Jolivet, C., Augusto, L., Trichet, P. and Arrouays, D.: Les sols du massif forestier des Landes de Gascogne: formation, histoire, propriétés et variabilité spatiale, Revue forestière française, 1, 7-30, 2007.

Jones, J.B. and Mulholland, P. J.: Carbon dioxide variation in a hardwood forest stream: an integrative measure of whole catchment ecosystem respiration, Ecosystems, 1, 183-196, 1998.

Jones, J.B., Jr., Stanley, E.H. and Mulholland, P.J.: Long-term decline in carbon dioxide supersaturation in rivers across contiguous United States, Geophys. Res. Lett., 30, 1495, doi:10.1029/2003GL017056, 2003.

Jonsson, A., Algesten, G., Bergstrom, A.K., Bishop, K., Sobek, S., Tranvik, L.J. and Jansson, M.: Integrating aquatic carbon fluxes in a boreal catchment carbon budget, Jour. Of Hydrol., 334, 141-150, 2007.

Kader, B.A and A.M. Yaglom: Mean fields and fluctuation moments in unstable stratified turbulent boundary layers, J. Fluid Mech., 212, 637-62, 1990.

Kaimal, J.C., Wyngaard, J.C, Izumi, Y. and O.R. Cote: Spectral characteristics of surface layer turbulence, Quarterly Journal of the Royal Meteorological Society, 98, 563-589, 1972.

Kaimal, J.C. and J.J. Finnigan: Atmospheric boundary layer flows: their structure and measurement, Oxford University Press, New York, 289 pp, 1994.

Kanduč, T., Szramek, K., Ogrinc, N. and Walter, L.M.: Origin and cycling of riverine inorganic carbon in the Sava river watershed Slovenia inferred from major solutes and stable carbon isotopes, Biogeochemistry, 86, 137-154, 2007.

Kathilankal, J.C. et al.: Tidal influences on carbon assimilation by a salt marsh, Environmental Research Letters, 3, 1-6, 2008.

Kawasaki, M.: Study on the dissolved organic carbon dynamics in the forested catchments in Japanese, MS Thesis, Kyoto University, Kyoto, 2002.

Keeling, C.D., and Whorf, T.P.: Atmospheric CO_2 records from sites in the SIO air sampling network, In: Trends: A compendium of data on global change. Carbon Dioxide Information Analysis Center, Oak Ridge National Laboratory, Oak Ridge, Tenn., USA, 2000.

Kempe, S., Pettine, M. and Cauwet, G.: Biogeochemistry of European Rivers, In Degens E.T., Kempe S. And Richey J.E. (Eds) Biogoeochemistry of Major World Rivers, John Wiley & Sons Ltd, Chichestel, 169-21, 1991.

Kjerfve, B.: Comparative oceanography of coastal lagoons, In Estuarine variability, ed. D.A. Wolfe, New York Academic, 63-81, 1985.

Kjerfve, B.: Coastal lagoons, chapter 1. In Kjerfve, B. (ed.), Coastal Lagoon Processes, Elsevier Oceanography Series, Amsterdam, 1-8, 1994.

Kling, G.W., Kipphut, G.W. and Miller, M.C.: Arctic lakes and streams as gas conduits to the atmosphere: implications for tundra carbon budgets, Science, 251, 298-301, 1991.

Kling, G.W., Kipphut, G.W. and Miller, M.C.: The flux of CO_2 and CH_4 from lakes and rivers in arctic Alaska, Hydrobiologia 240, 23-36, 1992.

Kondo, F. and O. Tsukamoto: Air-sea CO_2 flux by Eddy Covariance technique in the Equatorial Indian ocean, Journal of Oceanography, 66, 449-456, 2007.

Koné, Y.J.M., Abril, G., Kouadio, K.N., Delille, B. and Borges, A.V.: Seasonal variability of carbon dioxide in the rivers and lagoons of Ivory Coast (West Africa), Estuaries and Coasts, 32, 246-260, 2009.

Laplana, R., Billy, F., Beuffe, H. and Fleuranceau, J.: Localisation, quantification et dynamique des apports de nutriments au bassin d'Arcachon, Etude n°66, Cemagref-Bordeaux, 86 p., 1993.

Larsen, A. et al.: Spring phytoplankton bloom dynamics in Norwegian coastal waters: microbial community succession and diversity, Limnol. Oceanogr., 49, 180-190, 2004.

Laruelle, G.G, Dürr, H.H., Slomp, C.P. and Borges, A.V.: Evaluation of sinks and sources of CO_2 in the global coastal ocean using a spatially-explicit typology of estuaries and continental shelves, Geophysical Research letters, 37, L15607, doi:10.1029/2010GL043691, 2010.

Leavitt, S.W.: Carbon isotopes, stable, Encyclopedia of Earth Sciences Series, Springer-Verlag, 1-11, 2009.

Leclerc, M.Y. and G.W. Thurtell: Footprint prediction of scalar fluxes using a Markovian analysis, Boundary-Layer Meteor., 52, 247-258, 1990.

Leuschner, C., Landwehr, S. and Mehlig, U.: Limitation of carbon assimilation of intertidal Zostra noltii and Z. marina by dessication at low tide, Aquatic Botany, 62, 171-176, 1998.

Lorrain, A., Savoye, N., Chauvaud, L., Paulet, Y-M., Naulet, N.: Decarbonation and preservation method for the analysis of organic C and N contents and stable isotope ratios of low-carbonated suspended particulate material, Analytica Chimica Acta, 491, 125-133, 2003.

Ludwig, W., Probst, J.L. and Kempe, S.: Predicting the oceanic input of organic carbon by continental erosion, Glob. Biogeochem. Cycl., 10, 23-41, 1996.

Lundström, U.S., van Breemen, N. and Bain, D.: The podzolization process. A review, Geoderma, 94, 91-107, 2000.

M, N, O

Manaud, F., Bouchet, J.M., Deltreil, J.P., Maurer, D., Trut, G., Auby, I., Dreno, J.P., L'Yavanc, J., Masson, N. and Pellier, C. : Etude intégrée du Bassin d'Arcachon. Tome 1: Physique. Activités ressources vivantes, Rapport Interne DEL/Arcachon, 1997.

Mantoura, R.F.C. and Woodward, E.M.S.: Conservative behaviour of riverine dissolved organic carbon in the Severn Estuary: chemical and geochemical implications, Geochimica et Cosmochimica Acta, 47, 1293–1309, 1983.

Mantoura, R.F.C., Martin, J.M and Wollast, R.: Ocean margin processes, in Global Change, Chichester, UK: Wiley & Sons, 469 pp., 1991.

Mariotti, A. : Le carbone 13 en abondance naturelle, traceur de la dynamique de la matiere organique des sols et des paléoenvironnements continentaux, Cahier Orstrom 4, Série Pédologie, 26, 299-313, 1991.

Marra, J.: Net and gross productivity: weighing in with ^{14}C, Aquatic Microbial Ecology, doi:10.3354/ame01306, 2009.

Mauder, M. et al.: Quality control of CarboEurope flux data – Part 2: Inter-comparison of eddy-covariance software, Biogeosciences, 5, 451-462, 2008.

McRoy, C.P. and McMillan, C.: Production ecology and physiology of seagrasses, in: McRoy, C.P., Helferrich, C. (Eds.), Production Ecology and Physiology of Seagrasses. Dekler, New York, USA, 58-87, 1977.

Mehrbach, C., Culberson, C.H., Hawley, J.E. and Pytkowicz, R.N.: Measurement of the apparent dissociation constants of carbonic acid in seawater at atmospheric pressure, Limnology and Oceanography, 18, 897-907, 1973.

Meybeck, M.: River transport of organic carbon to the ocean, American Journal of Science 282, 401-450, 1982.

Meybeck, M.: Global chemical weathering of surficial rocks estimated from river dissolved loads, American J. Science, 287, 401-428, 1987.

Meybeck, M.: Riverine transport of atmospheric carbon: sources, global typology and budget. Water Air Soil Pollut. 70, 443-63, 1993.

Meybeck, M. and Vorosmarty, C.J.: Global transfer of carbon by rivers, Glob. Chan. Newslet., 37, 12-14, 1999.

Meybeck, M., Green, P. and Vorosmarty, C.J.: Global distribution of mountains and other major relief classes with regards to water runoff and population density, Mountain Research Development 21, 34-35, 2001.

Middelburg, J.J., Barranguet, C., Boschker, H.T.S., Hermann, P.M.J., Moens, T. and Heip, C.H.R.: The fate of intertidal microphytobenthos carbon: an *in situ* 13C-labeling study, Limnol. Oceanogr. 45, 1224-1234, 2000.

Middelburg, J.J., et al.: Respiration in coastal benthic communities, in Respiration in Aquatic Ecosystems, edited by P. A. del Giorgio and P. J. leB. Williams, pp. 206-224, Oxford Univ. Press, Oxford, U. K., ISBN:0-19-852709-8, 2005.

Migné, A., Davoult, D., Spilmont, N., Boucher, G., Gattuso, J.P. and H Rybarczyk : A closed-chamber CO_2 flux method for estimating primary production and respiration under emersed conditions, Marine Biology, 140, 865-869, 2002.

Migné A., Spilmont N., Davoult D. : *In situ* measurements of benthic primary production during emersion: seasonal variations and annual production in the Bay of Somme (eastern English Channel, France), *Cont. Shelf Res.* 24: 1437-1449, 2004.

Migné, A., Gévaert, F., Créach, A., Spilmont, N., Chevalier, E. and Davoult, D. : Photosynthetic activity of intertidal microphytobenthic communities during emersion : in situ measurements of Chlorophyll fluorescence (PAM) and CO_2 flux (IRGA), J. Phycol., 43, 864-873, 2007.

Miyajima, T., Yamada, Y., Hanba, Y.T., Yoshii, K., Koitabashi, T. and Wada, E.: Determining the stable isotope ratio of total dissolved inorganic carbon in lake water by GC/C/IRMS, Limnol. Oceanogr., 40, 994-1000, 1995.

Moncrieff, J.,-B. Et al. : A system to measure surface fluxes of momentum, sensible heat, water vapour and carbon dioxide, Journal of Hydrology, 188-189, 589-611, 1997.

Monteith, J.L., and M.H. Unsworth: Principles of Environmental Physics, 2nd ed., Edward Arnold, London, 291 pp, 1990.

Mook, W.G.: Stable carbon and oxygen isotopes of natural waters in the Netherlands, Isotope Hydrology, IAEA, Vienna, 163-190, 1970.

Mook, W.G., Bommerson, J.C. and Staverman, W.H.: Carbon isotope fractionation between dissolved bicarbonate and gaseous carbon dioxide, Earth Planet Sci. Lett., 22, 169-176, 1974.

Mook, W.G., Koopmans, M., Carter, A.F. and Keeling, C.D.: Seasonal, latitudinal, and secular variations in the abundance and isotopic ratios of atmospheric carbon dioxide. 1. results from land stations, J. Geophys. Res., 88, 10915-10933, 1983.

Mook, W. G. and Tan, F.C.: Stable carbon isotopes in rivers and estuaries. Degens E., Kempe S. and Richey J. Eds, Biogeochemistry of Major World Rivers, Wiley, 245-264, 1991.

Moore, C.J.: Frequency response corrections for eddy correlation systems, Boundary layer Meteorology, 37, 17-35, 1986.

Morison, J.I.L. et al.: Very high productivity of the C_4 aquatic grass Echinochloa polystachya in the Amazon floodplain confirmed by net ecosystem CO_2 flux measurements, Oecologia, 125, 400-411, 2000.

Mulholland, P. J.: Large-scale patterns in dissolved organic carbon concentration, flux, and sources, In S. Findlay and R. L. Sinsabaugh [eds.], Aquatic ecosystems-Interactivity of dissolved organic matter. Academic Press, 139-160, 2003.

Neal, C. and Hill, S.: Dissolved inorganic and organic carbon in moorland and forest streams: Plynlimon, mid-Wales, Journal of Hydrology, 153, 231-243, 1994.

Neal, C., Hilton, J., Wade, A.J., Neal, M. and Wickman, H.: Chlorophyll-a in the rivers of eastern England. Sci. Tot. Environ., 365, 84-104, 2006.

Neftel, A., Friedli, H., Moor, E., Lötscher, H., Oeschger, H., Siegenthaler, U. and Stauffer, B.: Historical CO_2 record from the Siple station ice core. In: Trends '93: A Compendium of Data on Global Change, [T.A. Boden, D.P. Kaiser, R.J. Sepanski, and F.W. Stoss (eds.)], Carbon Dioxide Inf. Anal. Cent., Oak Ridge, 11-14, 1994.

O'Connor, D. and Dobbins, W.: Mechanism of reaeration in natural streams, Transactions of the American Society of Civil Engineers, 123, 641-684, 1958.

Odum, H.T.: Primary production in flowing waters, Limnol. Oceanogr., 1, 102-117, 1956.

Okazaki, R.: Study on the export of organic carbon from a forested catchment in Japanese, MS Thesis, Kyoto University, Kyoto, 2001.

O'Leary, M.H.: Measurement of the isotope fractionation associated with diffusion of carbon dioxide in aqueous solution, Journal of Physical Chemistry, 88, 823-825, 1984.

Oquist, M.G., Wallin, M., Seibert, J., Bishop, K. and Laudon, H.: Dissolved inorganic carbon export across the soil/stream interface and its fate in a boreal headwater stream, Environ. Sci; Technol., 43, 7364-7369, 2009.

Ouisse, V., Migne, A. and Davoult, D.: Seasonal variations of community production, respiration and biomass of different primary producers in an intertidal Zostera noltii bed (Western English Channel, France), Hydrobiologia, 649, 3-11, 2010.

Owens, M., Edwards, R.W. and Gibbs, J.W.: Some reaeration studies in streams, International Journal of Air and Water Pollution, 8, 469-486, 1964.

P, Q, R

Pace, M.L. et al.: Whole-lake carbon-13 additions reveal terrestrial support of aquatic food webs, Nature, 427, 240-243, 2004.

Pardé, M. : Etudes hydrologiques sur les rivières françaises du sud oust de la France, Revue Géographique des Pyrénées et du sud ouest, 1192/8, T.XXVII, 1956.

Parker, S.R. Poulson, S.R., Gammons, C.H. and Degrandpre, M.D.: Biogeochemical controls on diel cycling of stable isotopes of dissolved O_2 and dissolved inorganic carbon in the Big Hole River, Montana, Environ. Sci. Technol., 39, 7134-7140, 2005.

Parsons, T.R., Takahashi, M. and Hargrave B.: Biological Oceanographic Processes, 3rd edn. Pergamon Press Ltd, Oxford: 330 pp., 1984.

Pernetta, J.C and Milliman, J.D.: Land-Ocean interactions in the coastal zone. Implementation plan, IGPB Rep., 33, 1-215, 1995.

Piñol, J. and Avila, A.: Streamwater pH, alkalinity, pCO_2 and discharge relationships in some forested Mediterranean catchments, Journal of Hydrology, 131, 205-225, 1992.

Plus, M., Auby, I., Verlaque, M. and Levavasseur, G.: Seasonal variations in photosynthetic irradiance response curves of macrophytes from a Mediterranean coastal lagoon, Aquatic Botany, 81(2), 157-173, 2005.

Plus, M., Stanisière, J.-Y., Maurer, D. and Dumas, F.: Caractérisation des composantes hydrodynamiques d'une lagune mésotidale, le Bassin d'Arcachon, Ifremer RST/LER/AR/06.007, 1-54, 2007.

Plus, M., Stanisière, J.-Y., Maurer, D. and Dumas, F. : Etude comparative des composantes hydrodynamiques de deux systèmes côtiers mésotidaux, les Bassins d'Arcachon et de Marennes-Oléron, Rapport commun LER-AR/LER-PC/DYNECO PHYSED, Ifremer, 1-25, 2008.

Plus, M., Dalloyau, S., Trut, G., Auby, I., de Montaudouin, X., Emery, E., Noël, C. and Viala, C.: Long-term evolution (1988-2008) of *Zostera* spp. Meadows in Arcachon bay (Bay of Biscay), Estuarine, Coastal and Shelf Science, 87, 357-366, 2010.

Polsenaere, P. and Abril, G.: Modelling CO_2 degassing from small acidic rivers using pCO_2, DIC and δ13C-DIC data, submitted to Geochemica et Cosmochimica Acta, 2010.

Polsenaere, P., Savoye, N., Etcheber, H., Canton, M., Poirier, D., Bouillon, S. and Abril, G.: Export and degassing of terrestrial carbon from small rivers and streams draining a temperate sandy podzolized catchment, submitted to L&O, 2010.

Polsenaere, P., Lamaud, E., Bretel, P., Bonnefond, J.M., Delille, B., Detandt, G., Loustau, D. and Abril, G.: Turbulent flux measurements by Eddy Correlation over a temperate intertidal flat in the southwest of France, submitted to Journal of Geophysical research, 2011.

Prentice, I.C., Farquhar, G.D., Fasham, M.J.R., Goulden, M.L., Heimann, M., Jaramillo, V.J., Kheshgi, H.S., Le Quéré, C., Scholes, R.J. and Wallace, D.W.R.: The Carbon Cycle and Atmospheric Carbon Dioxide. In: Climate Change 2001: The Scientific Basis. Contribution of Working Group I to the Third Assessment Report of the Intergovernmental Panel on Climate Change [Houghton, J.T., Y., Ding, D.J. Griggs, et al. (eds.)], Cambridge University Press, Cambridge, United Kingdom and New York, NY, USA, 185-237, 2001.

Pritchard, D.W.: What is an estuary? Physical point of view, In "Estuaries", G.H. Lauff (Ed.) Washington D.C., 158-179, 1967.

Probst, J.L.: Nitrogen and phosphorous exportation in the Garonne basin France, Jour. of Hydrol., 76, 281-305, 1985.

Probst, J.L.: Dissolved and suspended matter transported by the Girou River France: mechanical and chemical erosion rates in a calcareous molasse basin, Hydrol. Sci., 31, 71-79, 1986.

Rantakari, M., Mattsson, T., Kortelainen, P., Piirainen, S., Finér, L. and Ahtianen, M.: Organic and inorganic carbon concentrations and fluxes from managed and unmanaged boreal first-order catchments, Sci. Tot. Envir., 408, 1649-1658, 2010.

Raymond, P.A. and Cole, J.J.: Gas exchange in rivers and estuaries: choosing a gas transfer velocity, Estuaries, 24, 312-317, 2001.

Righi, P. and Wilbert, J.: The sandy podzolized soils from "Landes de Gascogne" France. Distribution and main characteristics, Science du sol, 4, 253-264, 1984.

Rimmelin, P., Dumon, J.C., Maneux, E. and Gonçalves, A.: Study of annual and seasonal dissolved inorganic nitrogen inputs into the Arcachon lagoon, Atlantic coast France, Est. Co. and Shelf Sci. 47, 649-659, 1998.

Reynolds, O.: On the dynamical theory of incompressible viscous fluids and the determination of criterion, Philosophical Transactions of Royal Society of London, A174, 935-982, 1895.

Rocha, A.V. and M.L. Goulden: Large interannual CO_2 and energy exchange variability in a freshwater marsh under consistent environmental conditions, Journal of Geophysical Research, 113, G04019, 1-12, 2008.

S, T

Sahlée, E., Smedman, A.-S., Rutgersson, A. and Högström U. : Spectra of CO_2 and water vapour in the marine atmospheric surface layer, Boundary-Layer Meteorology, 126, 279-295, 2008.

Savoye, N., Aminot, A., Tréguer, P., Fontugne, M., Naulet, N. and Kerouel, R.: Dynamics of particulate organic matter $\delta^{15}N$ and $\delta^{13}C$ during spring phytoplankton blooms in a macrotidal ecosystem Bay of Seine, France, Marine Ecology Progress Series, 255, 27-41, 2003.

Schindler, J.E. and Krabbenhoft, D.: The hyporheic zone as a source of dissolved organic carbon and carbon gases to a temperate forested stream, Biogeochemistry, 43, 157-174, 1998.

Serôdio, J., Vieira, S. and Cruz, S.: Photosynthetic activity, photoprotection and photoinhibition in intertidal microphytobenthos as studied in situ using variable chlorophyll fluorescence, Continental Shelf Research, 28, 1363-1375, 2008.

Sharp, J.H.: The dissolved organic carbon controversy: an update, Oceanography, 6, 45-50, 1993.

Silva, J., Santos, R., Calleja M.Ll. and C.M. Duarte: Submerged versus air-exposed intertidal macrophyte productivity: from physiological to community-level assessments, Journal of Experimental Marine Biology and Ecology, 317, 87-95, 2005.

Siegenthaler, U., Friedli, H., Loetscher, H., Moor, E., Neftel, A., Oeschger, H. and Stauffer, B.: Stable-isotope ratios and concentration of CO_2 in air from polar ice cores, Annals of Glaciology, 10, 1-6, 1988.

Smith, S. V. and Hollibaugh, J. T.: Coastal metabolism and the ocean organic carbon balance, Rev. Geophys., 31, 75-89, 1993.

Sobek, S., Tranvik, L.J. and Cole, J.J.: Temperature independence of carbon dioxide supersaturation in global lakes, Glob. Biogeochem. Cy., 19, GB2003, doi: 10.1029/2004GB002264, 2005.

Sobek, S., Söderbäck, B., Karlsson, S., Andersson, E. and Brunberg, A.K.: A carbon budget of a small humic lake: an example of the importance of lakes for organic matter cycling in boreal catchments, AMBIO, 35, 469-475, 2006.

Sobek, S., Tranvik, L.J., Prairie, Y.T., Kortelainen, P. and Cole, J.J.: Patterns and regulation of dissolved organic carbon: an analysis of 7500 widely distributed lakes, Limnol. Oceanogr., 52, 1208-1219, 2007.

Sophocleous, M.: Interactions between groundwater and surface water: the state of the science. Hydrogeol. Journ., 10, 52-67, 2002.

Soriano-Sierra, E.J.: Etude écologique des marais sales du basin d'Arcachon: structure et evolution des schorres, production et dégradation de leur végétation et échanges de matières particulaires entre les schorres et le bassin, thèse de doctorat, Université Bordeaux 1, 1992.

Spilmont, N., Migné, A., Lefebvre, A., Artigas, L. F., Rauch, M. and Davoult, D.: Temporal variability of intertidal benthic metabolism under emersed conditions in an exposed sandy beach (Wimereux, eastern English Channel, France). J. Sea Res. 53, 161-7, 2005.

Spilmont, N., Davoult, D. and Migné, A.: Benthic primary production during emersion: in situ measurements and potential primary production in the Seine Estuary (English Channel, France), Marine Pollution Bulletin, 54, 49-55, 2006.

Stella, P., Lamaud, E., Brunet, Y., Bonnefond, J.M., Loustau, D. and Irvine, M.: Simultaneous measurements of CO_2 and water exchanges over three agrosystems in South-West France, Biogeosciences, 2957-2971, 2009.

Stella, P., Loubet, B., Lamaud, E., Laville, P. and Cellier, P.: Ozone deposition onto bare soil: A new parameterisation, AGMET, doi :10.1016/j.agrformet.2011.01.015, 2011.

Strickland, J.D.H. and Parsons, T.R.: A practical handbook of sea-water analysis 2nd Edition, J. Fish. Res. Bd. Canada., 167-311, 1972.

Stum, W. and Morgan, J.J.: Aquatic chemistry: chemical equilibria and rates in natural waters, 3rd edition, Wiley-Interscience, New York, 1996.

Sutton, O.G.: Micrometeorology, Mc Gaw-Hill, New York, 333p., 1953.

Takahashi, T. et al.: Global sea-air CO_2 flux based on climatological surface ocean pCO_2, and seasonal biological and temperature effects, Deep Sea Research II, 49, 1601-1622, 2002.

Takahashi, T. et al.: Climatological mean and decadal change in surface ocean pCO_2, and net sea-air CO_2 flux over the global oceans, Deep-Sea Research II, 56, 554-574, 2009.

Teodoru, C.R, Del Giorgio, P.A., Prairie, Y.T. and Camire, M.: Patterns in pCO_2 in boreal streams and rivers of northern Quebec, Canada, Global Biogeochemical Cycles, 23, GB2012, DOI:10.1029/2008GB003404, 2009.

Thayer, G.W., Parker, P.L., Lacroix, M.W. and Fry, B.: The stable carbon isotope ratio of some components of an eelgrass (*Zostera marina*) bed, Oecologia (Berl.), 35, 1-12, 1978.

Tranvik, L.J.: Availability of dissolved organic carbon for planktonic bacteria in oligotrophic lakes of differing humic content, Microbial Ecol., 16, 311-322, 1988.

Tranvik, L.J. and Jansson, M.: Terrestrial export of organic carbon, Nature, 415, 861-862, 2002.

Tranvik, L.J. et al.: Lakes and reservoirs as regulators of carbon cycling and climate, Limnol. Oceanogr. 54, 2298-2314, 2009.

Trichet, P., Jolivet, C., Arrouays, D., Loustau, D., Bert, D. and Ranger, J. : Le maintien de la fertilité des sols forestiers landais dans le cadre de la sylviculture intensive du pin maritime, Etude et gestion des sols 6, 197-214, 1997.

V, W

Vachon, D., Prairie, Y.T. and Cole, J.J.: The relationship between near-surface turbulence and gas transfer velocity in freshwater systems and its effect on floating chamber measurements. Limnol. Oceanogr. 55(4): 1723-1732, 2010.

Van Hees, P.A.W., Jones, D.L., Finlay, R., Godbold, D.L. and Lundström, U.S.: The carbon we do not see-the impact of low molecular weight compounds on carbon dynamics and respiration in forest soils, Soil Biol. and Biochem., 37, 1-13, 2005.

Vermaat, J.E. and Verhagen, F.C.A.: Seasonal variation in the intertidal seagrass *Zostera noltii* Hornem: coupling demographic and physiological patterns, Aquatic Botany, 52, 259-281, 1996.

Vesala, T. et al.: Eddy covariance measurements of carbon exchange and latent and sensible heat fluxes over a boreal lake for a full open-water period, Journal of Geophysical Research, 111, D11101, 1-12, 2006.

Vestin, J.L.K., Norström, S.H., Bylund, D. And Lundström, U.S.: Soil solution and stream water chemistry in a forested catchment II: Influence of organic matter, Geoderma, 144, 271-278, 2008.

Veyssy, E., Etcheber, H., Lin, R. G., Buat-Menard, P. and Maneux, E.: Seasonal variation and origin of particulate organic carbon in the lower Garonne River at La Reole southwestern France, Hydrobiologia, 391, 113-126, 1999.

Vogel, J.C.: Variability of carbon isotope fractionation during photosynthesis, Stable Isotopes and Carbon Plant-Water Relations, 29-46, 1993.

Wachniew, P.: Isotopic composition of dissolved inorganic carbon in a large polluted river: the Vistula, Poland, Chemical Geology, 233, 293-308, 2006.

Wallin, M., Buffam, I., Oquist, M., Laudon, H and Bishop, K.: Temporal and spatial variability of dissolved inorganic carbon in a boreal stream network: concentrations and downstream fluxes, JGR, 115, 1-12, 2010.

Wang, Z.A. and Cai, W.J.: Carbon dioxide degassing and inorganic carbon export from a marsh-dominated estuary (the Duplin River): a marsh CO_2 pump, Limnol. Oceanogr., 49, 341-354, 2004.

Wanninkhof, R., Mulholland, P. J. and Elwood, J. W.: Gas exchange rates for a first-order stream determined with deliberate and natural tracers, Water Resources Research, 26, 1621-1630, 1990.

Wanninkhof, R.: Relationship between wind speed and gas exchange over the ocean, Journal of Geophysical Research, 97, 7373-7382, 1992.

Wanninkhof, R. and W.R. Mcgillis: A cubic relationship between air-sea CO_2 exchange and windspeed, Geophysical Research Letters, 26, 1889-1892, 1999.

Webb, E.K., Pearman, G. and Leuning, R.: Correction of flux measurements for density effects due to heat and water vapour transfer, Quarterly Journal of Royal Meteorological Society, 106, 85-100, 1980.

Weiss, R. F.: Carbon dioxide in water and seawater: the solubility of a non-ideal gas, Mar. Chem. 2, 203-215, 1974.

Woodwell, G.M. and P.H. Whittaker: Primary production in terrestrial communities, Am. Zool., 8, 19-30, 1968.

Worrall, F. and A. Lancaster: The release of CO_2 from riverwaters-The contribution of excess CO_2 from groundwater, Biogeochemistry, 76, 299-317, 2005.

Worrall, F., Guilbert, T. and Besien, T.: The flux of carbon rivers: the case for flux from England and Wales, Biogeochemistry, 86, 63-75, 2007.

Y, Z

Yan, Y. et al.: Closing the carbon budget of estuarine wetlands with tower-based measurements and MODIS time series, Glo. Cha. Biol., 14, 1690-1702, 2008.

Yang, C., Telmer, K. and Veizer, J.: Chemical dynamics of the 'St. Lawrence' riverine system: δH_2O, $\delta^{18}OH2O$, $\delta^{13}C_{DIC}$, $\delta^{34}S_{Sulfate}$, and Dissolved $^{87}Sr/^{86}Sr$, Geochim. Cosmochim. Acta, 60, 851-866, 1996.

Yentsch, C.M. and Menzel, D.W.: A method for the determination of phytoplankton chlorophyll and phaeophytin by fluorescence, Deep-Sea Res., 10, 221-231, 1963.

Zappa, C. J., et al. : Variation in surface turbulence and the gas transfer velocity over a tidal cycle in a macro-tidal estuary, Estuaries, 26(6), 1401-1415, 2003.

Zeebe, R.E. and Wolf-Gladrow, D.: CO_2 in seawater: equilibrium, kinetics, isotopes, Elsevier Oceanography Series, 65, 346, 2001.

Zhang, J., Quay, P.D. and Wilbour, D.O.: Carbon isotope fractionation during gas–water exchange and dissolution of CO_2, Geochimica et Cosmochimica Acta, 59, 107-114, 1995.

Zemmelink, H.J. et al.: Primary production and eddy correlation measurements of CO_2 exchange over an intertidal estuary, Geophysical Research Letters, 36, LI19606, 2009.

ANNEXES

ANNEXES

ANNEXE 1 : L'utilisation des images satellites dans l'estimation du couvert de l'herbier de *Zostera noltii* dans la lagune d'Arcachon

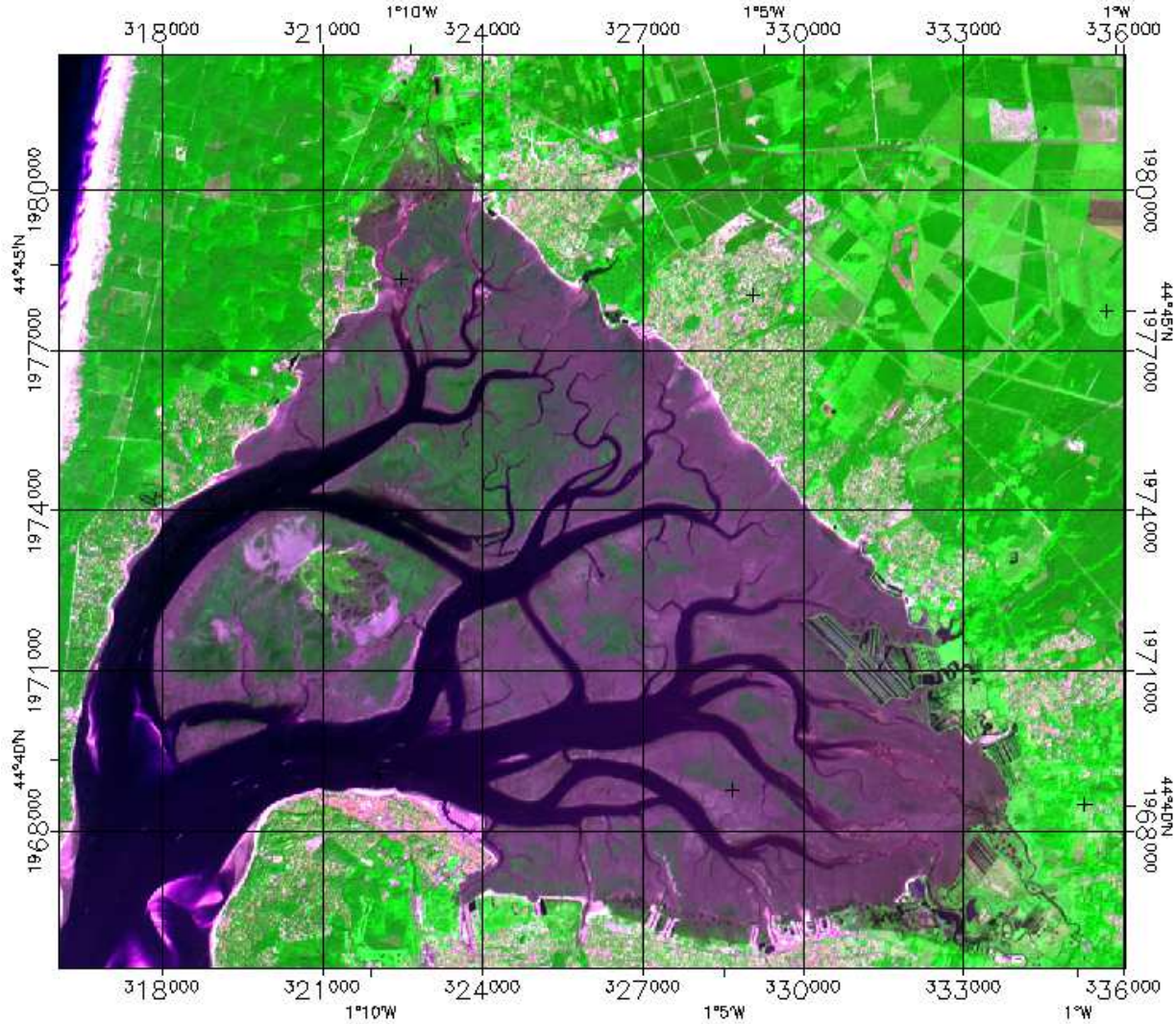

Exemple de la capture d'une image satellite SPOT de la lagune d'Arcachon (13 /09/07)

Afin d'estimer le couvert d'herbier de *Zostera noltii*, cinq images satellites SPOT correspondant à la lagune à basse mer ont été analysées (13/09/07, 17/10/2008, 08/09/2009, 24/06/2009 et 14/04/2010). Le couvert de l'herbier a été quantifié dans un cercle d'1 km de rayon autour du mat de l'Eddy Covariance aux deux stations, dans les 8 secteurs (45°) de direction de vent. Les images ont été analysées en utilisant la méthodologie basée sur l'index de végétation normalisé (Barillé et al., 2010). A l'exception des densités d'herbiers très faibles qui peuvent être confondues avec le microphytobenthos, les surfaces ainsi que les densités de couvert associées ont pu être estimées à partir de ces images. Des images de la base de données CNES/Kalideos ont été utilisées. Les images géo-référencées ont été téléchargées puis calibrées avec des mesures de réflectance sur le terrain. Les surfaces correspondant aux chenaux, récifs d'huitres et marais ont été masqués avant le calcul de l'index à l'échelle du pixel. La position et la densité de l'herbier ont été obtenues à partir de l'index cartographié à 2D. 36 observations GPS obtenues en automne 2009 ont été comparées à une image SPOT obtenue le 08/09/2009. Les résultats montrent que les observations menées corroborent l'image dans 90% des cas. Ce test valide l'approche utilisée et appliquée aux cinq images.

ANNEXE 2 : Présentation de la soutenance de thèse (29/04/2011)

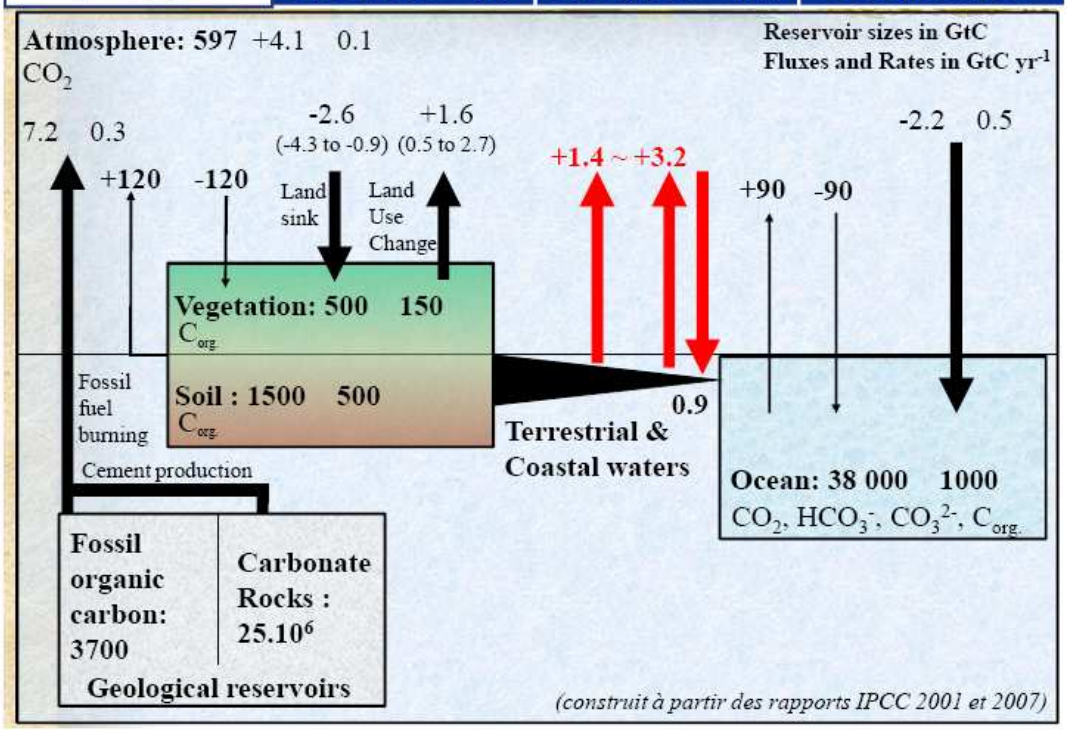

Introduction générale | Résultats et Discussion (I) | Résultats et Discussion (II) | Synthèse et Perspectives

- Zone côtière: 7% de l'océan global / active mais hétérogène et contrastée
- Prise en compte des **Zones côtières** dans les budgets de C depuis peu
  - **Plateaux continentaux : -0.21 0.36 Gt C an^{-1} (Laruelle et al., 2010)**
  - **Estuaires: +0.36 Gt C an^{-1} (Chen and Borges, 2009)**
  - **Marais salants, lagunes intertidales: ?**
  - **« Coastal wetlands »: 0.5% de la surface terrestre globale (660.10^3 km^2) (Lehner, B. and Döll, P.; 2004)**
- Compréhension du fonctionnement écologique de ces écosystèmes en termes de flux de C et d'En


Introduction générale
Résultats et Discussion (I)
Résultats et Discussion (II)
Synthèse et Perspectives
➢Production Nette de l'Ecosystème (NEP):
Accumulation nette de C dans un écosystème
NEP = GPP – CR
(NCP)
Respiration de la communauté
Production primaire brute
(Woodwell and Whittaker, 1968)
•Production Primaire Nette (NPP):
NPP = GPP - AR
Respiration des Autotrophes
•Respiration de la Communauté (CR):
CR = AR + HR
Autotrophes et Hétérotrophes
(Odum, 1956)
NEP > 0: AUTOTROPHE
NEP < 0: HÉTÉROTROPHE

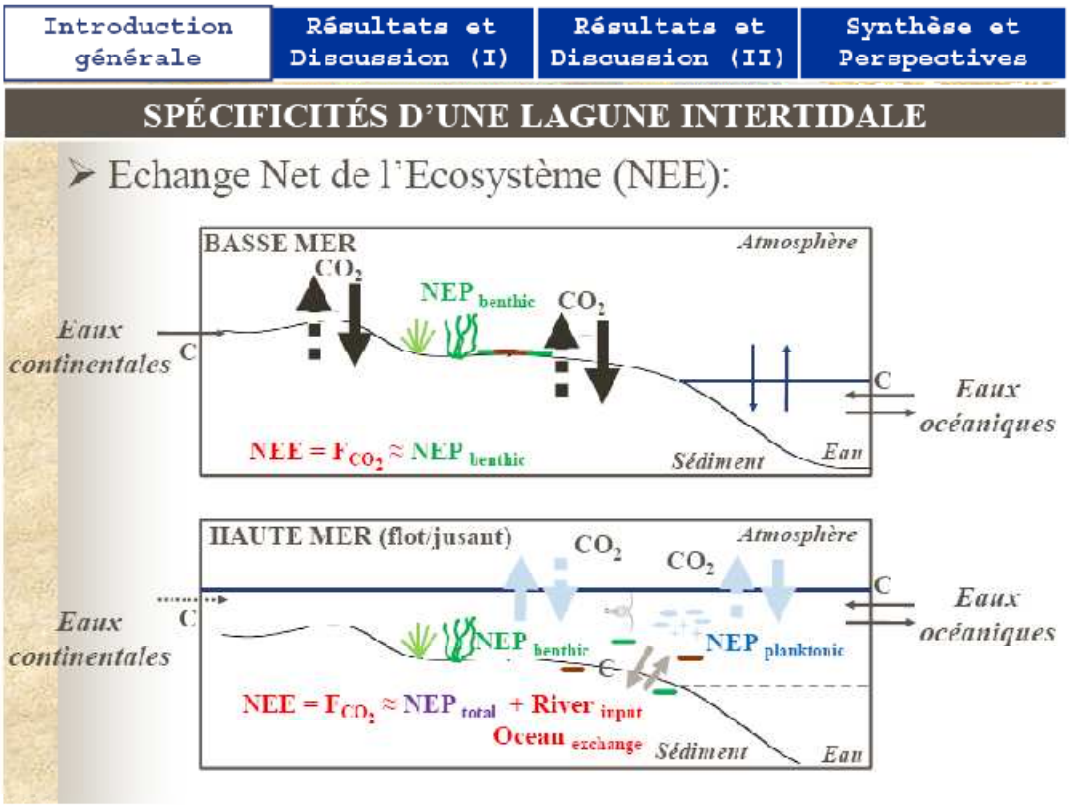
Introduction générale
Résultats et Discussion (I)
Résultats et Discussion (II)
Synthèse et Perspectives
SPÉCIFICITÉS D'UNE LAGUNE INTERTIDALE
➢ Echange Net de l'Ecosystème (NEE):
BASSE MER
Atmosphère
CO2
NEP benthic
CO2
Eaux continentales
C
C
Eaux océaniques
NEE = FCO2 ≈ NEP benthic
Sédiment
Eau
HAUTE MER (flot/jusant)
CO2
CO2
Atmosphère
Eaux continentales
C
C
Eaux océaniques
NEP benthic
NEP planktonic
NEE = FCO2 ≈ NEP total + River input
Ocean exchange
Sédiment
Eau

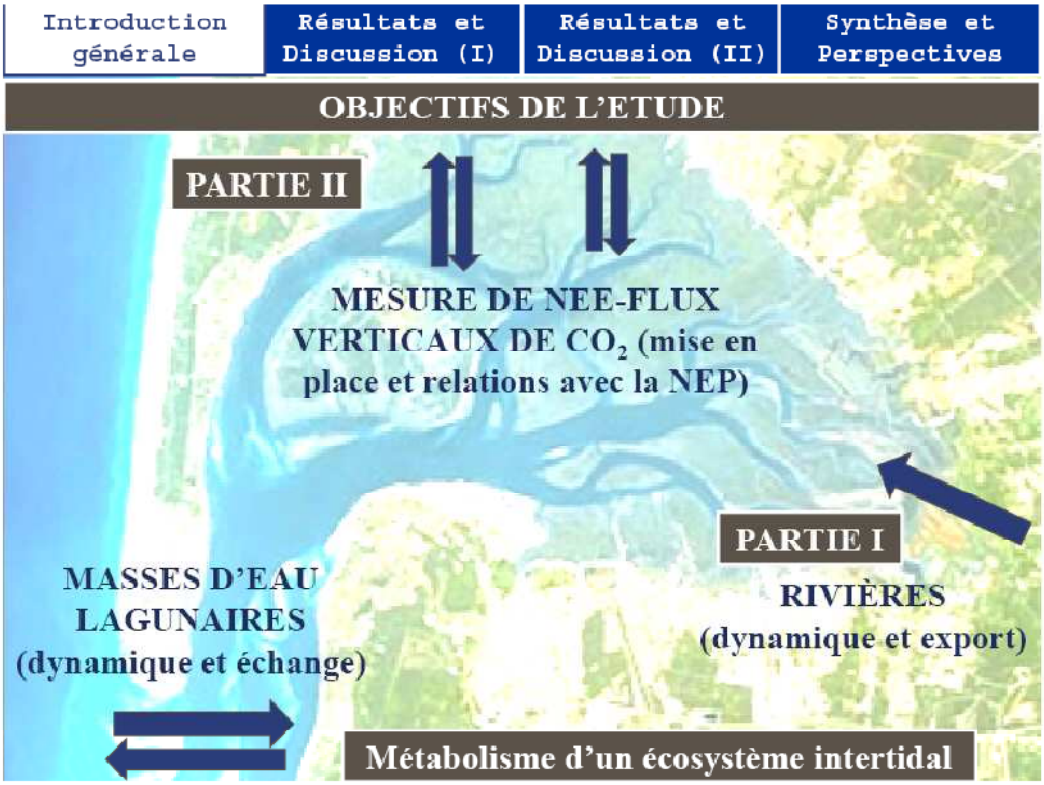
Introduction générale
Résultats et Discussion (I)
Résultats et Discussion (II)
Synthèse et Perspectives
OBJECTIFS DE L'ETUDE
PARTIE II
MESURE DE NEE-FLUX VERTICAUX DE CO_2 (mise en place et relations avec la NEP)
PARTIE I
RIVIÈRES
(dynamique et export)
MASSES D'EAU LAGUNAIRES
(dynamique et échange)
Métabolisme d'un écosystème intertidal

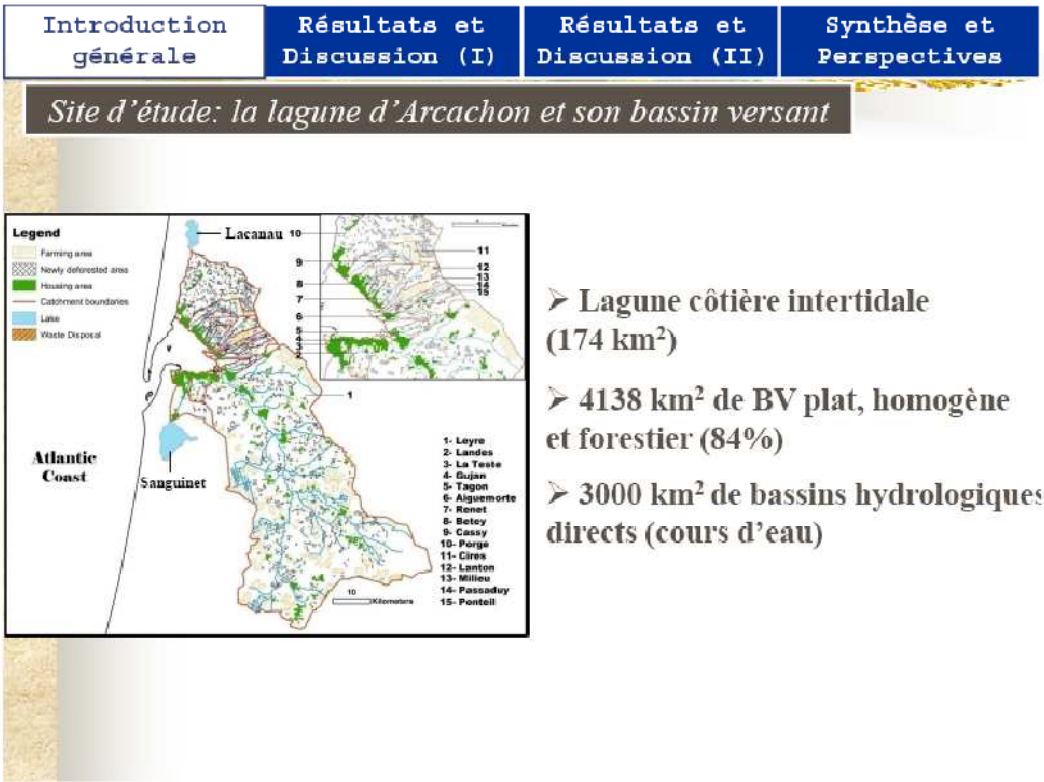
Introduction générale
Résultats et Discussion (I)
Résultats et Discussion (II)
Synthèse et Perspectives
Site d'étude: la lagune d'Arcachon et son bassin versant
Legend
Farming area
Newly deforested area
Housing area
Catchment boundaries
Lake
Waste Disposal
Lacanau
Atlantic Coast
Sanguinet
1- Leyre
2- Landes
3- La Teste
4- Gujan
5- Tagon
6- Alguemorte
7- Renet
8- Betey
9- Cassy
10- Porge
11- Ciros
12- Lanton
13- Milieu
14- Passaduy
15- Ponteil
➢ Lagune côtière intertidale (174 km²)
➢ 4138 km² de BV plat, homogène et forestier (84%)
➢ 3000 km² de bassins hydrologiques directs (cours d'eau)

Site d'étude: la lagune d'Arcachon

- **Platier soumis aux marées** (semi-diurnes)
  - Zone intertidale (gris): 117 km²
  - Zone subtidale (blanc): 57km²
- **Les échanges sur 1 cycle de marée:**
  - Avec l'océan: 300.10^6 m³ = 200
  - Apports eaux douces: $1{,}5.10^6$ m³
- **TR: 12.8 ~ 15.9 jours**

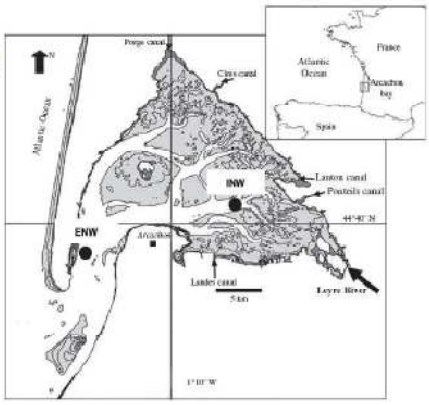

SYSTÈME HÉTÉROGÈNE BIEN MÉLANGÉ ET DYNAMIQUE, SOUMIS AUX INFLUENCES MARINES EN MAJORITÉ

Introduction générale | Résultats et Discussion (I) | Résultats et Discussion (II) | Synthèse et Perspectives

Site d'étude: la lagune d'Arcachon

- Sable sec de haute plage
- Sable sec
- Sable humide
- Sable très humide
- Sable très humide / m.o.
- Sable très humide / sous eau
- Sable sous eau
- Vase
- Vase à biofilm
- Zostères très peu denses
- Zostères peu denses
- Zostères densité moyenne
- Zostères dense
- Zostères très denses
- Spartine
- Spartine / schorre
- Schorre
- Végétation extérieure
- Eau

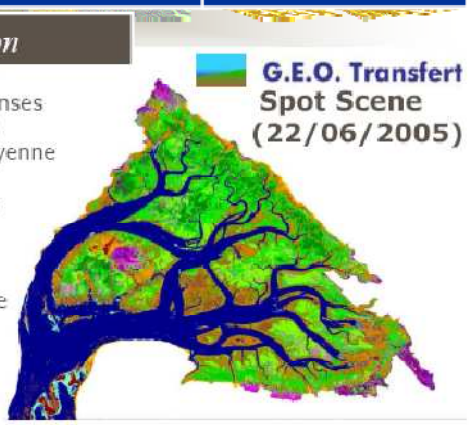

- Les différents ensembles du platier tidal:

Site d'étude: la lagune d'Arcachon

- Producteurs primaires benthiques et pélagiques:
  - *Zostera noltii* (127-181 g C m^{-2} an^{-1}) (Auby, 1991)
  - Microphytobenthos (104-114 g C m^{-2} an^{-1}) (Auby, 1991)
  - *Zostera marina*, Macroalgues, Plantes halophytes
  - Phytoplancton (103 g C m^{-2} an^{-1}) (Glé et al., 2008)

Introduction générale | Résultats et Discussion (I) | Résultats et Discussion (II) | Synthèse et Perspectives

MATERIELS ET METHODES

1. Dynamique et Apport de C par les rivières:

- ***Suivi annuel de février 2008 à février 2009***

2. Mesure des échanges de CO_2 entre la lagune d'Arcachon et l'atmosphère:

- ***Technique d'Eddy Covariance***
  - *Septembre/Octobre 2007*
  - *Juillet 2008*
  - *Septembre/Octobre 2008*
  - *Avril 2009*

Introduction générale | Résultats et Discussion (I) | Résultats et Discussion (II) | Synthèse et Perspectives

PARTIE I

DYNAMIQUE, EXPORT ET DÉGAZAGE DE CARBONE TERRESTRE VERS LA LAGUNE DEPUIS LES EAUX DE RIVIÈRE DE SON BASSIN VERSANT

Introduction générale | Résultats et Discussion (I) | Résultats et Discussion (II) | Synthèse et Perspectives

Stratégie d'échantillonnage des eaux de rivières du bassin versant

- Suivi 9 rivières (1 an)

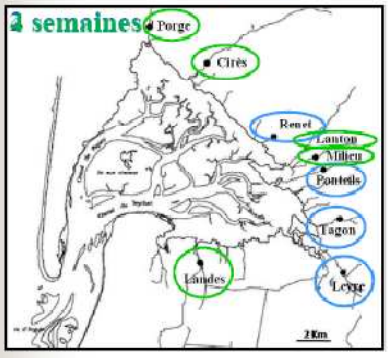

	Surface (km^2)	Runoff ($m^3 s^{-1}$)
Porge (Arès)	221.6	3.63
Cirès (Andernos)	48.7	0.63
Renet (Lanton)	17.9	0.61
Lanton (Lanton)	36.1	0.28
Milieu (Audenge)	21.3	0.63
Ponteils (Audenge)	23.3	0.23
Tagon (Biganos)	29.6	0.67
Leyre (Biganos)	2141.4	18.16
Landes (Gujan-Mestras)	116.6	0.52
Total	2656.5	25.34

- 1 rivière: La Leyre (4/5 des apports)
- 2 canaux: Lacs Lacanau et Cazaux → Lagune
- 6 ruisseaux
- 88% de la surface et 80% des débits échantillonnés

Stratégie d'échantillonnage des eaux de rivières du bassin versant

- Mesures des différentes formes du carbone et des paramètres associés
- Echantillonnages in situ et analyses en laboratoire
  - CARBONE INORGANIQUE: pCO_2, TA (= HCO_3^-), $\delta^{13}C$-DIC
  - CARBONE ORGANIQUE: DOC, POC, $\delta^{13}C$-POC, C/N
  - PARAMETRES ASSOCIES: MES, Chl *a*, T, …

Introduction générale | Résultats et Discussion (I) | Résultats et Discussion (II) | Synthèse et Perspectives

- Caractéristiques des cours d'eau: similitudes et différences

* Valeur faible
* Valeur élevée

• Podzols tempérés	COD ~ 4 à 11 mg L^{-1}
• Bassin versant de basse altitude • Taux d'érosion faibles • Eaux peu turbides	MES ~ 3 à 13 mg L^{-1} COP ~ 0.6 à 2.5 mg L^{-1} COP-% ~ 17.7 à 24.3%
• POC allochtone: sols et plantes terrestres en C_3 • Contribution du phytoplancton faible	Chl *a* ~ 0.4 à 5 µg L^{-1} C/N ~ 12 à 20 $\delta^{13}C$-COP ~ -29.2 à -28.1‰ COP /Chl *a* ~ 580 à 4220
• Prédominance des roches silicatées , eaux acides • CO_2 : respiration terrestre + eaux souterraines	pCO_2 ~ 1600 à 6500 ppmv TA ~ 0.104 à 0.55 mmol L^{-1} pH ~ 6.09 à 7.03 $\delta^{13}C$-DIC ~ -20.4 à -13.3‰

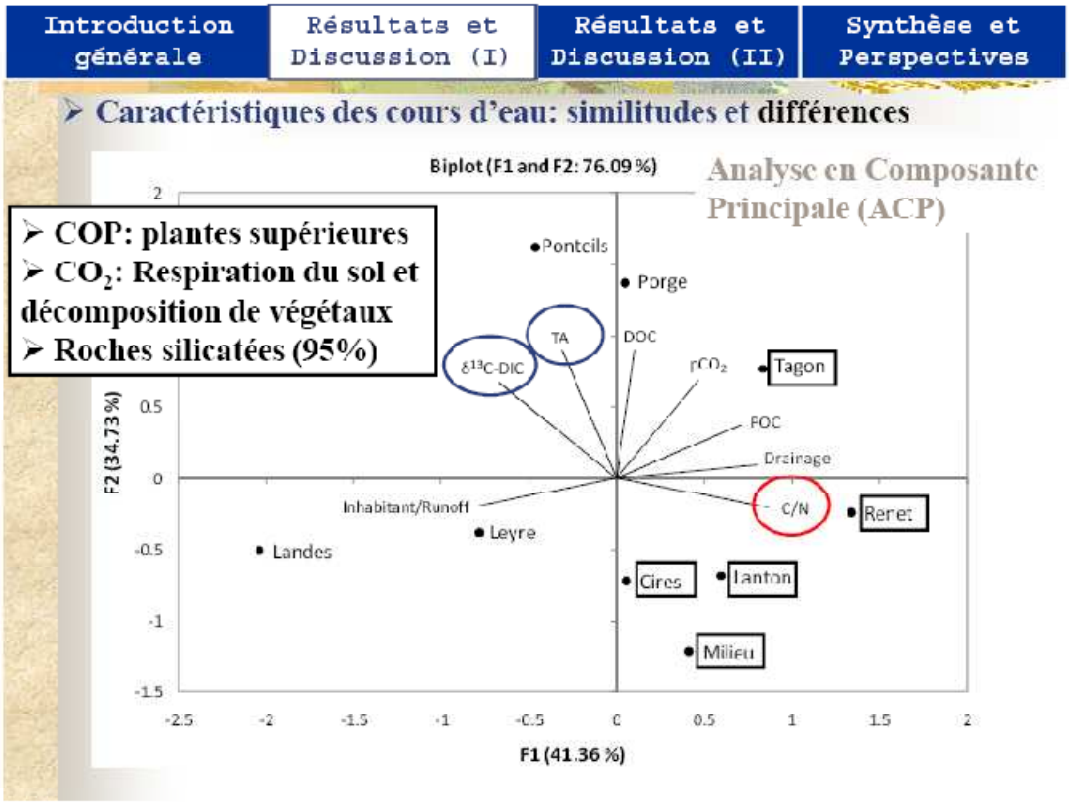
Introduction générale
Résultats et Discussion (I)
Résultats et Discussion (II)
Synthèse et Perspectives
Caractéristiques des cours d'eau: similitudes et différences
Biplot (F1 and F2: 76.09 %)
Analyse en Composante Principale (ACP)
COP: plantes supérieures
CO_2: Respiration du sol et décomposition de végétaux
Roches silicatées (95%)
Pontcils
Porge
TA
DOC
δ^{13}C-DIC
pCO_2
Tagon
FOC
Drainage
Inhabitant/Runoff
C/N
Rere
Leyre
Landes
Cires
Lanton
Milieu
F2 (34.73 %)
F1 (41.36 %)

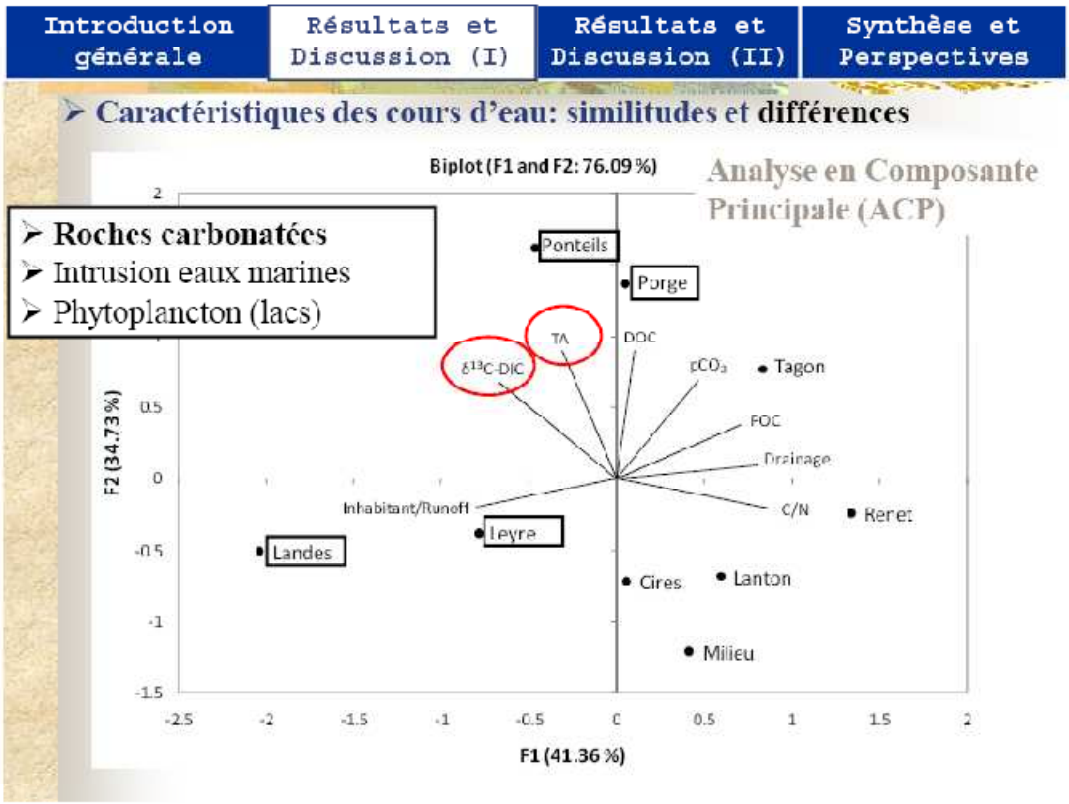
Introduction générale
Résultats et Discussion (I)
Résultats et Discussion (II)
Synthèse et Perspectives
Caractéristiques des cours d'eau: similitudes et différences
Biplot (F1 and F2: 76.09 %)
Analyse en Composante Principale (ACP)
Roches carbonatées
Intrusion eaux marines
Phytoplancton (lacs)
Ponteils
Porge
TA
DOC
δ^{13}C-DIC
pCO_2
Tagon
FOC
Drainage
Inhabitant/Runoff
C/N
Rere
Leyre
Landes
Cires
Lanton
Milieu
F2 (34.73 %)
F1 (41.36 %)

➢ Caractéristiques des cours d'eau: similitudes et différences

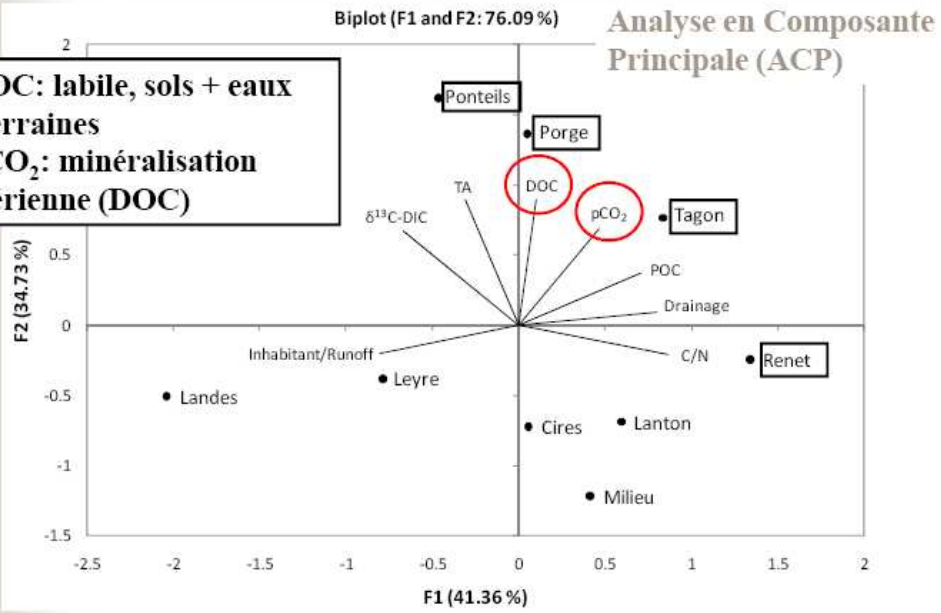

➢ Variations temporelles, saisonnières du carbone dans les cours d'eau

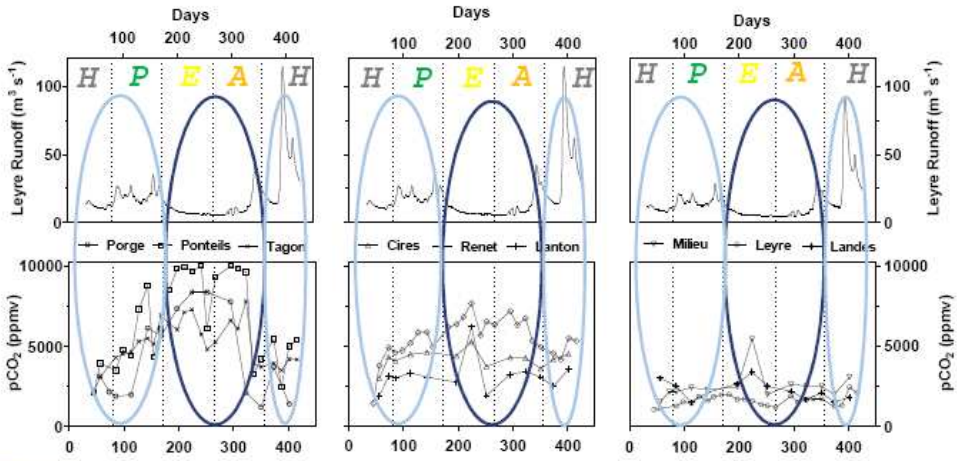

→ En général, les paramètres du DIC ↑ en été-automne et ↓ en hiver-printemps

➢ Variations temporelles, saisonnières du carbone dans les cours d'eau

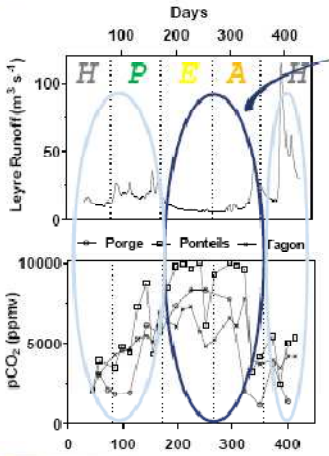

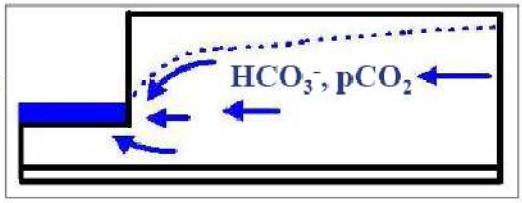

(1) La nappe alimente la rivière (décharge)

Introduction générale | Résultats et Discussion (I) | Résultats et Discussion (II) | Synthèse et Perspectives

➢ Variations temporelles, saisonnières du carbone dans les cours d'eau

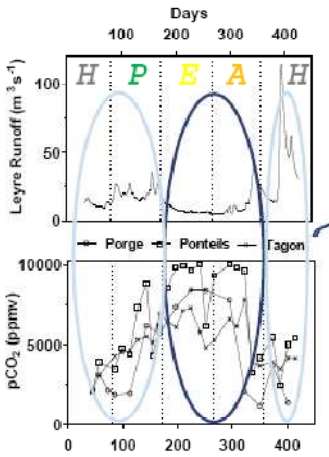

(2) La rivière alimente la nappe (recharge)

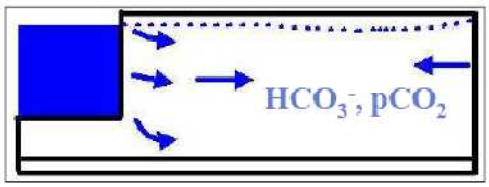

➢Export et dégazage du carbone terrestre depuis les eaux de rivière

- « StreamCO$_2$-DEGAS » → Bilan de masse et Equilibration isotopique air/eau
- Estimation du dégazage de CO$_2$ depuis les rivières vers l'atmosphère à partir de pCO$_2$, TA et δ^{13}C-DIC mesurés *in situ*
- Appliqué et validé sur 3 rivières
- Hypothèses: eaux acides (4.7-7.2) et non productives (Chl *a* < 4 ug L^{-1})
- L'idée: au fur et à mesure du dégazage, δ^{13}C-DIC ↑ et pCO$_2$ ↓

Introduction générale | Résultats et Discussion (I) | Résultats et Discussion (II) | Synthèse et Perspectives

➢Export et dégazage du carbone terrestre depuis les eaux de rivière

• Principe du modèle "StreamCO$_2$-DEGAS"

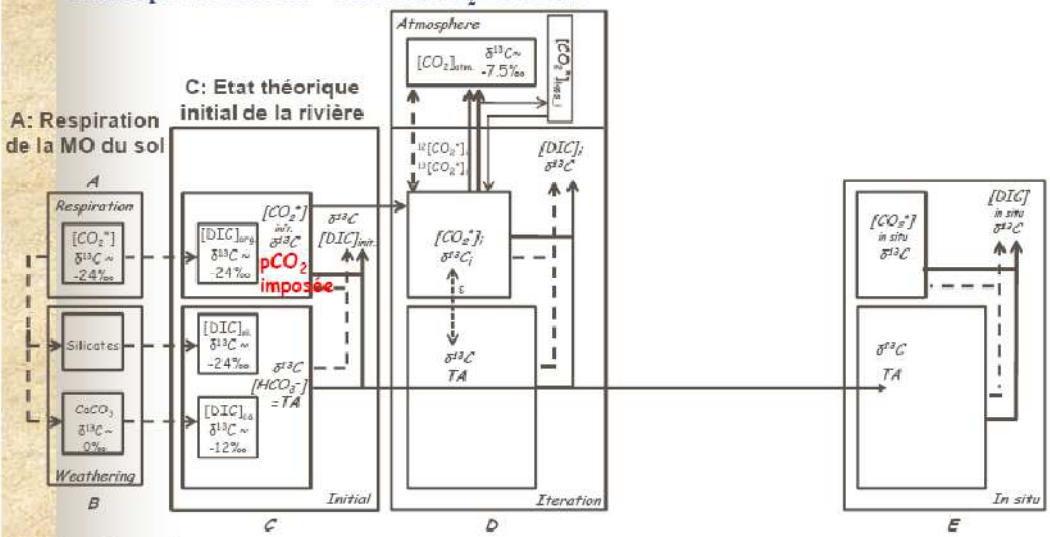

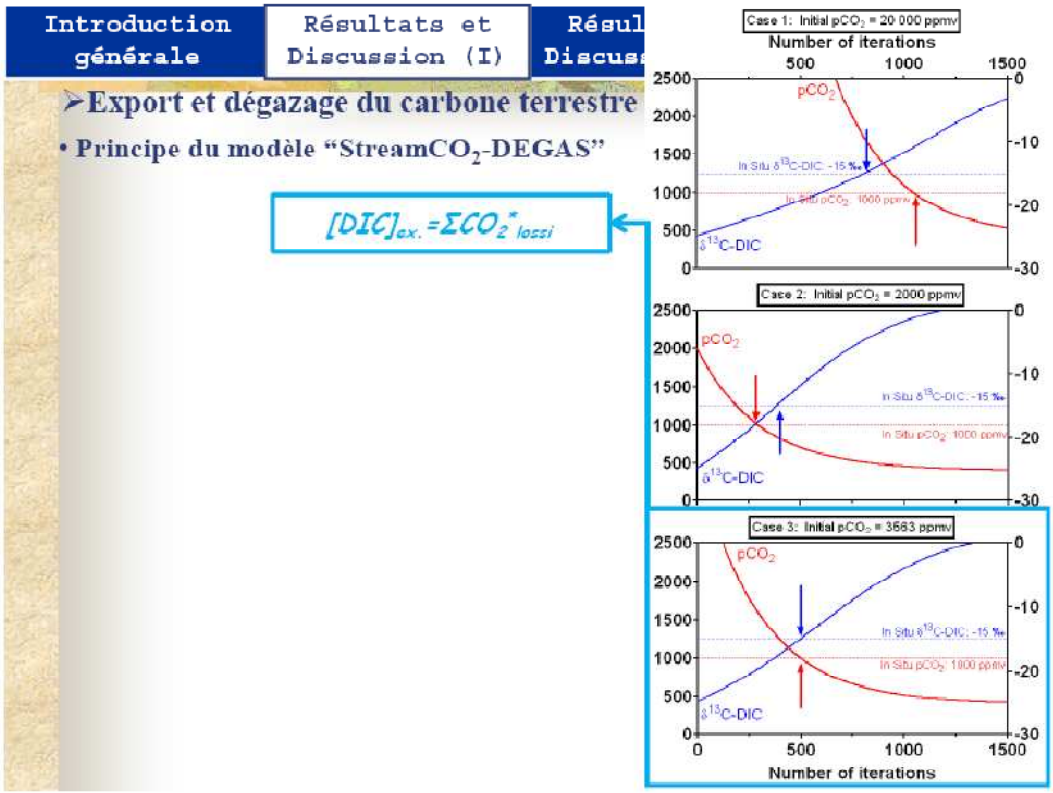
Introduction générale
Résultats et Discussion (I)
Résul
Discuss
➢Export et dégazage du carbone terrestre
• Principe du modèle "StreamCO2-DEGAS"
[DIC]ex. =ΣCO2* lossi
Case 1: Initial pCO2 = 20 000 ppmv
Number of iterations
pCO2
δ13C-DIC
Case 2: Initial pCO2 = 2000 ppmv
Case 3: Initial pCO2 = 3583 ppmv
0
500
1000
1500
2000
2500
-10
-20
-30

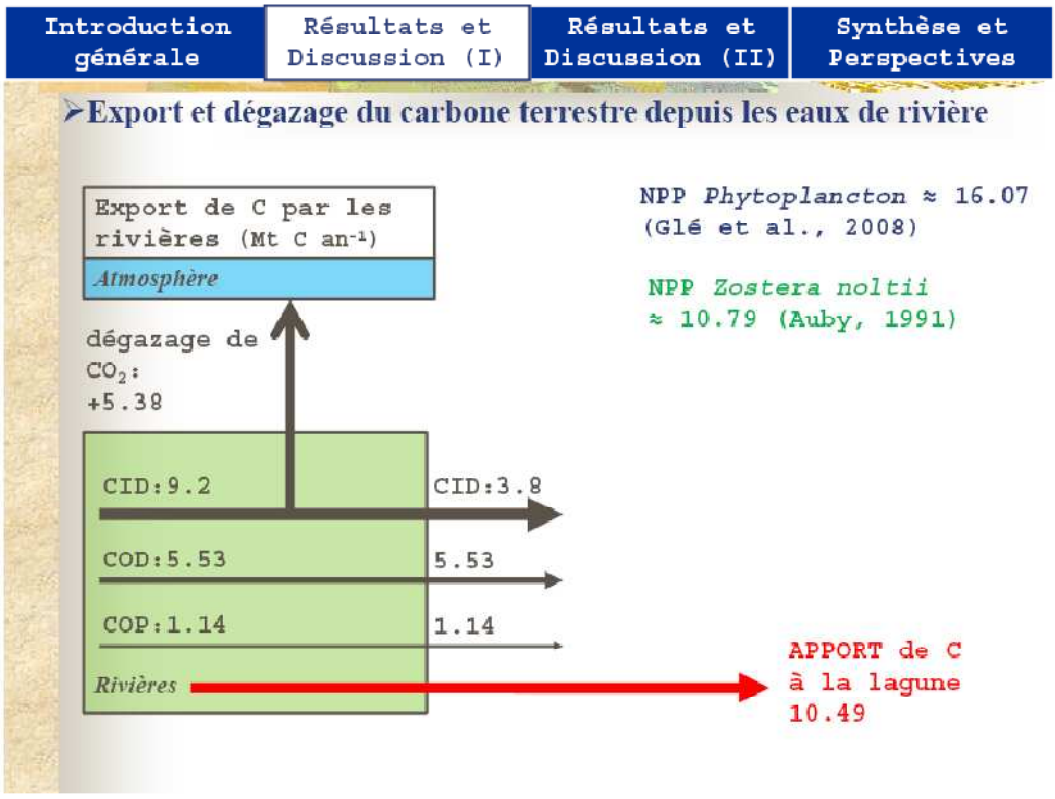
Introduction générale
Résultats et Discussion (I)
Résultats et Discussion (II)
Synthèse et Perspectives
➢Export et dégazage du carbone terrestre depuis les eaux de rivière
Export de C par les rivières (Mt C an-1)
Atmosphère
dégazage de CO2: +5.38
CID:9.2
CID:3.8
COD:5.53
5.53
COP:1.14
1.14
Rivières
NPP Phytoplancton ≈ 16.07 (Glé et al., 2008)
NPP Zostera noltii ≈ 10.79 (Auby, 1991)
APPORT de C à la lagune 10.49

PARTIE II

MESURE DES FLUX VERTICAUX DE CO_2 PAR EDDY COVARIANCE DANS LA LAGUNE D'ARCACHON

Introduction générale | Résultats et Discussion (I) | Résultats et Discussion (II) | Synthèse et Perspectives

➢ **Introduction à la technique d'Eddy Covariance (EC)**

→ Mesure et calcul de **flux turbulents** dans la **couche limite atmosphérique**

• Le **flux** d'air → flux horizontal d'eddy rotatifs (3D) de ≠ tailles et fréquences (composante verticale).

• Les tourbillons se forment dans la **couche limite**:

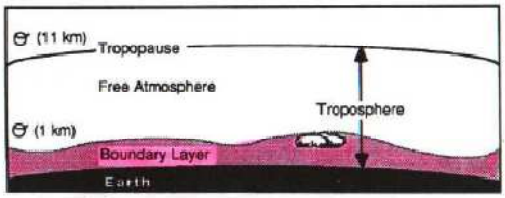

➢ Introduction à la technique d'Eddy Covariance (EC)

• Processus responsables de la turbulence:

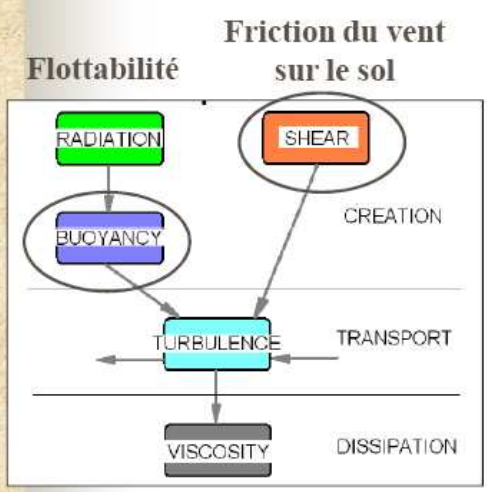

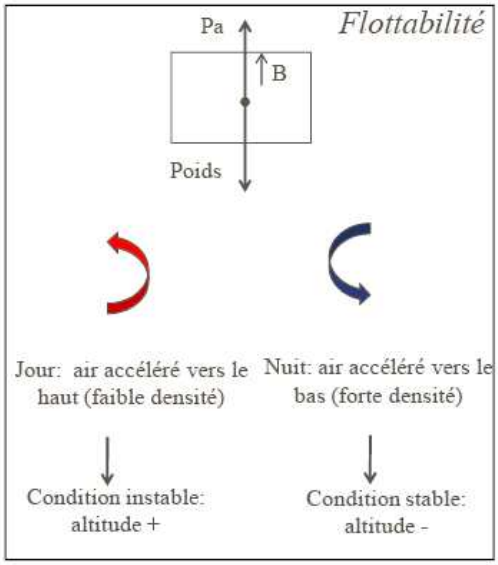

Introduction générale | Résultats et Discussion (I) | Résultats et Discussion (II) | Synthèse et Perspectives

➢ Introduction à la technique d'Eddy Covariance (EC)

• Exemple de signal turbulent:

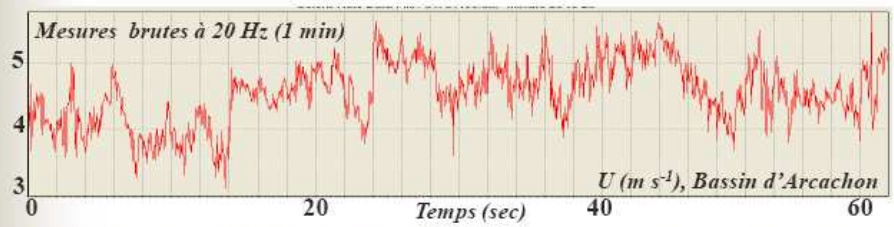

→ Irrégulier, quasi-aléatoire mais :

Transformation du Temps → Fréquence

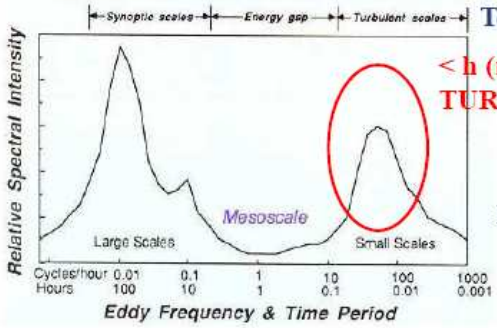

< h (min, sec)
TURBULENCE

Différentes échelles

➢ Introduction à la technique d'Eddy Covariance (EC)

• Le flux turbulent vertical moyen:

Covariance entre les fluctuations de la vitesse verticale du vent (w') et celles de la concentration du scalaire en question (ρ_c') (i.e. CO_2).

$$F_c = \overline{w' \rho_c'}$$

Avec x' = x – $\overline{x}$ (Décomposition de Reynolds d'une valeur instantanée (x) en une moyenne ($\overline{x}$) et une fluctuation (x'))

• **Sous-entend un certain nombre d'hypothèses:**

- Mesure dans la CL et l'aire d'intérêt
- Stationnarité
- Terrain horizontal et homogène › flux verticaux indépendants de la hauteur, fluctuations de densité négligeables

Introduction générale | Résultats et Discussion (I) | Résultats et Discussion (II) | Synthèse et Perspectives

➢ Le système d'Eddy Covariance (EC) dans le bassin d'Arcachon

• Mesures à très **haute fréquence**, en **continu** aux **interfaces air/eau** et **air/sédiment**, de manière **non intrusive** à l'**échelle de l'écosystème**

(1) *CSAT3*: U_x, U_y, U_z (m s^{-1}) / 20Hz

(2) *Licor 7500*: [CO_2], [H_2O] (mmol m^{-3}) / 20Hz

(3) *SKP215*: PAR (µmol.m^{-2}.s^{-1}) / 60sec.

(4) Vaisala *WXT510*: vent, température, humidité, pluie… / 60sec.

➢ Le système d'Eddy Covariance (EC) dans le bassin d'Arcachon

Automne 2008
25 septembre au 17 octobre 2008
(Station 1)

N 44 42'59.15
W 01 08'36.96

Eté 2008
01 au 7 juillet 2008
(Station 1)

Printemps 2009
01 au 13 avril 2009
(Station 1)

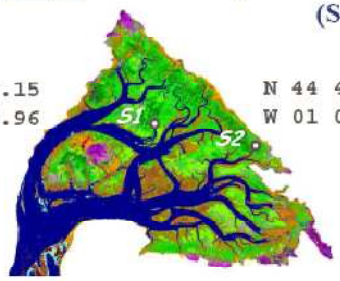

Automne 2007
30 septembre au 03 octobre 2007
(Station 2)

N 44 42'19.96
W 01 04'01.35

➢ Obtention de données haute fréquence et validation de la technique dans la lagune d'Arcachon

Déploiement du système sur le terrain, traitement du signal, analyse des données.

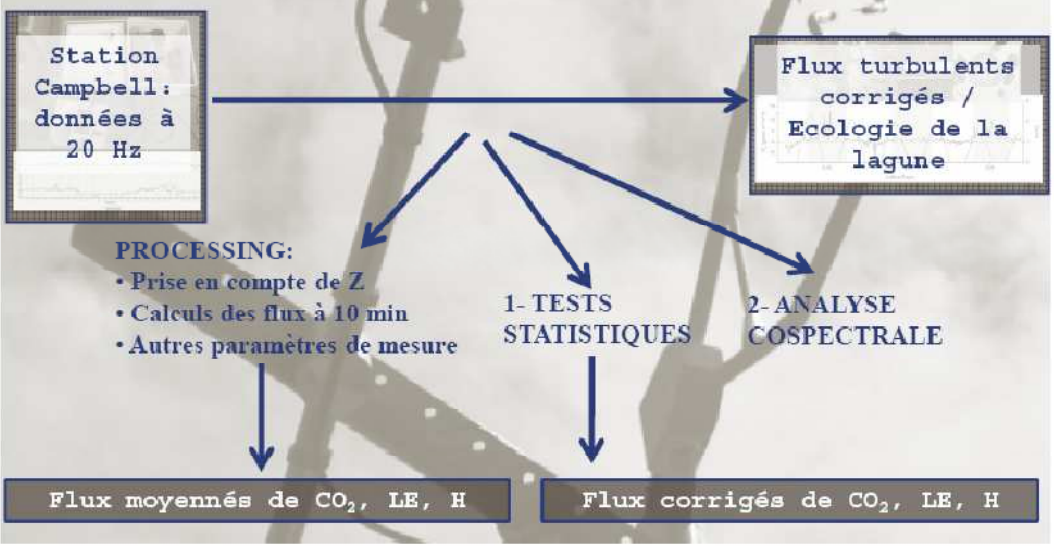

➢ **Traitement de données et validation de l'EC**

1- Données corrigées ← Tests de stationnarité (Foken and Wichura, 1996) et des caractéristiques de turbulence intégrée (Foken et al., 1991)

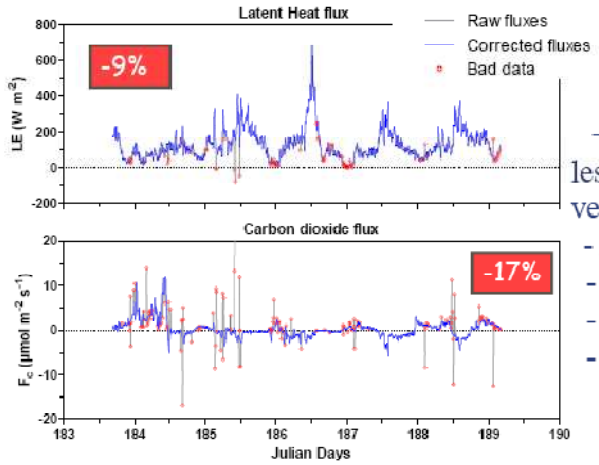

→ Peu de données biaisées sur les séries de mesure. Pour les flux verticaux de CO_2:
- Automne 2007 (St. 2): 27%
- Été 2008 (St. 1): 17%
- Automne 2008 (St. 1): 17%
- Printemps 2009 (St. 1): 13%

Introduction générale | Résultats et Discussion (I) | Résultats et Discussion (II) | Synthèse et Perspectives

➢ **Traitement de données et validation de l'EC**

2- Analyse cospectrale → Principe

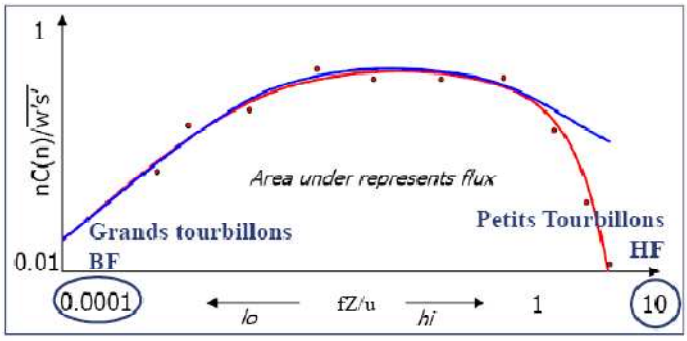

- **La distribution de la covariance de w' et s' par fréquence (Fourier transformation).**
- **L'aire sous la courbe ≈ flux mesuré**
- **La quantité de flux transporté à chaque fréquence (perte en HF ou BF)**

➢ Traitement de données et validation de l'EC

2- Analyse cospectrale: Hauteur de mesure

Mesure haute

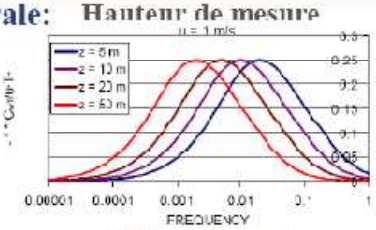

Mesure près de la surface

Vitesse de vent

Tourbillons grands et lents

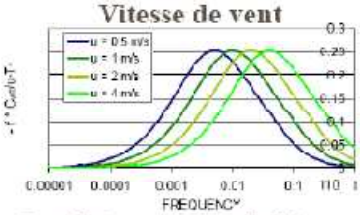

Tourbillons petits et rapides

Conditions atmosphériques

Instabilité
(i.e. journée ensoleillée calme)

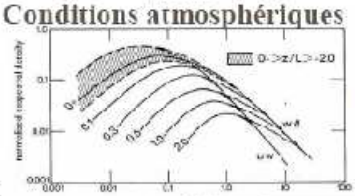

Stabilité
(i.e. nuit claire et calme)

BASSE FREQUENCE ⟷ HAUTE FREQUENCE

Introduction générale | Résultats et Discussion (I) | Résultats et Discussion (II) | Synthèse et Perspectives

➢ Traitement de données et validation de l'EC

2- Analyse cospectrale:

Juillet 2008

Bien définis et similaires aux HF: *f* et *Z* adéquates

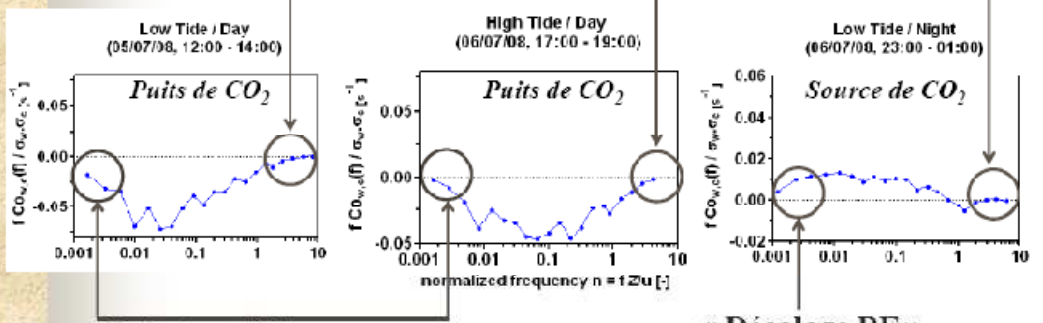

Décalage BF
→ Instabilité atmosphérique
→ Larges structures convectives
→ Pertes mineures à BM le jour (Z)

« Décalage BF »
→ Hétérogénéité spatiale

➢ Échanges de CO_2 / Fonctionnement écologique de la lagune

• Dynamique temporelle des flux de CO_2 avec l'atmosphère

Juillet 2008 (St.1)

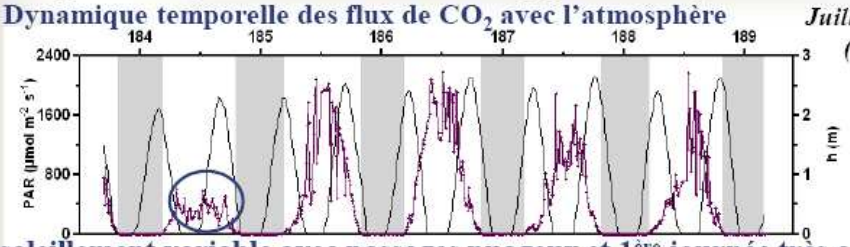

Ensoleillement variable avec passages nuageux et 1ère journée très couverte / émersion ≈ 4h – immersion ≈ 9h

Introduction générale | Résultats et Discussion (I) | Résultats et Discussion (II) | Synthèse et Perspectives

➢ Échanges de CO_2 / Fonctionnement écologique de la lagune

• Dynamique temporelle des flux de CO_2 avec l'atmosphère

Juillet 2008 (St.1)

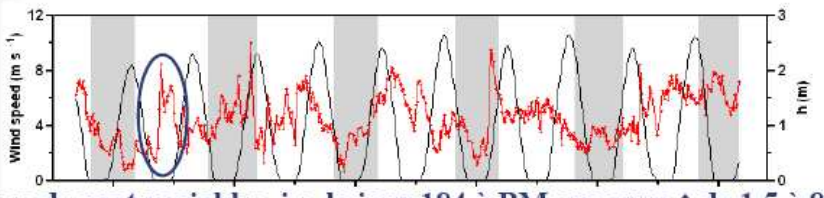

Vitesses de vent variables, i.e. le jour 184 à BM avec une ↑ de 1.5 à 8.5 m s^{-1}

➢ Échanges de CO_2 / Fonctionnement écologique de la lagune

• Dynamique temporelle des flux de CO_2 avec l'atmosphère

Juillet 2008 (St.1)

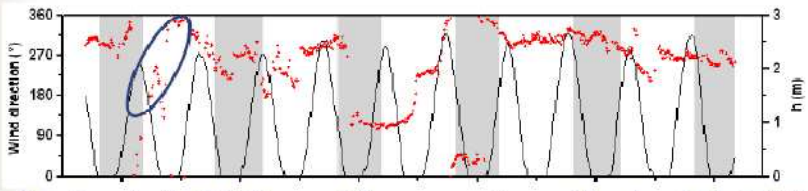

Vents dominants de ONO avec Changements rapides, i.e. 184: OSO → NNO

Introduction générale | Résultats et Discussion (I) | Résultats et Discussion (II) | Synthèse et Perspectives

➢ Échanges de CO_2 / Fonctionnement écologique de la lagune

• Dynamique temporelle des flux de CO_2 avec l'atmosphère

Conditions perturbées:

F_c → POSITIFS
DESTOCKAGE (physique)

A Basse Mer, la Nuit
F_c POSITIFS → SOURCES DE CO_2

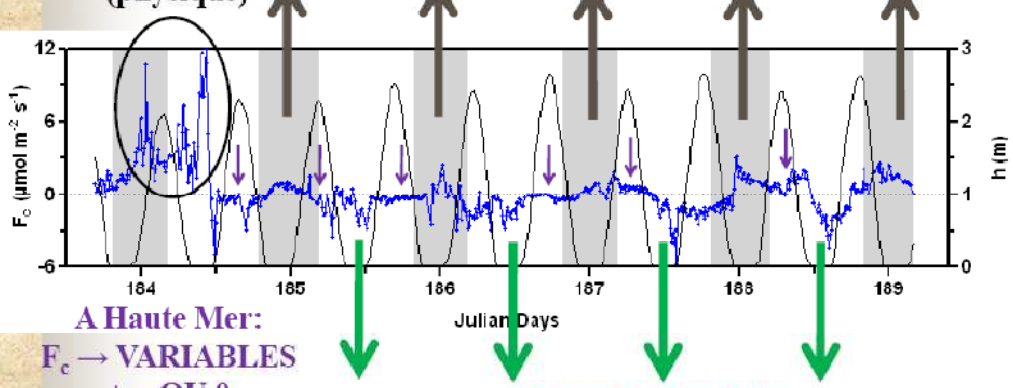

A Haute Mer:
F_c → VARIABLES
+, - OU 0
EFFET LIMITANT

A Basse Mer, le Jour:
F_c NEGATIFS → PUITS DE CO_2

➢ Échanges de CO_2 / Fonctionnement écologique de la lagune

• Dynamique temporelle des flux de CO_2 avec l'atmosphère

SOURCES DE CO_2

F_c ($\mu mol\ m^{-2}\ s^{-1}$)	BM/Jour		BM/Nuit		HM/Jour		HM/Nuit	
September/October 2007 (Station 2)	-1.66	1.70	2.73	3.67	0.42	1.06	1.88	2.38
July 2008 (Station 1)	-0.31	3.29	0.94	0.81	-0.20	1.38	0.75	1.93
September/October 2008 (Station 1)	-0.71	2.27	0.19	1.07	-0.14	0.66	-0.27	1.32
April 2009 (Station 1)	-2.67	1.99	-1.30	1.37*	-1.71	1.45	-3.17	2.36

PUITS DE CO_2

Introduction générale | Résultats et Discussion (I) | Résultats et Discussion (II) | Synthèse et Perspectives

➢ Échanges de CO_2 / Fonctionnement écologique de la lagune

• Dynamique temporelle des flux de CO_2 avec l'atmosphère

F_c ($\mu mol\ m^{-2}\ s^{-1}$)	BM/Jour		BM/Nuit		HM/Jour		HM/Nuit	
September/October 2007 (Station 2)	-1.66	1.70	2.73	3.67	0.42	1.06	1.88	2.38
July 2008 (Station 1)	-0.31	3.29	0.94	0.81	-0.20	1.38	0.75	1.93
September/October 2008 (Station 1)	-0.71	2.27	0.19	1.07	-0.14	0.66	-0.27	1.32
April 2009 (Station 1)	-2.67	1.99	-1.30	1.37*	-1.71	1.45	-3.17	2.36

PUITS-SOURCES

Dynamique des communautés phytoplanctoniques (Glé et al., 2007 et 2008)

➢ Échanges de CO_2 / Fonctionnement écologique de la lagune

• Dynamique temporelle des flux de CO_2 avec l'atmosphère

F_c ($\mu mol\ m^{-2}\ s^{-1}$)	BM/Jour		BM/Nuit		HM/Jour		HM/Nuit	
September/October 2007 (Station 2)	-1.66	1.70	2.73	3.67	0.42	1.06	1.88	2.38
July 2008 (Station 1)	-0.31	3.29	0.94	0.81	-0.20	1.38	0.75	1.93
September/October 2008 (Station 1)	-0.71	2.27	0.19	1.07	-0.14	0.66	-0.27	1.32
April 2009 (Station 1)	-2.67	1.99	-1.30	1.37*	-1.71	1.45	-3.17	2.36

VARIATIONS SPATIO-TEMPORELLES (F_c, GPP, CR, NCP, couvert herbier)

Introduction générale | Résultats et Discussion (I) | Résultats et Discussion (II) | Synthèse et Perspectives

➢ Échanges de CO_2 / Fonctionnement écologique de la lagune

Couplage simultané image satellite / Flux de CO_2 par EC

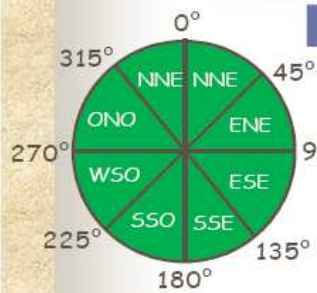

Couvert de *Zostera noltii* par secteurs de vent

Marée Basse Jour

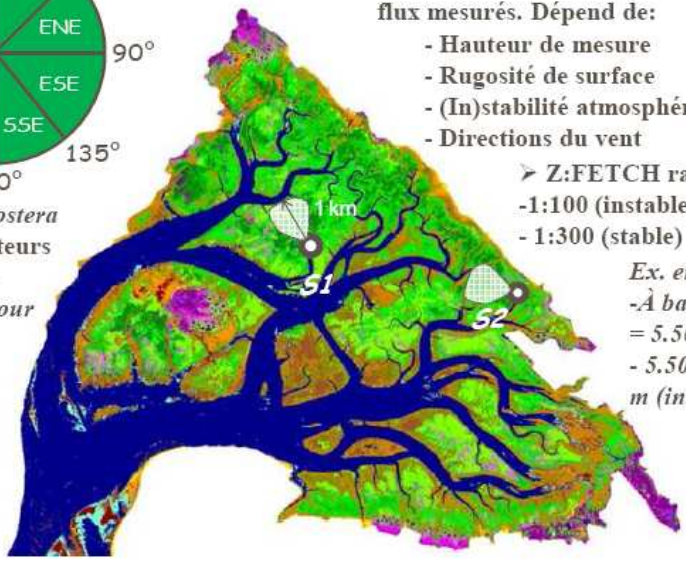

FOOTPRINT: zone représentative des flux mesurés. Dépend de:

- Hauteur de mesure
- Rugosité de surface
- (In)stabilité atmosphérique
- Directions du vent

➢ Z:FETCH ratio

-1:100 (instable)

- 1:300 (stable)

Ex. en juillet 2008,

-À basse mer, Z_{max} = 5.50 m

- 5.50:500 m < 1000 m (instable)

➢ Échanges de CO_2 / Fonctionnement écologique de la lagune

• Variations spatiales

▪ Forte différence spatiale dans le couvert de *Zostera noltii* entre les deux stations en Automne (au maximum de biomasse et densité).

92 10% — 17/10/2008 (Station 1) ≠ 22 14% — 13/09/2007 (Station 2)

▪ Aux deux stations: changements rapides des flux de CO_2 (NCP) avec la direction du vent et le couvert de l'herbier.

Introduction générale | Résultats et Discussion (I) | Résultats et Discussion (II) | Synthèse et Perspectives

➢ Échanges de CO_2 / Fonctionnement écologique de la lagune

• Variations spatiales

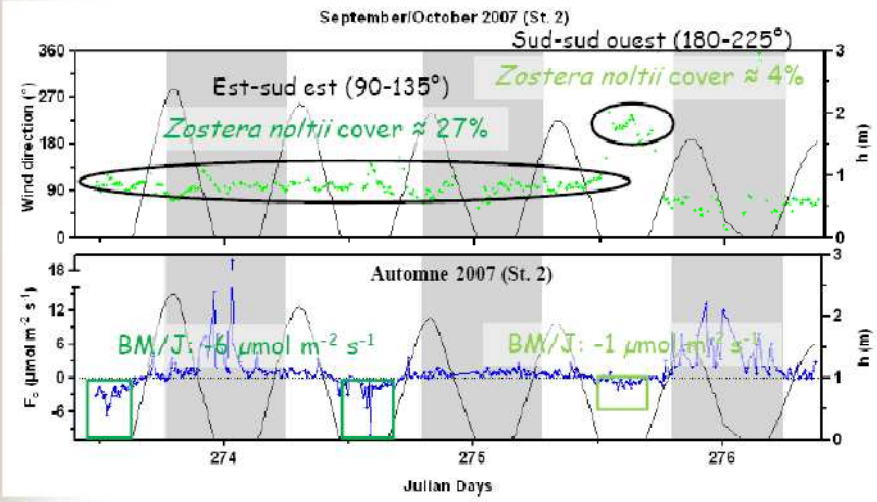

➢ Échanges de CO_2 / Fonctionnement écologique de la lagune

• Variations spatiales

- *Zostera noltii* → NCP Station 1 (Station 2)
- Partition NCP (-F_c à BM/J), CR (F_c à BM/N) et GPP: NCP = GPP - CR

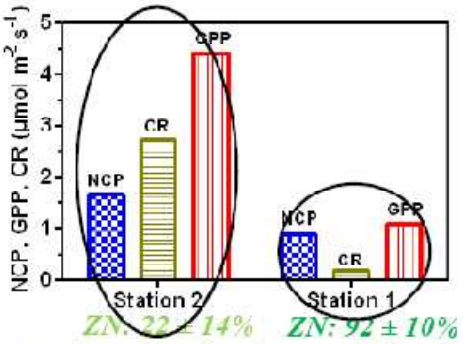

ZN: 22 ± 14% *ZN: 92 ± 10%*

- St. 2: Vase nue avec microphytobenthos → GPP et la CR (NCP)
- Source de MO labile → hétérotrophes benthiques

→ CYCLE METABOLIQUE RAPIDE DU MICROPHYTOBENTHOS, St. 2 (échelle tidale/semaine) ≠ CYCLE LONG DE ZN, St. 1 (saisonnière)

Introduction générale | Résultats et Discussion (I) | Résultats et Discussion (II) | Synthèse et Perspectives

➢ Échanges de CO_2 / Fonctionnement écologique de la lagune

• Variations saisonnières à la Station 1

- Prédominance de ZN (été et automne) + Contrôle de la NCP: 1.5 ± 1.2 (Juillet) et 0.9 ± 1.7 µmol m^{-2} s^{-1} (Sept-Oct.)

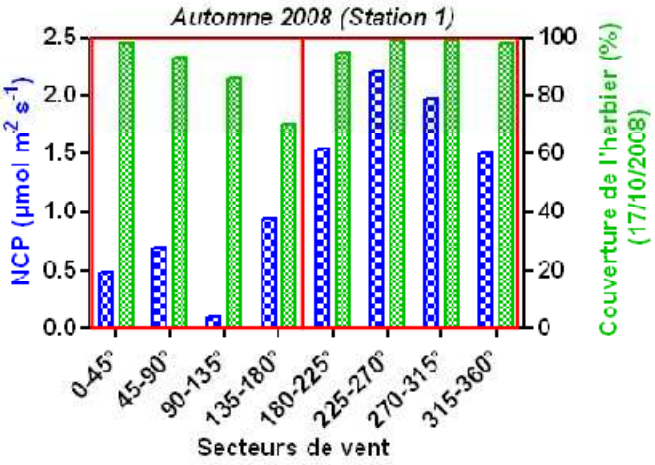

➢ Échanges de CO_2 / Fonctionnement écologique de la lagune

• Variations saisonnières à la Station 1

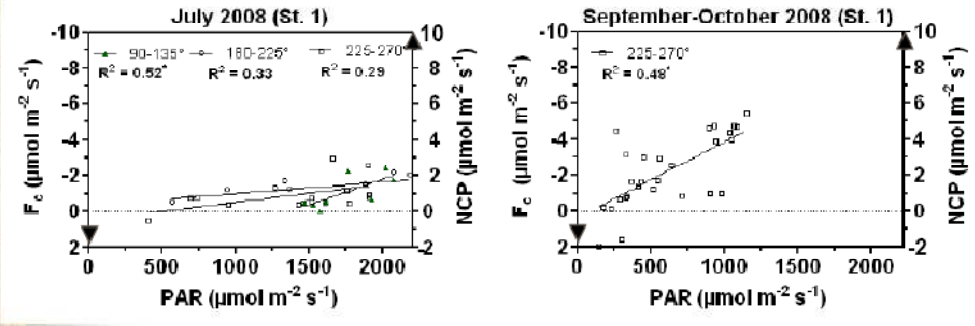

▪ Relations NCP/PAR positives ou F_c/PAR négatives → Adaptation herbier aux conditions environnementales de BM/Jour

Introduction générale | Résultats et Discussion (I) | Résultats et Discussion (II) | Synthèse et Perspectives

➢ Échanges de CO_2 / Fonctionnement écologique de la lagune

• Variations saisonnières à la Station 1

▪ Au printemps, NCP: 2.7 ± 1.2 µmol m^{-2} s^{-1} → ?

○ ZN ○ Microphytobenthos tapis

▪ % de couvert de ZN « élevé » mais:

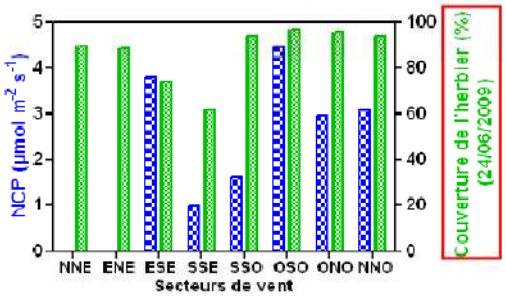

➢ Échanges de CO_2 / Fonctionnement écologique de la lagune

• Variations saisonnières à la Station 1

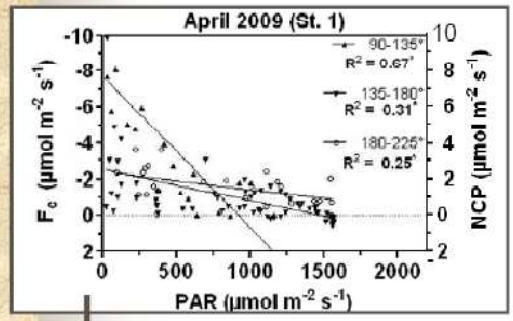

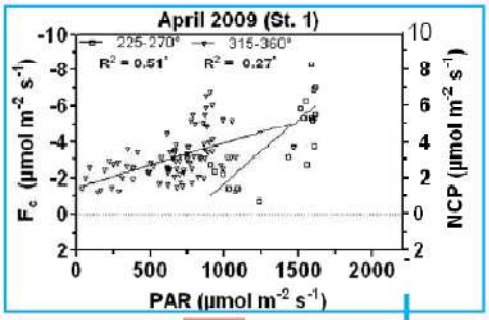

NCP/PAR - → Vase nue avec Microphytobenthos (Photo-acclimatation)

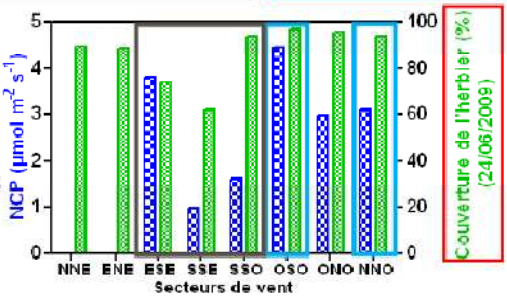

NCP/PAR + → *Zostera noltii*

Introduction générale | Résultats et Discussion (I) | Résultats et Discussion (II) | Synthèse et Perspectives

➢ Échanges de CO_2 / Fonctionnement écologique de la lagune

• Variations saisonnières à la Station 1

- Au printemps, NCP: 2.7 ± 1.2 µmol m^{-2} s^{-1} → ?
  - ZN
  - Microphytobenthos tapis
- % de couvert de ZN « élevé » mais:

Prédominance du microphytobenthos sur le sédiment et comme épiphytes sur les quelques pousses de ZN

APPORTS DE L'ÉTUDE SUR LE BUDGET DE CARBONE DE LA LAGUNE ET LES PERSPECTIVES POSSIBLES

Introduction générale | Résultats et Discussion (I) | Résultats et Discussion (II) | Synthèse et Perspectives

➢ Les apports de ce travail et les inconnues restantes

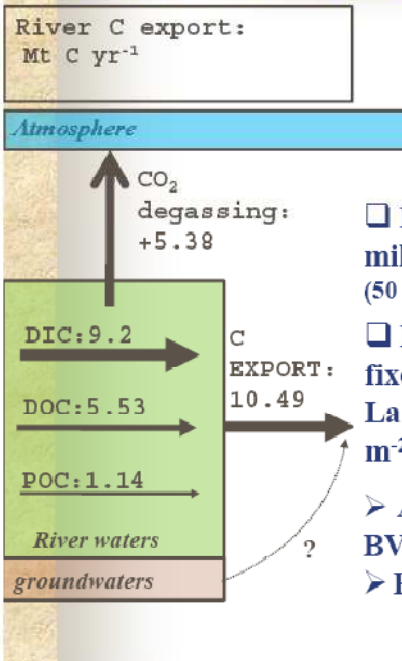

❑ Perte de C depuis le milieu terrestre vers le milieu aquatique: 115 g C m^{-2} an^{-1}
(50 vers l'atmosphère + 65 vers la lagune)

❑ Part significative (1/3) de la quantité de C fixée sur terre,
La forêt du Bray: fixation moyenne de 345 g C m^{-2} an^{-1}

➢ Affiner le bilan de C de la forêt landaise du BV

➢ Préciser les relations sol/nappe/rivière

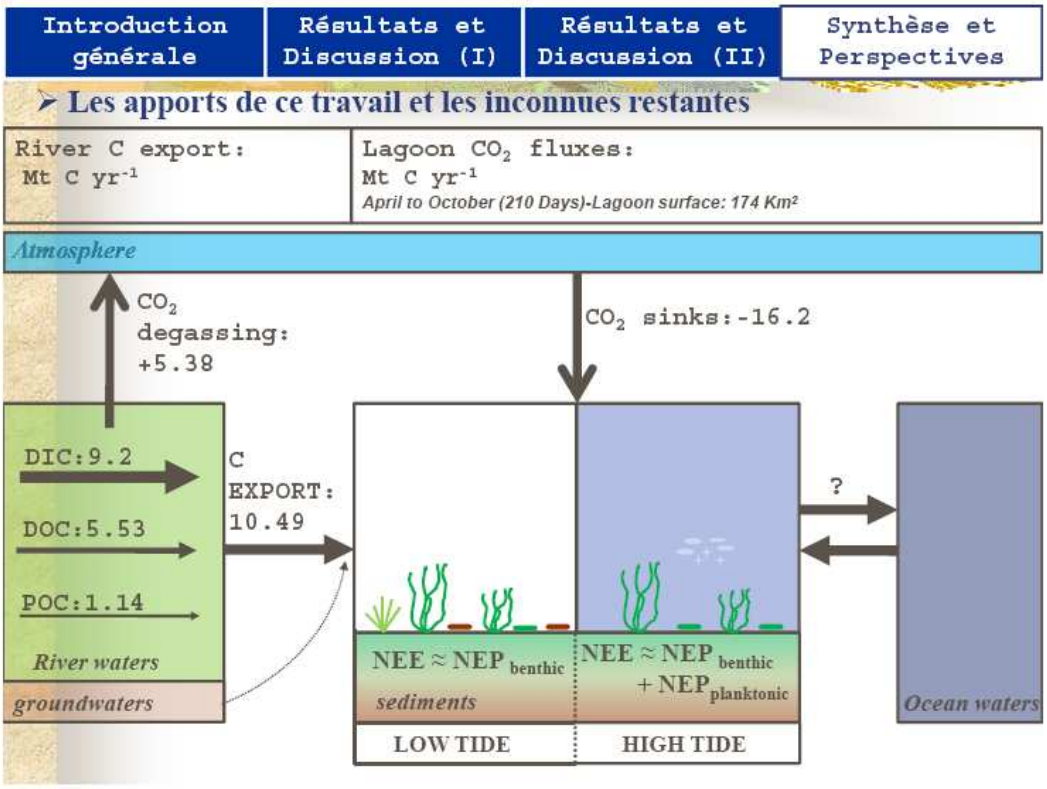
Introduction générale
Résultats et Discussion (I)
Résultats et Discussion (II)
Synthèse et Perspectives
Les apports de ce travail et les inconnues restantes
River C export: Mt C yr-1
Lagoon CO2 fluxes: Mt C yr-1
April to October (210 Days)-Lagoon surface: 174 Km²
Atmosphere
CO2 degassing: +5.38
CO2 sinks:-16.2
DIC:9.2
DOC:5.53
POC:1.14
River waters
groundwaters
C EXPORT: 10.49
NEE ≈ NEP benthic
sediments
NEE ≈ NEP benthic + NEP planktonic
?
Ocean waters
LOW TIDE
HIGH TIDE

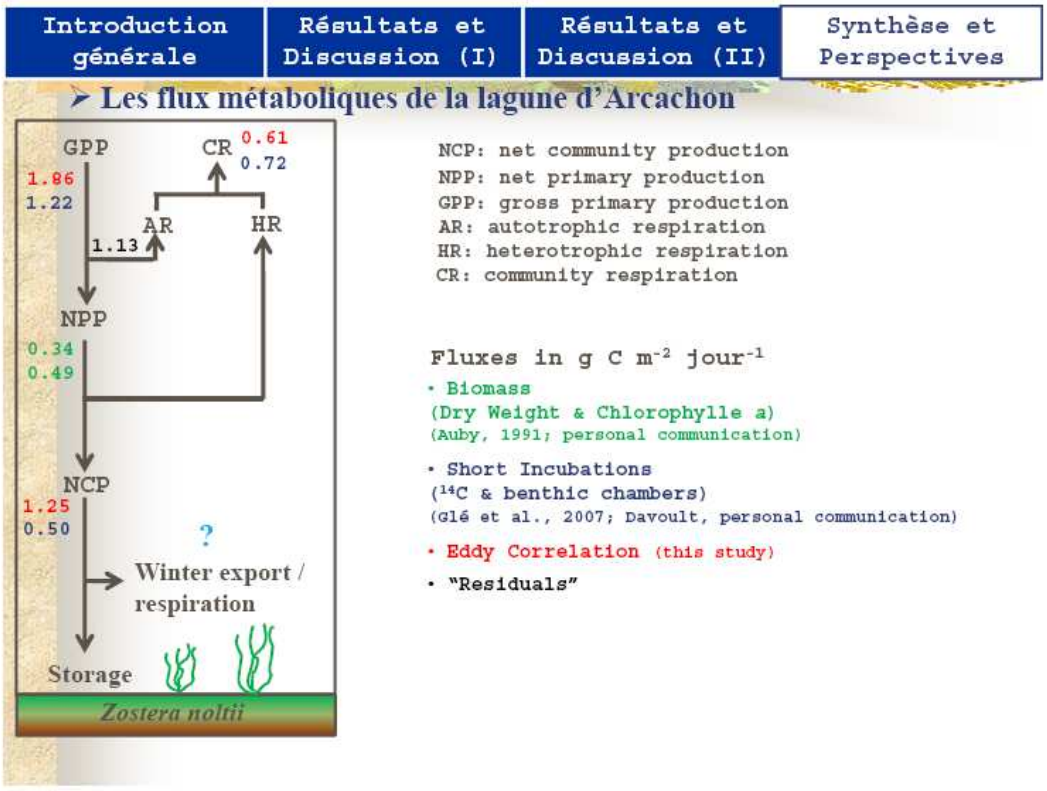
Introduction générale
Résultats et Discussion (I)
Résultats et Discussion (II)
Synthèse et Perspectives
Les flux métaboliques de la lagune d'Arcachon
GPP
1.86
1.22
CR 0.61 0.72
AR
HR
1.13
NPP
0.34
0.49
NCP
1.25
0.50
?
Winter export / respiration
Storage
Zostera noltii
NCP: net community production
NPP: net primary production
GPP: gross primary production
AR: autotrophic respiration
HR: heterotrophic respiration
CR: community respiration
Fluxes in g C m-2 jour-1
• Biomass
(Dry Weight & Chlorophylle a)
(Auby, 1991; personal communication)
• Short Incubations
(14C & benthic chambers)
(Glé et al., 2007; Davoult, personal communication)
• Eddy Correlation (this study)
• "Residuals"

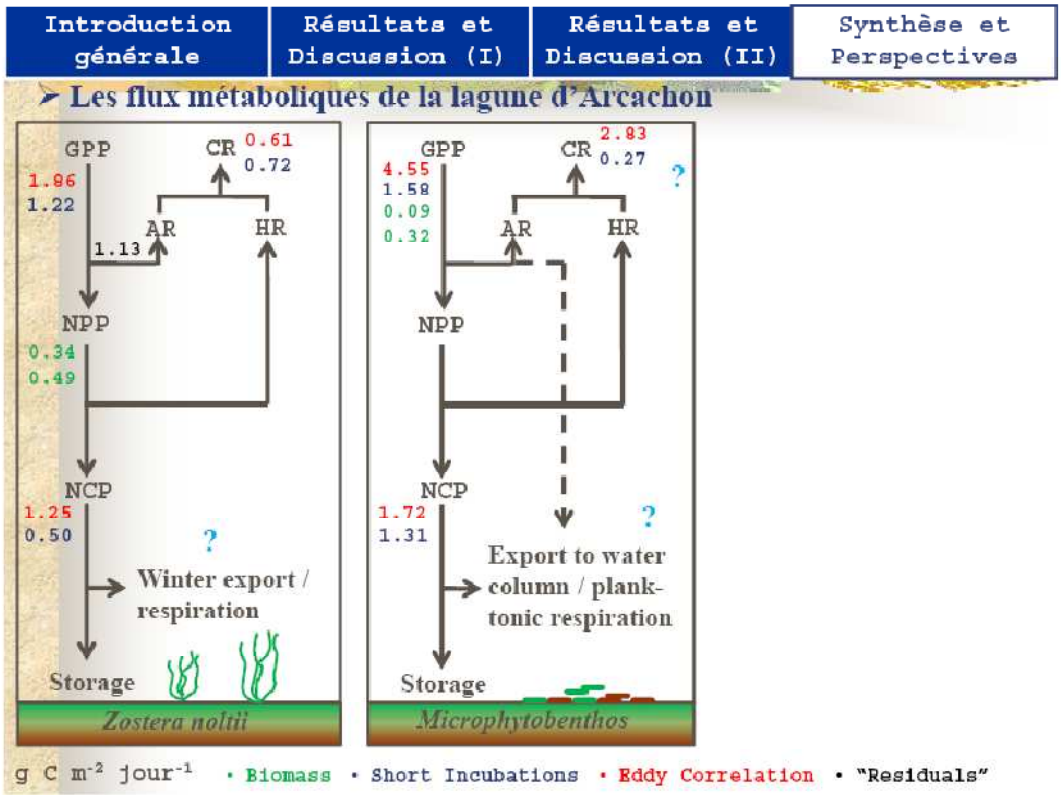
Introduction générale
Résultats et Discussion (I)
Résultats et Discussion (II)
Synthèse et Perspectives
Les flux métaboliques de la lagune d'Arcachon
GPP
CR
AR
HR
NPP
NCP
1.96
1.22
0.61
0.72
1.13
0.34
0.49
1.25
0.50
?
Winter export / respiration
Storage
Zostera noltii
4.55
1.58
0.09
0.32
2.93
0.27
1.72
1.31
Export to water column / planktonic respiration
Microphytobenthos
g C m-2 jour-1
• Biomass
• Short Incubations
• Eddy Correlation
• "Residuals"

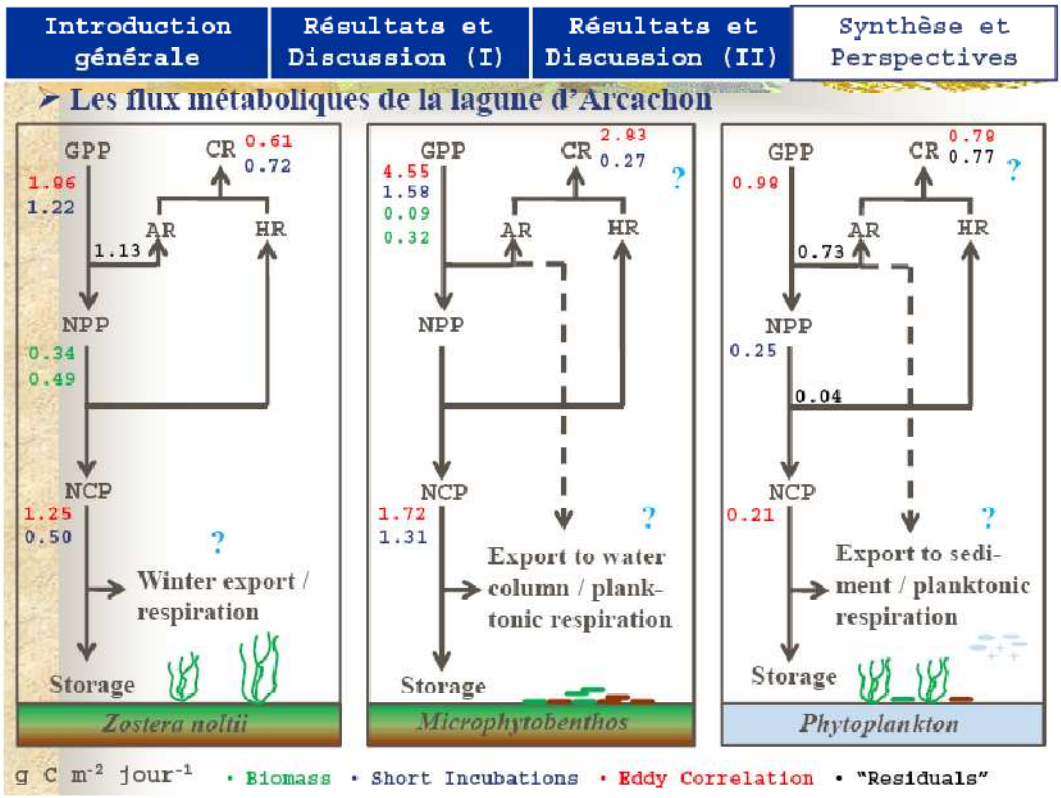
Introduction générale
Résultats et Discussion (I)
Résultats et Discussion (II)
Synthèse et Perspectives
Les flux métaboliques de la lagune d'Arcachon
GPP
CR
AR
HR
NPP
NCP
1.96
1.22
0.61
0.72
1.13
0.34
0.49
1.25
0.50
?
Winter export / respiration
Storage
Zostera noltii
4.55
1.58
0.09
0.32
2.93
0.27
1.72
1.31
Export to water column / planktonic respiration
Microphytobenthos
0.99
0.79
0.77
0.73
0.25
0.04
0.21
Export to sediment / planktonic respiration
Phytoplankton
g C m-2 jour-1
• Biomass
• Short Incubations
• Eddy Correlation
• "Residuals"

Introduction générale	Résultats et Discussion (I)	Résultats et Discussion (II)	Synthèse et Perspectives

- ❑ Echanges atmosphériques hivernaux
- ❑ Couplage entre ≠ méthodes
- ❑ La respiration planctonique
- ❑ Couplage EC atmosphérique et sous marine
- ❑ Station pérenne d'EC/image (herbier)
- ❑ Dynamique + échanges avec l'océan

ANNEXE 3 : Missions, communications et publications scientifiques

MISSIONS SCIENTIFIQUES

- ***Août-Septembre 2010***

CARBAMA (23 jours): Etude biogéochimique sur la dynamique et le cycle du carbone (CO_2, CH_4, DIC, DOC, POC, O_2, Chl *a*, Lipides, $\delta^{13}C$) dans le système Amazone (Brésil). Projet soutenu par l'ANR CARBAMA (Carbon Cycle in the Amazone River). Coordinateur: Gwenaël Abril.

- ***Mars 2008***

FORCLIM-PECH5 (10 jours): Etude géochimique et écologique de la colonne d'eau et des dépôts turbiditiques dans la baie de Biscay (France). Projet soutenu par l'ANR FORCLIM.

- ***Janvier 2008***

Protidal2 (5 jours): Etude biogéochimique des zones subtidale et intertidale du basin d'Arcachon (France). Projet soutenu par l'ANR PROTIDAL.

- ***Septembre-Octobre 2007***

PNEC-Bentidal-Meso Program (9 jours): Etude biogéochimique et microbiologique des zones subtidale et intertidale du basin d'Arcachon (France). Projet soutenu par le programme PNEC "Modes de fonctionnement des systèmes semi-fermés du littoral atlantique".

COMMUNICATIONS ORALES ET POSTERS

- ***Symposium international***

Polsenaere P. and Abril G. (2010) / Oral
A model to estimate CO_2 degassing from small acidic streams and rivers, based on pCO_2, DIC and $\delta^{13}C_{DIC}$. AGU Ocean Sciences Meeting 8-13 August.
Iguassu Falls/Brazil

Polsenaere P., Bretel P. and Abril G. (2008) / Poster
Atmospheric CO_2 exchanges in the Arcachon lagoon: an integrative measure of intertidal ecosystem metabolism. ASLO Summer Meeting, Interactions on the Edge, June 8-13, 2008.
St. John's, Newfoundland/Canada

Polsenaere P., Bretel P. and Abril G. (2008) / Poster
CO_2 Fluxes by Eddy Correlation in the Arcachon lagoon: an integrative measure of intertidal ecosystem metabolism. XI International Symposium on Oceanography of the Bay of Biscay, 2-4 April 2008.
San Sebastián/Spain

• ***Présentations nationales (Oraux)***

Polsenaere P., Abril G., Bretel P. and Detandt G. (May 2010)
Journée Ecole Doctorale « Science et Environnement »: Echanges de CO_2 atmosphérique dans la lagune d'Arcachon et relations avec le métabolisme intertidal.
Université Bordeaux 1/France

Polsenaere P., Abril G., Bretel P. and Detandt G. (March 2010)
Echanges de CO_2 atmosphérique dans la lagune d'Arcachon et relations avec le métabolisme intertidal. Restitution Projet Région ASCOBAR.
Université Bordeaux 1/France

Polsenaere P., Abril G. and Bretel P. (April 2009)
Journée des **« thésards »**: Echanges de CO_2 atmosphérique dans la lagune d'Arcachon et relations avec le métabolisme intertidal.
Université Bordeaux 1/France

Polsenaere P., Abril G. and Bretel P. (April 2009)
Journée autour du « Bassin d'Arcachon »: Echanges de CO_2 atmosphérique dans la lagune d'Arcachon et relations avec le métabolisme intertidal.
Station Marine d'Arcachon/France

Abril G., **Polsenaere P.**, Bretel P. and Detandt G. (March 2009)
Mesures automatiques des flux de CO_2 atmosphériques dans le Bassin d'Arcachon: vers une quantification du métabolisme du milieu intertidal.
Conseil Régional d'Aquitaine, Bordeaux/France

Polsenaere P., Bretel P. And Abril G. (November 2007)
Echanges de CO_2 atmosphérique dans le basin d'Arcachon: une mesure intégrative du métabolisme intertidal.
Conseil Régional d'Aquitaine, Bordeaux/France

PUBLICATIONS SCIENTIFIQUES

Polsenaere P. and G. Abril
Modelling CO_2 degassing from small acidic rivers using pCO_2, DIC and δ^{13}C-DIC data.
Soumis à *Geochimica et Cosmochimica Acta*

Polsenaere P., Savoye N., Etcheber H., Canton M., Poirier D., Bouillon S. and G. Abril
Export and degassing of terrestrial carbon from small rivers and streams draining a temperate sandy podsolised catchment.
Soumis à *Limnology and Oceanography*

Polsenaere P., Lamaud E., Bretel P., Bonnefond J.-M., Delille B., Detandt G., Loustau D. and G. Abril
Turbulent flux measurements by Eddy Correlation over a temperate intertidal flat in southwestern France.
Soumis à *Journal of Geophysical Research*

Polsenaere P., Lamaud E., Bonnefond, J.-M., Lafon V., Bretel, P., Delille, B., Deborde, J., Loustau, D. and G. Abril
Spatial and temporal CO_2 exchange measured by Eddy Correlation over a temperate intertidal flat and their relationships to net ecosystem production.
Soumis à *Biogeosciences*

Canton M., Anschutz P., Coynel A., **Polsenaere P.** and D. Poirier
Nutrient export to an Eastern Atlantic coastal zone: first modelling and nitrogen mass balance.
Biogeochemistry, DOI 10.1007/s10533-010-9558-7, 2010

EXPERIENCES EN ENSEIGNEMENT

- ***2007/2010***

Monitorat à l'UFR des **Sciences Biologiques** en Licence et Master (3 ans, 290 heures). Enseignements dispenses en travaux pratiques, travaux dirigés et amphithéâtre. Spécialités: écophysiologie aquatique, ecotoxicologie aquatique, production primaire, relations trophiques et génétiques des populations.
Université Bordeaux 1/France

- ***2009/2010***

Participation au projet "Carboschools" Aquitaine: initiation aux mesures de pCO_2 dans l'estuaire de la Gironde (Lycée)
Blaye/Bordeaux